Research in Natural Laminar Flow and Laminar-Flow Control

Compiled by
Jerry N. Hefner and Frances E. Sabo
Langley Research Center
Hampton, Virginia

NASA

National Aeronautics
and Space Administration

Scientific and Technical
Information Division

1987

PREFACE

Since the mid 1970's, NASA, industry, and universities have worked together to conduct important research focused at developing laminar-flow technology that could reduce fuel consumption for general aviation, commuter, and transport aircraft by as much as 40 to 50 percent. This research, which was initiated under the NASA Aircraft Energy Efficiency Program and continued through the Research and Technology Base Program, has proved very successful with many significant and impressive results having been obtained.

This symposium was planned in view of the recent accomplishments within the areas of laminar-flow control and natural laminar flow and the potential benefits of laminar-flow technology to the civil and military aircraft communities in the United States. The symposium included technical sessions on advanced theory and design tool development, wind tunnel and flight research, transition measurement and detection techniques, low and high Reynolds number research, and subsonic and supersonic research.

iii

CONTENTS

Part 1

SESSION 1: OVERVIEWS
Chairman: R. V. Harris, Jr.

SESSION 2: JETSTAR LEFT PROGRAM
Chairman: R. D. Wagner

PRECEDING PAGE BLANK NOT FILMED

SESSION 3: ADVANCED STABILITY THEORY AND ITS APPLICATION
Chairman: D. M. Bushnell

Part 2[*]

SESSION 4: BASIC WIND TUNNEL RESEARCH/TECHNIQUES
Chairman: W. D. Harvey

*Part 2 is presented under separate cover.

SESSION 5:   COMPUTATIONAL TRANSITIONAL RESEARCH
Chairman: P. J. Bobbitt

*Part 3 is presented under separate cover.

SESSION 8: SUPERSONIC TRANSITION/LFC RESEARCH
Chairman: R. W. Barnwell

ATTENDEES

WILLIAM J. ALFORD, Jr.
DEI

TED AYERS
NASA-DFRF

JENNIFER L. BAER-RIEDHART
NASA-DFRF

WAYNE BALDWIN
AFWAL/FIMG

MARK J. BERGEE
LOCKHEED-CALIFORNIA COMPANY

SCOTT BERRY
ESC

MARK EUGENE BEYER
OMAC

S. BIRINGEN
UNIVERSITY OF COLORADO

JOHN BLASCOVICH
GRUMMAN CORPORATION

MICHAEL D. BONDY
NASA-DFRF

ALAN B. CAIN
McDONNELL DOUGLAS

GARY D. CARLSON
NASA-DFRF

FANG-JENG CHEN
HIGH TECHNOLOGY CORPORATION

RODNEY L. CLARK
AFWAL/FIMM

FAYETTE S. COLLIER
HIGH TECHNOLOGY CORPORATION

KENNETH C. CORNELIUS
LOCKHEED-GEORGIA CO.

EDWIN G. CHAPLIN
OMAC, INC.

S. DODBELE
VIGYAN

R. O. DODSON
BOEING

CO DONALDSON
TITAN ASSOCIATES

CORNELIUS DRIVER
EAGLE ENGINEERING, INC.

NABIL M. EL-HADY
ODU

DAVE ELLIS
CESSNA

JEANNE EVANS
TELEDYNE RYAN AERONAUTICAL

G. K. FAUST
GENERAL ELECTRIC

DAVID F. FISHER
NASA-AMES-DRYDEN

EDWARD A. GABRIEL
FAA

HEINZ A. GERHARDT
NORTHROP CORPORATION

DR. GERALD GREGOREK
OHIO STATE UNIVERSITY

SURESH GORADIA
VIRA

GLENN J. GRUBER
PRATT & WHITNEY

M. HUSSAINI
ICASE

DOUG HALL
NADC

PHIL HALL
ICASE

THORWALD HERBERT
VPI&SU

MICHAEL L. HINSON
GATES LEARJET CORP.

VENKIT S. IYER
VIGYAN RESEARCH ASSOC., INC.

LISA A. JENNETT
NASA-DRYDEN

JOSEPH B. JOHNSON
NASA-DRYDEN

M. JONES
PRC-KENTRON

CHANTAL JOUBERT
McDONNELL DOUGLAS CORP.

VIJAY KALBURGI
ODU

OSAMA KANDIL
ODU

ABRAHAM KAREM
LEADING SYSTEMS, INC.

K. KAUPS
DOULGAS AIRCRAFT CO.

EDWARD J. KERSCHEN
UNIVERSITY OF ARIZONA

MARK E. KIRCHNER
BOEING COMM. AIRPLANE CO.

MAX KLOTZCHE
DOUGLAS AIRCRAFT

MARTIN A KNUTSON
NASA-DRYDEN

THOMAS R. LACEY
McDONNELL AIRCRAFT CO.

ROY H. LANGE
LOCKHEED-GEORGIA CO.

SPIRO LEROUDIS
OFFICE OF NAVAL RESEARCH

JOHN O. LINDGREN
DOUGLAS AIRCRAFT CO.

GARY L. LINK
BOEING

T. M. LIU
ROHR INDUSTRIES, INC.

LAURENCE K. LOFTIN, JR.
SELF

W. K. LONDENBERG
GDS/FT. WORTH DIV.

WESLEY K. LORD
PRATT & WHITNEY

LESLIE M. MACK
JET PROPULSION LABORATORY

DR. MUJEEB MALIK
HIGH TECHNOLOGY CORPORATION

DONALD L. MALLICK
NASA-DRYDEN

SIVA M. MANGALAM
AS&M, INC.

MARK D. MAUGHMER
PENN STATE UNIVERSITY

FRED W. MAY
BOEING MILITARY AIRPLANE CO.

WILLIAM D. McCAULEY
TRW

BARNES W. McCORMICK
PENN STATE UNIVERSITY

DAVID E. MCNAY
DOUGLAS AIRCRAFT COMPANY

ROBERT R. MEYER
NASA-DRYDEN

LAWRENCE C. MONTOYA
NASA-DFRF

MARK V. MORKOVIN
ILLINOIS INSTITUTE OF TECH.

DR. THOMAS J. MUELLER
UNIVERSITY OF NOTRE DAME

PARMA MUNGUR
GENERAL ELECTRIC

JOHN W. MURDOCK
THE AEROSPACE CORPORATION

WILLIAM R. MURPHY
GULFSTREAM AEROSPACE CORP.

DEL NAGEL
BOEING

A. NAYFEH
VPI&SU

RON NEAL
BEECH AIRCRAFT

ORAN NICKS
TEXAS A&M

CLIFF OBARA
PRC-KENTRON

ARNOLD OTCHIN
TELEDYNE RYAN AERONAUTICAL

WILLIAM M. OTTO
OTTO LABORATORIES, INC.

PARESH PARIKH
VIRA, INC.

WILFRED E. PEARCE
DOUGLAS AIRCRAFT COMPANY

BRUCE PETERMAN
CESSNA

WERNER PFENNINGER
AS&M

DAVID PICKETT
BOEING MILITARY AIRPLANE CO.

DR. ARTHUR G. POWELL
DOUGLAS AIRCRAFT CO.

JOHN W. RAWLS, JR.
PRC-KENTRON

KENNETH H. ROGERS
DOUGLAS AIRCRAFT COMPANY

OLLIE J. ROSE
PRC-KENTRON

ROGER A. ROZENDAAL
BOEING COMM. AIRPLANE CO.

JIM RUNYAN
BOEING COMM. AIRPLANE CO.

DALLAS M. RYLE
LOCKHEED-GEORGIA COMPANY

F. CHRIS SAUTTER
PENN STATE UNIVERSITY

PAUL SHANG
NAVAL SHIP R&D CENTER

A. J. SMITH
SELF

GREGORY E. SMITH
DYNAMIC ENGINEERING, INC.

NORBERT F. SMITH
McDONNELL DOUGLAS

ROBERT J. STEWART
GULFSTREAM

DENNIS M. STRAUSSFOGEL
PENNSYLVANIA STATE UNIV.

G. TEMANSON
BOEING

BIANCA M. TRUJILLO
NASA-DRYDEN

CHANDRA S. VEMURU
AS&M, INC.

PAUL VIJGEN
UNIVERSITY OF KANSAS

SALLY WATSON-VIKEN
COMPLERE

GIUSEPPE VOLPE
GRUMMAN CORP. RES. CTR.

KENNETH B. WALKLEY
DYNAMIC ENGINEERING, INC.

RICHARD T. WHITCOMB
SELF

MICHAEL WUSK
ODU

LANGLEY RESEARCH CENTER ATTENDEES

RICHARD BARNWELL
HSAD

DENNIS BARTLETT
LSAD

DR. H. LEE BEACH
D/AERO

WILLIAM D. BEASLEY
TAD

IVAN E. BECKWITH
HSAD

PERCY J. BOBBITT
TAD

ALBERT L. BRASLOW
SELF

CUYLER W. BROOKS, JR.
TAD

DENNIS M. BUSHNELL
HSAD

RICHARD L. CAMPBELL
TAD

DEBRA CARRAWAY
IRD

A. M. CARY, JR.
HSAD

WILLIAM CORLETT
HSAD

THEODORE R. CREEL
HSAD

CINDY CROOM
LSAD

RAY DAGENHART
TAD

PAMELA DAVIS
SDD

RICHARD E. DAVIS
FED

DANIEL J. DICARLO
LSAD

SAM DOLLYHIGH
AVD

DOUGLAS DWOYER
HSAD

JAMES FERRIS
TAD

TOM FOUGHNER
TAD

DAVID HAHNE
LSAD

ROBERT HALL
TAD

JAMES HALLISSY
TAD

CHARLES D. HARRIS
TAK

JULIUS E. HARRIS
HSAD

ROY V. HARRIS, JR.
D/AERO

WILLIAM D. HARVEY
TAD

EARL C. HASTINGS
LSAD

JERRY N. HEFNER
AVD

TODD HODGES
MD

BRUCE HOLMES
LSAD

CHARLES JOHNSON
TAD

JOSEPH L. JOHNSON
LSAD

ROBERT A. JONES
HSAD

FRANK JORDAN
LSAD

PIERCE L. LAWING
TRAD

DAL V. MADDALON
LSAD

LUCIO MAESTRELLO
TAD

JACK MOLLOY
OFFICE OF D/AERO

GREGORY S. MANUEL
LSAD

ROBERT J. MCGHEE
TAD

JIM MEYERS
IRD

HARRY MORGAN
LSAD

C. E. K. MORRIS, JR.
AVD

SHELBY J. MORRIS
AVD

LEON MORRISETTE
HSAD

DAN MURRI
LSAD

RICHARD H. PETERSEN
DIRECTOR

PAM PHILLIPS
TAD

JAMES L. PITTMAN
HSAD

LAWRENCE E. PUTNAM
TAD

JAMES A. SCHOENSTER
AcoD

WILLIAM SEWALL
TAD

DAN SOMERS
TAD

JERRY SOUTH
OFFICE OF DIRECTOR

JOHN P. STACK
TAD

P. CALVIN STAINBACK
TAD

DAVID STEPHENS
AD

ERIC C. STEWART
LSAD

JOSEPH W. STICKLE
LSAD

H. PAUL STOUGH III
LSAD

HARRY A. VERSTYNEN, JR.
FAA

NICHOLAS G. VRETAKIS
AFSC LIAISON OFFICE

ED WAGGONER
TAD

RICHARD D. WAGNER
LSAD

BETTY S. WALKER
TAD

RALPH WATSON
HSAD

JOHN WHITCOMB
MD

RICHARD WOOD
HSAD

LONG YIP
LSAD

JAMES YOUNGBLOOD
SSD

TOM ZANG
HSAD

|

NASA LAMINAR-FLOW PROGRAM-
PAST, PRESENT, FUTURE

Roy V. Harris, Jr. and Jerry N. Hefner
NASA Langley Research Center
Hampton, Virginia

CHRONOLOGY OF LAMINAR FLOW RESEARCH

Research in the area of laminar flow control dates back to the 1930's when early applications of stability theory led to the observation that laminar boundary layers can be stabilized by either favorable pressure gradients or small amounts of wall suction. (An excellent summary of this early work is presented in reference 1.) Research was performed in many countries to explore approaches for achieving extensive laminar flow with these concepts. Stabilization of boundary-layer disturbances and instabilities by pressure gradient and shaping became known as natural laminar flow (NLF), and NACA research led to the development of the six-series NLF airfoil. International research on stabilization by suction, referred to as LFC with suction, was intensive at the same time and culminated in the United States in the 1960's with flight tests of a relatively unswept suction glove on an F-94 aircraft (reference 2) and the X-21 flight tests (references 3-6) of a totally new swept LFC wing on a reconfigured WB-66 aircraft.

Little laminar flow research was conducted from the mid-1960's to the mid-1970's. However, as a result of the increased aircraft fuel costs caused by the Arab Oil Embargo of the early 1970's, NASA again resumed laminar flow control research in 1976 as part of the Aircraft Energy Efficiency Program (ACEE); this research, which was later continued under the Research and Technology Base Program, is the subject of this NASA Symposium on Natural Laminar Flow and Laminar Flow Control Research.

2
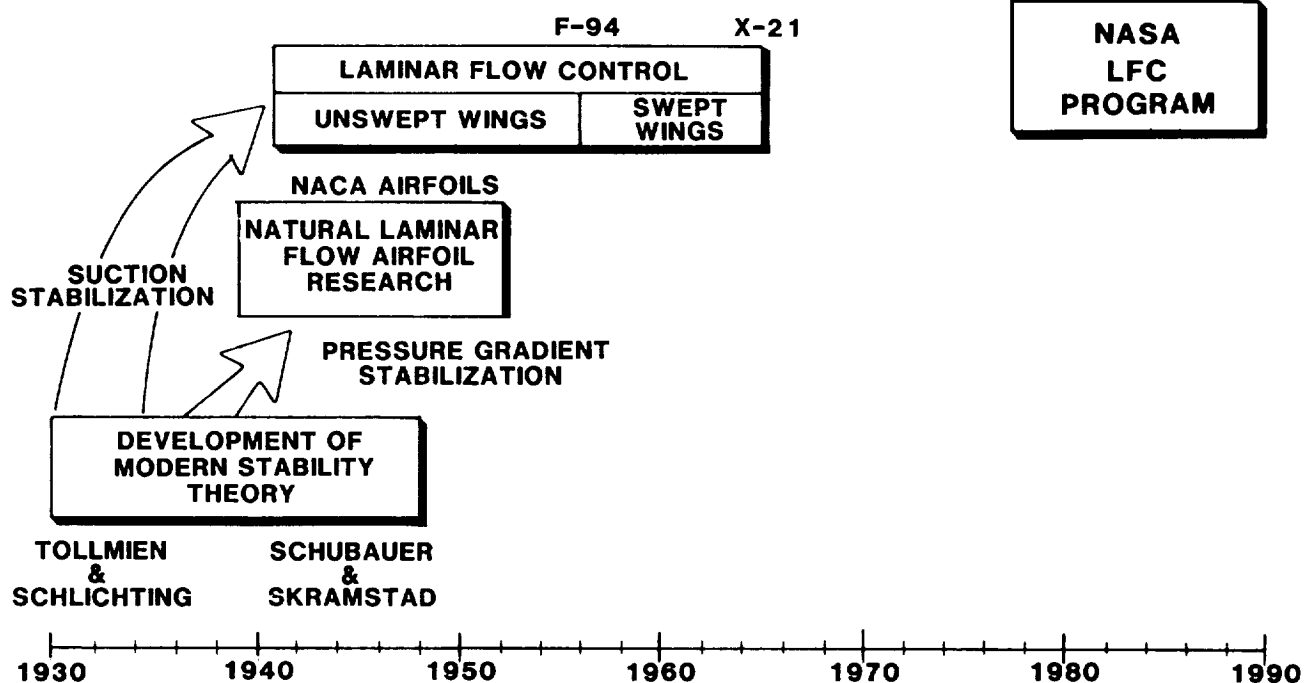
X-21 BOUNDARY-LAYER-CONTROL AIRPLANE IN FLIGHT

In the flight tests of the X-21 aircraft, laminar flow with full-chord slotted suction surfaces was achieved repeatedly over almost all of the intended laminar upper wing area to chord Reynolds numbers of approximately 20×10^6. Extensive laminar flow was also achieved on a nonroutine basis to wing chord Reynolds numbers as high as 47×10^6. Although this flight experiment showed that extensive laminar flow could be achieved in flight with slotted suction surfaces, unresolved concerns regarding maintenance and reliability of LFC systems prevented serious consideration of LFC as a design option for aircraft at that time. Principal concerns were the practicality of producing wing surfaces sufficiently smooth and wave-free to meet laminar-flow criteria and maintaining the wing surface quality in normal airline service operations.

NASA research since 1976 has addressed the maintenance and reliability concerns that were unresolved in the X-21 flights and is focused on developing the technology for application of LFC to transport aircraft. This paper provides an overview of the NASA Laminar Flow Program--its status and its future direction.

UPPER SURFACE

LOWER SURFACE

■ LAMINAR BOUNDARY LAYER
▨ NON-SUCTION REGIONS
▤ TURBULENT BOUNDARY LAYER IN SUCTION REGIONS

MAINTENANCE OF LAMINAR FLOW FOR VISCOUS DRAG REDUCTION

Under the NASA Laminar Flow Program, computational, wind-tunnel, flight, and systems research is being focused at providing the required data base and design methodology to reduce the risks associated with both near- and far-term applications of laminar flow technology. Two approaches are being emphasized to delay the transition process and maintain laminar flow beyond the usual transition Reynolds numbers of 4 x 10^6 or less: i.e., natural laminar flow (NLF) which uses favorable pressure gradients and shaping and laminar flow control with suction (LFC) through slotted or perforated surfaces. Natural laminar flow has the advantage of being a passive approach; however, it may be limited to sweep angles of approximately 20° or less and chord Reynolds numbers of less than 20 x 10^6. Laminar flow control with suction is more complex but will probably be required to some extent in order to achieve extensive laminar flow beyond chord Reynolds numbers of about 20 x 10^6 and for wing sweep angles in excess of about 20-25°.

- Pressure gradient/shaping
- Suction through slotted or perforated surfaces
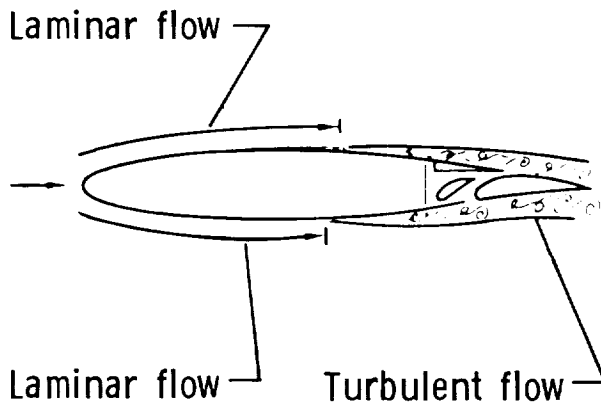
Laminar flow

Laminar flow   Turbulent flow

Natural Laminar Flow

Laminar flow

Laminar flow   Turbulent flow
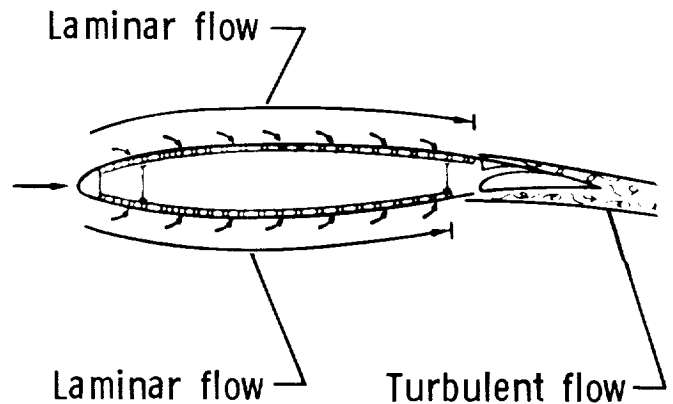
Laminar Flow Control

FACTORS AFFECTING LAMINAR FLOW

The multiplicity of factors affecting laminar flow (reference 7) has made the Laminar Flow Control Program a high-risk research undertaking. The most fundamental of these factors are the Reynolds number at which laminar flow becomes turbulent, the degree of wing sweep used, and the airfoil geometry. Understanding the importance of these and the many other factors illustrated on the figure and how they relate to each other continues to be a critical part of the research program.

FLOW CONDITIONS
- MACH NUMBER
- REYNOLDS NUMBER
- DISTURBANCE ENVIRONMENT

STRUCTURE
- SURFACE DEFORMATION UNDER LOAD

GEOMETRY
- SWEEP
- AIRFOIL SHAPE

NOISE
- ENGINES
- SUCTION PUMPS

SURFACE CONDITION
- CORROSION
- CLOGGING
- REPAIRS

MANUFACTURING QUALITY
- WAVINESS, SMOOTHNESS
- JOINTS (STEPS, GAPS)

SUCTION SYSTEM
- SURFACE OPENINGS
- SUCTION DISTRIBUTION

LEADING EDGE CONDITION
- INSECTS, DIRT
- EROSION
- ICING

ATMOSPHERIC CONDITIONS
- ICE CRYSTALS
- RAIN

NASA LAMINAR FLOW CONTROL PROGRAM

The Laminar Flow Program is composed of four primary elements. These include: (1) aerodynamic design tools and methodology including the essential transition criteria; (2) wind-tunnel and flight calibration and validation of these transition criteria, design tools and methodology; (3) design and integration of LFC systems into advanced wing structures; and (4) performance and reliability of laminar flow concepts in the "real-world" environment. In this research program, NASA continues to work closely with both industry and universities to ensure technology readiness for laminar flow control in the 1990's.

Aero design tools and methodology	Design/integration of LFC systems

NLF, LFC, & HLFC TECHNOLOGY

Wind-tunnel/flight verification of aero design tools and methodology	Performance/reliability in "Real World" environment
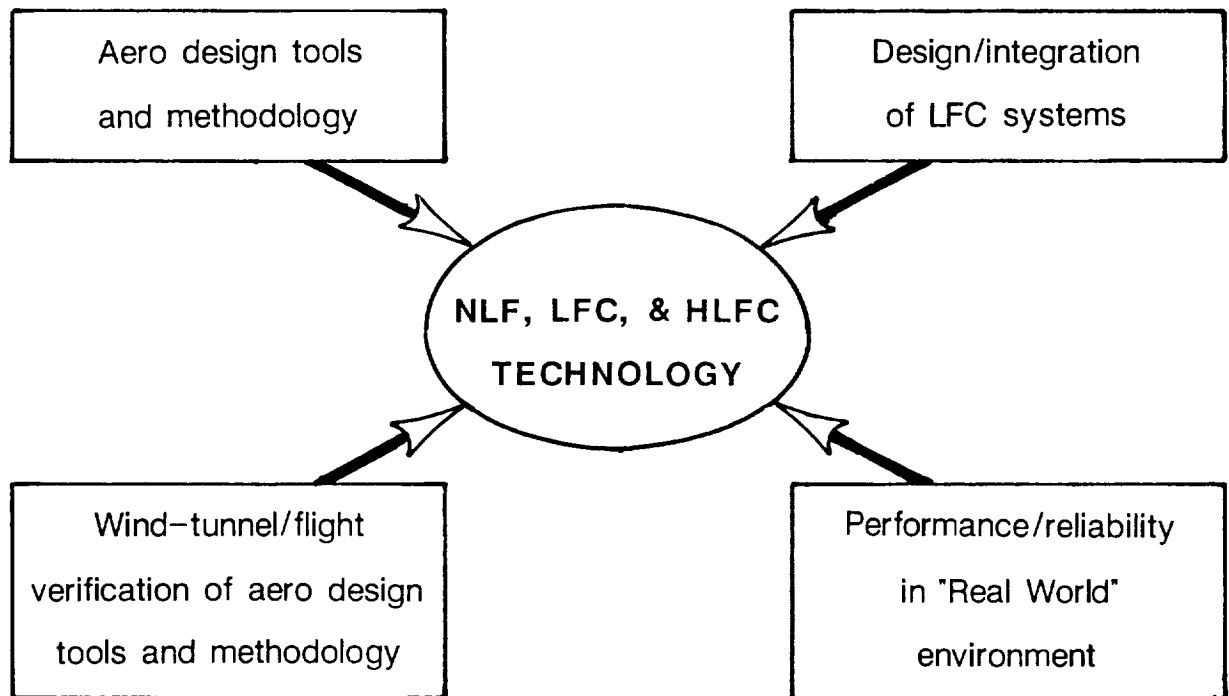
NASA AIRFOIL DEVELOPMENT

Development of advanced computational design tools including stability theories and transition criteria (e.g., references 8-19 which appear in the proceedings) have enabled a new class of low-drag laminar flow airfoils to be developed. NLF airfoils for a wide range of applications, as shown on the figure, and suction LFC airfoils for larger transport aircraft have been designed and tested. Some applications are discussed in references 20-25 which also appear in the proceedings. The NLF (1)-0414F, HSNLF (1)-0213F and the SCLFC (1)-0513F airfoils are discussed in references 20-22 and 25-26.
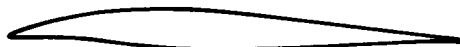
LRN(1)-1010
Low altitude

HSNLF(1)-0213F
Business Jet

NLF(1)-1015
High altitude

NLF(2)-0415
Commuter

NLF(1)-0414F
General aviation

SCLFC(1)-0513F
Transport

VISCOUS DRAG REDUCTION
NATURAL LAMINAR FLOW

The general aviation industry has enthusiastically accepted the new NASA NLF airfoil concepts and is already incorporating them into their advanced designs. Some of these airfoils have recently been tested on a Swearingen SX-300, a Mooney 301, and a Cessna 210. Results of the flight tests with the NLF (1)-0414 airfoil on the Cessna 210 airplane are reported in reference 27. In these flight tests, laminar flow was achieved on the upper and lower wing surfaces to approximately 70-percent chord. Loss of laminar flow did not significantly degrade the lift performance of the wing, and the flight experiments validated both the predicted performance and that obtained in wind-tunnel tests.
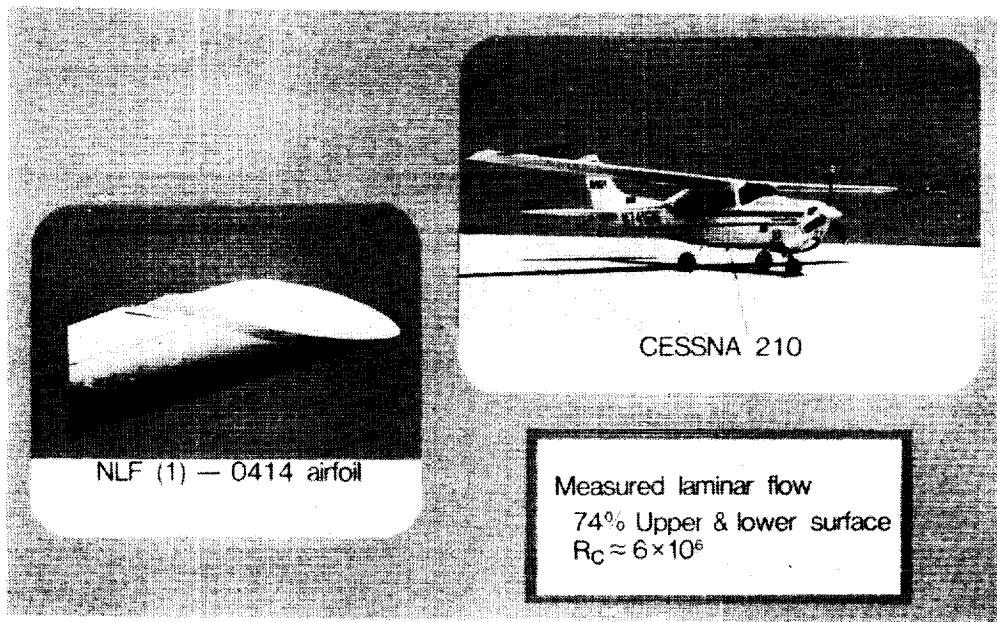
NLF (1) — 0414 airfoil

CESSNA 210

Measured laminar flow
74% Upper & lower surface
$R_C \approx 6 \times 10^6$

ADVANCED TRANSITION MEASUREMENT TECHNIQUES

The calibration and validation of aerodynamic design tools and methodology for NLF and LFC applications require the ability to accurately determine the extent of laminar flow or the location where the laminar boundary layer undergoes transition. A number of advanced transition detection and measurement techniques have been developed to provide the required definitive data in both flight and wind-tunnel investigations. Four such techniques are shown on the figure and are discussed in references 28 and 29.

Turbulent wedge
Roughness particle
Transition front

Transition Visualization in Flight by Liquid Crystal Color Changes

$.030$ in U_∞

1.0 in

Prototype Laminar Crossflow Vorticity Sensor

Copper lead wires   .0623 in. spacing between elements

Any 3 elements
Outer elements - Resistance thermometers
Center element - Hot-film

Polyimide film substrate U_∞

Advanced Laminar Separation Sensor Array

Boeing model transonic wind tunnel

Test section

Interferometer & associated electronics

Advanced Optical Technique for Transition Detection in Compressible Flows

PROGRESS ON ADVANCED LFC AIRFOIL DEVELOPMENT

Subsonic/transonic laminar flow and transition research to validate stability theory, transition prediction criteria, and the aerodynamic LFC design tools continues to be conducted in wind-tunnel facilities at NASA Langley Research Center and in both university and industry laboratories. The most complex and difficult of these experiments is the supercritical LFC airfoil experiment being conducted in the Langley Research Center 8-Foot Transonic Pressure Tunnel (TPT) (reference 30). Extensive modifications to the 8' TPT were necessary for this experiment. These included modifications to reduce tunnel turbulence levels and installation of a honeycomb and five screens in the settling chamber and a sonic choke ahead of the diffuser. A contoured liner was installed in the test section to produce an infinite swept-wing flow over the model surface.

This experiment employs an advanced LFC airfoil incorporating the latest supercritical airfoil technology with features intended to simplify the achievement of laminar flow. The airfoil, shown on the figure, has supercritical flow on both the upper and lower surfaces and a drag divergence Mach number comparable to advanced turbulent supercritical airfoils, but with laminar flow, has nearly an order of magnitude higher lift-to-drag ratio. Full-chord suction with either slotted surfaces or perforated surfaces is being investigated. Results of this research are discussed in references 25 and 26.

The tests with the slotted suction surface have been completed and show that supercritical technology can be successfully combined with LFC technology to produce a supercritical LFC airfoil having at least 60-percent less drag than the comparable turbulent supercritical airfoil. Tests with the perforated suction surfaces will begin in the spring of 1987.
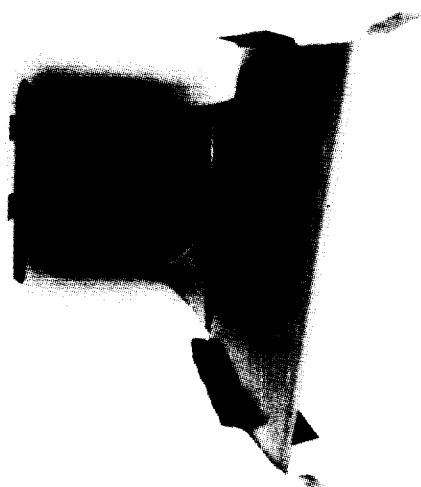
7 FOOT MODEL INSTALLED
IN 8 FOOT TPT
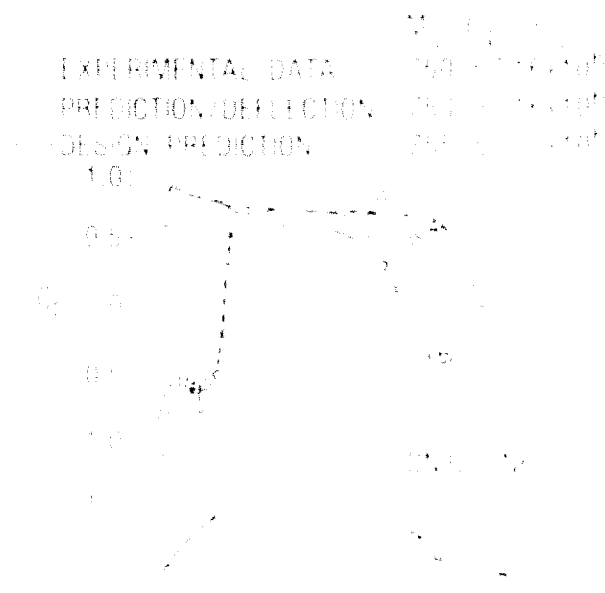
FLIGHT EXPERIMENTS
SUPPORTING DESIGN TOOL DEVELOPMENT

Flight research is a very important extension of the wind-tunnel research being conducted in the Laminar Flow Control Program. Since the maintenance of laminar flow is a boundary-layer stability problem, it is crucial that definitive laminar flow research be conducted at the appropriate unit and chord Reynolds numbers, Mach number, and in the correct disturbance environment. In wind tunnels, the disturbance environment is generally not representative of that in flight; wind tunnels typically have high turbulence levels that can adversely affect the transition phenomena. Also, to achieve large chord Reynolds numbers in wind tunnels, the unit Reynolds number must be large to compensate for relatively small models; this exacerbates the allowable roughness and waviness requirements associated with fabricating the smooth model.

Five important flight experiments are illustrated on the figure. The Lear 28/29 flight tests have provided access to the transonic flight environment for NLF research and for evaluation of advanced transition measurement techniques. The 757 NLF flight tests provided near-field acoustic data on a transport at cruise for the first time and showed that laminar flow can be maintained on wings near wing-mounted engines. The F-111 flight tests and the F-14 Variable Sweep Transition Flight Experiment (VSTFE) are providing the data base essential to the evaluation of sweep, Mach number, and Reynolds number on transition and NLF at transonic speeds. The OV-1 NLF nacelle experiments are providing data to validate acoustic theory and to assess the feasibility of NLF on nacelles. The research with the 757, F-14, and OV-1 is discussed in references 31 to 33 which appear in the proceedings; research on the F-111 and Lear 28/29 is discussed in references 34 and 35, respectively.

LEAR 28/29 NLF   757 NLF

F-14 VSTFE

OV-1 NLF NACELLES   F-111
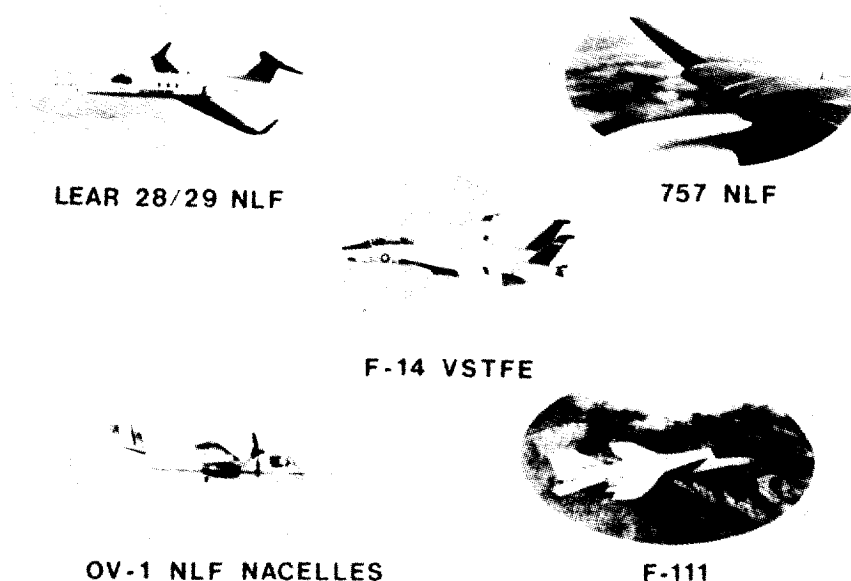
LFC WING PANEL DEVELOPMENT

Wing structural design is the central problem in the definition of a practical large commercial LFC transport. Under the ACEE Program, contracts were awarded to the Lockheed-Georgia Company and the Douglas Aircraft Company to develop LFC wing panel concepts and evaluate their feasibility.

The Lockheed-Georgia Company design employs a ducting network integrated into the primary wing structure and extensively uses graphite epoxy composite materials. (The details of this concept are discussed in reference 36.) The main feature of the Lockheed concept is that it employs slotted suction through a titanium skin with fluid-dispensing slots in the leading edge for de-icing and protection from insect contamination; it was found in earlier work (ref. 7) that insects do not adhere to wet leading edges. Suction is applied on both the upper and lower surfaces of the wing.

The Douglas Aircraft Company concept (discussed in reference 37) uses perforated suction strips in the titanium skin with less ducting in the primary structure. A retractable Krueger device in the leading edge serves as a line-of-sight shield for protection from insects; as a supplement, spray nozzles behind the shield are used to wet the leading edge. Suction is applied only on the upper wing surface.

Since these concepts appeared so promising, they were used in the subsequent Leading-Edge Flight Test (LEFT) Program on the NASA Jetstar aircraft being flown from the Ames-Dryden Flight Research Facility. Currently, new concepts for fabricating LFC panels are being explored; these include superplastic forming and diffusion bonding. Also, methods of fabricating panel joints which can meet the smoothness criteria for laminar flow over the airplane life-cycle are being developed.

LOCKHEED
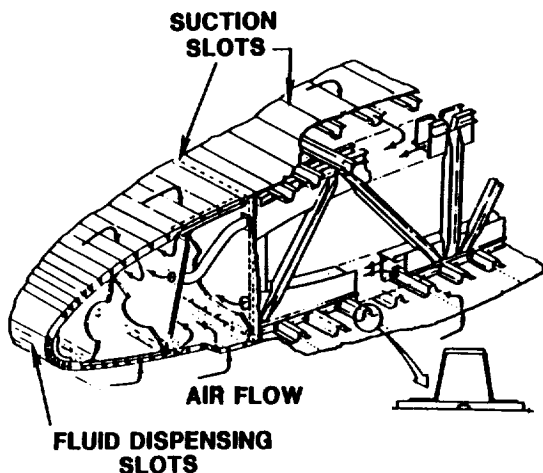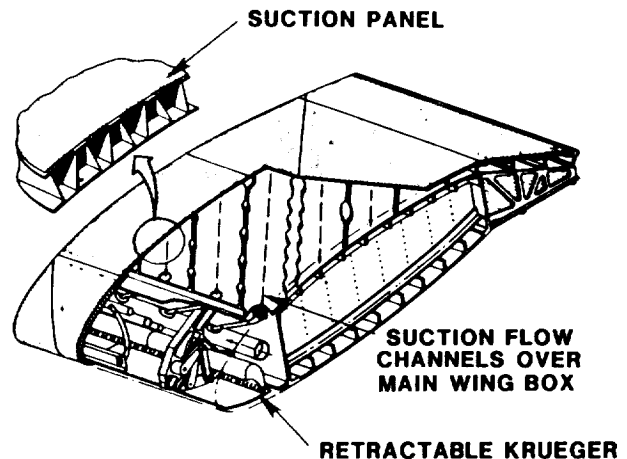
SUCTION SLOTS

AIR FLOW

FLUID DISPENSING SLOTS

DOUGLAS

SUCTION PANEL

SUCTION FLOW CHANNELS OVER MAIN WING BOX

RETRACTABLE KRUEGER

NASA JETSTAR
LFC LEADING-EDGE FLIGHT TEST

The most formidable problem facing practical LFC application is the integration of the de-icing, insect protection, and suction systems into the wing leading edge. Since the Lockheed-Georgia Company and the Douglas Aircraft Company had developed concepts for integrating these systems into the wing structure of transport aircraft, contracts were awarded to these companies to design and fabricate practical leading-edge test articles to be installed and flight tested on the NASA Jetstar. The objective of this research was to evaluate the performance and reliability of these systems in the "real world" environment.

The flight research program has successfully demonstrated that practical and reliable leading-edge systems can be designed and fabricated, and that these systems perform extremely well in an airline environment without any unusual maintenance requirements. Results of this research are discussed in references 38 to 41 and appear in the proceedings.
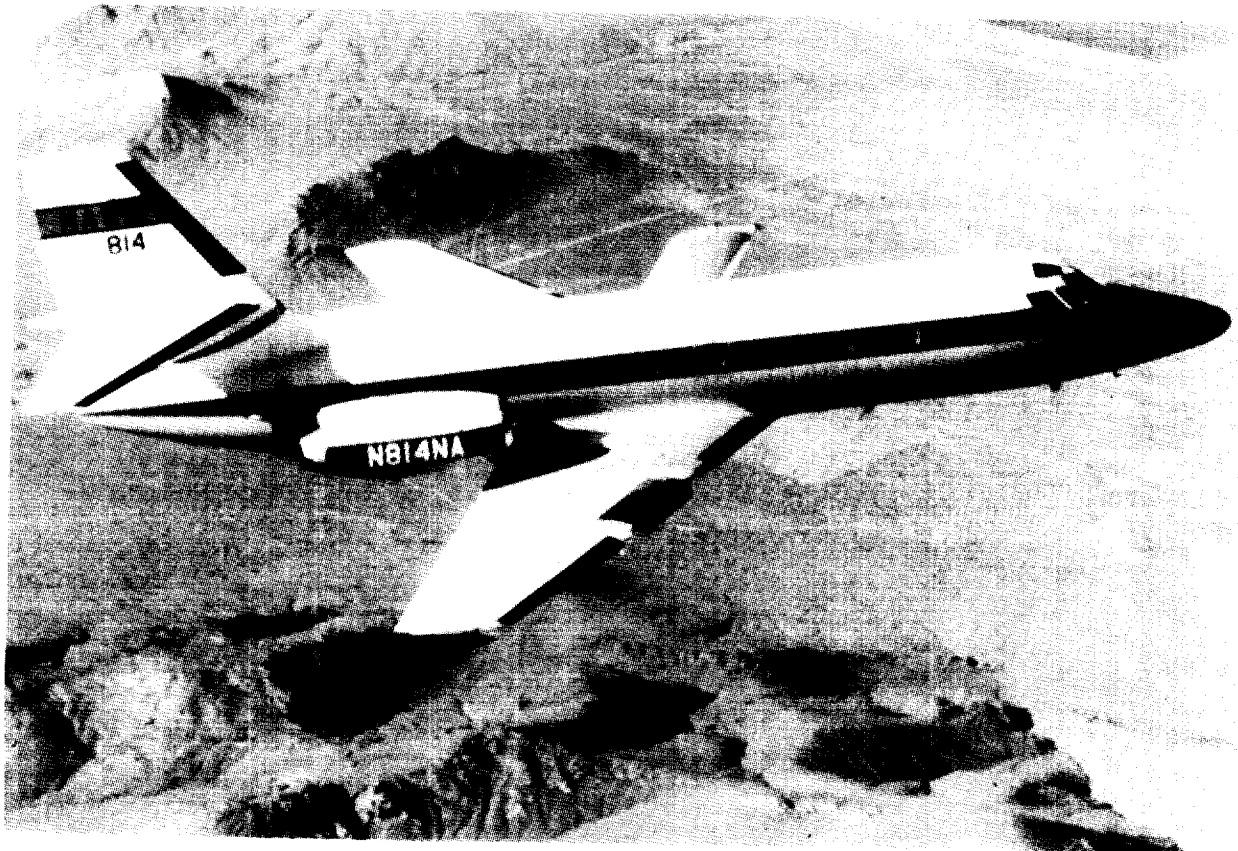
ORIGINAL PAGE
BLACK AND WHITE PHOTOGRAPH

HYBRID LFC FLIGHT EXPERIMENT

The next step for subsonic/transonic laminar flow research is to evaluate hybrid laminar flow control (HLFC). HLFC combines suction LFC and NLF to achieve extensive laminar flow and is probably most applicable for wing chord Reynolds numbers to 40 x 10^6 and wing sweep angles between 20 - 30°. The concept of particular interest for near-term transport application uses suction in the leading edge ahead of the front spar with a slightly favorable or roof-top pressure gradient over the wing box; the goal is to maintain laminar flow to approximately 60-percent chord. HLFC has the advantages of being less complex than full-chord LFC, requiring less suction, and allowing the use of a more conventional wing box structure.

The performance of HLFC at practical Reynolds numbers and Mach numbers in the "real world" environment has not been determined. Therefore, a cooperative NASA, USAF, and industry HLFC Flight Research Experiment is being planned. This experiment will be conducted on a partial-span HLFC test article mounted on a transport aircraft wing at chord Reynolds numbers approaching 40 x 10^6. The goals of this research include: HLFC and perforated suction performance at high Reynolds numbers, environmental effects, off-design performance, and design tool and methodology validation. Since the Jetstar LEFT Program only evaluated the leading-edge problem, the HLFC flight experiment will be designed to achieve extensive laminar flow at realistic flight Reynolds numbers.

Typical Wing Section
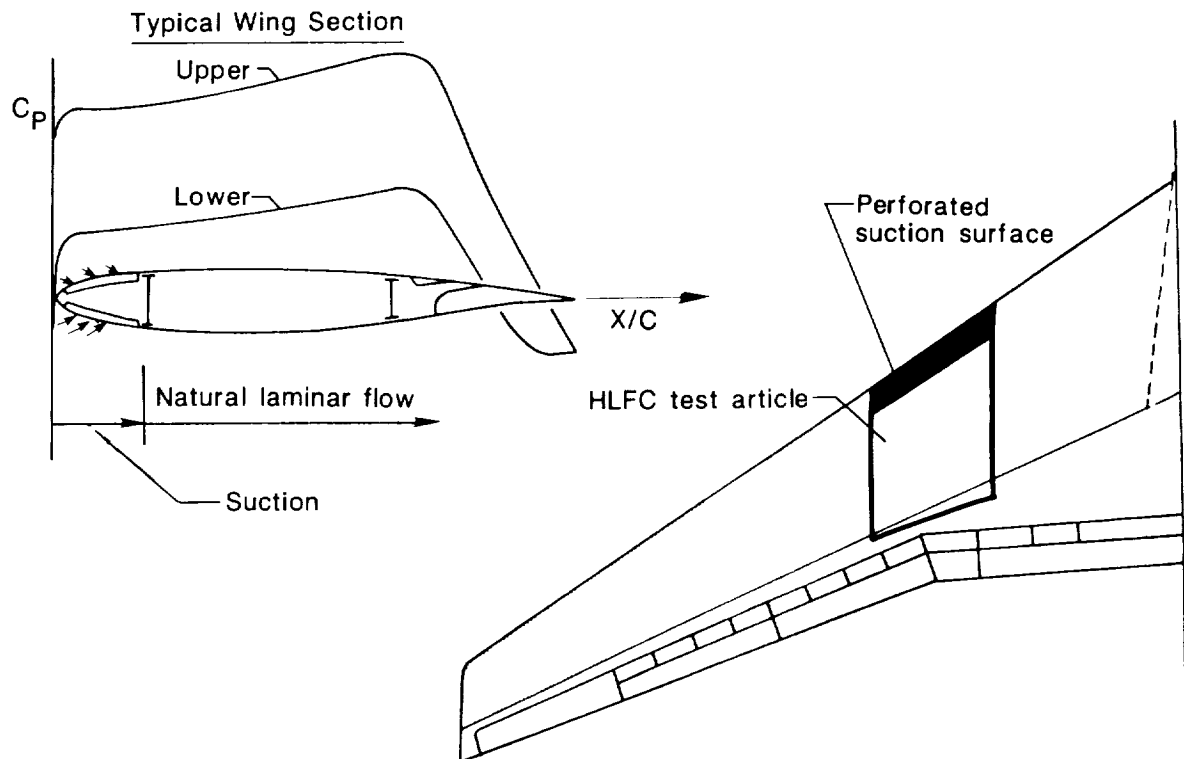
POTENTIAL BENEFITS OF SUPERSONIC LFC

LFC may be more important to supersonic cruise than it is to subsonic/transonic cruise because of its potential impact on the critical areas shown on the figure. Unfortunately, whether extensive laminar flow can be practically maintained at supersonic speeds has not yet been established. Therefore, using the experience and knowledge gained from the subsonic/transonic laminar flow program, the next major thrust in the NASA Laminar Flow Program will be supersonic LFC.

Currently, the supersonic LFC program is being developed with problem areas and research directions being identified. The physics of supersonic transition and LFC is already being investigated including the effects of roughness and waviness, unit Reynolds number, acoustic environment, disturbance amplification through shocks, and suction through perforated surfaces. Stability theories and boundary-layer transition criteria, developed for compressible subsonic and transonic flows, are also being evaluated to determine their applicability to supersonic LFC (reference 43).

- Increased L/D

- Reduced surface temperature

- Reduced gross weight

- Reduced sonic boom

- Increased seat-miles per gallon of fuel

SUPERSONIC LOW-DISTURBANCE TUNNEL

Definitive data for evaluating LFC and transition physics and for developing and validating stability theories and transition criteria must be obtained in ground facilities with low background disturbance levels or in flight. Unfortunately, the turbulence levels in essentially all existing supersonic and hypersonic wind tunnels are sufficiently high to alter the transition phenomena in these facilities. For the past 10 years, research at the NASA Langley Research Center has been conducted to develop a low-disturbance Mach 3.5 wind tunnel. A pilot model of this facility has been built, and transition Reynolds numbers equivalent to those obtained in flight have been measured on cones in this facility; this is the first time flight transition Reynolds numbers have been obtained in a supersonic ground facility (reference 44 discusses this unique facility.) Much of the current research on supersonic transition physics is now being conducted in this pilot facility. (See references 45 and 46 which appear in the proceedings.) Construction of the full-size Supersonic Low-Disturbance Tunnel is now being considered for future NASA funding. An alternate Mach 6 nozzle is also being developed for hypersonic transition research.

$$R_L \leq 15 \times 10^6$$
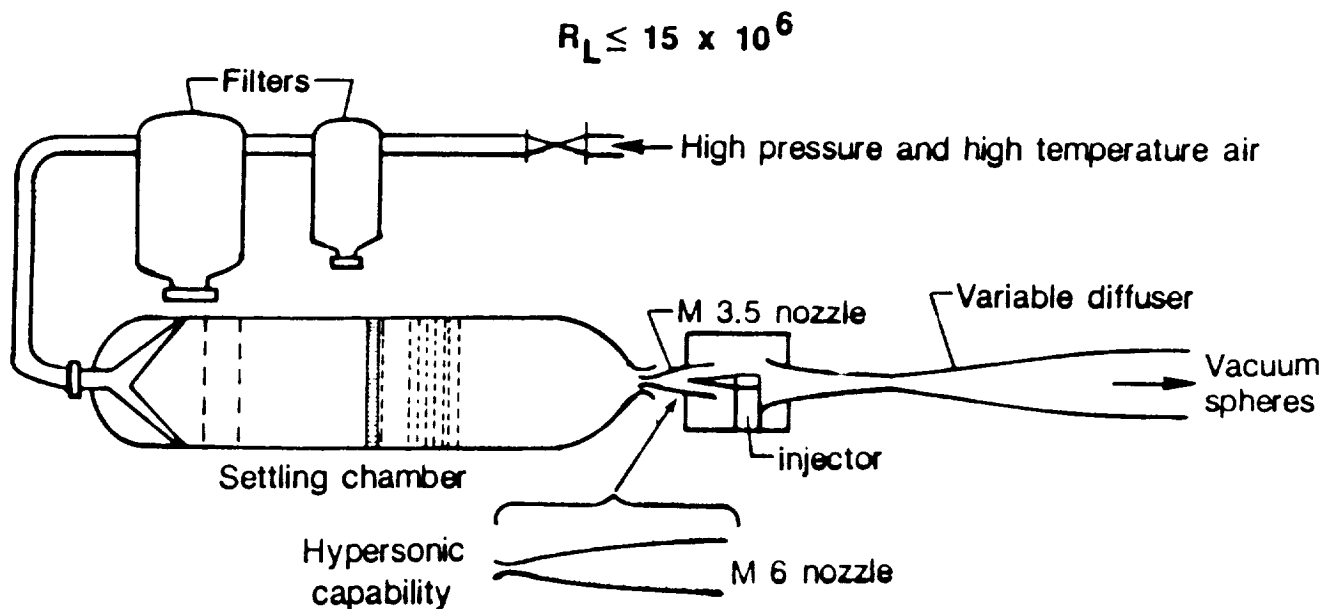
SUPERSONIC FLIGHT TRANSITION MEASUREMENTS

Supersonic swept-wing data of the quality necessary for exploring the transition phenomena, evaluating compressible flow transition criteria at supersonic speeds, and assessing the feasibility of obtaining significant laminar flow at supersonic speeds is almost non-existent. A window of opportunity for obtaining some of this much needed data became available in late 1985 and early 1986. Clean-up gloves to achieve the needed smooth surface finish were installed on the leading edge of a F-15 at the Ames-Dryden Flight Research Facility and on the leading edges of the wing and vertical tail of an F-106 at the Langley Research Center. Surface pressure and hot-film data were obtained in flight tests with both aircraft. Results of these exploratory investigations, which are helping to better define future supersonic LFC flight research, are discussed in reference 47.

F-15
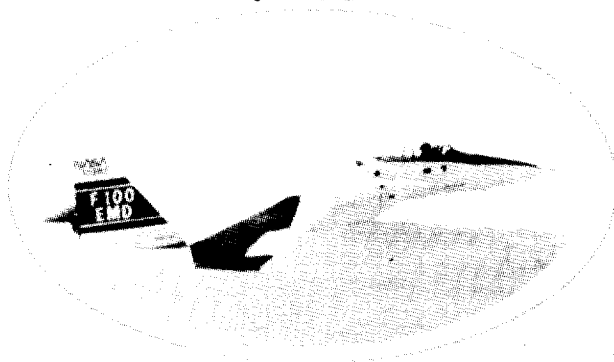
F-106B
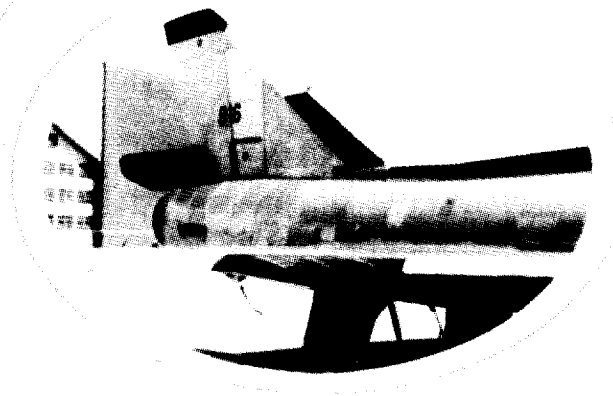
ORIGINAL PAGE
BLACK AND WHITE PHOTOGRAPH

F-106 SUPERSONIC LAMINAR FLOW EXPERIMENT

As a result of the exploratory transition experiments on the F-15 and F-106, the feasibility of a supersonic LFC experiment on the F-106 or other aircraft is now being investigated. Suction through a slotted or perforated suction surface would be applied in the leading-edge region of the wing or vertical tail with a glove installed aft of the suction surface to provide the desired pressure distribution. Surface pressures, hot-film data, and liquid crystal flow visualization data would be employed to examine the extent of laminar flow achieved and the effect of suction in stabilizing supersonic laminar boundary layers. The experimental test article might look something like that shown on the figure.
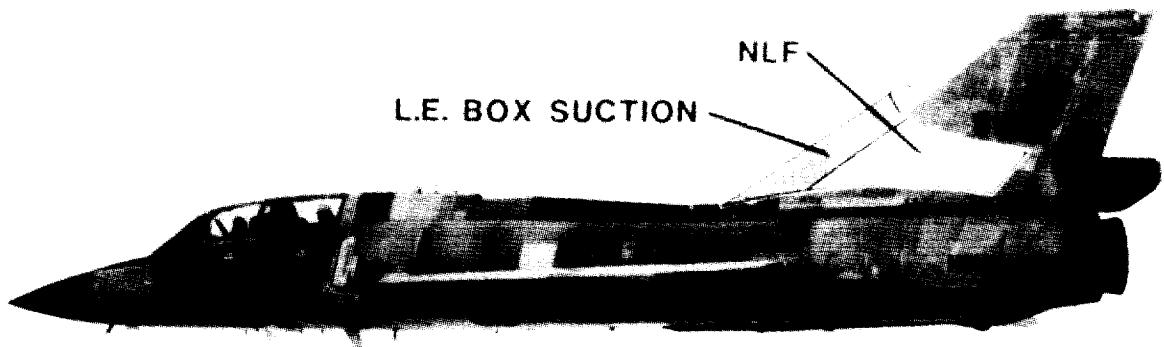
NLF

L.E. BOX SUCTION

SUMMARY

- Results obtained over past 10 years are impressive

- General aviation industry now using NLF in their new aircraft designs

- Success in laminar flow research has provided impetus for looking at HLFC for near-term transport applications

- Focus of laminar flow research being directed toward

    - High Reynolds number effects associated with HLFC applications

    - Supersonic laminar flow control

REFERENCES

1. Bushnell, D. M; and Tuttle, M. H.: Survey and Bibliography on Attainment of Laminar Flow Control in Air Using Pressure Gradient and Suction. NASA RP-1035, vol. 1, 1979.

2. Groth, E. E.; Carmichael, B. H.; White, R. C.; and Pfenninger, W.: Low Drag Boundary Layer Suction Experiments in Flight on the Wing Glove of a F-94A Airplane - Phase II: Suction Through 69 Slots. NA1-57-318, BLC-94 (Contract AF-33 (616) - 3168), Northrop Aircraft, February 1957.

3. Antonatus, P. P.: Laminar Flow Control Concepts and Applications. Astronautics and Aeronautics, vol. 4, no. 7, July 1966, pp. 32-36.

4. Nenni, J. P.; and Gluyas, G. L.: Aerodynamic Design and Analysis on an LFC Surface. Astronautics and Aeronautics, vol. 4, no. 7, July 1966.

5. White, R. C.; Suddreth, R. W.; and Wheldon, W. G.: Laminar Flow Control on the X-21. Astronautics and Aeronautics, vol. 4, no. 7, July 1966, pp. 38-43.

6. Pfenninger, W.; and Reed, V. D.: Laminar-Flow Research and Experiments. vol. 4, no. 7, July 1966, pp. 44-47, 49-50.

7. Maddalon, D. V.; and Wagner, R. D.: Operational Considerations for Laminar Flow Aircraft. Laminar Flow Aircraft Certification Workshop, NASA SP-2413, May 1986, pp. 247-266.

8. Malik, M.: Stability Theory Applications to Laminar Flow Control. NASA Symposium on NLF and LFC Research, NASA CP 2487, 1987, pp. 219-244.

9. Nayfeh, A.: Nonparallel Stability of Boundary Layers. NASA Symposium on NLF and LFC Research, NASA CP 2487, 1987, pp. 245-259.

10. Hall, P.: Interaction of Tollmien-Schlichting Waves and Görtler Vortices. NASA Symposium on NLF and LFC Research, NASA CP 2487, 1987, pp. 261-271.

11. Kerschen, E.: Boundary-Layer Receptivity and Laminar Flow Airfoil Design. NASA Symposium on NLF and LFC Research, NASA CP 2487, 1987, pp. 273-287.

12. Kalburgi, V.; Mangalam, S.; Dagenhart, J.; and Tiwari, S.: Gortler Instability on an Airfoil. NASA Symposium on NLF and LFC Resesarch, NASA CP 2487, 1987, pp. 289-300.

13. Nayfeh, A.: Effect of Roughness on the Stability of Boundary Layers. NASA Symposium on NLF and LFC Research, NASA CP 2487, 1987, pp. 301-315.

14. Bushnell, D. M.; Hussaini, V.; and Zang, T.: Sensitivity of LFC Techniques in the Non-linear Regime. NASA Symposium on NLF and LFC Research, NASA CP 2487, 1987, pp. 491-516.

15. Harris, J.; Iyer, V.; and Radwan, S.: Numerical Solutions of the Compressible 3-D Boundary Layer Equations for Aerospace Configurations With Emphasis on LFC. NASA Symposium on NLF and LFC Research, NASA CP 2487, 1987, pp. 517-545.

16. Goradia, S.; and Morgan, H.: Theoretical Methods and Design Studies for NLF and HLFC Swept Wings at Subsonic and Supersonic Speeds. NASA Symposium on NLF and LFC Research, NASA CP 2487, 1987, pp. 547-575.

17. Biringen, S.; and Caruso, M.: Numerical Experiments in Transition Control in Wall-Bounded Shear Flows. NASA Symposium on NLF and LFC Research, NASA CP 2487, 1987, pp. 577-592.

18. Maestrello, L.: Parikh, P.; and Bayliss, A.: Application of Sound and Temperature to a Control Boundary-Layer Transition. NASA Symposium on NLF and LFC Research, NASA CP 2487, 1987, pp. 593-616.

19. Rawls, J. W.: Near-Field Noise Prediction of an Aircraft in Cruise. NASA Symposium on NLF and LFC Research. NASA CP 2487, 1987, pp. 617-636.

20. Viken, J.; Viken, S.; Pfenninger, W.; Morgan, H.; and Campbell, R.: Design of the Low-Speed NLF(1)-0414F and High-Speed HSNLF(1)-0213 Airfoils With High-Lift Systems. NASA CP 2487, 1987, pp. 637-671.

21. Murri, D.; McGhee, R.; Jordan, F.; Davis, P.; and Viken, J.: Wind-Tunnel Results of the Low-Speed NLF(1)-0414F Airfoil. NASA Symposium on NLF and LFC Research. NASA CP 2487, 1987, pp. 673-726.

22. Kolesar, C.: Design and Test of a Natural Laminar Flow Large Reynolds Number Airfoil With High Design Cruise Lift Coefficient. NASA Symposium on NLF and LFC Research, NASA CP 2487, 1987, pp. 727-751.

23. Waggoner, E.; Campbell, R.; Phillips, P.; and Hallissy, J.: Design and Test of an NLF Wing Glove for the Variable-Sweep Transition Flight Experiment. NASA Symposium on NLF and LFC Research, NASA CP 2487, 1987, pp. 753-776.

24. Maughmer, M.; and Somers, D.: Design of an Airfoil for a High Altitude Long-Endurance, Remotely Piloted Vehicle. NASA Symposium on NLF and LFC Research. NASA CP 2487, 1987, pp. 777-794.

25. Brooks, C.; and Harris, C.: Results of LFC Experiment on Slotted, Swept Supercritical Airfoil in Langley's 8-Foot Transonic Pressure Tunnel. NASA Symposium on NLF and LFC Research, NASA CP 2487, 1987, pp. 453-469.

26. Berry, S.; Dagenhart, J.; Brooks, C.; and Harris, C: Boundary Layer Stability Analysis of LaRC 8-Foot LFC Experimental Data. NASA Symposium on NLF and LFC Research, NASA CP 2487, 1987, pp. 471-489.

27. Befus, J.; Latas, J.; Nelson, E.; Carr, J.; and Ellis, D.: In-Flight Measurements of Lift, Drag, and Pitching Moments on an Advanced NLF Wing on a Cessna Model T210. Presented at the NASA Symposium on NLF and LFC Research, March 16-19, 1987.

28. Holmes, B.; Carraway, D.; Manuel, G.; and Croom, C.: Advanced Measurement Techniques. Part I. NASA Symposium on NLF and LFC Research. NASA CP 2487, 1987, pp. 317-340.

29. Johnson, C.; Stainback, P.; Carraway, D.; Stack, P.; Yeaton, R.; Dagenhart, J.; Hall, R.; and Lawing, P.: Advanced Measurement Techniques. Part II. NASA Symposium on NLF and LFC Research. NASA CP 2487, 1987, pp. 341-419.

30. Harvey, W. D.; and Pride, J. D.: NASA Langley Laminar Flow Control Airfoil Experiment. NASA CP-2218, September 1981, pp. 1-42.

31. Runyan, L.; Bielak, G.; Rehbahani, R.; Chen, A.; and Rozendaal, R.: 757 NLF Glove Flight Test Results. NASA Symposium on NLF and LFC Research. NASA CP 2487, 1987, pp. 795-818.

32. Meyer, R.; Bartlett, D.; and Trujillo, B.: F-14 VSTFE and Results for the Clean-Up Flight Test Program. NASA Symposium on NLF and LFC Research. NASA CP 2487, 1987, pp. 819-844.

33. Hastings, E.; Faust, G.; Mungur, P.; Obara, C.; Dodbele, S.; Schoenster, J.; and Jones, M.: Status Report on a Natural Laminar Flow Flight Experiment. NASA Symposium on NLF and LFC Research. NASA CP 2487, 1987, pp. 887-921.

34. Montoya, L. C.; Steers, L. L.; Christopher, D.; and Trujillo, B.: F-111 TACT Natural Laminar Flow Glove Flight Results. NASA CP-2208, September 1981.

35. Holmes, B. J.; Croom, C. C.; Gall, P. D.; Manuel, G. S.; and Carraway, D. L.: Advanced Transition Measurement Methods for Flight Applications. AIAA/AHS/CASI/DGLR/IES/ISA/ITEA/SETP/SFTE 3rd Flight Testing Conference, Las Vegas, Nevada, April 2-4, 1986, AIAA Paper No. 86-9786.

36. Lange, R. H.: Design Integration of Laminar Flow Control for Transport Aircraft. Journal of Aircraft, vol. 21, August 1987, pp. 612-617.

37. Pearce, W. E.: Progress at Douglas on Laminar Flow Control Applied to Commercial Transport Aircraft. Proceedings of the 13th ICAS Congress, and AIAA Aircraft Systems and Technology Conference, Seattle, Washington, vol. 2, August 22-27, 1982, pp. 811-817.

38. Fisher, D; and Fischer, M.: The Development Flight Tests of the Jetstar LFC Leading-Edge Flight Experiment. NASA Symposium on NLF and LFC Research, NASA CP 2487, 1987, pp. 117-140.

39. Powell, A.: The Right Wing of the L.E.F.T. Airplane. NASA Symposium on NLF and LFC Research, NASA CP 2487, 1987, pp. 141-161.

40. Davis, R.; Maddalon, D.; and Wagner, R.: Performance of Laminar Flow Leading-Edge Test Articles in Cloud Encounters. NASA Symposium on NLF and LFC Research, NASA CP 2487, 1987, pp. 163-193.

41. Maddalon, D.; Fisher, D.; Jennett, L.; and Fischer, M.: Simulated Airline Service Experience with Laminar Flow Control Leading-Edge System. NASA Symposium on NLF and LFC Research, NASA CP 2487, 1987, pp. 195-218.

I

42. Montoya, L.; and Maddalon, D.: Suction Discontinuities in LFC Leading-Edge Surfaces. Presented at the NASA Symposium on NLF and LFC Research, March 16-19, 1987.

43. Bushnell, D. M.; and Malik, M.: Supersonic Laminar Flow Control. NASA Symposium on NLF and LFC Research, NASA CP 2487, 1987, pp. 923-946.

44. Beckwith, I.; Chen, F.; and Malik, M.: Design and Fabrication Requirements for Low Noise Supersonic/Hypersonic Wind Tunnels. NASA Symposium on NLF and LFC Researach. NASA CP 2487, 1987, pp. 947-964.

45. Morrisette, L.; and Creel, T.: Effects of Wall Surface Defects on Boundary Layer Transition in Quiet and Noisy Supersonic Flow. NASA Symposium on NLF and LFC Research. NASA CP 2487, 1987, pp. 965-980.

46. Creel, T.; Malik, M.; and Beckwith, I.: Experimental and Theoretical Investigation of Boundary Layer Instability Mechanisms on a Swept Leading Edge at Mach 3.5. NASA Symposium on NLF and LFC Research. NASA CP 2487, 1987, pp. 981-995.

47. Collier, F.; Rose, O.; Miller, D.; and Johnson, C.: Supersonic Boundary-Layer Transition on the LaRC F-106 and DFRF F-15 Aircraft. NASA Symposium on NLF and LFC Research. NASA CP 2487, 1987, pp. 997-1024.

LAMINAR FLOW: CHALLENGE AND POTENTIAL

M. E. Kirchner
Boeing Commercial Airplane Company
Seattle, Washington

INTRODUCTION

Commercial air transportation has experienced revolutionary technology advances since WWII. These technology advances have resulted in an explosive growth in passenger traffic. Today, however, many technologies have matured, and maintaining a similar growth rate will be a challenge. We have come to the point where more complex technology must be addressed. At the Boeing Company we see the potential benefits of laminar flow as being worthy of the challenge.

A brief history of the technology and its application to subsonic and supersonic air transportation is presented.

- Laminar flow—the potential
    - Subsonic
    - Supersonic

- Laminar flow perspective

- Laminar flow at Boeing

- Laminar flow—the challenge

LAMINAR FLOW POTENTIAL - SUBSONIC

Many claims have been made over the past several decades regarding the potential advantages of "laminarizing" a transport-type airplane. These claims have ranged from wildly optimistic projections to the pessimistic prognosis that it is technically feasible but economically and operationally absurd.

To place these views in perspective, consider the results of a limited number of trade-studies relating to the fuel savings anticipated from full and partial laminarization of transport aircraft. As shown in this figure, the increments in projected fuel savings are significant. The projections vary considerably depending on the nature of the laminar-flow control concept employed, the extent of the airframe components to be laminarized, and the mission range of the vehicle. The conclusion one draws from these limited data is that, for long range subsonic transports, the potential fuel saving from laminar flow control (LFC) is worth investigating.

SUBSONIC TRANSPORT FUEL SAVING
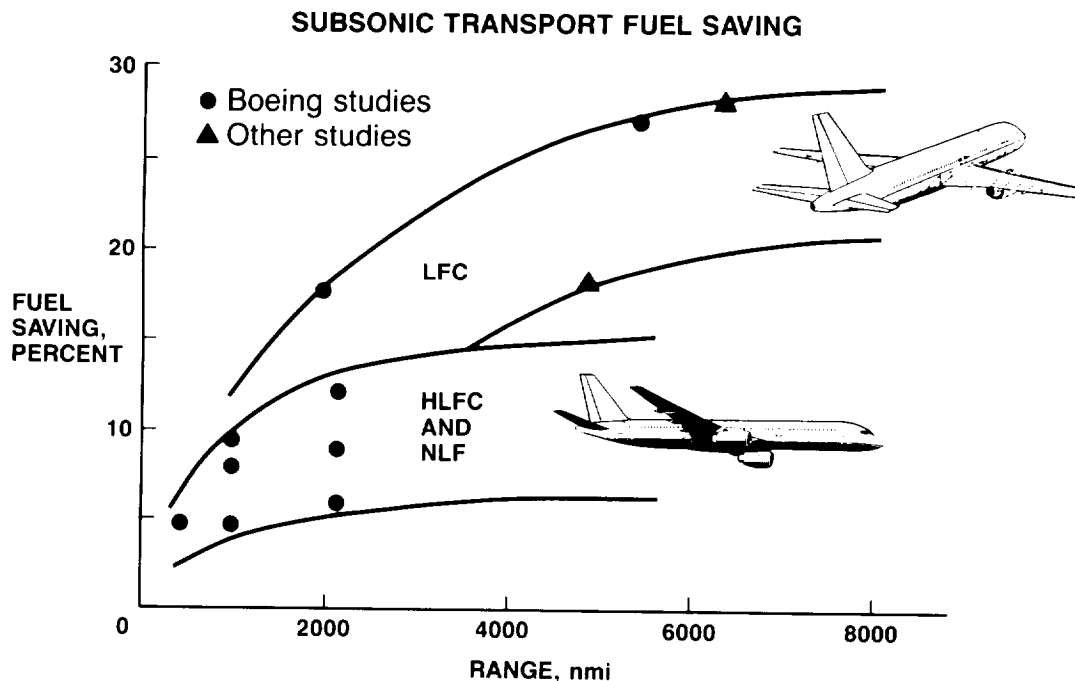
LAMINAR FLOW POTENTIAL - SUPERSONIC

While fuel saving benefits for subsonic transport applications may be substantial, the advantages of laminar flow technology in high speed transport applications may be even greater. From a purely aerodynamic viewpoint, past studies of typical SST configurations have illustrated the potential increases in cruise lift-drag ratio obtainable as a function of the extent of laminar flow achieved. Results of this type are shown in the left hand portion of the figure for both older and advanced SST configurations.

The graph on the right hand side of the figure displays the experimental data (refs. 1-2) upon which present performance improvement estimates can be based. The data are limited and suggest the need for improved supersonic wind tunnels with quiet test sections to supplement flight experiments. Such further work is essential to address the following two major questions for high speed civil transports (HSCT):

- What is the achievable transition Reynolds number (RN) on realistically complex configurations?

- What are the structural requirements of candidate laminarized configurations?

(L/D) IMPROVEMENT
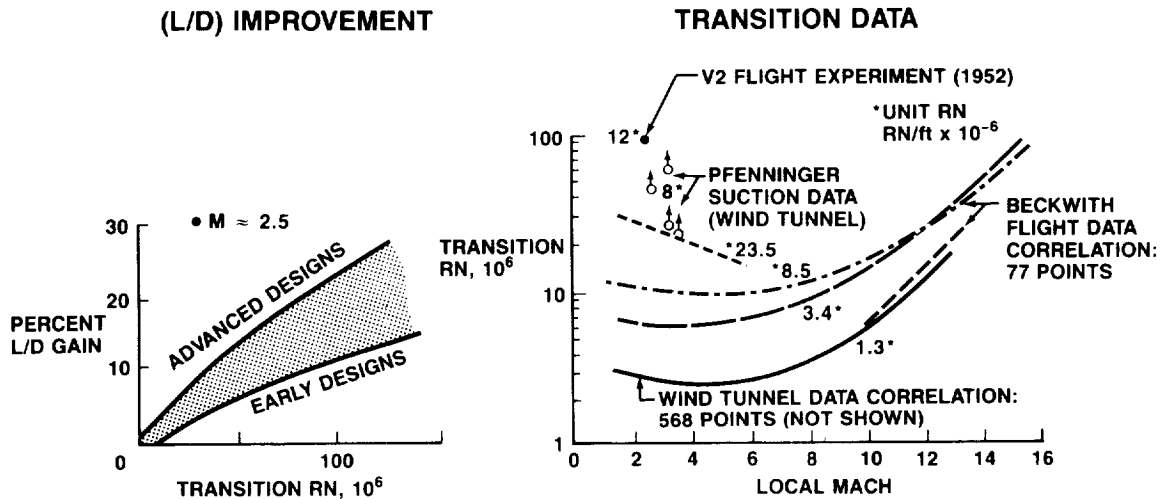
TRANSITION DATA

MAJOR UNKNOWNS
- Achievable transition RN on complex HSCT configuration
- Structural feasibility of LFC on HSCT

LAMINAR FLOW POTENTIAL - SUPERSONIC (conc.)

While the performance advantages of laminarizing a high speed transport can be readily identified, other more subtle advantages may also be exploited to make the overall airframe system more attractive.

As listed in this figure, an important benefit in laminarization may be the substantial reductions obtainable in both skin temperature and fuel temperature as a function of mission time. Reduced aerodynamic heating has many important implications. In high speed transport applications this must be considered at the outset of a design feasibility study. Besides the immediate impact on materials selection, the feasibility of structural concepts to be employed must also be assessed. Further, major choices in a whole range of aircraft systems will be significantly influenced by the degree to which laminar flow can reduce the net heat load on the airframe.

If the aerodynamic gains anticipated from laminarization of a significant portion of the airframe can be achieved, then associated reductions in airplane gross weight and sonic boom intensity can be expected.

Work remains to be done to clarify the important benefits as well as the possible problems encountered in thermal cycling.

- Aerodynamic heating reduced

- Structural/materials/systems benefits

- Reduced load on fuel heat sink

- Gross weight reduced

- Sonic boom reduction

- Thermal cycling possible problem

LFC PERSPECTIVE

The previous figures have shown some of the reasons for our interest in laminar flow. With potential gains of the magnitude shown, the obvious question is why laminar flow control isn't being applied? To put this matter in context, the data for long range transport aircraft shown in this figure have been assembled from several sources (Dept. of Transportation* and ref. 3).

Since the era of the DC-3 we have seen dramatic improvements in commercial airplane performance and direct operating cost (DOC) reduction. For several decades fuel costs remained low and the contribution of the fuel to DOC remained relatively small. Only since the early 1970s has this equation changed, and, with the advent of OPEC and other related factors, we have entered an era where fuel prices have fluctuated dramatically. While detailed predictions of future fuel costs are controversial, the probability of a generally upward trend over time seems certain. From the viewpoint of our commercial airline customers, the cost of fuel is a major element of their overall DOC and will continue to influence their purchase decisions.
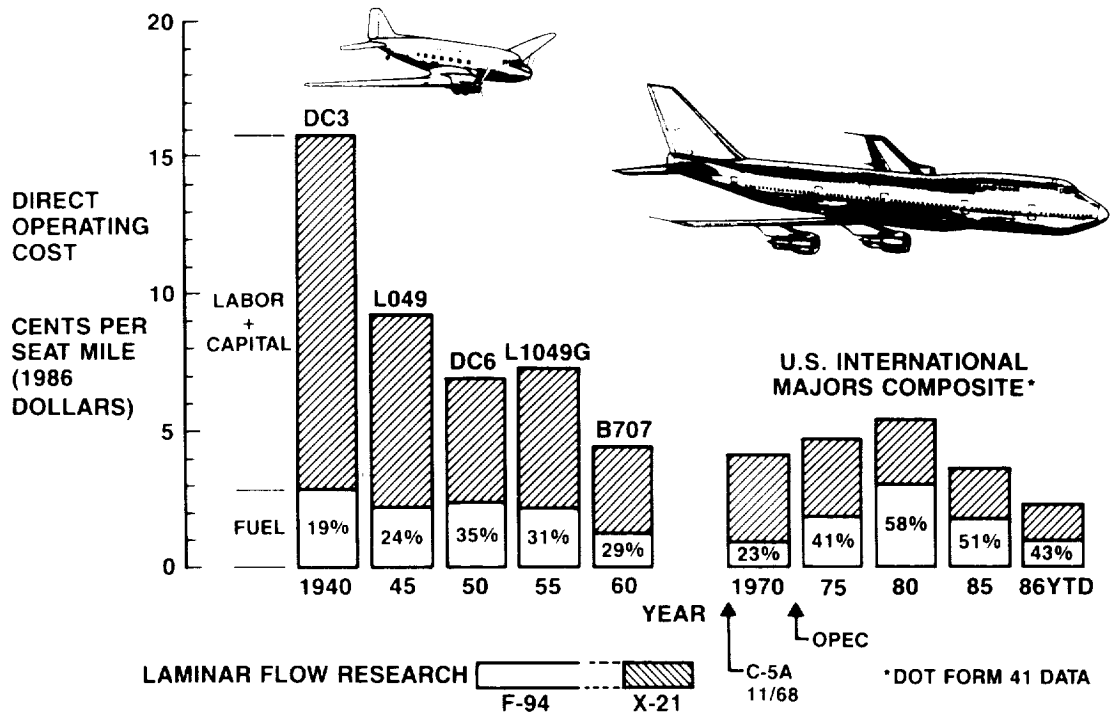
WHY LAMINAR FLOW HAS NOT BEEN USED

While the economics of long range transport operation does much to explain the lack of emphasis on laminar flow technology development, it does not fully address the question of why this technology has not been used.

One reason is that early experience with natural laminar flow airplanes was rather negative. There was not enough appreciation for the effects of skin surface condition and waviness. Smooth structure simply could not be built in those days. Recently, however, when we carefully smoothed the wing of a 30-year old T-33 trainer, we got extensive runs of laminar flow over almost the entire flight envelope.

The unfortunate history of the X-21 is another factor. Perhaps this program occurred too soon but it was driven by the potential application to the C-5. According to a summary (ref. 4) given at the 1974 NASA Langley laminar flow workshop, the X-21 "failed" in spite of many impressive accomplishments. Due to an incorrect design detail, that in retrospect appears easily avoidable, primary objectives of the test program were not met. Progress on the C-5 program could not wait for the design of a new wing and thus, laminar flow lost a major opportunity to display its real potential. The technical community recommended continuing a research program, but funds could not be made available. For laminar flow research this began a hiatus which was to last a decade.

Given its history, laminar flow technology was clearly not ready for application in a commercial environment. The risk was much too great, and necessary performance gains were more easily achievable through other, more conventional technologies such as propulsion, structures, materials, and avionics. Generally speaking, the risk-benefit ratio for laminar flow had to be improved.

Failures of early application
+
Low cost of fuel
+
Competing technologies
+
Competition for funds

High risk/reward ratio

WHAT IS NEW IN LAMINAR FLOW

What factors are operative today to alter the previous risk-benefit ratio for laminar flow applications. The two major factors are 1) a greater need for performance improvements in today's increasingly competitive market, and 2) technological advances that have significantly reduced the risks of application.

To illustrate the advances in laminar flow technology, we have selected the three examples in the figure:

o   Better understanding of laminar flow problems.

   A resurgence of interest in laminar flow, in connection with the NASA ACEE program, led to a number of very constructive flight test programs. These programs have given us a far better basis for assessing the potential for achieving practical laminar flow systems for subsonic aircraft. Typified by the NASA Leading Edge Flight Test (LEFT) program, these efforts have given us a much better understanding of laminar flow problems and how to address them.

- **BETTER UNDERSTANDING OF LAMINAR FLOW PROBLEMS**

- **NEW MATERIALS AND PROCESSES**

ELECTRON BEAM DRILLING
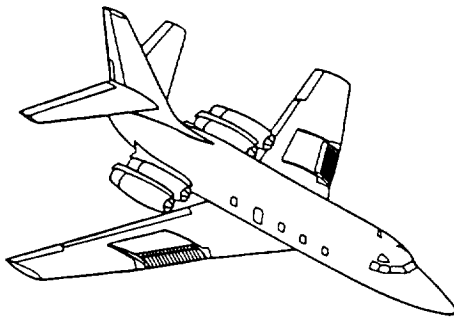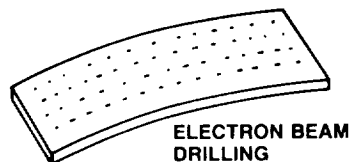
- **BETTER COMPUTATIONAL AERODYNAMIC METHOD**
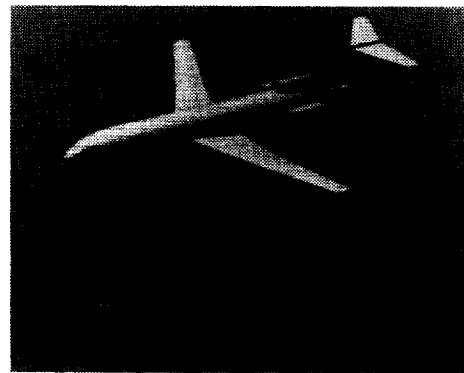
- TRANSONIC, VISCOUS FLOW WING ANALYSIS AND DESIGN
- BOUNDARY LAYER STABILITY AND TRANSITION ANALYSIS

WHAT IS NEW IN LAMINAR FLOW (conc.)

o New materials and processes.

Significant advances have been made in both materials and, perhaps more significantly, manufacturing processes. For example, electron beam drilling of titanium sheet stock now permits large scale fabrication of porous laminar flow surfaces which are economically viable and corrosion resistant.

o Better computational aerodynamic methods.

Advances in computational aerodynamics enable improvements in two of the major risk/cost reducing factors of laminar flow development. First, we now have the capability to both analyze and design realistically complex wing-body combinations in a transonic flow. This enables the efficient development of wing and tail surfaces capable of meeting the requirements of either natural laminar flow (NLF), hybrid laminar flow control (HLFC), or full LFC systems. Second, mechanization of sophisticated boundary-layer-stability analyses allows the routine evaluation of a wide range of wing geometries. Such analyses simply were not performed in the past because of the unacceptable amounts of time and money they required.

CURRENT SITUATION

Our continued efforts to develop commercially acceptable laminar flow technology is dictated by the improved risk-benefit relationship. We need answers to a relatively few, but important, technical questions such as flight data at Reynolds numbers and wing sweep representative of subsonic transports to determine aerodynamic and operational effectiveness.

In the remainder of this presentation, I would like to discuss laminar flow work done by the Boeing Company under NASA contract and Company funded investigations.

- Technical advances/competitive pressures dictate continued effort
- Questions needing answers now
    - How much NLF aft of suction surface?
    - Operational reliability/maintainability?
    - Economics?
- It is time to address these issues

T-33 NATURAL LAMINAR FLOW FLIGHT TESTING

A Boeing-funded research program was undertaken to supplement the experiments conducted in the NASA sponsored LEFT program and to provide Boeing with experience in laminar flow flight testing. A series of tests were conducted in two sequential phases between 1984 and 1986 utilizing a T-33 jet trainer. The program had the following basic objectives:

Phase I. Testing of Baseline T-33 Wing (Smoothed) -1984

o Develop testing techniques and instrumentation for laminar flow flight research.
o Study the behavior of natural laminar flow on an unswept wing at high subsonic speeds (i.e. Mach numbers up to approx. 0.7 at altitudes up to 35,000 feet).

Phase II. Testing of a 20 Degree Swept NLF Glove-1985/86

o Verify NLF wing design philosophy.
o Verify transition prediction methods.
o Refine surface smoothness criteria.
o Perform in-flight measurements of extent of laminar flow and surface pressure distributions.
o Determine effects of selected surface protuberances (e.g. rivet heads, skin joints).

BOEING FUNDED TESTS (1984-86)
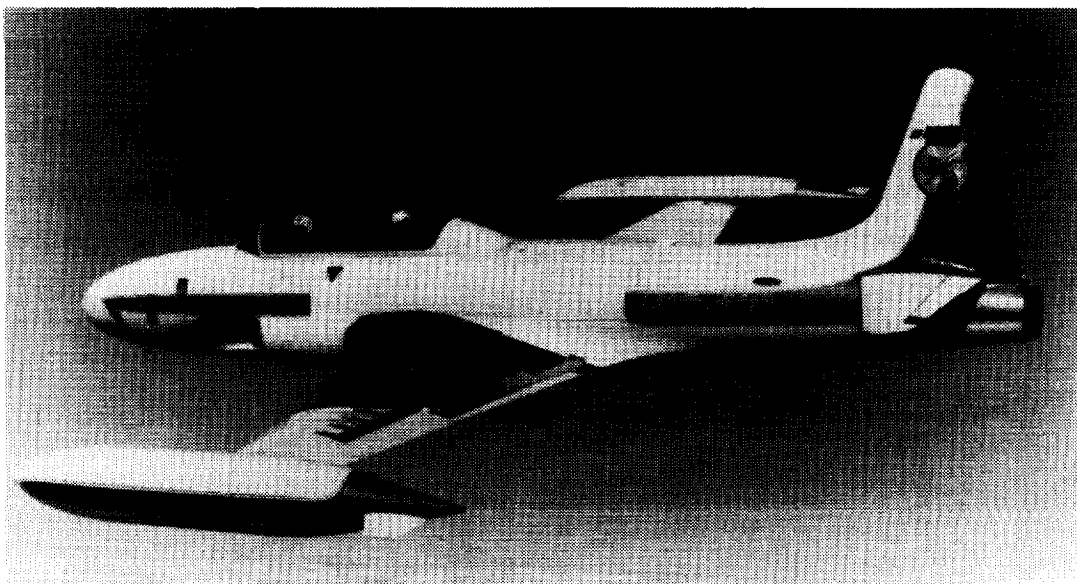
T-33 NATURAL LAMINAR FLOW FLIGHT TESTING
(cont'd)

The program was highly successful. It demonstrated the cost effectiveness of using a fairly small and relatively inexpensive airplane to acquire large quantities of very useful experimental data. In this manner, key decisions could be made prior to commitment to a more sophisticated and complex test program requiring a modern transport-sized airplane.

In almost all respects, the T-33 program met or exceeded its objectives. While the achieveable flight test envelope for an airplane like a T-33 is limited, the following observations were made:

Phase I. Basic (Smoothed) Wing

- Extensive natural laminar flow was present over the smoothed test section of the basic T-33 wing throughout a wide range of test conditions.
- A hot-film gage technique was found to be more informative and more reliable in detecting boundary layer transition than flow visualization using evaporative coatings or pressure sampling probes.

T-33 NATURAL LAMINAR FLOW FLIGHT TESTING
(conc.)

Phase II. Boeing Designed and Fabricated 20 Degree Sweep NLF Glove

o Extensive laminar flow (in excess of 40% chord on the upper surface at some test conditions) was achieved on both upper and lower surfaces of the glove.

o The extent of laminar flow was more sensitive to off-design conditions on the swept glove than on the basic (unswept) wing.

o Transition predictions based on stability theory (ref. 5) were verified reasonably well.

o Wing pressure distributions were predicted by three-dimensional transonic flow theory.

o Critical rivet heights in the region of the wing leading edge are dependent on unit Reynolds number, location and pressure distribution.

o Transition indication by liquid crystal coatings (as shown in the figure and described in ref. 6) was demonstrated. While highly promising as an in-flight flow visualization technique, the success of the method is sensitive to a number of variables and requires further development.

T-33 WITH NLF GLOVE
FALL 1986

ORIGINAL PAGE IS
OF POOR QUALITY
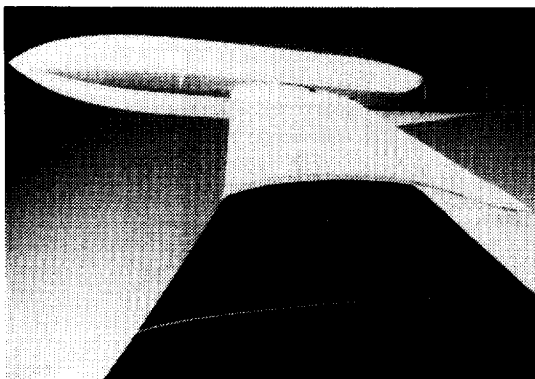
MACH NO. = 0.61
20,000 ft
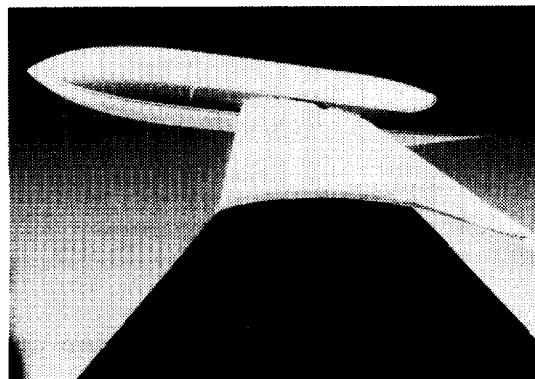
MACH NO. = 0.65
20,000 ft

LAMINAR FLOW AIRFOIL TEST (1977-78)

While the T-33 flight experiments just described are among the latest Boeing Company efforts in laminar flow research, the company has been involved in exploring the basic issues for many years. As an example, an important test series, jointly funded by Boeing and NASA, was conducted in 1977-78 in the Boeing Research Wind Tunnel (BRWT). The large scale 30° swept airfoil model developed for these test is shown in the figure. The airfoil section was specially designed to provide an upper surface pressure distribution in the presence of the wind tunnel walls that is typical of a laminar flow airplane's outboard wing at cruise conditions (M=0.8, C_L=0.5). Provision was made for slot suction over the first 30% of the chord on the upper surface and 15% of chord on the lower surface.

The principal aims of these tests (ref. 7) were to demonstrate that the suction system would function properly, to establish the required suction distribution for maximum efficiency and to explore the sensitivity to changes in suction intensity. Subsequent testing was performed to explore the sensitivity of the LFC system to various disturbance effects such as surface imperfections, off-design operating conditions and tunnel noise.

These tests gave us considerable confidence in our design and analysis tools and provided needed experience with a variety of techniques for monitoring and diagnosing the state of a boundary layer. Additional wind tunnel tests under contract to NASA are planned.

- Boeing IR&D and NASA contract
- 20-ft chord model
- Model tailored for free air pressure distribution

PLAN VIEW

FLOW ▷ — ADJUSTABLE FLAP

|— 20 ft —|

SIDE VIEW

FLOW ▷ SWEEP 30 deg — REGION OF UNDISTURBED FLOW

— SLOTTED TEST SURFACE

$V_{MAX} \approx$ 215 ft/s
$R_{e_{max}} \approx$ 25 x 10^6
TURBULENCE LEVEL: t ≈ 0.15%
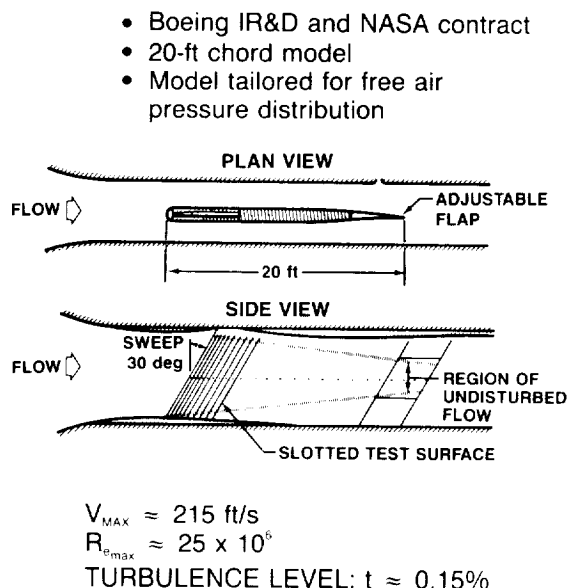
MODEL IN BOEING RESEARCH WIND TUNNEL

ORIGINAL PAGE
BLACK AND WHITE PHOTOGRAPH
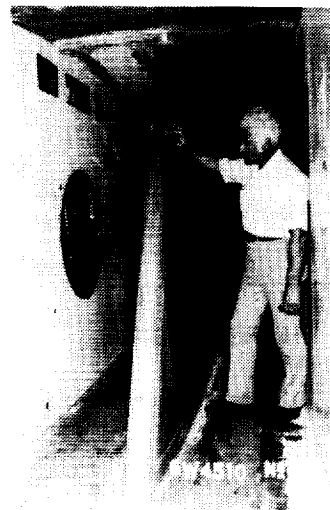
F-14 VSTFE PROGRAM SUPPORT

The F-14 Variable Sweep Test Flight Experiment (VSTFE) program is the latest in an important NASA-funded sequence of experiments with variable sweep aircraft to systematically explore the important effect of wing sweep on boundary-layer stability and transition - an effect not sufficiently understood when the X-21 program began. Boeing participation in these later programs has been continuous, with emphasis on developing and refining the computer-based capability to analyze and predict three-dimensional boundary-layer stability characteristics over a wide range of wing geometries and flight conditions. Details of the most recent work on this fundamentally important enabling technology for laminar flow are described in the paper by Rozendaal (ref. 5).

NASA CONTRACTS 1984-87

39
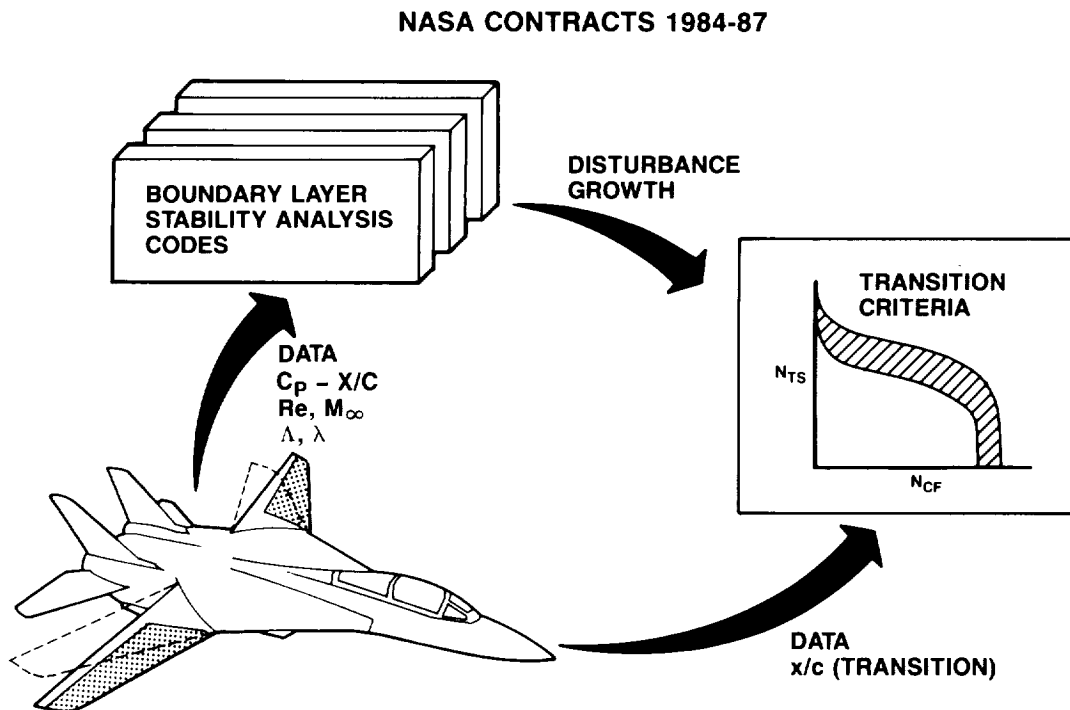
BOEING 757 NLF GLOVE

These tests of a Boeing designed and fabricated NLF glove were performed during 1985 under NASA contract. A fundamental objective was to determine possible adverse effects of engine noise impingement on an NLF surface under realistic operational conditions. The results of the tests are described in detail in ref. 8.

The important result of these experiments has been the demonstration that engine noise effects are limited to the under-surface of the wing. This opens a configuration option of major significance in a range of possible future hybrid laminar flow applications.

- **FLIGHT TESTS 1985**
- **NASA CONTRACT**

ORIGINAL PAGE IS
OE POOR QUALITY

ORIGINAL PAGE
BLACK AND WHITE PHOTOGRAPH

KRUEGER FLAP/INSECT SHIELD DESIGN AND TEST

Two important concerns in deriving a practical laminar flow airplane system are the provision for an adequate high-lift system and a means of protecting the relevant aerodynamic surfaces from insect contamination during low altitude operations. As part of our recent laminar flow efforts, the design and validation of an appropriate leading-edge high-lift device/insect shield was undertaken. The objectives of this work were to:

- o Develop a shielding device that would protect a wing upper surface from insect contamination during ground roll, take-off, initial climb and landing approach.
- o Develop such a leading-edge shielding device that also produces high-lift performance equivalent to existing slat/Krueger flap devices used on our present product line.
- o Develop computational and experimental techniques for design and validation of such a leading-edge device.

KRUEGER FLAP/INSECT SHIELD DESIGN AND TEST
(conc.)

This work during 1986 involved design of a "foldable bullnose" Krueger leading-edge flap, development of a computer code capable of predicting insect trajectories within the flow field associated with a multi-element airfoil, and the conduct of a wind tunnel test in the Boeing Research Wind Tunnel. Typical results are shown in the figure. The conclusions drawn from this work include:

o   A practical leading-edge device, which is both an adequate insect shield and high-lift device, can be developed.

o   Such a Krueger device is mechanically compatible with existing transport wings with slat-type leading-edge devices.

o   High-lift performance need not be seriously compromised in providing adequate insect shielding.

o   Experimental techniques (e.g. means of injecting live insects into a wind tunnel test section) now exist to allow experimental validation of insect impact predictions.

- BOEING IR&D

LOW ANGLE OF ATTACK (α = 0 deg)
LARGE INSECTS

HIGH ANGLE OF ATTACK (α = 8 deg)
SMALL INSECTS

CALCULATED TRAJECTORIES
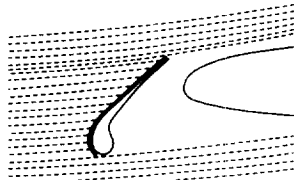
INSECT IMPACTS
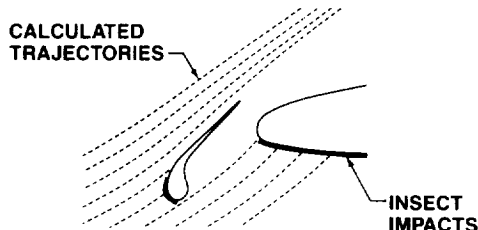
BOEING 5-ft by 8-ft RESEARCH WIND TUNNEL
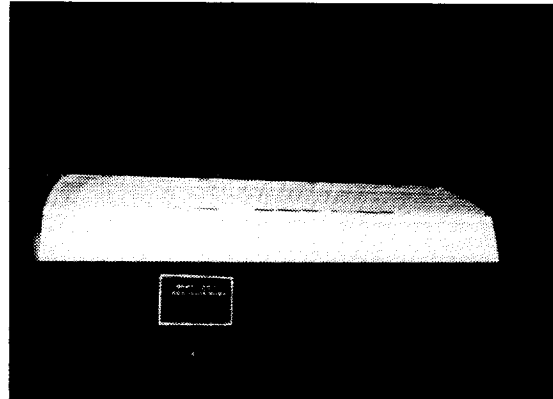
KRUEGER FLAP/INSECT SHIELD
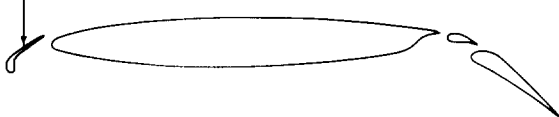
- Krueger is an effective insect shield
- Foldable bullnose type Krueger has good high-lift performance

LAMINAR FLOW - THE CHALLENGE

As shown in the figure, the development in laminar flow has been systematic and the results obtained are impressive.

Based on the enormous amount of laminar flow work to be reported in this Symposium it is clear that the technical community is making progress toward establishing technical feasibility. Our next research challenge is the attainment of the predicted extents of laminar flow on an HLFC aircraft with the characteristics of a modern transport.
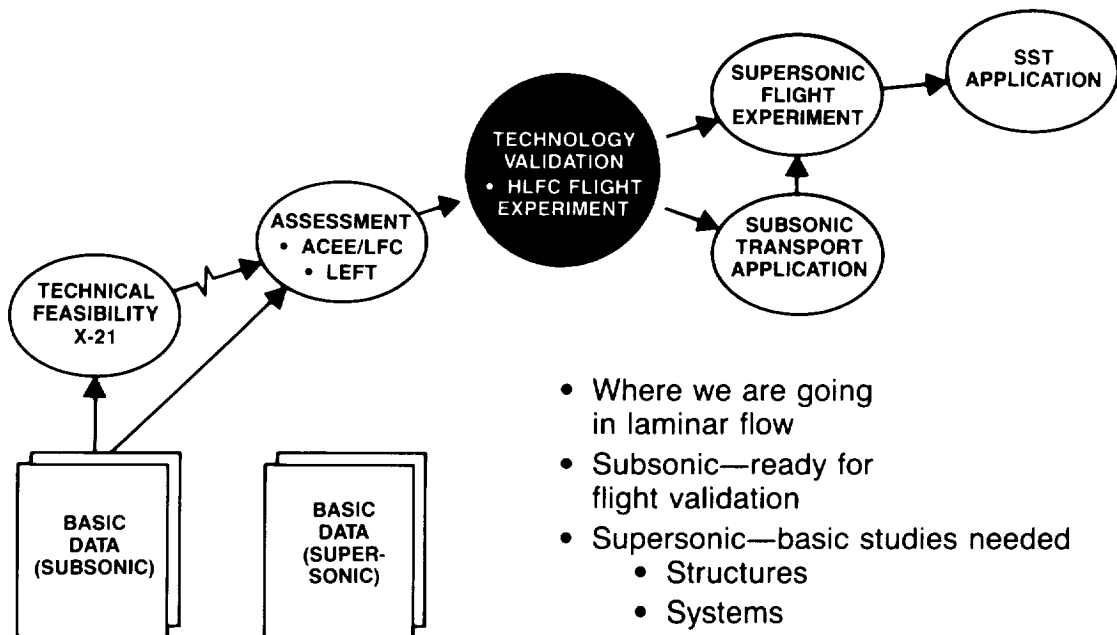
- Where we are going in laminar flow
- Subsonic—ready for flight validation
- Supersonic—basic studies needed
  - Structures
  - Systems

ACKNOWLEDGMENT

REFERENCES

1. Beckwith, I. E., "Development of High Reynolds Number Quiet Tunnel for Transition Research", AIAA Journal, Vol 13, No. 3, March 1975, pp. 300-6.

2. Pfenninger, W., "USAF and Navy Sponsored Northrop LFC Research Between 1949 and 1967", in "Workshop on Laminar Flow Control", compiled by C. T. D'Aiutolo, NASA-Langley Research Center, April 6-7, 1976, pp. 14-50.

3. Montle, L. K. and Steiner, J. E., "Post World War II Commercial Transport Design History", presented at AIAA Aircraft Systems and Technology Meeting, Dayton, Ohio, August 11, 1981.

4. Kitowski, J. V., "USAF Review of the X-21A Program", in "Workshop on Laminar Flow Control" compiled by C. T. D'Aiutolo, NASA-Langley Research Center, April 6-7, 1976, pp. 239-73.

5. Rozendaal, R. A., "VSTFE-Stability Code Development and Clean-Up Glove Data Analysis", Symposium on Natural Laminar Flow Control Research, NASA-Langley Research Center, NASA CP 2487, March 16-19, 1987, pp. 845-859.

6. Holmes, B. J., Croom, C. C., Gall, P. D. Manuel, G. S., and Carraway, D. L., "Advanced Transition Measurement Methods for Flight Applications", AIAA-86-9786, Las Vegas, NV, April 2-4, 1986.

7. BCAC Preliminary Design Department, "Evaluation of Laminar Flow Control System Concepts for Subsonic Commercial Transport Aircraft", NASA CR 158976, December, 1978.

8. Runyan, L. J., Bielak, G. W., Behbehani, R., Chen, A. W., and Rozendaal, R. A., "757 NLF Glove Flight Test Results", Symposium on Natural Laminar Flow and Laminar Flow Control Research, NASA-Langley Research Center, NASA CP 2487, March 16-19, 1987, pp. 795-818.

LFC - A MATURING CONCEPT*

John Morris
Douglas Aircraft Company
McDonnell-Douglas Corporation
Long Beach, California

INTRODUCTION

The existence of both turbulent and laminar flows has been known for a long time, but it was not until the middle of the last century that the first systematic tests with fluids were conducted to establish the physical relationships and governing laws. The importance of turbulent and laminar airflows in aeronautics was recognized as early as the 1930s, but actual laminar flow control (LFC) investigations were not undertaken seriously until the 1940s.

This overview briefly touches on some of the historical developments of LFC leading up to current activities. It then examines the technical problems being addressed and potential long-term LFC applications. Past and current Douglas activities are examined and the required future testing involving hybrid laminar flow control (HLFC) is discussed (Figure 1).

---

1. HISTORICAL DEVELOPMENT OF LFC

2. TECHNICAL PROBLEMS ADDRESSED

3. POTENTIAL LONG-TERM APPLICATION

4. DOUGLAS PAST AND CURRENT ACTIVITIES

5. REQUIRED FUTURE TESTING: HLFC

FIGURE 1. LFC OVERVIEW

There are three principal laminarization technologies for aircraft:

1. Natural laminar flow (NLF) for moderately swept wings (generally less than 21 degrees) relying on a favorable pressure gradient. This concept is most suitable for general aviation aircraft.

2. Suction laminar flow control (LFC), which can laminarize highly swept wings with significant cross-flow and attachment line instabilities, and with adverse pressure gradients. The total potential for LFC includes wings, tails, nacelles, and "clean" regions of fuselages.

3. Hybrid LFC (HLFC), which is based on suction LFC from leading edge to front spar and natural laminar flow aft of the spar. This is the simplest and most economical suction LFC application (Figure 2).

NATURAL LAMINAR FLOW (NLF)
- MODERATELY SWEPT WINGS, ⊿ 21 DEGREES
- FAVORABLE PRESSURE GRADIENT
- SUITABLE FOR GENERAL AVIATION

SUCTION LAMINAR FLOW CONTROL (LFC)
- CAN LAMINARIZE HIGHLY SWEPT WINGS WITH CROSS-FLOW AND ATTACHMENT LINE INSTABILITIES AND ADVERSE PRESSURE GRADIENTS
- POTENTIAL FOR MAXIMUM LAMINARIZATION OF WINGS, TAILS. NACELLES, AND "CLEAN" REGIONS OF BODIES

HYBRID LFC (HLFC)
- SUCTION LFC FROM LEADING EDGE TO FRONT SPAR
- NATURAL LAMINAR FLOW AFT OF SUCTION REGION
- SIMPLEST/MOST ECONOMICAL SUCTION LFC APPLICATION

FIGURE 2. PRINCIPAL LAMINARIZATION TECHNOLOGIES FOR AIRCRAFT

HISTORICAL DEVELOPMENT OF LFC

The initial suction LFC investigations (Figure 3) were conducted in the 1940s by the British, Germans, and Swiss in Europe and by NACA in the United States. During the next decade, Northrop and the U.S Air Force developed and tested a slotted LFC glove concept on an F-94 aircraft. At Mississippi State University, experiments were conducted using a glider with a fabric wing and pricked perforations. Finally, at the RAE in Great Britain, a de Haviland Vampire (Figure 4) was equipped with a coarse perforated glove and flown extensively. This was followed in the 1960s by the most ambitious program undertaken until then — the X-21 (Figure 5). A Northrop/USAF project, the X-21 was a derivative of the B-66 with a new wing featuring suction slots on both upper and lower surfaces. One pod under each wing housed the compressors for the suction systems.

The experience from these different development efforts was largely encouraging, but much work still remained until a truly practical solution would emerge. Laminar flow was achieved over major portions of the X-21 wing, but difficulties were experienced, in particular with the more demanding inboard sections close to the fuselage.

One objective of this LFC testing was to improve the range capability of military aircraft at a time when jet engines still displayed poor fuel efficiency. However, at that time the bypass engines began to emerge and the interest in LFC faded,
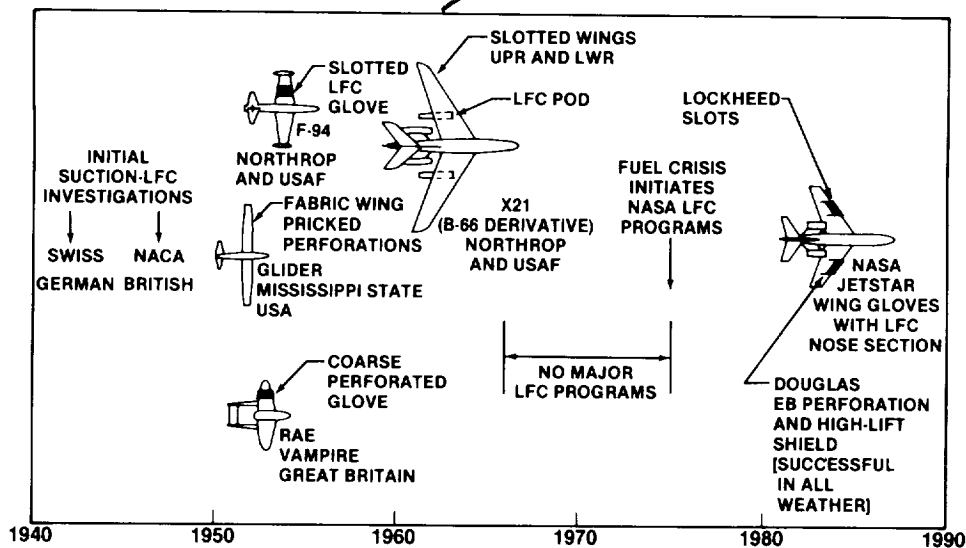
FIGURE 3. SUCTION-LFC FLIGHT TEST PROGRAMS
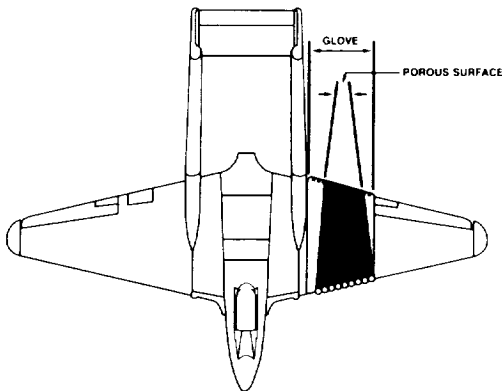
FIGURE 4. DE HAVILLAND VAMPIRE EQUIPPED WITH
COARSE PERFORATED GLOVE
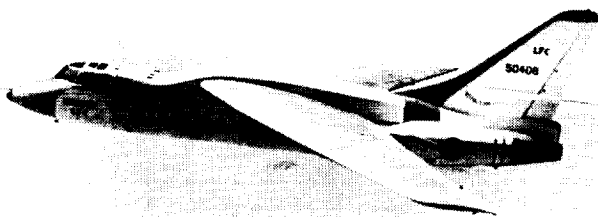
FIGURE 5. X-21 LFC TEST PLANE

remaining low for approximately a decade until the fuel crisis struck the industry and NASA initiated LFC programs in the mid-1970s.

The current NASA Jetstar program has been highly successful, yielding invaluable experience with two different approaches: the Douglas electron-beam-perforated approach on one wing and the Lockheed slot system on the other. The Douglas system will be discussed later in this paper.

TECHNICAL PROBLEMS AND SOLUTIONS FOR LFC

A number of practical technical problems have been identified, and the required solutions have been developed by industry and tested in flight by NASA (Figure 6). The solution to the leading edge problems of contamination and/or icing is clearly the retractable shield in combination with liquid efflux.

Wing sweep created the problems of attach line instability and cross-flow instability. The successful solution here is distributed suction with perforations that are not sensitive to the flow direction.

Other problems are related to surface characteristics such as roughness, steps, gaps, and variances. The solutions here involve close-tolerance external jig control or accurate mold surfaces, and the avoidance of surface joints or slots that can cause discontinuities.

Finally, there are potential problems with the suction involving boundary layer disturbance and clogging. The solutions have been provided by the electron beam (EB) technology,

PROBLEMS	SOLUTIONS
LE: CONTAMINATION ICING	RETRACTABLE SHIELD LIQUID EFFLUX
SWEEP: ATTACH LINE INSTABILITY CROSS-FLOW	DISTRIBUTED SUCTION WITH PERFORATIONS
SURFACE: ROUGHNESS STEPS GAPS WAVINESS	EXTERNAL JIG CONTROL ACCURATE MOLD SURFACES CONTINUOUS SURFACES
SUCTION: BOUNDARY LAYER DISTURBANCE CLOGGING	FINE PERFORATIONS TAPERED PERFORATIONS EB TECHNOLOGY

FIGURE 6. TECHNICAL PROBLEMS AND SOLUTIONS
FOR LFC

which generates extremely fine perforations of the desired high density and tapers these perforations to prevent clogging.

POTENTIAL LONG-TERM APPLICATION OF LFC

The potential long-term applications of LFC are substantial (Figure 7). However, additional testing must be done before LFC can be applied with confidence on production airplanes. The initial application will center around the hybrid laminar flow control (HLFC) solution, which promises a drag reduction of about 10 percent. Further gains are possible by using suction in other regions of the wing, the horizontal and vertical tails, the nacelles, and certain "clean" regions of the fuselage. Total drag improvements could then eventually reach as much as 25 percent, with the actual levels depending on the extent of complexity justified by future fuel costs for optimum economics.
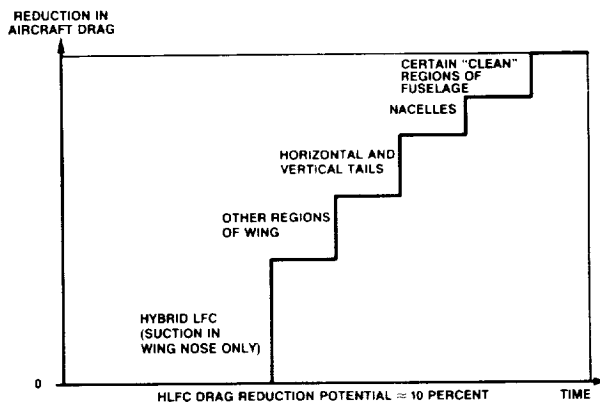
FIGURE 7. POTENTIAL LONG-TERM APPLICATION OF LFC

PAST AND CURRENT DOUGLAS ACTIVITIES

Three major developments that resulted from past Douglas LFC efforts are listed in Figure 8 and will be discussed in detail later. These developments have been instrumental in helping to correct some of the shortcomings encountered in the early LFC tests, both in Europe and the U.S. In particular, as shown in Figure 9, the previous LFC suction surfaces left much to be desired. Slotted surfaces involved difficult and costly machining, and surface deformation frequently occurred as the slots released locked-in stresses. Furthermore, spanwise flow along the attachment line, including fuselage boundary layer contamination, could not be controlled using spanwise suction slots. A porous surface offers a better solution since it is not sensitive to the flow direction, which changes rapidly in the leading edge region.

ELECTRON-BEAM-PERFORATED SUCTION SURFACE

SIMPLIFIED LFC SUCTION PANEL

RETRACTABLE HIGH-LIFT SHIELD

FIGURE 8. LFC TECHNOLOGY DEVELOPMENTS AT DOUGLAS

The earlier porous surface obtained through the sintering process was easily clogged. It was poor structurally and multiple sintered inserts resulted in inadequate joint smoothness. Other perforation techniques available at the time resulted in holes that were too large, and mechanical drilling proved to be prohibitively expensive.

SLOTTED SURFACES
- MACHINING DIFFICULT AND COSTLY
- SURFACE DEFORMATIONS AFTER SLOTTING
- ATTACHMENT LINE INSTABILITY } SPANWISE
- FUSELAGE BOUNDARY LAYER CONTAMINATION } FLOW

POROUS SURFACES
- SINTERED
  - CLOGGING
  - POOR STRUCTURALLY
  - JOINT SMOOTHNESS

- PERFORATED
  - PRACTICAL HOLES TOO LARGE
  - MECHANICAL DRILLING TOO EXPENSIVE

FIGURE 9. PREVIOUS PROBLEMS WITH LFC SUCTION SURFACES

Douglas selected EB-perforated titanium for LFC suction surfaces, as shown in Figure 10. This process economically produces sufficiently fine tapered perforations with satisfactory accuracy and consistency. The outstanding characteristics of this approach are listed in Figure 11. Foremost are high wing strength and stiffness, both in bending and torsion with uniform porosity unaffected under load. Furthermore, the panel is corrosion- and damage-resistant and can be readily repaired. Any local reduction in porosity following repair will not cause a loss of LFC. Finally, the external airflow direction is not critical. A number of large LFC panel structural test specimens with EB-perforated surfaces have been built and successfully tested (Figure 12). The panel strength and strain characteristics exceeded those required for wing panels of either aluminum or carbon composite construction.

Initially, Douglas visualized the entire upper wing surface under LFC suction with an arrangement as shown in Figure 13. The integral suction flow channels in the panel that lead to the wing flow channels and spanwise ducts are clearly visible. Also shown is the retracted leading edge high-lift
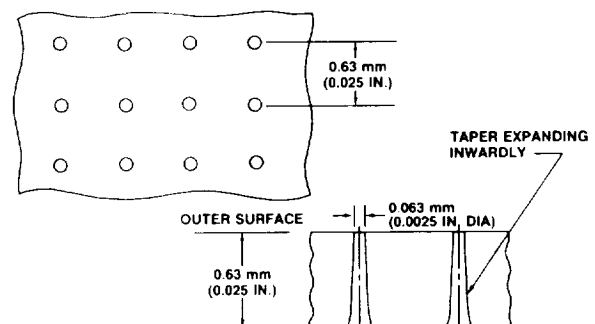
FIGURE 10. SUCTION SURFACE ELECTRON-BEAM-PERFORATED TITANIUM

HIGH STRENGTH - CONTRIBUTES TO WING STRENGTH AND STIFFNESS IN BENDING AND TORSION

POROSITY UNIFORM - UNAFFECTED BY STRESS/STRAIN

DOES NOT CLOG - SELF-CLEARING BECAUSE OF TAPERED HOLES
- SIMPLE STEAM CLEANING EFFECTIVE

CORROSION-RESISTANT

DAMAGE-RESISTANT - REPAIR PRACTICAL

EXTERNAL AIRFLOW DIRECTION NOT CRITICAL

FIGURE 11. ELECTRON-BEAM-PERFORATED TITANIUM CHARACTERISTICS
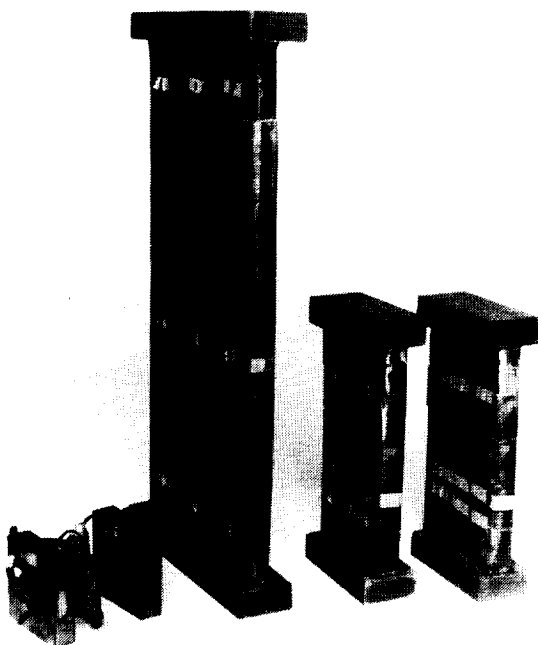
FIGURE 12. LFC PANEL STRUCTURAL TEST SPECIMENS

ELECTRON-BEAM-PERFORATED TITANIUM SURFACE

SUCTION FLOW CHANNELS OVER MAIN WING BOX

RETRACTABLE HIGH-LIFT SHIELD
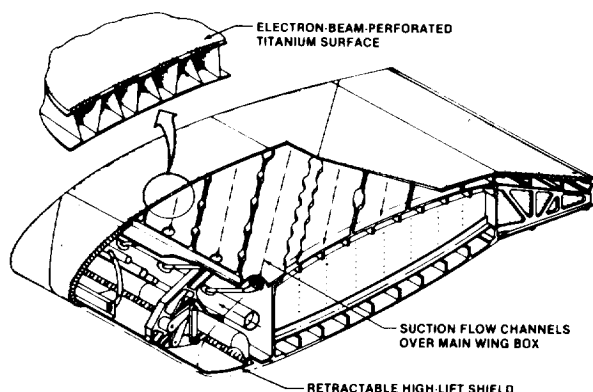
FIGURE 13. DOUGLAS/NASA POROUS-UPPER-SURFACE LFC CONCEPT

device, which acts as a shield to prevent surface contamination at low altitudes, particularly during takeoff, approach, and landing.

While analyzing this concept, it became clear that there are many advantages in laminarizing only the upper wing surface (Figure 14). LFC is used most effectively on that surface, which causes two-thirds of the total wing skin friction, particularly with an efficient wing that cruises at a high-lift coefficient. This is possible with the high-lift shield that allows the use of a smaller wing, thereby eliminating any sizing penalty relative to an advanced turbulent wing, which obviously would have a leading edge device. Other benefits are easy access to wing systems; a simpler, less expensive suction system; and lower maintenance cost.

TWO-THIRDS OF TOTAL SKIN FRICTION ON UPPER SURFACE (LFC USED MORE EFFECTIVELY)

ALLOWS USE OF RETRACTABLE HIGH-LIFT SHIELD (SMALLER WING WITH HIGHER C_{LMAX} + CONTAMINATION AVOIDANCE)

NO SIZING PENALTY RELATIVE TO ADVANCED TURBULENT WING

LAMINAR SURFACE NOT EXPOSED TO FOD

ALLOWS NORMAL ACCESS TO WING SYSTEMS

SIMPLER SYSTEM WITH LOWER COST

LESS SUCTION POWER REQUIRED

LOWER MAINTENANCE COST

FIGURE 14. ADVANTAGES OF LAMINARIZING UPPER WING SURFACE ONLY

The large LFC high-speed wind tunnel panels shown in Figure 15 were manfactured by Douglas. They have been installed on the swept-wing model now being tested by NASA in the 8-foot tunnel at Langley.

Douglas participated in the extensive NASA Jetstar flight test program (Figure 16). The objective was to demonstrate the effectiveness of LFC leading edge systems under representative flight conditions. The starboard wing was equipped with the Douglas EB-perforated wing panel (Figure 17) and related equipment and systems, while the port wing carried corresponding installations using the Lockheed slot system. The Douglas concept is illustrated in Figure 18, which shows the suction panel and the small retractable shield with its de-icing system and supplementary fluid spray nozzles. In addition to the LFC leading edge system performance, the contamination avoidance system was tested in simulated airline service operations. These tests were conducted from three different bases (Figure 19) into a variety of airports to obtain a representative cross section of operational conditions with regard to climate, environment, and seasonal fluctuation.

The small leading edge shield was found to provide very effective protection against the kind of insect contamination that can be encountered at lower altitudes. The results from one particular flight without use of the liquid system, are shown in Figure 20. The contrast to the unprotected left wing is striking.

49
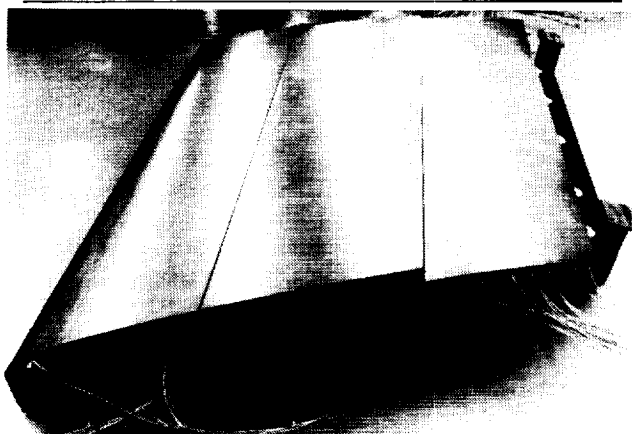
FIGURE 15. LFC HIGH-SPEED WIND TUNNEL PANELS

OBJECTIVE
- DEMONSTRATE BY FLIGHT RESEARCH THE EFFECTIVENESS OF LFC LEADING EDGE SYSTEMS UNDER REPRESENTATIVE FLIGHT CONDITIONS

FLIGHT TEST PROGRAM
- LFC LEADING EDGE SYSTEM PERFORMANCE
- CONTAMINATION AVOIDANCE SYSTEMS PERFORMANCE
- SIMULATED AIRLINE SERVICE OPERATIONS

FIGURE 16. LFC JETSTAR FLIGHT TEST PROGRAM
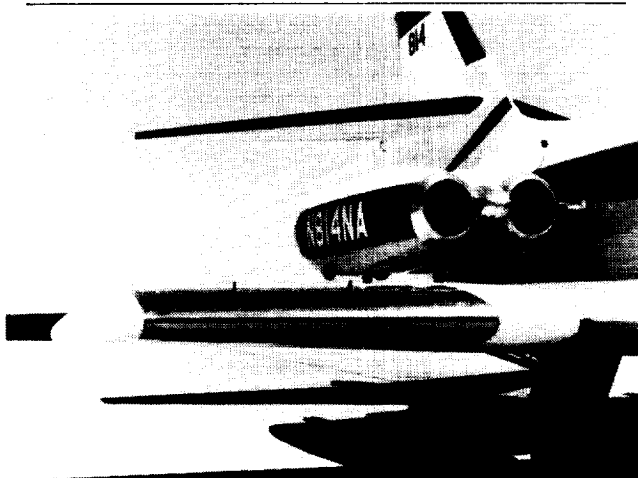
FIGURE 17. LAMINAR FLOW CONTROL
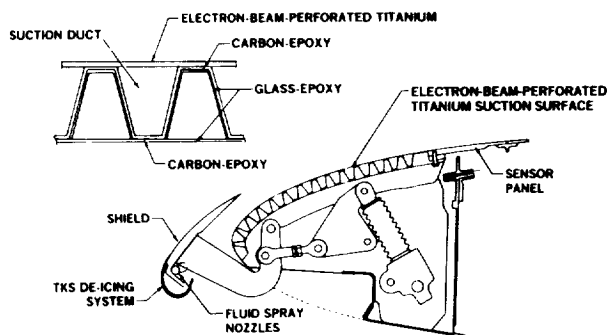
FIGURE 18. DOUGLAS TEST ARTICLE

HOME BASE	DATE
☐ ATLANTA	JULY 85
☐ PITTSBURGH	SEPTEMBER 85
☐ CLEVELAND	FEBRUARY 86

59 FLIGHTS TO 45 AIRPORTS
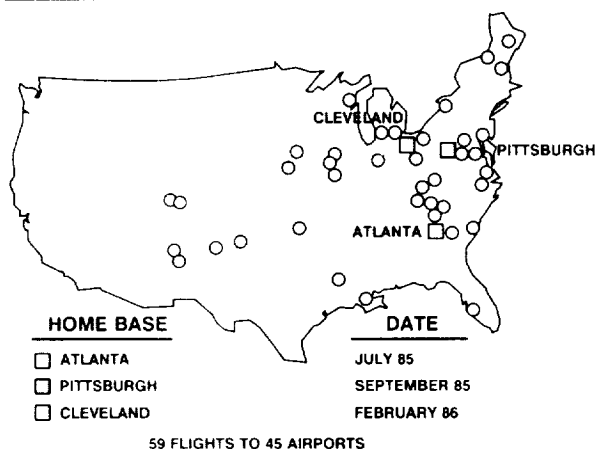
FIGURE 19. SIMULATED SERVICE FLIGHT TESTS
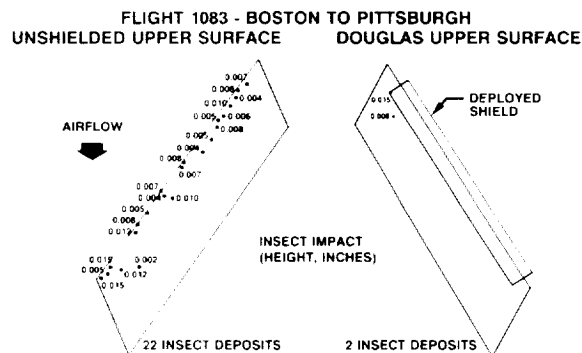
FIGURE 20. INSECT CONTAMINATION ON JETSTAR DURING DESCENT

Other aspects of airline service simulation involved overnight accumulation of ice and snow on the wings (Figure 21) with subsequent removal through normal glycol spraying before flight (Figure 22), which proved entirely adequate for subsequent LFC operation.

In summary, the performance of the Douglas LFC system during 3 years of flight testing has been excellent (Figure 23). LFC was achieved on the initial test flight. LFC was lost only during flights through ice crystals, but was immediately restored when clear air was reached. Overall, LFC was reliably obtained throughout simulated airline service flying that reflected a wide variety of winter and summer conditions, including ice, snow, heavy rain, and airborne insect infestation. No surface maintenance has been needed, and there has been no deterioration of the LFC panel or its performance during the 3 years of flight testing.

REQUIRED FUTURE TESTING: HLFC

A simpler approach to achieving LFC on swept wings is currently under investigation. In this approach, suction is used only in the leading edge region to counteract attachment line and cross-flow instabilities, and a favorable pressure gradient

50
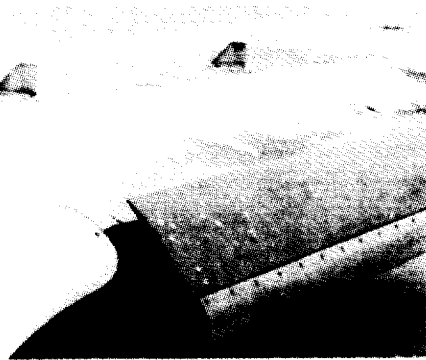
FIGURE 21. OVERNIGHT ACCUMULATION OF ICE AND SNOW
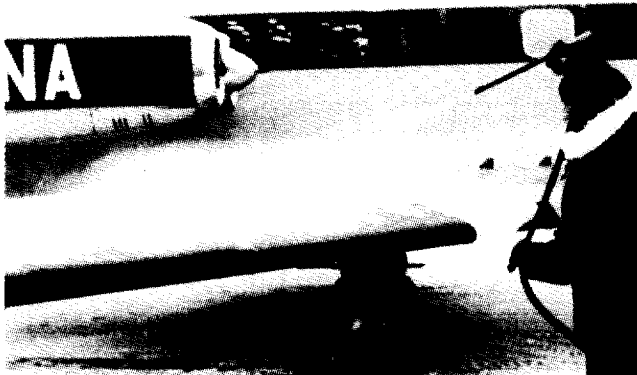
FIGURE 22. GLYCOL SPRAYING BEFORE FLIGHT

LFC ACHIEVED ON INITIAL TEST FLIGHT

LFC RECOVERED IMMEDIATELY FOLLOWING FLIGHT THROUGH ICE CRYSTALS

LFC OBTAINED RELIABLY THROUGHOUT SIMULATED AIRLINE SERVICE FLYING - 59 FLIGHTS/45 AIRPORTS

- SUMMER:
  - AIRBORNE INSECT INFESTATION
  - HEAVY RAIN STORMS

- WINTER:
  - OVERNIGHT EXPOSURE TO ICE AND SNOW
  - IN-FLIGHT ICING CONDITIONS

NO DETERIORATION OF LFC POROUS SURFACE OR PERFORMANCE IN 3 YEARS OF FLIGHT TESTING

FIGURE 23. PERFORMANCE OF DOUGLAS LFC LEADING EDGE DURING JETSTAR FLIGHT TESTS

is used further aft to maintain laminar flow over the main wing box region (Figure 24).

This concept, known as hybrid laminar flow control (HLFC), offers many advantages (Figure 25). These include reduced suction power requirements, simplification of the suction system, uncompromised wing structural efficiency and fuel volume, and reduced initial cost and maintenance requirements. This concept needs to be tested in flight.

OBJECTIVE - ECONOMICAL LFC WITH EFFICIENT STRUCTURE
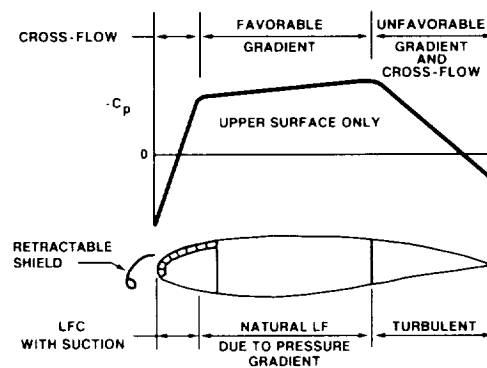
FIGURE 24. HYBRID LAMINAR FLOW CONTROL (HLFC)

SIMPLEST PRACTICAL LFC SYSTEM

LESS SUCTION POWER REQUIRED

WING BOX STRUCTURE AND FUEL TANK UNAFFECTED

LOWER INITIAL COST

LOW INVESTMENT RISK
- SAME AIRFOIL SECTION AS TURBULENT DESIGN

REDUCED MAINTENANCE COST

FIGURE 25. ADVANTAGES OF HLFC

The objectives of such full-scale testing are numerous. Apart from demonstrating the basic HLFC concept at an appropriate Mach number and Reynolds number, environmental effects and off-design flight performance can be investigated. The results of this program, if successful, can reduce design risks in making future industry applications.

DOUGLAS LFC PROGRAM SUMMARY

The electron-beam-perforated suction surface and its simplified suction ducting has been shown to provide reliable leading edge LFC in flight, and the high-lift shield effectively protects the LFC surface from contamination.

The development of needed technology for a practical and reliable LFC system is thus already well advanced. However, HLFC is so far an unproven concept, and full-scale flight testing is clearly needed to further advance the state of the art (Figure 26).

EB-PERFORATED SUCTION SURFACE IS PROVIDING RELIABLE LFC ON LEADING EDGE IN FLIGHT

HIGH-LIFT SHIELD IS PROTECTING LFC SURFACE EFFECTIVELY

DEVELOPMENT OF TECHNOLOGY NEEDED FOR A PRACTICAL AND RELIABLE LFC SYSTEM IS ALREADY WELL ADVANCED

HLFC IS AN UNPROVEN CONCEPT THAT NEEDS TO BE TESTED

FIGURE 26. DOUGLAS LFC PROGRAM SUMMARY

|

LOCKHEED LAMINAR-FLOW CONTROL SYSTEMS DEVELOPMENT AND APPLICATIONS

Roy H. Lange
Lockheed-Georgia Company
Marietta, GA

ABSTRACT

This paper summarizes progress at the Lockheed-Georgia Company from 1974 to the present in the practical application of laminar-flow control (LFC) to subsonic transport aircraft. Those efforts include preliminary design system studies of commercial and military transports and experimental investigations leading to the development of the leading-edge flight test article installed on the NASA JetStar flight test aircraft. The benefits of LFC on drag, fuel efficiency, lift-to-drag ratio, and operating costs are compared with those for turbulent flow aircraft. The current activities in the NASA Industry Laminar-Flow Enabling Technologies Development contract include summaries of activities in the Task 1 development of a slotted-surface structural concept using advanced aluminum materials and the Task 2 preliminary conceptual design study of global-range military HLFC transports. The final section in the paper addresses the need for an experimental flight program on a swept wing aircraft with hybrid laminar-flow control (HLFC) to obtain data at high Reynolds numbers and at Mach numbers representative of long-range subsonic transport aircraft operation.

INTRODUCTION

Among the many concepts for aircraft drag reduction, laminar-flow control (LFC) has indicated the greatest potential for skin-friction drag reduction. A review of early progress since 1939 in analytical and experimental investigations of boundary-layer transition and methods for achievement of laminar flow is contained in a paper by Braslow and Muraca (ref. 1). The achievement of laminar-flow control in flight was obtained by the British on Vampire aircraft in 1951-1955 and the U.S. Air Force/ Northrop tests on the F-94 and X-21 in the mid 1950's and early 1960's. The X-21 program was a significant milestone not only for the extensive regions of laminar flow obtained in flight at chord Reynolds numbers up to 40 million but also for the LFC design criteria established and validated and crossflow instabilities identified due to wing sweepback (refs. 2-5). The premature termination of the X-21 program prevented the accumulation of the desired data base on service experience for an operational aircraft, and thus the economics and day-by-day reliability of an LFC aircraft still remain uncertain.

The Lockheed motivation in LFC activities has been directed to the eventual application to long-range or long-endurance military strategic aircraft systems. Early work includes the application of LFC by Lockheed and Northrop in 1962 on the C-141 aircraft and in 1966 on the C-5A (ref. 6). However, little further work was done on LFC until the effects of the fuel crisis in 1973 directed attention to the use of advanced technologies for improved fuel efficiency. Another significant milestone occurred when LFC was reactivated as one of the elements in the NASA Aircraft Energy Efficiency, ACEE, program in 1976 (refs. 7-9) and is continuing to the present.

This paper summarizes progress at the Lockheed-Georgia Company from 1974 to the present in the practical application of LFC to subsonic transport aircraft. These efforts include preliminary system design studies, airfoil development, boundary-layer analyses, integrated structural design, the suction system, manufacturing methods, and a final integrated aircraft configuration. Experimental investigations include wind tunnel tests, low-speed flight tests, and tests of structural specimens. The benefits of LFC on drag, fuel efficiency, and operating costs are compared with current as well as a counterpart advanced technology turbulent transport. The

development of the leading-edge flight test article installed on the NASA JetStar flight test aircraft is discussed. A review of the above activities since 1974 is given in an AIAA paper by Lange (ref. 10). The current efforts in the NASA Laminar-Flow Enabling Technologies Development contract include summaries of activities in the Task 1 development of a slotted-surface structural concept using advanced aluminum materials and the Task 2 preliminary conceptual design study of global-range military HLFC transports. The paper also addresses the need for a flight experimental program on a swept wing aircraft with HLFC to obtain data at high Reynolds numbers and at Mach numbers representative of long-range subsonic transport aircraft operation.

LFC PROGRAM HISTORY

NASA, in concert with industry, has been sponsoring LFC technology development activities for the past 11 years to achieve LFC technology readiness in the 1990's. NASA/Lockheed LFC contract efforts presented in Figures 1 and 2 cover a time span from 1974 to mid 1986. These charts are provided as background material and only the highlights will be discussed in this paper. The reader is provided with references to these activities for more details. Lockheed Independent Research and Development is identified in these figures and these activities have been devoted primarily to preliminary system design studies of large payload, long-range military airlift aircraft. As shown in Figure 1, Lockheed performed the initial feasibility study of advanced technology LFC aircraft beginning in October 1974. The favorable results of this initial study provided the impetus to additional investigations of LFC outer skin panels (ref. 11), a JetStar leading-edge flap modification (ref. 12), a study of cruise noise/LFC noise criteria, and the evaluation of LFC system concepts (refs. 13-15).

On April 6-7, 1976, the NASA-Langley Research Center conducted a Workshop on Laminar-Flow Control. The program was arranged as a forum for informal papers and discussions on LFC experience from government and industry. Included in the discussions were the effects of advances in technology on the performance and costs of LFC, the outlook for LFC as perceived by government and industry, and critical concerns and possible solutions. One result of the Workshop was additional contacts by Lockheed with airlines and other aircraft operators relative to LFC transport aircraft. A concensus of industry and airline concerns on LFC was obtained. Three major areas of concern include the development of LFC structure and subsystems with acceptable weight and cost, problems of manufacturing of the required LFC structure, and the operational reliability on a day-by-day basis. The following sections of this paper review the status of NASA and industry activity up to the present time related to these concerns.

Major LFC development programs funded in 1980 under the NASA ACEE program shown in Figure 2 include wing surface panel structural development (refs. 16 and 17) and the design, fabrication, and flight test of leading-edge articles (ref. 18). Because of the loss in NASA funding, the wing structural development program was terminated in 1981 before progress on major objectives could be made. The leading-edge flight test article program will be discussed in a later section. Modifications were made to the NASA-Langley Research Center 8-Foot Transonic Tunnel to accommodate a special sweptback, slotted-surface, laminar-flow control airfoil (ref. 19). The objective of continuing tests is to evaluate the effectiveness of suction through both slotted and perforated surfaces in supercritical flow. The airfoil is mounted at a fixed

angle of attack for a lift coefficient of 0.55, and test conditions include Mach numbers up to 0.82 and Reynolds numbers up to 20 million (ref. 20).

SYSTEM STUDIES RESULTS

The intensive evaluation of LFC system concepts in NASA contract NAS1-14631 (ref. 15) resulted in the preliminary design of the Lockheed LFC transport shown in Figure 3. It is a wide-body configuration designed to carry 400 passengers and baggage over an intercontinental range of 6500 nautical miles at M = 0.80 cruise speeds with adequate fuel to account for adverse winds, intermittent LFC disruption due to atmospheric conditions at cruise, and international fuel reserves. The total payload of the aircraft including passengers and baggage is 84,800 pounds.

The general arrangement drawing of the Lockheed LFC transport aircraft is presented in Figure 4. The aircraft is a low-wing T-tail monoplane with four aft-mounted engines. An independently driven LFC suction unit is located in a fairing under each wing root. Fuel is carried in the wing, including the wing center-section box. The wing has 25° sweep at the leading edge, an aspect ratio of 11.6, and a wing loading of 111.8 pounds per square foot. Full-span flaps, including drooped ailerons, provide the required airport performance for a 10,000-foot runway. Leading-edge, high-lift devices are not required. Partial-span spoilers are provided. Small-chord (10 percent) secondary flaps incorporated into the main flaps provide upper surface pressure gradient and shock position control for off-design operation, and serve as active controls to minimize structural requirements. The takeoff gross weight of the aircraft is 592,205 pounds. LFC suction capability is provided on upper and lower wing surfaces from 0 to 75 percent chord and on the empennage from 0 to 65 percent chord. The effectiveness of the Lockheed design approach in the integration of LFC-peculiar items resulted in the relatively low weight of 4.4 percent of the empty weight incurred for LFC. The dedicated slots at the leading edge for dispensing the flow of a liquid to present contamination of the surface during takeoff and climb out required an amount of fluid per flight which is 2.6 percent of the gross weight of the aircraft.

The benefits of LFC shown in Figure 5 were determined by comparison of the performance of the LFC aircraft and an equivalent advanced technology turbulent aircraft which performed the same mission as that of the LFC aircraft. The calculations of aircraft drag indicate a 60 percent reduction in the wing and empennage drag, resulting from the effects of LFC in reducing skin-friction drag. The corresponding reduction in total aircraft drag due to LFC is 15 percent. The weight empty of the LFC aircraft is about 1 percent greater than the turbulent aircraft but the takeoff gross weight of the LFC aircraft is 8 percent lower, primarily due to the 22 percent reduction in fuel required for the long-range mission. The lower fuel burned provides a 4 percent reduction in direct operating costs (DOC).

During the time period of the intensive system evaluation studies of commercial LFC transport studies under contract NAS1-14631, Lockheed was continuing its preliminary design studies of military cargo airlift aircraft under Independent Research and Development projects. A general arrangement drawing of one of the military LFC transports presented in Figure 6 shows a M = 0.68 cruise speed with four times the payload of the 400 passenger commercial transport in the NASA study. With a lower amount of sweep in the wing, the aspect ratio was increased to 15, and for the 6000-nautical-mile-range capability, the takeoff gross weight is about 1.2 million pounds. The results of these military LFC transport studies were presented at a

special meeting on laminar-flow control conducted by the Defense Advanced Research Projects Agency on May 2, 1978. The parametric study included cruise Mach numbers from 0.65 to 0.80 and ranges from 6,000 nautical miles to 12,000 nautical miles. Fuel savings of 16 percent were indicated for the laminar-flow control aircraft as compared to that for the turbulent flow aircraft for the same mission characteristics.

NASA LEADING-EDGE SYSTEMS FLIGHT TEST PROGRAM

Encouraged by the progress made in the development and validation of leading-edge cleaning, anti-icing, and suction systems so vital to the success of an LFC transport, Lockheed and Douglas developed flight test articles with NASA funding that were installed and tested on the NASA-Dryden Flight Research Facility JetStar aircraft. The Lockheed activity is reported in reference 18. An early review of the total NASA program is given by Wagner and Fischer in reference 21. In addition to the development of the leading-edge test article, Lockheed had the added responsibility for providing the aircraft structural and support system design and integration.

The schematic diagram in Figure 7 shows the NASA JetStar flight test airplane with the McDonnell-Douglas perforated leading-edge flight test article on one wing and the Lockheed slotted test article on the other wing. Both LFC suction concepts are logical candidates, and the flight tests were made to determine the effectiveness of these system concepts for leading-edge cleaning, anti-icing, and cruise suction LFC conditions. The test articles were instrumented for measuring boundary-layer conditions, suction flows, and other basic aircraft flight parameters. After ground and flight check-out and acceptance tests, the aircraft was operated in a simulated airline service phase to accumulate the operational flight data required. The total flight program is reviewed by NASA in reference 22.

The Lockheed leading-edge test article shown in a cross-section view in Figure 8 is a sandwich construction consisting of a 0.016-inch-thick titanium outer skin bonded to a substructure of graphite/epoxy face sheets with a Nomex honeycomb core.

Suction slots are cut in the titanium outer skin by a high-speed steel jeweler's saw to provide fine spanwise slots about 0.0035 inch wide on both upper and lower surfaces back to the front spar location. The suction flow passes through the wing outer skin into slot ducts which have metering holes into the collector ducts imbedded in the honeycomb. The insert protection and anti-icing are accomplished by dispensing the cleaning/anti-icing fluid over the wing surface through the slots above and below the wing flow attachment line as denoted by slots C and D on Figure 8. These slots are purged of the fluid during climbout and provide suction to achieve laminar flow at cruise conditions in combination with the slots denoted by U and L.

A problem in fabrication of the leading-edge test article was discovered upon suction flow check out of the final article. It was determined that migration of the adhesive during the titanium-to-graphite faced core bonding process had plugged up a few of the slots, metering holes on collector ducts in a random manner on the test article. The attendant loss of suction flow in these locations prevented the local attainment of conditions necessary for laminar flow. As a result, the attainment of laminar flow over the entire test article could not be realized during the flight testing.

57

A close-up photograph of the Lockheed test article installed on the NASA JetStar LFC flight test aircraft is provided in Figure 9. Figure 10 is a photograph of the aircraft in flight.

LAMINAR FLOW ENABLING TECHNOLOGY DEVELOPMENT

At a meeting held at the NASA-Langley Research Center on January 19-20, 1984, NASA discussed plans for LFC new initiatives and technology development with representatives from Boeing, McDonnell-Douglas, and Lockheed. These discussions eventually resulted in request for proposals (RFP) being released for laminar flow enabling technologies development and the award of task-type contracts to Boeing, McDonnell-Douglas, and Lockheed.

In order to provide for a near-term application of laminar-flow control, a more simplified concept referred to as hybrid laminar-flow control (HLFC) has been established for current activities. The HLFC concept, shown in Figure 11, has the active suction system restricted to the region ahead of the front spar of the wing. Aft of the active suction region the airfoil shape is tailored to achieve the maximum extent of laminar flow, and this is expected to extend to 50 percent or more of the wing chord. HLFC studies by Boeing are reported in reference 23. The HLFC concept avoids a number of concerns by the industry and the airlines, in particular, suction surfaces and ducting are not required in the main wing box areas which also contain the fuel for the aircraft. Thus the weight and complexity of the suction systems is greatly reduced and the possible hazards with the fuel are eliminated. The suction in the leading-edge region can control the cross flow disturbances for swept wings and the airfoil tailoring over the wing box can stabilize two-dimensional disturbances.

The two tasks in the NASA/Lockheed Laminar-Flow Enabling Technology Development Contract No. NAS1-18036 are listed in Figure 12 and will now be discussed. Contract NAS1-18036 is a 48 month task-type contract that was effective in December 1985. The NASA/Industry Laminar-Flow Enabling Technology Development Program is another significant step in the path leading to the achievement of the potential benefits of LFC for future transport aircraft.

TASK 1 - ADVANCED ALUMINUM SLOTTED-SURFACE STRUCTURAL CONCEPT DEVELOPMENT

The primary objective of Task 1 was to design and fabricate a small demonstration article as shown in Figure 13. This new structural arrangement of a slotted surface uses advanced aluminum material and manufacturing techniques. The program demonstrates the producibility of the design using a powder metal aluminum alloy outer skin, superplastic forming, diffusion bonding, and a low density aluminum-lithium inner skin. Fabrication techniques were selected to eliminate assembly difficulties encountered in the previous composite design of the JetStar flight test article.

The bonded assembly was placed in an indexing fixture which rates the part for slotting. Slotting was done with a 1-inch-diameter jeweler's saw with an 0.0025 inch thickness. The saw was mounted on a motor set up on a computer-controlled gantry.

Slot widths of 0.003 were obtained with this process on the demonstration article. Powder aluminum IN9052 was selected for the outer skin because of its high corrosion resistance properties similar to titanium used in the previous test articles. Thus the slots cut in this material should maintain their desired geometry and not degrade with time and operation.

A close-up view of a single spanwise duct in Figure 14 shows the materials and joining processes. The outer skin and the inner sheet used to form the slot duct are fabricated from powder metal aluminum alloy IN9052 and diffusion bonded using a Texas Instruments bonding and expansion process. Diffusion bonding was selected in this area because of its high shear strength and to avoid the use of adhesive bonding in the slot, slot duct, and metering hole regions. Texas Instruments, located in Attleboro, Massachusetts, was selected to fabricate the outer skin and slot ducts.

Texas Instruments uses a cold roll bonding process. Prior to bonding, metal surfaces are chemically and mechanically cleaned to provide contaminant-free surfaces. Bonding is achieved by passing the metal sheets through a specially designed rolling mill where extremely high reduction in the sheet gages forces the layers into intimate contact. During this bonding process, the new surface is exposed, providing bonding surfaces which are virtually defect-free. A thermal expansion process is introduced by placing stop-off materials between the layers of metal before bonding. This thermal treatment causes the material to expand into shaped dies at the locations of the stop-off. The end result is a shaped configuration of the slot duct diffusion bonded to the outer skin, with shear strengths nearly equal to the shear strength of the monolithic alloy.

The collector duct is superplastically formed from 7475 aluminum alloy. The structure is closed using low-density aluminum-lithium alloy. Interfaces between the slot duct sheet and the collector duct and between the collector duct and the aluminum-lithium inner skin are adhesively bonded using FM300 adhesive.

Lockheed was responsible for the fabrication of the inner portion of the demonstration article including the collector duct and inner skin and for the final assembly.

Photographs of a sample of the outer skin and slot duct cross section and of a top view showing the slots are provided in Figure 15.

TASK 2 - GLOBAL RANGE MILITARY TRANSPORT STUDY

The objective of Task 2 was to determine by means of preliminary system design studies the benefits derived from the use of hybrid laminar-flow control (HLFC) for military transports designed to achieve the payload/range requirements of global range aircraft. As shown in Figure 16 the Air Force Project Forecast II effort has identified system PS-03 Multirole Global Range Aircraft as a subsonic element in global force projection. It is anticipated that this global range aircraft must have exceptional aerodynamic and propulsive efficiency to achieve the mission characteristics. Previous Lockheed preliminary design studies have shown significant increase in aerodynamic efficiency by the application of LFC to military transport aircraft. It is also expected that the HLFC or natural laminar flow, NLF, will also provide improved efficiency for System PS-05 High-Altitude, Long-Endurance, Unmanned Aircraft, the PS-22 Multimission Remotely Piloted Vehicle, and the PS-35 Airborne Surveillance System.

A recent study of military laminar-flow control transport aircraft was conducted by Lockheed under an Air Force contract study, "Technology Alternatives for Airlift Deployment" (ref. 24). A sketch of the military LFC transport given in Figure 17 is for a Mach 0.80 cruise aircraft with a payload of 212,000 pounds, a range of 5800 nautical miles, and a takeoff gross weight of 786,700 pounds. The aircraft utilized LFC from the leading edge back to 65 percent of the wing chord and to 75 percent chord on the empennage surfaces. As compared to a comparable turbulent flow transport the LFC transport showed a 40 percent increase in range for the same payload but with an attendant 10 percent increase in structural weight.

The laminar-flow control transport showed a 14 percent reduction in mission fuel as compared to that for the turbulent flow aircraft. The fuselage-mounted engine location is a compromise among considerations of weight and balance, nose wheel lift off at takeoff and, of course, avoidance of wing-mounted engines.

The scope of the Task 2 preliminary design study of contract NAS1-18036 is included in five study elements: (1) Basic Data Assumptions, (2) Mission Character-istics, (3) Configuration Development, (4) Configuration Selection, and (5) Analysis of Laminar-Flow Benefits. In element (1), the approach is to utilize the technology data base in the Lockheed Generalized Aircraft Sizing and Performance (GASP) com-puter program used in the Air Force Technology Alternatives for Airlift Deployment (TAFAD) study. Modification is made to the data base to account for the change to the hybrid laminar-flow control concept from the previous LFC concept. Mission characteristics such as payload, range, cruise Mach number, airfield performance, and operational concepts have been mutually agreed upon among NASA, the Air Force, and Lockheed. The baseline mission characteristics presented in Figure 18 are based upon the following considerations: the payload of 132,500 pounds is generic for multi-purpose missions of the Air Force under study by Lockheed under AFWAL contract (see ref. 25); cruise speed of Mach 0.77 will be increased to Mach 0.80; initial cruise altitude will be a fallout to provide best cruise efficiency for the Pratt & Whitney STF-686 turbofan propulsion system and initial results of about 31,000 feet were increased to 36,000 feet; the initial takeoff field length and field length at the midpoint are representative of those for long-range transoceanic flights; and the radius-type payload/range with no refueling at the mid-point provides military force projection to many parts of the world of interest to the Air Force. The range capability provides access to Pacific Rim countries which are important to operators of commercial transport aircraft.

The HLFC design ground rules listed in Figure 19 are, with a few exceptions, basically self-explanatory and consistent with previous LFC studies. Turbulent flow is assumed to occur during 6 percent of cruise time to assure mission completion should atmospheric conditions preclude the use of HLFC for short periods during cruise. The 12 percent excess cruise thrust provides the capability to maintain cruise altitude and/or speed with the HLFC system inactive. The wing sweep was varied for both the HLFC and comparison turbulent flow aircraft in the parametric sizing studies as will be discussed later. The number in the flight crew provides for rest cycles for this long-range mission. It was assumed that technology readi-ness of 1994 will provide an initial operational capability (IOC) for the year 2000.

Results of the ongoing parametric design studies of Task 2 are provided in Fig-ure 20 of an initial baseline HLFC design concept for the long-range mission and at a cruise Mach number of 0.77. The design concept features the fuselage-mounted engines similar to the previous Air Force TAFAD study (ref. 24). In addition, geometric features include a wing sweep of 20°, an aspect ratio of 13.86, and a wing span of

60

259 feet. Performance characteristics include a takeoff gross weight of 594,548 pounds, mission fuel of 253,330 pounds, and a lift-to-drag ratio of 30.9. As mentioned earlier, wing sweeps of 20° and 25° were investigated in the parametric sizing runs for the HLFC aircraft. A comparison of the parametric data for the two sweep cases showed mixed results with the 20° sweep design indicating slightly higher lift-to-drag ratio than the 25° design but the 25° design indicating slightly less fuel burned and takeoff gross weight. The 20° sweep design was selected because it was expected that less leading-edge cross flow would be encountered than that for the higher sweep design.

Parametric sizing data were derived for the turbulent flow aircraft with the wing sweep varying from 25° to 40° for identical mission requirements as those for the HLFC designs. The data indicate a superiority of the 30° sweep design based on an overall comparison of minimum fuel burned, maximum lift-to-drag ratio, and minimum takeoff gross weight. A general arrangement drawing of the baseline 30° sweep turbulent design presented in Figure 21 features wing-mounted engines, an aspect ratio of 13.5, and a wing span of 256 feet. Performance characteristics include a takeoff gross weight of 616,125 pounds, mission fuel of 291,401 pounds, and a lift-to-drag ratio of 26.

The benefits of HLFC presented in Figure 22 were determined by a comparison of the performance of HLFC designs with that for the baseline turbulent design, which performed the same mission as that of the HLFC designs. Data for the HLFC baseline design and two variations from that design are presented in the three columns of Figure 22 and the percentage changes are all referenced to the baseline turbulent design. As presented in the first column, the baseline HLFC design as compared to the baseline turbulent flow design indicates an increase in operating empty weight of 5.4 percent, a decrease in takeoff gross weight of 4 percent, a decrease in fuel consumption of 13.4 percent, and an increase in lift-to-drag ratio of 18.4 percent. The second column of Figure 22 shows the effects of deleting laminar-flow control from the empennage of the HLFC aircraft; and the results, as expected, are small with slightly higher aircraft weights, an improvement in the fuel consumption, and little change in the lift-to-drag ratio. The effects of deleting HLFC on the lower wing surfaces show significant adverse effects on aircraft weights, fuel consumption, and lift-to-drag ratio. As compared to the HLFC baseline aircraft, the overall effect of a decrease in lift-to-drag ratio of 32 percent and an increase in fuel consumption of 41 percent gives an increase in takeoff gross weight of 85 percent. Although not shown on Figure 22, an increase in initial cruise altitude of the HLFC design to 36,000 feet has a slightly adverse effect on the weights and fuel consumption and an improvement in the lift-to-drag ratio.

It should be noted that the aspect ratios of both turbulent flow and HLFC design concepts are relatively high as compared to the state-of-the-art and to near-term projections. Although a number of conceptual design studies have utilized design concepts with aspect ratios from 13 to 16 and even higher, there is concern that such aspect ratios will be achievable on a fully operational, flight worthy and certified aircraft in the next 5 to 10 years. The global range Task 2 study will address this concern with a study of a lower aspect ratio design.

In summary, these studies of the application of HLFC to global range military transport aircraft show a significant increase in lift-to-drag ratio (18 percent), decrease in fuel consumption (13 percent), and decrease in takeoff gross weight (4 percent) for a 5 percent increase in empty weight as compared to that for global range turbulent flow aircraft.

STATUS AND RECOMMENDATIONS FOR FURTHER WORK

It is clear that substantial progress has been made in the NASA/Industry technology development of laminar-flow control over the past 10 years as indicated in Figure 23. The recently completed flight tests of LFC leading-edge systems have successfully demonstrated solutions to leading-edge contamination. These tests have also obtained laminar flow over both slotted and perforated surfaces for a variety of flight conditions and from operation out of many airport operating environments.

The current NASA/Industry Laminar-Flow Enabling Technology Development projects initiated in 1985 are continuing to provide direction to the achievement of technology readiness for application of LFC to future long-range transport aircraft. As discussed previously the simplified HLFC concept reduces the complexity of LFC and thus provides for one more near-term application of this technology. The significant benefits of HLFC indicated in the global range aircraft studies described herein provide the justification for an accelerated effort to develop the desired data base on HLFC for application to long-range transport aircraft. With the present state of the art in HLFC technology, additional development is required especially for application to long-range transport aircraft in the high Reynolds number regime. The current LFC data base in wind tunnel and flight tests is limited to a maximum Reynolds number of about 20 million. This situation leads to the next logical step in the development of HLFC.

What is now needed in HLFC, as outlined in Figure 24, is an experimental flight program on a swept wing aircraft to obtain the required data at high Reynolds numbers, i.e., 30 to 50 million, and at cruise Mach numbers and altitudes representative of long-range transport operation. These tests are needed to obtain the physical flow properties of the boundary layer including leading-edge crossflow and two-dimensional disturbances aft of the leading edge and over the main wing box area. These data can only be obtained by means of flight tests on a representative subsonic speed, long-range aircraft. A program of this type is a logical extension of the ongoing NASA program in laminar flow and laminar-flow control research. Such a program has been discussed with NASA by Lockheed utilizing the C-141 as the flight test aircraft. To this end it is gratifying to note the issue of NASA RFP 1-42-3610.0049, "High Reynolds Number Hybrid Laminar-Flow Control (HLFC) Flight Experiment," in a cooperative effort with the Air Force Wright Aeronautical Laboratories. This flight investigation is envisioned as the final step in the achievement of the technology readiness for application of HLFC to long-range transport aircraft in the mid to late 1990's.

SUMMARY AND CONCLUSIONS

The summary and concluding remarks for this paper are outlined in Figure 25. Considerable progress has been made in the NASA/Industry LFC program from its inception in October 1974. Furthermore this work has provided the United States with a competitive edge over our foreign competitors. In order to maintain this edge, a high Reynolds number flight test program on a subsonic speed, swept wing aircraft with HLFC should be initiated at the earliest possible time. It is hereby noted that NASA has issued an RFP for such a program in a cooperative effort with the Air Force Wright Aeronautical Laboratories.

Industry as yet does not have the required data base to proceed with the design and fabrication of an HLFC aircraft for operational use. The global range aircraft

study has shown significant benefits for HLFC application on the order of an 18 percent increase in lift-to-drag ratio and a 13 percent reduction in fuel consumption as compared with turbulent flow aircraft. These results warrant an accelerated effort to develop the HLFC technology data base required for technology readiness.

REFERENCES

1. Braslow, Albert L., and Muraca, Ralph J., "A Perspective of Laminar-Fuel Control," AIAA Paper 78-1528, Los Angeles, CA, August 1978.

2. Antonatos, P. P., "Laminar Flow Control - Concepts and Applications," Astronautics and Aeronautics, July 1966, pp. 32-36.

3. Whites, R. C., Sudderth, R. W., and Wheldon, W. G., "Laminar Flow Control on the X-21," Astronautics and Aeronautics, July 1966, pp. 38-43.

4. Pfenninger, Werner, and Reed, Verlin D., "Laminar-Flow Research and Experiments," Astronautics and Aeronautics, July 1966, pp. 44-50.

5. Nenni, Joseph, and Gluyas, George L., "Aerodynamic Design and Analysis of an LFC Surface," Astronautics and Aeronautics, July 1966, pp. 52-57.

6. Chuprun, John, and Cahill, Jones F., "LFC on Large Logistics Aircraft," Astronautics and Aeronautics, July 1966, pp. 58-62.

7. Kramer, J. J., "Planning a New Era in Air Transportation Efficiency," Astronautics and Aeronautics, July/August 1978, pp. 26-28.

8. Conner, D. W., "CTOL Concepts and Technology Development," Astronautics and Aeronautics, July/August 1978, pp. 29-37.

9. Leonard, R. W., "Airframes and Aerodynamics," Astronautics and Aeronautics, July/August 1978, pp. 28-46.

10. Lange, R. H., "Design Integration of Laminar Flow Control for Transport Aircraft," Journal of Aircraft, Vol. 21, No. 8, August 1984, pp. 612-617.

11. Meade, L. E., Kays, A. O., Ferrill, R. S., and Young, H. R., "Development of the Technology for the Fabrication of Reliable Laminar Flow Control Panels," NASA CR 145168, prepared by the Lockheed-Georgia Company, October 1976.

12. Peterson, J. B., Jr., and Fisher, D. F., "Flight Investigation of Insect Contamination and Its Alleviation," NASA CP 2036, Part I, Feb.-Mar. 1978, pp. 357-373.

13. Sturgeon, R. F., "The Development and Evaluation of Advanced Technology Laminar-Flow-Control Subsonic Transport Aircraft," AIAA Paper 79-96, Huntsville, Alabama, January 1978.

14. Sturgeon, R. F., "Toward a Laminar-Flow Control Transport," CTOL Transport Technology 1978, NASA Conference Publication 2036, February 28 - March 3, 1978.

15. Sturgeon, R. F., "Evaluation of LFC System Concepts for Subsonic Commercial Transport Aircraft," NASA CR 159253, prepared by Lockheed-Georgia Company, Sept. 1980.

16. Lineberger, L. B., Beall, R. T., and Gilbert, G. J., "Development of Laminar Flow Control Wing Surface Composite Structures," NASA CR 172330, prepared by the Lockheed-Georgia Company, May 1984.

17. Lineberger, L. B., "Structural Tests and Development of a Laminar Flow Control Wing Surface Composite Chordwise Joint," NASA CR 172462, prepared by the Lockheed-Georgia Company, December 1984.

18. Etchberger, F. R., "LFC Leading Edge Glove Flight - Aircraft Modification Design, Test Article Development, and Systems Integration," NASA CR 172136, prepared by Lockheed-Georgia Company, Nov. 1983.

19. Harvey, W. D., and Pride, J. D., Jr., "NASA Langley Laminar Flow Control Airfoil Experiment," NASA CP 2218, September 1981, pp. 1-42.

20. Harvey, W. D., Harris, C. D., Brooks, C. W., Jr., and Bobbitt, P. J., "Experimental Results on a Swept Supercritical Airfoil With Suction via the Langley 8-Foot Transonic Pressure Tunnel." AIAA Shear Flow Control Conference, Boulder, Colorado, March 12-14, 1985.

21. Wagner, Richard D., and Fischer, Michael C., "Developments in the NASA Transport Aircraft Laminar Flow Program," AIAA Paper 83-0090, Reno, Nevada, January 1983.

22. Wagner, Richard D., Maddalon, Dal V., and Fischer, Michael C., "Technology Developments for Laminar Boundary Layer Control on Subsonic Transport Aircraft," presented at the 54th Meeting of the FLID Dynamics Panel Symposium on Improvement of Aerodynamic Performance Through Boundary Layer Control and High Lift Systems, Brussels, Belgium, May 21-23, 1984.

23. Anon., "Hybrid Laminar Flow Control Study," NASA CR-165930, prepared by Boeing Commercial Aircraft Company, October 1982.

24. Moore, J. W., Craven, E. P., Farmer, B. T., Simica, C. A., and Stevens, R. J., "Technology Alternatives for Airlift Deployment," Air Force Wright Aeronautical Laboratory Report AFWAL-TR-85-3001, prepared by Lockheed-Georgia Company, April 1985.

25. Smethers, Rollo G., and Honrath, John F., "Configuration Integration for Large Multi-Purpose Aircraft," Air Force Wright Aeronautical Laboratory Report AFWAL-TR-85-3075, prepared by Lockheed-Georgia Company, September 1985.

	1974	1975	1976	1977	1978	1979	1980
APPLICATION OF ADVANCED TECHNOLOGIES TO LFC SYSTEMS - CONTRACT NAS1-13694		▭					
JETSTAR L. E. FLAP MODIFICATION - CONTRACT NAS4-2340			▭				
DEVELOPMENT OF LFC PANELS - CONTRACT NAS1-14409			▭				
PREDICTION OF CRUISE NOISE/ LFC NOISE CRITERIA - CONTRACT NAS1-14946					▭		
EVALUATION OF LFC SYSTEM CONCEPTS - CONTRACT NAS1-14631				▭▭▭▭			
INDEPENDENT RESEARCH AND DEVELOPMENT			▭▭▭▭▭				

Figure 1. Lockheed LFC program history.

	1980	1981	1982	1983	1984	1985	1986
WING STRUCTURAL SYSTEMS DEVELOPMENT PROGRAM - CONTRACT NAS1-16235, 17487		▭			▭		
LEADING-EDGE FLIGHT TEST PROGRAM - CONTRACT NAS1-16219				FIRST FLIGHT ▽	▭▭▭▭▭▭		
JETSTAR LFC MODIFICATION SUPPORT - CONTRACT NAS2-11397				▭			
NASA WIND TUNNEL PROGRAM		ENTRY TEST ▽ ▽					
INDEPENDENT RESEARCH AND DEVELOPMENT							
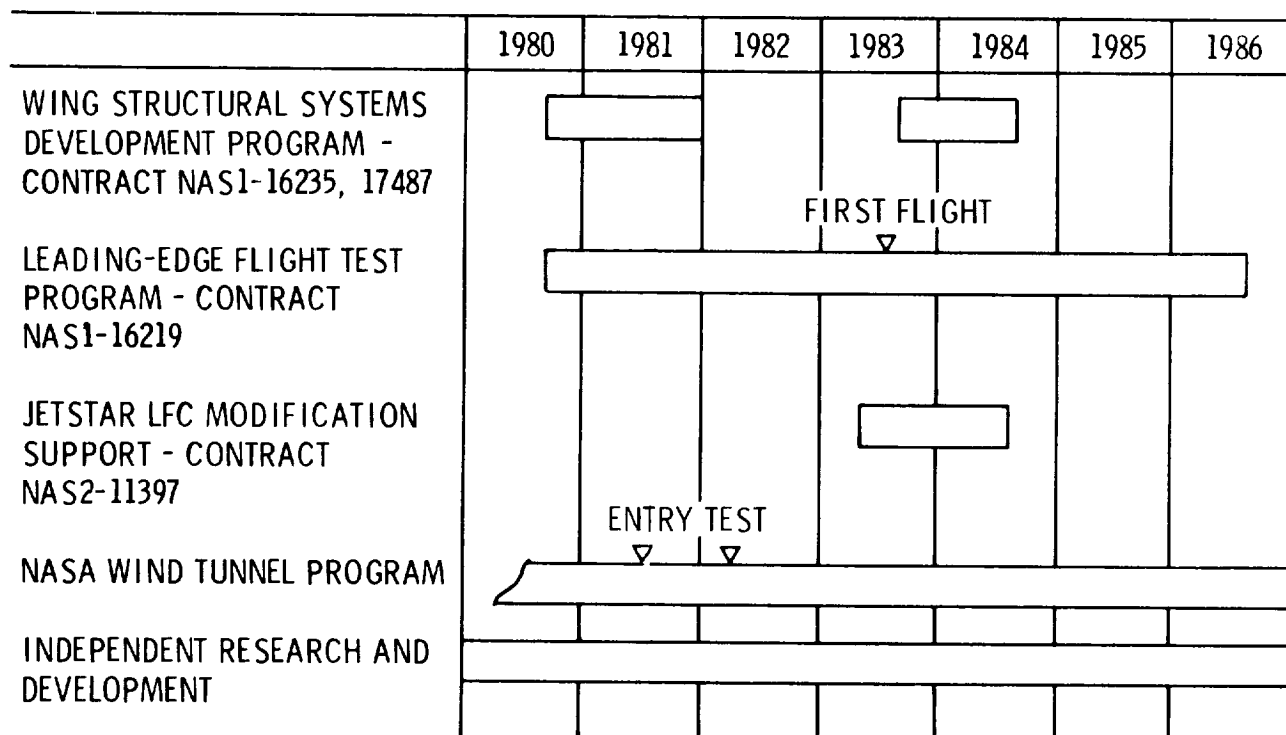
Figure 2. Lockheed LFC program history (Concluded).
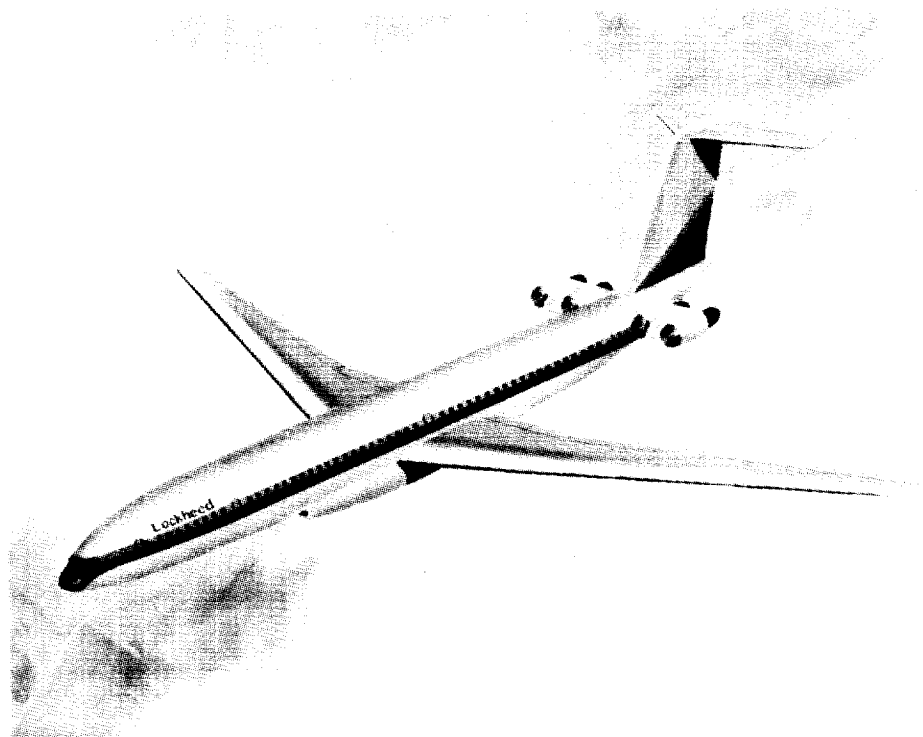
Figure 3. Laminar-flow control passenger transport.

Payload	400 Pax.
Range	6500 N.M.
Speed	0.80 Mach
Gross Weight	592,205 LB
Aspect Ratio	11.6

254.2 Ft

250.0 Ft

62.8 Ft
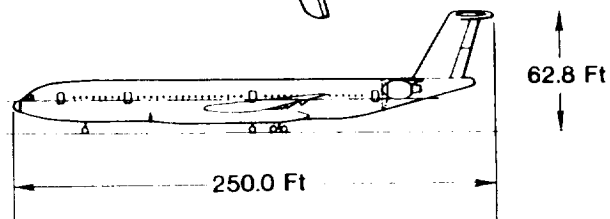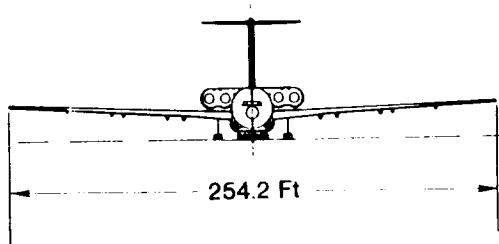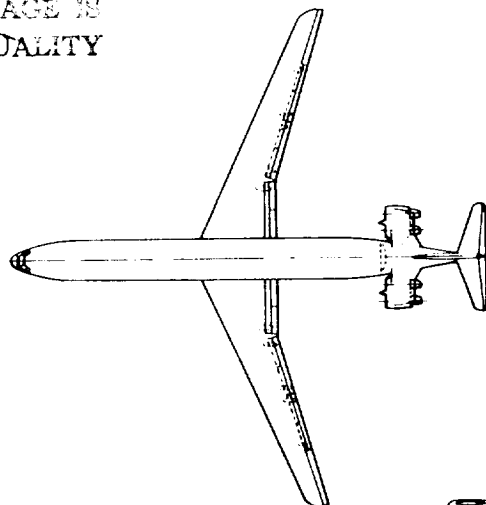
Figure 4. General arrangement of LFC transport.

	Change-%
Drag	
Wings/Empennage	**-60**
Total Aircraft	**-15**
Weight	
Empty Weight	**+1**
Gross Weight	**-8**
Fuel Consumption	**-22**
Direct Operating Cost	**-4**

Figure 5. Benefits of laminar-flow control.

Speed	0.68 Mach
Payload	350,000 Lb
Range	6000 NM
Operating Weight	468,700 Lb
Gross Weight	1,194,200 Lb
Block Fuel	350,600 Lb
Aspect Ratio	15.0

384 Ft

74 Ft

311 Ft
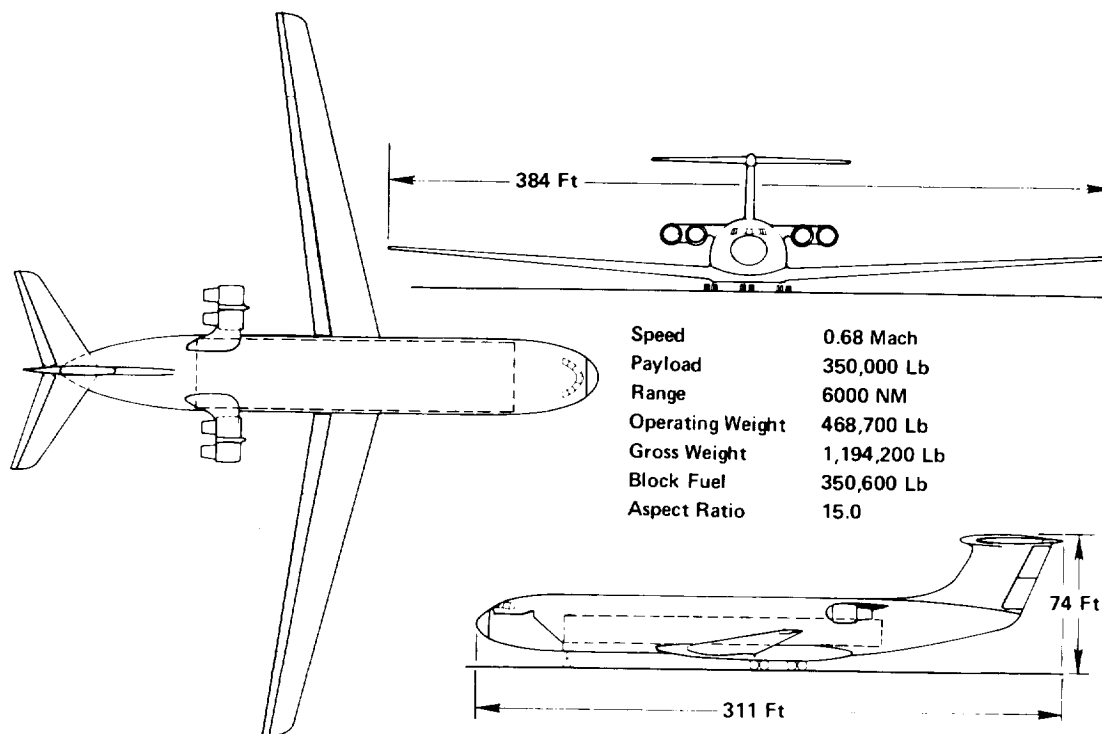
Figure 6. LFC military transport.

Lockheed-Georgia Test Article
Slotted Surface
Integral Structural Design

McDonnell-Douglas Test Article
Perforated Surface
Non-Integral Structural Design
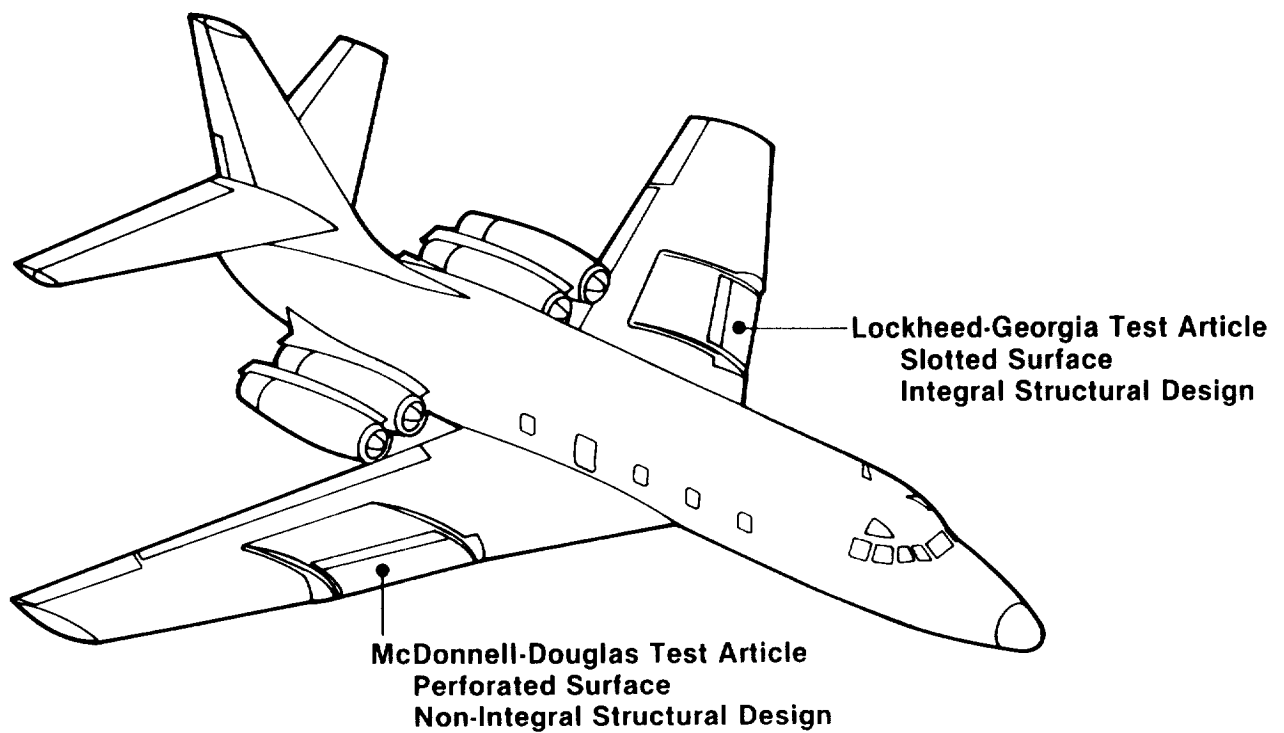
Figure 7. NASA JetStar and test articles.

U – UPPER SURFACE DEDICATED SUCTION SLOTS

L – LOWER SURFACE DEDICATED SUCTION SLOTS

C – DEDICATED CLEANING/ANTI-ICING SLOTS

D – DUAL PURPOSE SLOTS
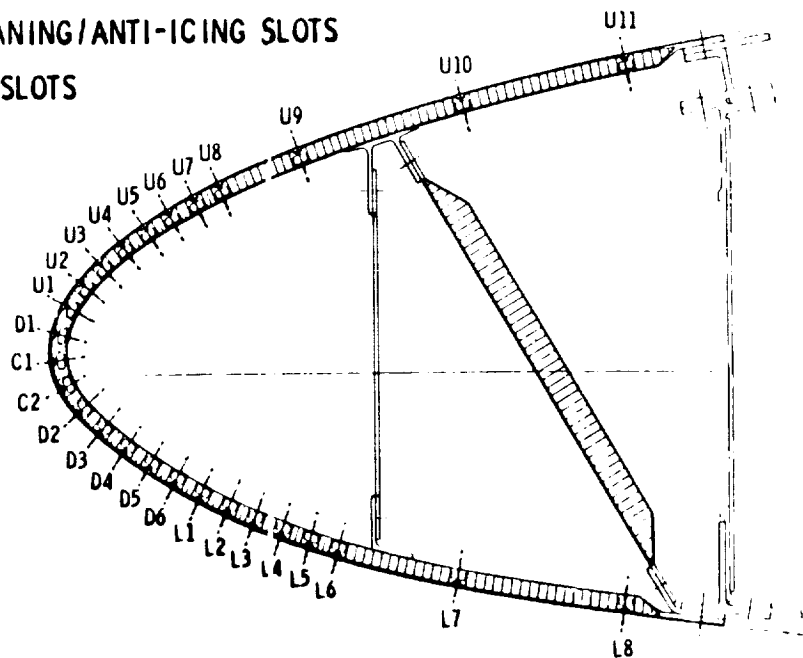
Figure 8. Slot locations on test article.

Figure 9. Photograph of Lockheed test article.
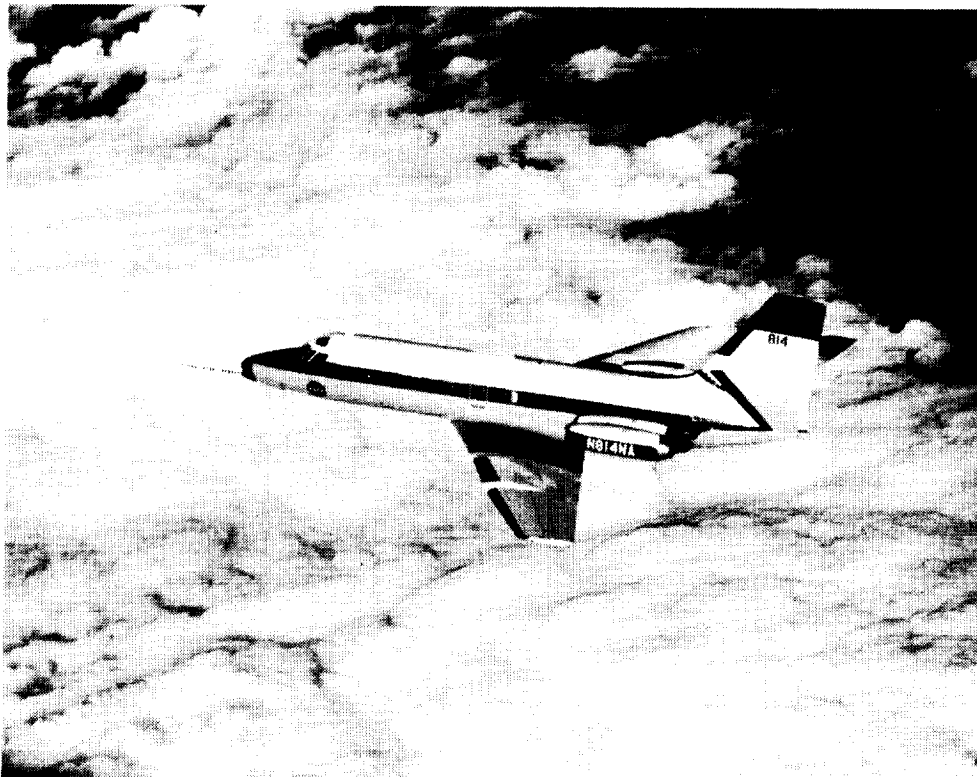
Figure 10. Photograph of NASA JetStar test aircraft.

69

LEADING EDGE
TREATMENT

AIRFOIL TAILORING TO MAINTAIN
NATURAL LAMINAR FLOW

- CLEANING AND
  ANTI-ICE SYSTEM

- SUCTION
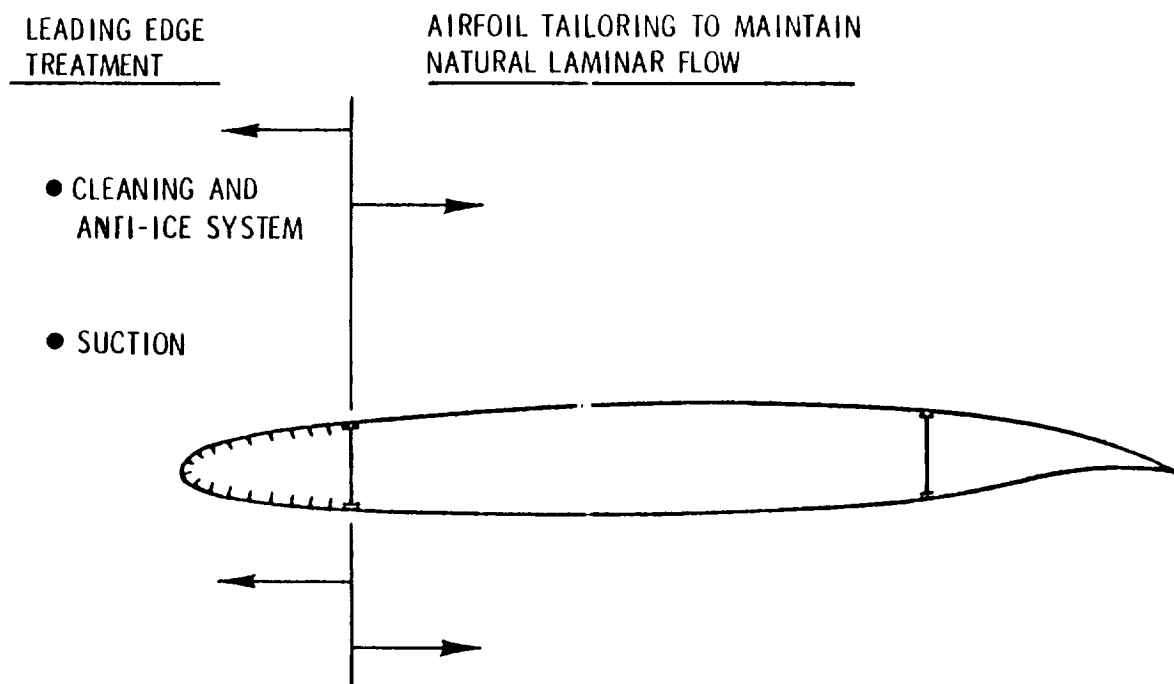
Figure 11.   Schematic of hybrid laminar-flow control concept.

48 MONTH TASK-TYPE CONTRACT - NAS1-18036

	1986	1987	1988	1989	1990
TASK 1 - ALUMINUM ALLOY L.E. SLOTTED-SURFACE STRUCTURAL CONCEPT, EVAL/DEMO					
TASK 2 - GLOBAL RANGE MILITARY TRANSPORT STUDY					
INDEPENDENT RESEARCH AND DEVELOPMENT					

Figure 12.   Laminar flow enabling technology development.

70
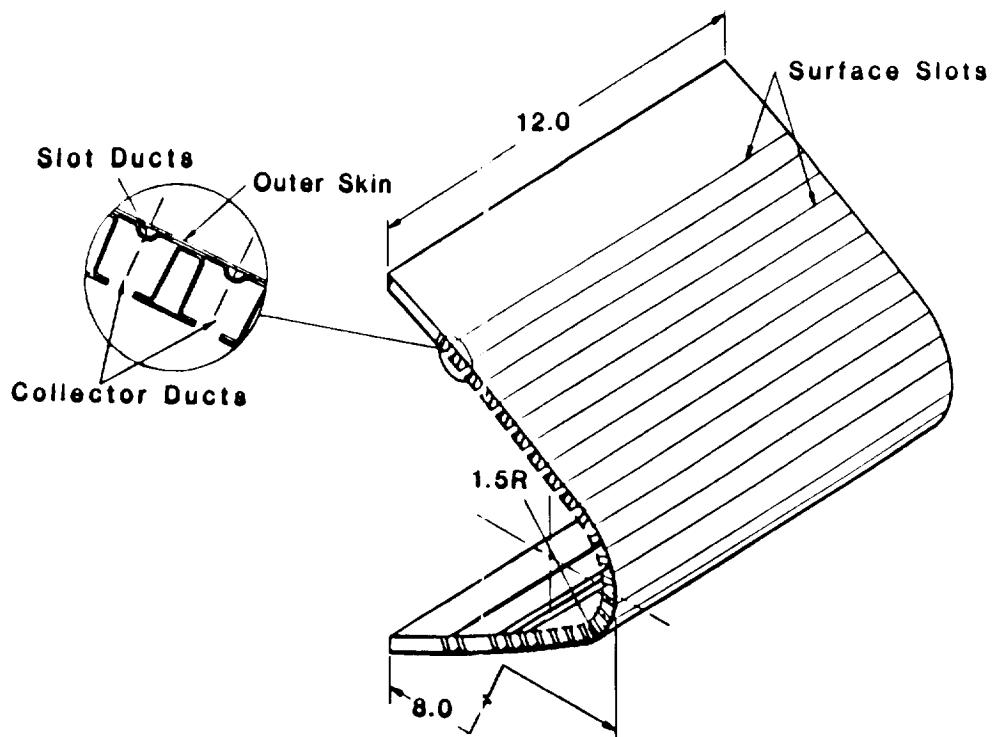
Figure 13. Leading-edge structure demonstration article.
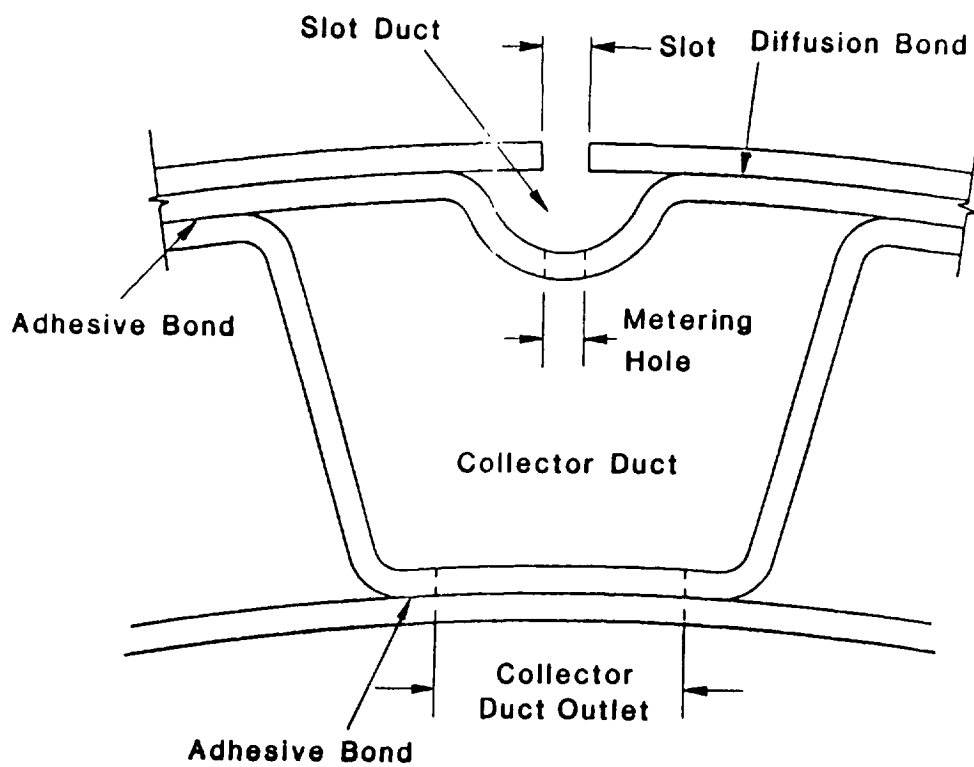
Figure 14. Leading-edge section bonding processes.

Cross-Section   Top View
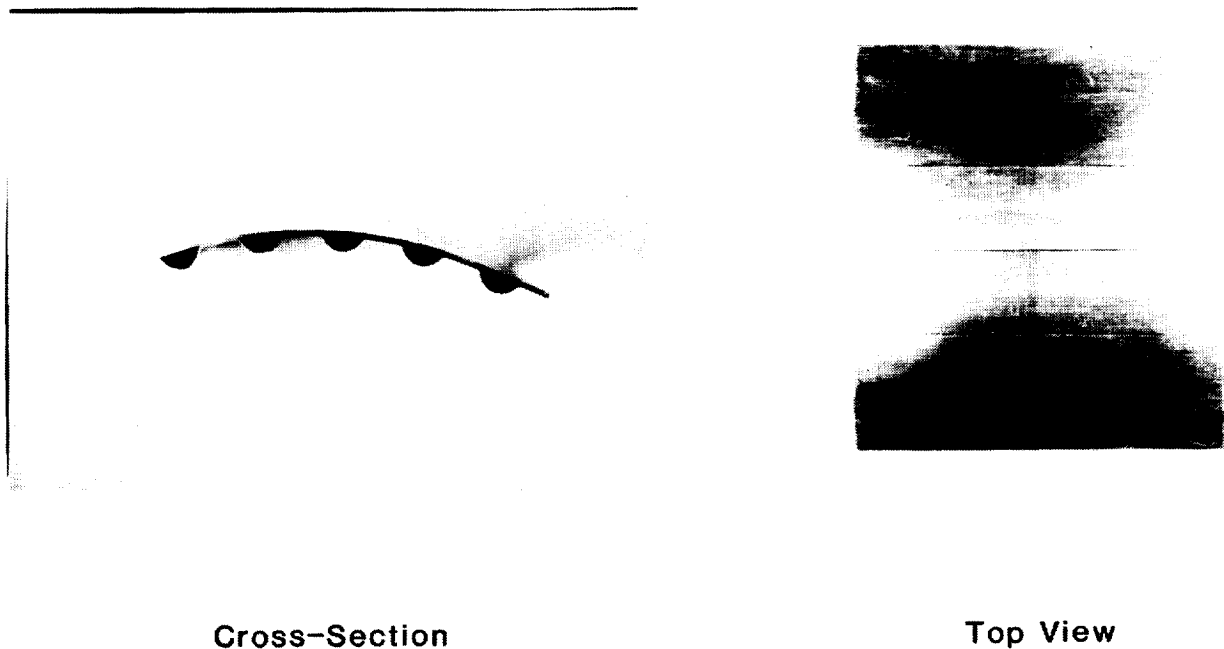
Figure 15. Diffusion bonded IN9052 panel.

PS-01   INTRATHEATER VSTOL TRANSPORT AIRCRAFT
PS-03   MULTIROLE GLOBAL RANGE AIRCRAFT
PS-05   HIGH ALTITUDE, LONG ENDURANCE, UNMANNED AIRCRAFT

PS-04   SUPERSONIC VSTOL TACTICAL AIRCRAFT
PS-22   MULTIMISSION REMOTELY PILOTED VEHICLE

PS-35   AIRBORNE SURVEILLANCE SYSTEM
PS-07   SPECIAL OPERATIONS AIRCRAFT

Figure 16. Air Force Project Forecast II.
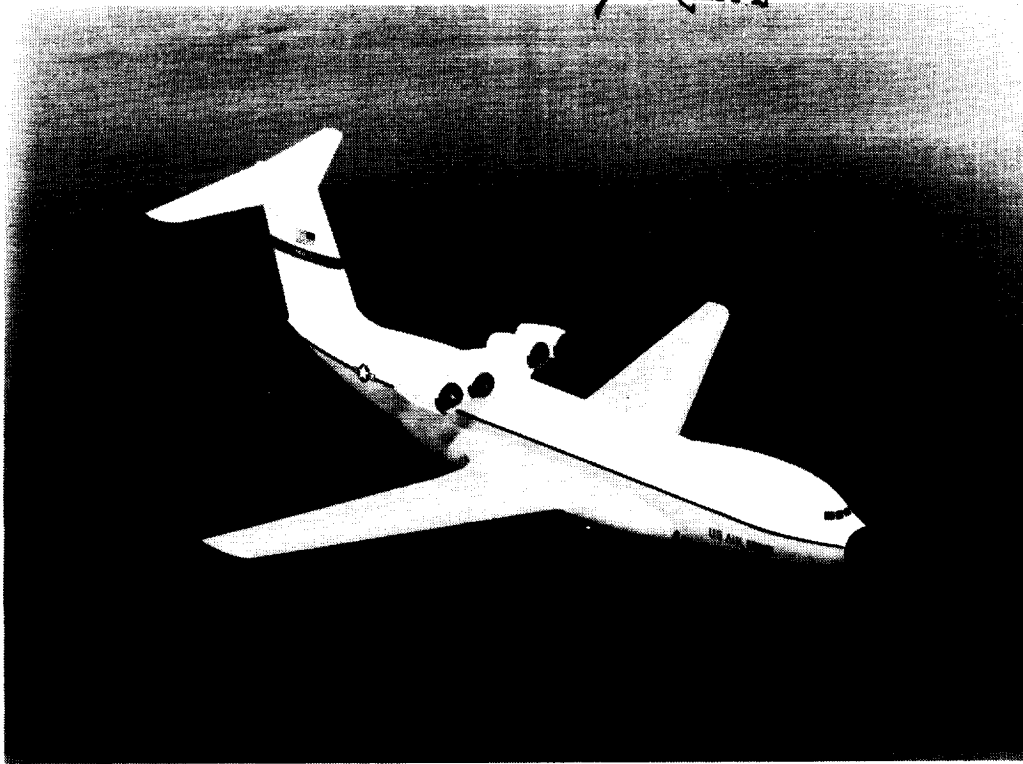
Figure 17.   Military LFC transport in TAFAD study.

- PAYLOAD = 132,500 LB @ 2.5g

- CRUISE SPEED = 0.77 MACH

- INITIAL CRUISE ALTITUDE = FALLOUT VALUE

- AIRFIELD (CFL) = 10,000 FT @ S.L. STD, DAY

- FLYOUT 6,500 NM WITH FULL PAYLOAD AND RETURN
  6,500 NM WITH ZERO PAYLOAD

- FIELD LENGTH @ MIDPOINT ≲ 8,000 FT @ S.L. STD, DAY

Figure 18.   HLFC Global Range Transport Mission characteristics.

- WING AND EMPENNAGE ACTIVE SUCTION = 15% CHORD

- WING FRONT AND REAR BEAM @ 15 AND 65% CHORD

- HLFC ACTIVATED ONLY UPON REACHING INITIAL CRUISE ALTITUDE

- TURBULENT FLOW = 6% CRUISE TIME

- 12% MINIMUM EXCESS CRUISE THRUST AVAILABLE

- WING L.E. SWEEP (DEGREES) - BAT = 25, BASIC = 20

- EMPENNAGE SURFACE SWEEP = 23 DEGREES @ 1/4 CHORD

- WING T.E. FLAPS = 25% WING CHORD

- INDEPENDENT HLFC SUCTION POWER SYSTEM

- ACCOMMODATIONS = 3 PILOTS, 1 LOADMASTER, AND TWO BUNKS

Figure 19.   HLFC Global Range Transport Design ground rules.

PAYLOAD -	132,500 LB
RANGE -	6,500 NM
MACH NO. -	0.77
ALTITUDE -	31,685 FT
TOGW -	594,548 LB
FUEL -	253,330 LB
L/D -	30.91
MAC -	22.68 FT
SPAN -	259.74 FT
AR -	13.86
L.E. SWEEP -	20 DEG
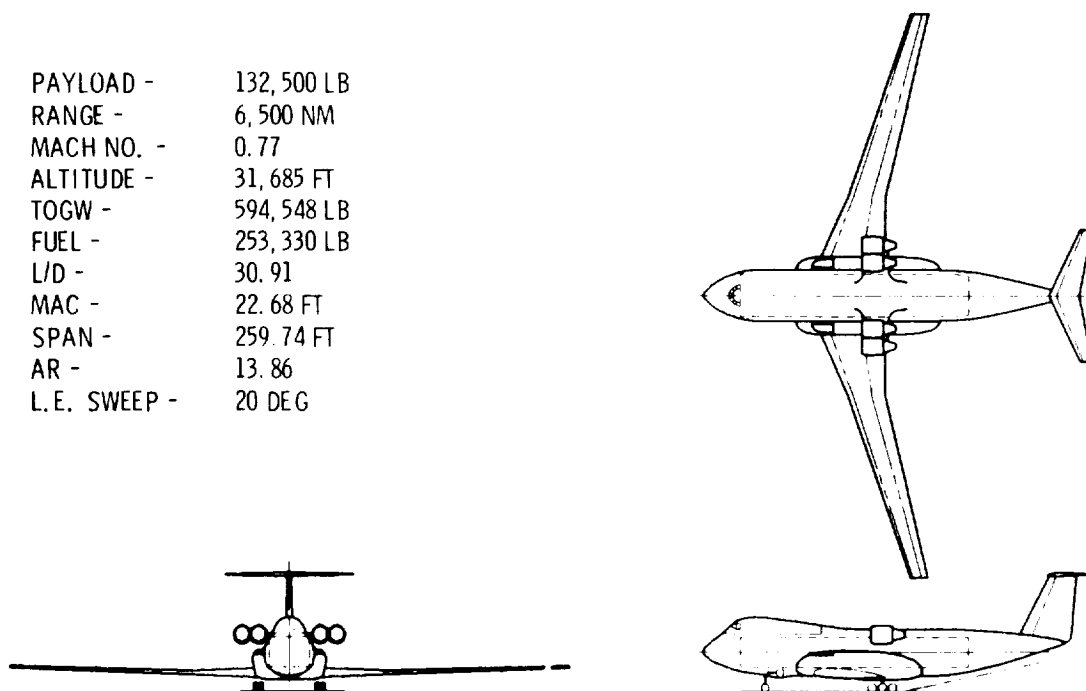
Figure 20.   HLFC initial baseline design concept.

74

PAYLOAD -   132, 500 LB
RANGE -   6, 500 NM
MACH NO. -   0. 77
ALTITUDE -   32, 119 FT
TOGW -   616, 125 LB
FUEL -   291, 401 LB
L/D -   25. 99
MAC -   22. 88 FT
SPAN -   255. 91 FT
AR -   13. 54
C/4 SWEEP - 30 DEG
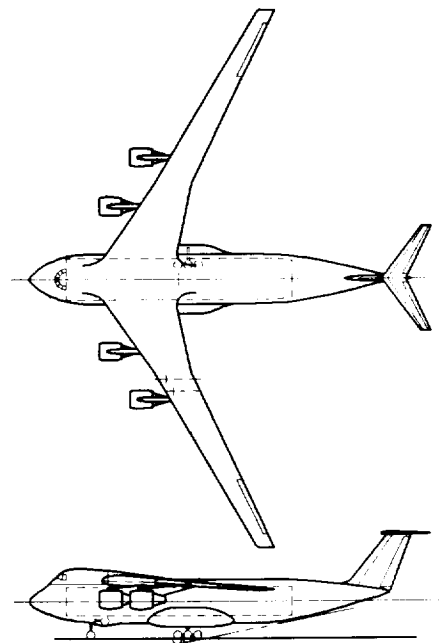
Figure 21. Turbulent flow baseline design concept.

CHANGE %

	HLFC BASELINE	NO HLFC ON EMP.	NO LOWER SURF. HLFC
WEIGHTS			
OPERATING EMPTY	5.4	5.4	7.9
GROSS	−4.0	−4.2	−0.6
FUEL CONSUMPTION	−13.4	−13.7	−7.9
LIFT TO DRAG RATIO	18.4	18.2	12.5

Figure 22. Benefits of HLFC.

SUBSTANTIAL PROGRESS MADE IN NASA/INDUSTRY PROGRAM
OVER PAST 10 YEARS

- CURRENT FLIGHT TESTS HAVE DEMONSTRATED SOLUTION TO LEADING EDGE CONTAMINATION PROBLEM. LAMINAR FLOW OBTAINED ON SLOTTED AND PERFORATED SURFACES

- $2.28 MILLION, 4 YEAR ENABLING TECHNOLOGY DEVELOPMENT EFFORT STARTING IN LATE 1985 IS PART OF NASA R&T BASE FUNDING.

- A SIMPLIFIED HYBRID LFC CONCEPT PROVIDES NEAR TERM APPLICATION AND ACCELERATED EFFORT IS WARRANTED

- LFC DATA BASE IN WIND TUNNEL AND FLIGHT TESTS HAS BEEN LIMITED TO A MAXIMUM REYNOLDS NUMBER OF 20 MILLION

Figure 23. Status of laminar-flow control activities.

NEED FLIGHT EXPERIMENTAL PROGRAM ON SWEPT WING AIRCRAFT WITH
HYBRID LFC TO OBTAIN REQUIRED DATA AT HIGH REYNOLDS NUMBERS,
30 - 50 MILLION, REPRESENTATIVE OF TRANSPORT AIRCRAFT OPERATION

- OBTAIN PHYSICAL FLOW PROPERTIES OF THE BOUNDARY LAYER INCLUDING L.E. CROSSFLOW AND TOLLMIEN-SCHLICHTING EFFECTS AND TRANSITION LOCATION

- COMPARE PHYSICAL FLOW WITH THAT PREDICTED BY TRANSONIC VISCOUS FLOW COMPUTATIONAL METHODS

- THESE HIGH REYNOLDS NUMBER TRANSONIC DATA CANNOT BE OBTAINED IN WIND TUNNEL TESTS

- NO DATA BASE OF THIS TYPE EXISTS FOR THE DESIGN OF A HYBRID LFC SYSTEM FOR TRANSPORT AIRCRAFT

- THIS PROGRAM CLEARLY FITS NASA ROLE IN TECHNOLOGY DEVELOPMENT FOR EMERGING TECHNOLOGIES

Figure 24. Future development needs in hybrid LFC.

- MUST MAINTAIN OUR EDGE OVER FOREIGN COMPETITION. THIS IS BEST DONE BY THE HYBRID LFC FLIGHT EXPERIMENTAL PROGRAM

- THERE IS FOREIGN ACTIVITY UNDER WAY ON NATURAL LAMINAR FLOW BY AIRBUS, DORNIER, MBB AND ONERA

- SOME BUDGET REDUCTIONS ARE ALREADY BEING IMPOSED ON THE NASA VISCOUS DRAG REDUCTION PROGRAM.

- INDUSTRY IS NOT YET READY TO PROCEED WITH THE DESIGN AND FABRICATION OF A HYBRID LFC SYSTEM DUE TO THE LACK OF REQUIRED DATA BASE FOR TRANSPORT AIRCRAFT APPLICATION

- THE ATTAINMENT OF THE REQUIRED PHYSICAL FLOW DATA BASE IS BEST ACCOMPLISHED BY CONTINUATION OF THE CURRENT NASA/INDUSTRY LAMINAR FLOW PROGRAM

Figure 25. Concluding remarks.

LAMINAR FLOW - THE CESSNA PERSPECTIVE

B. E. Peterman
Cessna Aircraft Company
Wichita, Kansas

ABSTRACT

A review of Natural Laminar Flow (NLF) and Laminar-Flow Control activities over the last twenty years at Cessna Aircraft Company is presented. Expected NLF benefits and remaining challenges are then described.

INTRODUCTION

The question might well be, "Why is Cessna involved in NLF Research and Development?" It's simply that we're convinced that there is a worthwhile prize in terms of speed increase, or engine size and fuel flow decrease. In other words, airplane efficiency _can_ be improved and we want to apply the improvements to our products.

We are indebted to NASA for reviving the interest in this fundamental phenomenon and its control. Our involvement in the subject at Cessna goes back over twenty years — both in research and production application — so in a sense it's not new. But, the understanding and resulting benefits continue to increase and NASA's involvement is essential and applauded.

Work in NLF is like seeking a sunken treasure. After becoming convinced that it's worth going after, comes the realization that success will most likely come only by systematic and persistent pursuit of the goal. We believe that we remain on that course.

CESSNA BACKGROUND

The Cessna NLF experience goes back to the mid-1960's when Cessna and a number of other General Aviation manufacturers began using NASA 6-Series laminar flow airfoils.

Cessna 177 Cardinal	— 64 Series Airfoil
Cessna 210G Centurion	— 64 Series Airfoil
Piper Comanche	— 64 Series Airfoil
Piper Cherokee	— 65 Series Airfoil
Mooney Mark 20	— 63 and 64 Series Airfoils
Beech Musketeer	— 63 Series Airfoil
Bede BD-1*	— 63 Series Airfoil

(*later Grumman-American Yankee)

In addition to the two models shown and other production derivatives, Cessna built prototypes of two twin-engine models with 6-Series airfoils that did not go into production.

Our results with laminar flow airfoils in the 1960's and early 1970's was mixed. We know from more recent tests that some laminar flow was achieved but drag reduction based on gross performance measurements at the time was not overwhelming. At the time it was felt that conventional construction methods prevented achieving the laminar flow for which the airfoil sections were developed. Further, although the 210 was successful with the basic 6-Series airfoil, other applications required modification either to improve stall characteristics or in an attempt to improve performance.

In 1981 when Bruce Holmes of NASA initiated a review of NLF, Cessna cooperated with flight tests of transition point visualization (Fig. 1). These tests utilized a sublimating chemical and contributed to the realization that there was more NLF with real-world aircraft construction than had been earlier thought.   As shown on the right of Figure 1, there is little difference in the extent of laminar flow between the inboard section, which was smoothed and painted, and the outboard section, which was only painted.   We also all began to realize that more NLF than expected meant that airplane drag had been apportioned incorrectly.   More importantly, it meant that NLF was worth pursuing, especially since Holmes' investigations showed that bugs and other irregularities were not as detrimental as expected.

Figure 1

This research led to Citation III transition measurements which introduced higher speeds and modest wing sweep. Hot film transition measurement techniques were refined during these tests. Figure 2 shows the test aircraft on the left and laminar flow results on the right. The lack of laminar flow behind the stall strip is in contrast to that which exists on the remainder of the test section. No significance should be attached to the speed brake position at the time the photo was taken.

ORIGINAL PAGE
BLACK AND WHITE PHOTOGRAPH
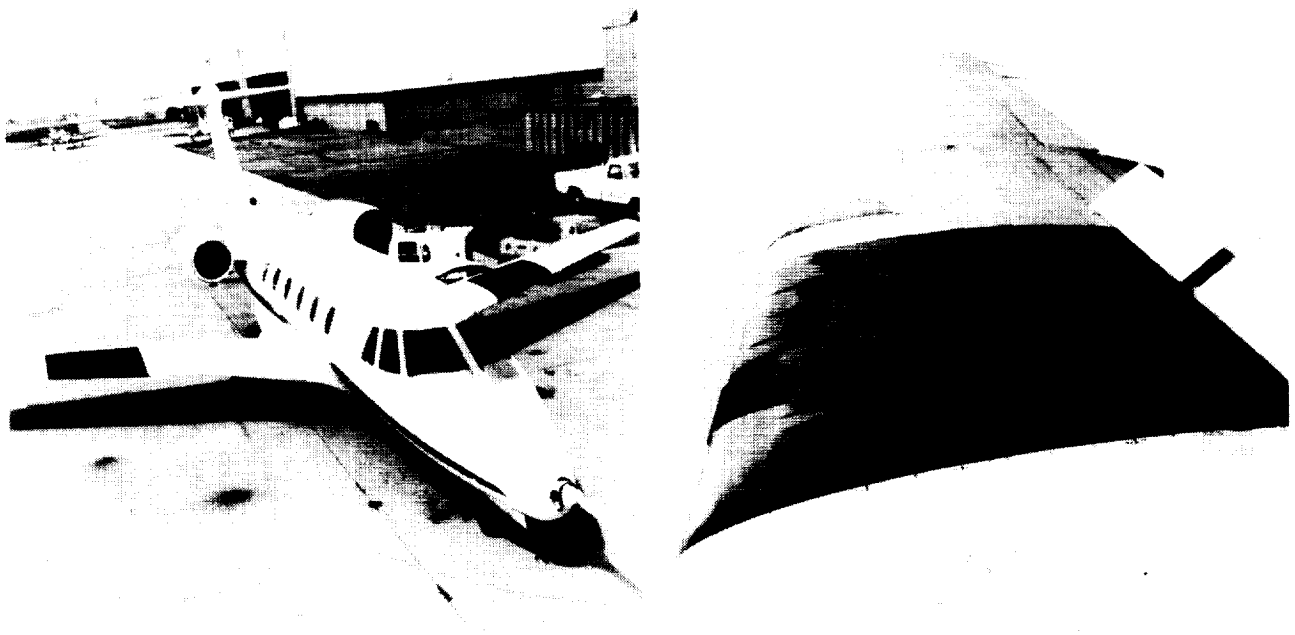
Figure 2

C-2

RECENT WING NLF RESEARCH: AIRFOIL IMPROVEMENTS

Additional tests on a Cessna 210 involved measurements above a 20,000 foot altitude on a modified airfoil designed by Gerry Gregorek at Ohio State. Good laminar runs were obtained on the lower surface as shown in Figure 3.

Figure 3

As our interest in NLF continued to increase, the 210 prototype wing was modified as shown in Figure 4 with the NLF (1)-0414(F) airfoil designed by J. K. Viken of Complere, Inc. and W. Pfenninger of Analytical Services and Materials, Inc. The program involved construction and flight tests by Cessna and both full-scale and small-scale wind tunnel tests by NASA.

A mixture of polyester resin and glass microballoons was applied to the basic metal construction wing and contoured using sailplane profiling methods. Local waviness was less than 0.003 inch per 2 inches, with most of the forward 70% chord within 0.001 inch per 2 inches. With these tight tolerances, which were more rigorous than necessary, the results were spectacular! Also, since the wing had conventional flaps, ailerons, and spoilers, the need for other means of lift and roll control was avoided.

The wing worked as predicted with runs of laminar flow at cruise to approximately 70% chord; section drag (as measured with an integrating wake rake) matched values obtained in the wind tunnel. No unusual behavior occurred when transition was induced at the leading edge with a trip strip, and stall behavior was good. In other words, a very workable wing was obtained.

The speed increment between having no laminar flow (transition at 5%c) and full laminar flow on the wing was 14 Kts or about 7%.
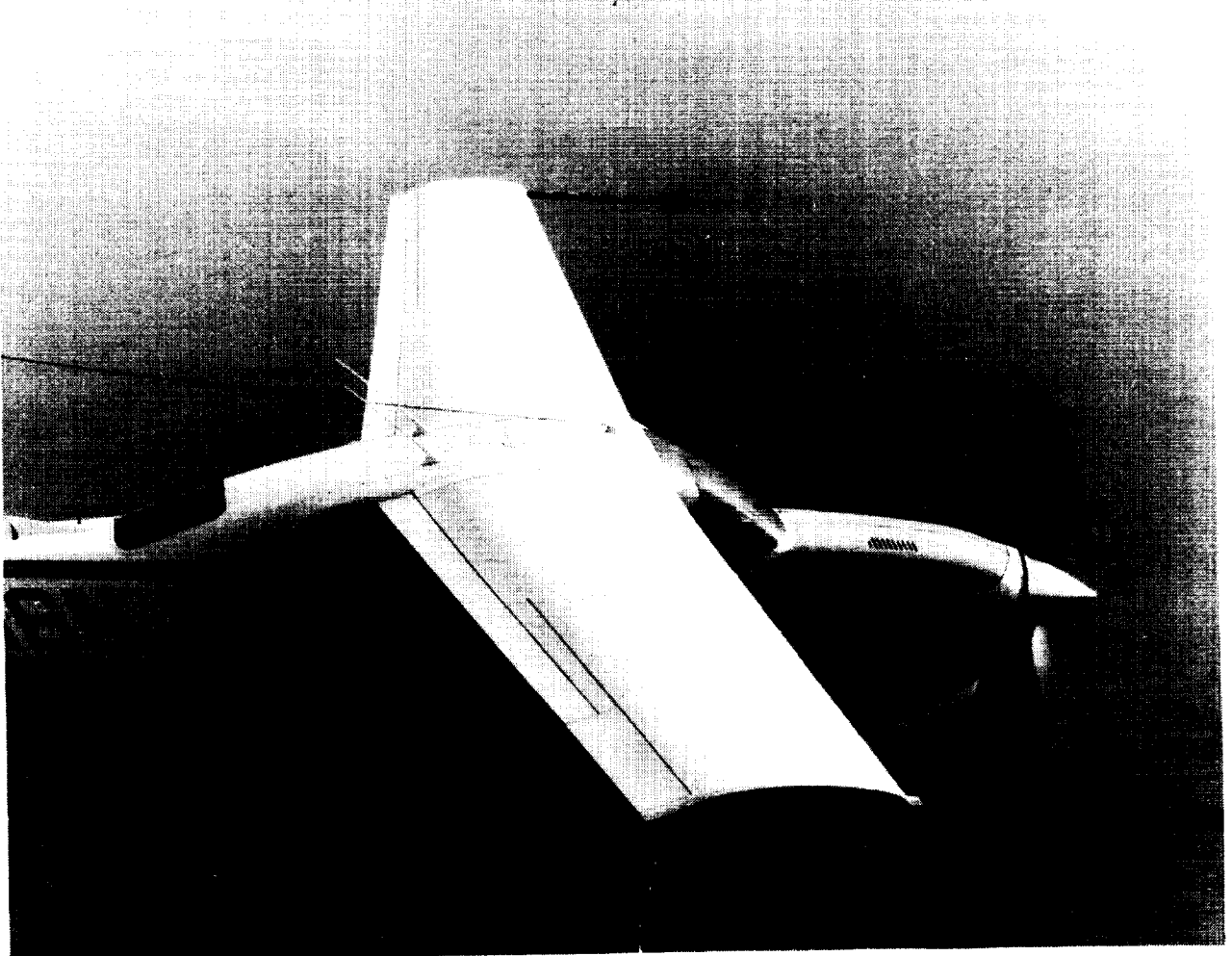
Figure 4

THREE-DIMENSIONAL BODY NLF RESEARCH

NASA has been working the problem of NLF on 3-D bodies for several years. From lofts of the Cessna T303 fuselage nose provided to NASA by Cessna, computer models of the shape were developed and it was concluded that the nose shapes had good potential for laminar flow. Flight tests in conjunction with Kansas University and NASA are now in the final stage. Preliminary results are encouraging with laminar runs beyond the propeller plane. Figure 5 depicts the test aircraft and results of an initial flight.

ORIGINAL PAGE IS
OF POOR QUALITY
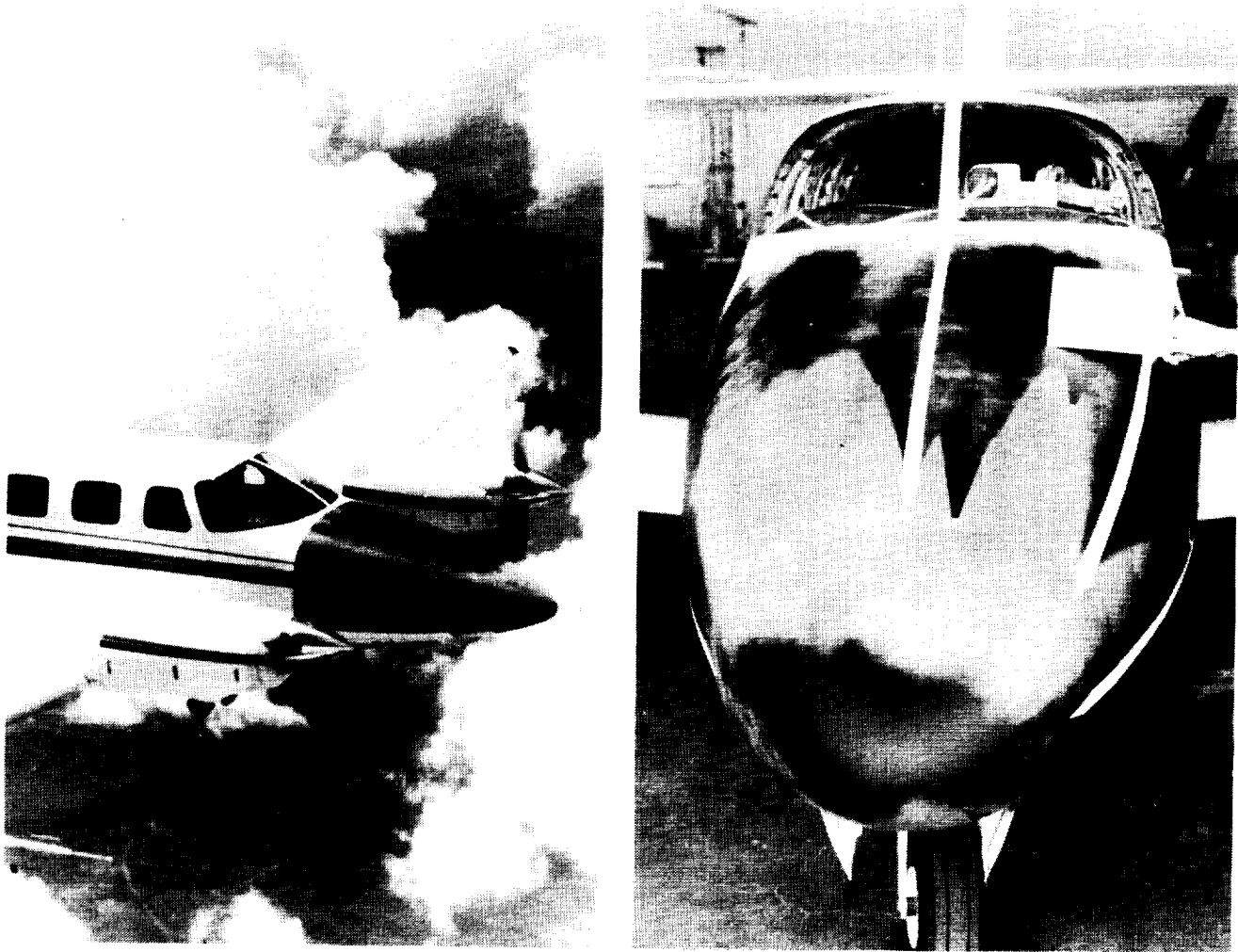
Figure 5

The companion to natural laminar flow is laminar-flow control. While the mechanical simplicity of achieving laminar flow by careful tailoring of pressure distribution through contour design is desirable, this may not always be possible. In that case, laminar-flow control through boundary-layer suction may be appropriate.

Cessna's experience with laminar-flow control consists of experiments on the Citation III nacelle under contract to Rohr Industries (Fig. 6).

The nacelle was lengthened approximately 10 inches and the exterior surface of the forward 40% was re-skinned with DYNAROHR^{TM}, which has a woven wire exterior surface with honeycomb backup. Suction was applied through the honeycomb. By adjusting the honeycomb size and interior suction, surface suction was controlled as desired.

During the tests, piping connected the surface pressure system to a low pressure tank in the fuselage. Surface pressures were measured and an array of hot film gages were used to determine boundary-layer transition from laminar to turbulent flow. The tests occurred in August and September of 1986 and all data were forwarded to Rohr.

Figure 6

EXPECTED NLF BENEFITS

A comparative study has been made, based on a conventional six-place, single engine aircraft weighing approximately 4700 lb. In one case, flow on the wing and tail was assumed turbulent and in the other, laminar. The NLF speed advantage is 12.5%, and specific range is over 11% better. If the laminar flow of current aircraft is considered, the benefits may be slightly less but still well worth the effort.

NLF CHALLENGES

A. Practical Construction

The new NLF wing has yet to be made on a production airplane. The Cessna 210 test wing is an aerodynamic proof-of-concept article. While it has conventional flaps, ailerons, spoilers and some access panels, it has not been fitted with landing lights, radar pods, pitot tubes, fuel or deicing. However, it is believed that these can be accommodated by paying attention to design details and carefully checking the results. No doubt some unsuspected opportunities will be found as the wing is developed further.

The question of metal versus composites remains, and either is probably acceptable. Therefore, cost and weight will determine which is better for the marketplace. In either approach, the wing surface will have to be built in a female mold for contour control, especially at rib locations. However, this has already been done with both metal and composites, so cost control is the only challenge.

B. Ice Protection

It is generally accepted that conventional deice boots will not be acceptable. The newer versions that have been or are being developed to minimize discontinuities may find acceptance. It is too early to say. Careful tests must be conducted.

TKS, glycol exuding systems are a definite possibility for NLF wings and tail surfaces. This system is used on the latest Citation SII business jet. Although B. J. Holmes' work (ref. 1) has shown that bugs aren't as significant a problem as first suspected, the TKS system has a bug clearing advantage. However, the cost may be prohibitive for small aircraft.

The newest possibility for NLF wing deicing is electro-impulse, which allows a smooth exterior surface. Cessna is quite familiar with this approach since icing flight tests were conducted on a Cessna Model 206 with the system applied to both the wing and tail leading edges and to the wing struts. Some of the testing was done in conjunction with Wichita State University working under NASA and State of Kansas sponsorship; the remainder has been done with in-house funding. As the system is being developed and structural fatigue considerations are being resolved, Cessna is grappling with making leading edges removable with joints that NLF will tolerate.

Thus, deicing is felt to be a solvable problem but it remains to be accomplished in the NLF environment.

C. Transonic NLF

As mentioned earlier, limited experiments have been conducted on the Citation III. NASA is working the transonic NLF problem with some promising results. While compressibility is beneficial, wing sweep is detrimental. It appears that by careful airfoil design and the use of a minimum sweep to prevent drag rise, useful runs of laminar flow may be achieved up to Mach 0.8. It is worth pursuing but will take extensive wind tunnel and flight testing.

D. Certification Rules

Cessna's main concern about this challenge is that it not become disproportionate. Aircraft with varying amounts of NLF have been produced for over twenty years. Although there is a drag change when NLF is lost, acceptable flight characteristics must be maintained; results to date indicate no compromise in safety. Each new certification should not become a research project. In determination to inform the pilot of the effects of losing laminar flow, straight-forward checks and a reasonable amount of testing must be provided. Further, practical data need to be presented, both for certification and in pilot manuals. These items become a real challenge in today's environment – but it may help to remember that NLF isn't new to production aircraft. It would also be beneficial to have test results with a modern NLF wing in the areas of certification concerns before new rule making is started.

SUMMARY

Cessna's perspective is based on over twenty years involvement in laminar flow work, for both research and application to production aircraft. Natural laminar flow is attainable and the more learned, the greater the potential gain. Manufacturing and deicing challenges will be overcome; methods are currently available but achieving solutions with acceptable production costs remains a goal. Nonetheless, aircraft with significant NLF will prevail. Efforts to keep certification reasonable must continue.

The basic thrust at Cessna is to attain greater and greater amounts of natural laminar flow. It provides the design simplicity and greatly aids in achieving significant improvements in aircraft performance.

REFERENCE

1. B. J. Holmes, C. J. Obara, and Long P. Yip: Natural Laminar-Flow Experiments on a Modern Airplane Surface, NASA TP-2256, June 1984.

LONG-RANGE LFC TRANSPORT

W. Pfenninger
Analytical Services & Materials Inc.,
Hampton, Virginia

LONG RANGE LFC TRANSPORT

A potential design for high-subsonic speed Laminar Flow Control (LFC) transport that can carry large payloads to any place on earth without refuelling is discussed (see Fig. 1). A cruise lift-to-drag ratio (L/D) of 39.4 appears feasible with 70% laminar flow on the wings, tails, nacelles, and struts, and a fully turbulent fuselage. Strut-braced wings with large span and aspect ratio are used to achieve lower induced drag-to-lift ratio. Additional performance gains appear possible with fuselage laminarization. An example of a 180,000 kg take-off gross weight LFC transport airplane with 50,000 kg payload (250 passengers plus cargo) and a cruising speed of $M_{cruise} = 0.83$ is described.

Figure 1

90
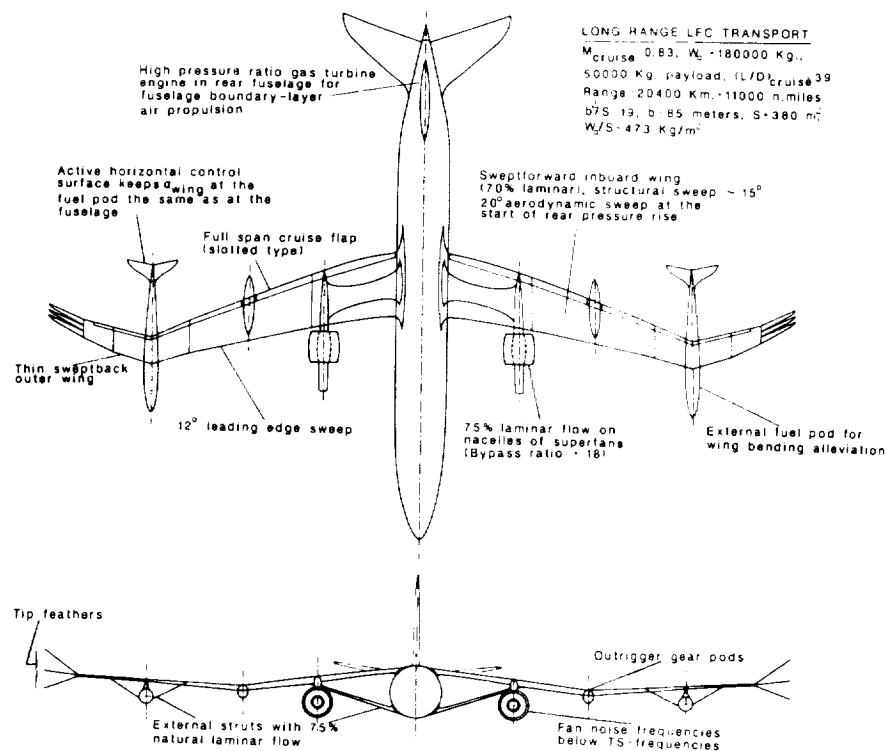
REDUCTION OF WING PROFILE DRAG

The variation of wing profile drag, C_{D_∞} , with chord Reynolds number, Re_c, is shown in Fig. 2 for various degrees of suction laminarization, as indicated by the transition location $(x/c)_T$. The wing profile drag coefficient at $Re_c = 30 \times 10^6$ is 0.0067 for a fully turbulent flow, 0.0024 with 70% laminarization, and 0.0010 with 100% laminar flow. These numbers include suction drag penalty. The additional drag due to sweep, especially at high Reynolds numbers, is primarily the result of higher suction rates required in the front and rear part of the wing to control sweep-induced boundary-layer crossflow instability.

(A)
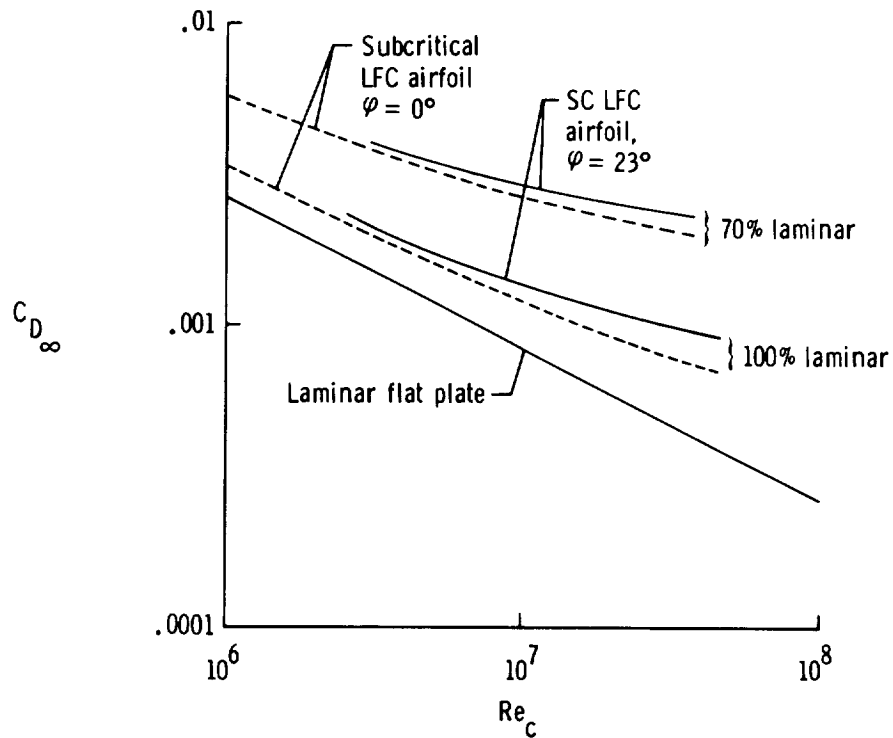
Figure 2
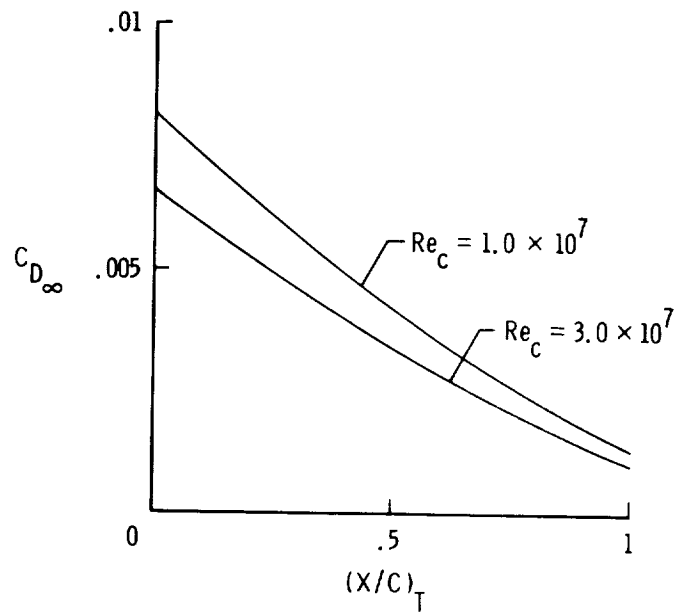
(B)

Figure 2

LAMINARIZATION OF SWEPT LFC WINGS

Boundary layer crossflow instability, as well as spanwise turbulent contamination along the wing attachment line, critically affect the design of strongly swept LFC wings at high Re_c. Swept LFC wings are inherently more sensitive to 3-D leading-edge roughness: in addition to higher local flow velocities in the leading-edge region of the swept wing, the streamwise disturbance vorticity induced by 3-D roughness is adversely superimposed on the sweep-induced streamwise vorticities to cause early transition. Indeed, leading-edge flyspecks often caused extensive loss of laminar flow in the X-21 LFC wing with its 33^0 swept leading edge at $M_\infty = 0.75$ and 12,000 meters altitude (Ref. 1) while full chord laminar flow was often observed on the F94 LFC wing glove with its 10^0 swept leading edge at $M_\infty = 0.65$ and altitudes above 6,000 - 7,000 meters (Ref. 2), despite the presence of leading-edge flyspecks. Similarly, atmospheric ice crystals apparently did not influence transition on the F94 LFC glove, while they often caused extensive loss of laminar flow on the X-21 wing. Therefore, to alleviate these sweep-induced problems, wing sweep should be reduced by raising the 2-D airfoil design Mach number $M_{\infty_{Design}}$, while maintaining satisfactory off-design characteristics. To simplify the wing design and minimize the LFC wing weight penalty, natural laminar flow should be maintained in the area of wing bending structure.

SC LFC AIRFOIL DESIGN CONSIDERATIONS:

DESIGN TOWARD HIGH MACH NUMBERS

The design Mach number, $M_{\infty_{Design}}$, of supercritical (SC) LFC airfoils is increased by thinning the airfoil either over the entire chord or by undercutting the structurally less-critical front and rear lower surfaces, resulting in relatively sharp-nosed SC airfoils (see examples of derivatives of SC LFC airfoil X63T18S: Fig. 3a and 3(b)). Lift is carried primarily in the front and rear sections of the wing, while the lower-surface center bulge, operating close to sonic condition, contributes primarily to airfoil thickness. The design Mach number is further increased by having an extensive low supersonic flat rooftop pressure distribution (M = 1.08 - 1.10) on the upper surface, preceded far upstream by a supersonic pressure minimum ($M \approx 1.20$ at s/c = 0.015 to 0.02), and followed by a steep subsonic rear pressure rise region where low drag boundary-layer suction is applied for full-chord laminarization. Alternately, a satisfactory steep pressure rise appears possible without suction on a slotted (2- element) airfoil by optimally subdividing the rear pressure rise on the wing and the slotted trailing edge cruise flap. Whitcomb's first SC airfoil had, indeed, such a slotted trailing edge flap, except that the flap chord had been larger (Ref. 3). The flow exit Mach number at the flap was then about sonic, resulting in an excessively sensitive flow in the flap gap and a non-optimum subdivision of the rear pressure rise over wing and flap.

(A)

Figure 3

(B)

Figure 3

DESIGN OF LEADING-EDGE REGION

The superiority of supercritical airfoils (that have an extensive upper surface flat rooftop pressure distribution at low supersonic speeds, preceded by a front supersonic minimum) is explained as follows: The relatively strong expansion waves, radiating from the high-velocity region of the supersonic pressure minimum, are reflected from the sonic line as strong compression waves to the surface. This reduces the supersonic flow velocities further downstream in the flat rooftop area. As a result, the height of the supersonic bubble decreases. Alternately, the design Mach number increases for a given supersonic bubble height. The same result follows from elementary considerations: Since the supersonic flow of the front upper surface decays relatively fast towards the sonic line as a result of the small radius of curvature, substantially higher supersonic Mach numbers and correspondingly increased lift appear possible in the leading-edge region of the upper surface without significantly affecting the height of the supersonic bubble. This results in an increase in design lift coefficient, $C_{L_{Design}}$ or design Mach number (at a given $C_{L_{Design}}$). As the radius of curvature of the upper surface continuously increases in the downstream direction, the supersonic flow in the pressure-rise area downstream of the front pressure minimum must progressively decelerate and asymptotically join the extensive flat rooftop pressure distribution. The upper-surface nose contour of the SC LFC X66 airfoil (Fig. 4(a)) is characteristic to SC airfoils with a far upstream supersonic pressure minimum; it decisively influences the entire flow of the supersonic zone of the upper surface. Figure 4(b) shows the leading-edge contour of a similar SC LFC airfoil but with a substantially blunter nose and a similar supersonic pressure minimum on the front upper surface, i.e., the same considerations apply to SC airfoils with blunter leading edges.

$$0.1C$$

(A)

Figure 4

0.1C

(B)
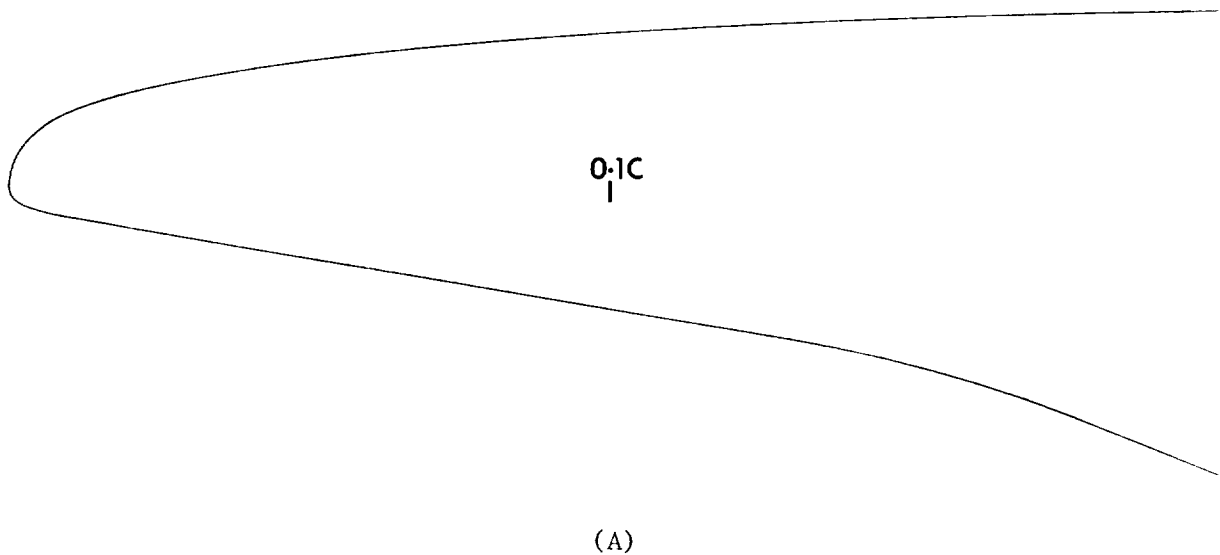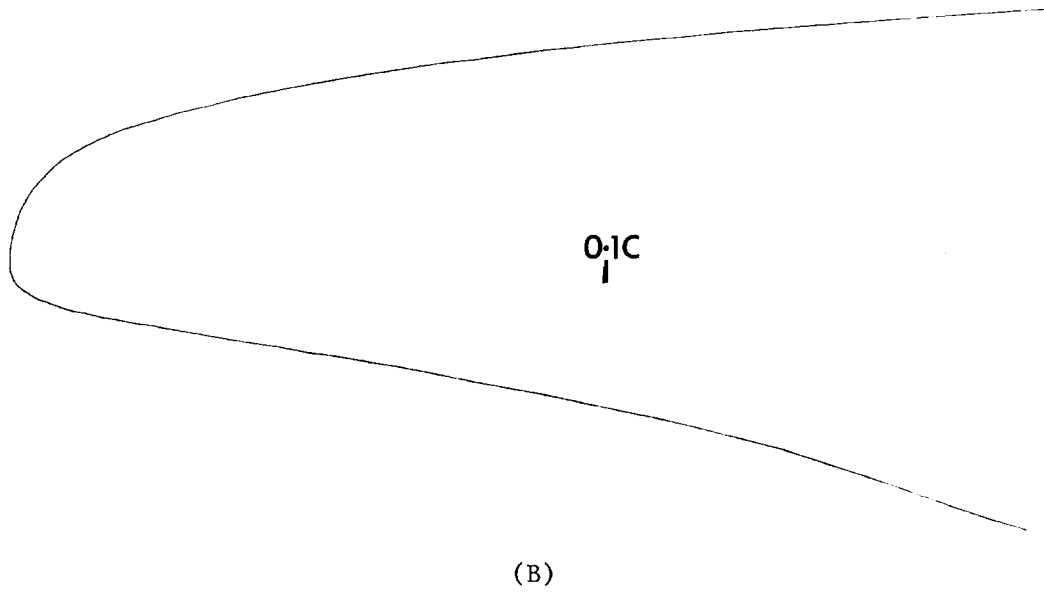
Figure 4

SHOCK PREVENTION ON SC AIRFOILS
AT OFF-DESIGN MACH NUMBERS

To delay or prevent off-design shock formation on SC LFC airfoils with a pressure minimum on the front upper surface at $M_\infty < M_{\infty_{Design}}$, tangency of the upper surface hodograph streamline with the hodograph characteristics (equivalent to limit line formation) must be delayed or avoided. This is possible by flattening the upper surface hodograph streamline, such that the flow on the upper surface decelerates sufficiently slowly and continuously in the hodograph plane over a particularly wide angular range of upper surface flow inclination angles form the location of the pressure minimum to the rooftop zone (see upper surface hodograph streamline of airfoil X66, Fig. 5). This implies that the supersonic pressure minimum should be located as far upstream as practical in a strongly inclined upper surface area. To further ensure a continuous upper surface flow deceleration in the hodograph plane for the prevention of shock formation in the entire $M_\infty - range$ below $M_{\infty_{Design}}$, the chordwise pressure gradients downstream of the front pressure minimum at design must be tailored to the local upper surface curvature, i.e., these pressure gradients must progressively decrease in downstream direction and asymptotically approach the flat rooftop value. Indeed, a Korn-Garabedian analysis for the similar X63T18S airfoil (Ref. 4) has not shown any double shock formation at $M_\infty < M_{\infty_{Design}}$ at constant α_{wing}.
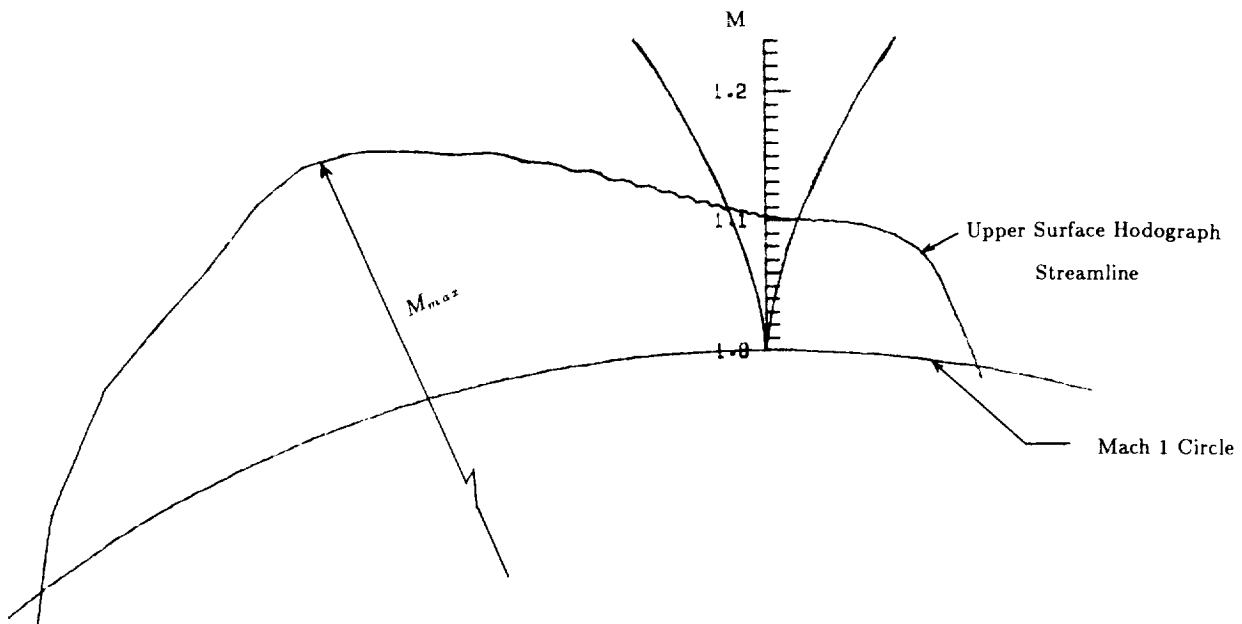
Figure 5

SHOCK-FREE DESIGN OF SC AIRFOILS

A Korn-Garabedian analysis (Ref. 4) of SC LFC airfoils with and without a particularly sharp front supersonic pressure minimum on the upper surface show a superior upper shock-free low-drag C_L − *limit* for the peaked airfoil compared to the airfoil with a flat supersonic rooftop pressure distribution and no front pressure minimum (Fig. 6). Since the supersonic flow on SC airfoils responds essentially to angular flow changes, the lift coefficient, C_L, of SC LFC airfoils should be varied by changing the airfoil camber at a constant angle-of-attack, α_{wing}, by deflecting a small-chord full-span trailing-edge cruise flap. A slotted flap for a SC LFC airfoil without suction in the steep rear pressure-rise area of the upper surface is preferred.

Figure 6

(B)

Figure 6

LAMINARIZATION OF SWEPT WINGS:

BOUNDARY-LAYER CROSSFLOW INSTABILITY

On SC LFC airfoils with a front supersonic pressure minimum on the upper surface, the boundary-layer crossflow, generated in the acceleration zone can be largely cancelled by a boundary-layer crossflow of opposite sign, generated in the pressure-rise zone downstream of the front pressure minimum (Fig. 7). If the boundary-layer crossflow can be minimized in the front acceleration zone of the upper surface by thinning the leading edge (undercutting the front lower surface), accelerating the flow rapidly to the supersonic pressure minimum, and/or applying local suction preferably in the area where the boundary-layer crossflow is about neutrally stable, then the crossflow instability is practically absent in the flat rooftop area of the upper surface and streamwise vortex - interaction with amplified Tollmien-Schlichting (TS) waves is practically eliminated in this area. For relatively sharp-nosed SC LFC airfoils of the X66- type, generally no suction is needed for the control of boundary- layer crossflow instability in the front acceleration zone up to $Re_c = 30$ million with 23^0 sweep.
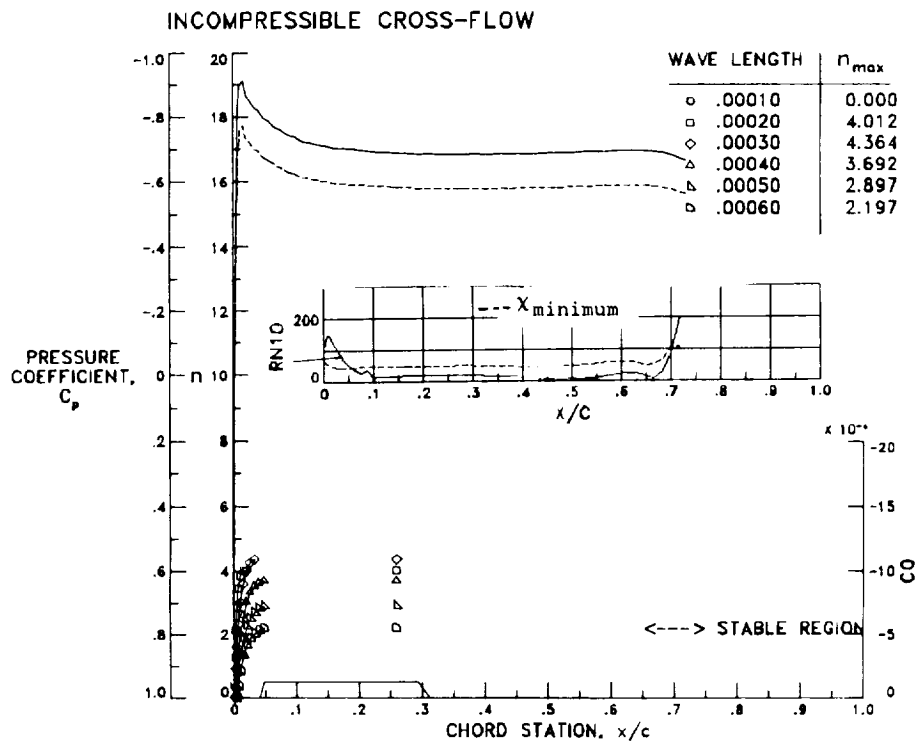
Figure 7

EFFECT OF TAPER

On tapered swept-back or swept-forward SC wings, the isobar sweep decreases or increases, respectively, from the wing leading edge to the trailing edge to superimpose an additional streamwise flow deceleration or acceleration (Fig. 8). The TS-instability in the flat rooftop region of the upper surface of X66-type SC LFC wings is then influenced in a favorable manner on tapered swept-forward wings and vice-versa on swept-back LFC wings, optimized for a high cruise Mach number, will have a slightly adverse upper-surface rooftop pressure distribution, preceded by a more pronounced supersonic pressure minimum. Additional spanwise suction strips may then be required in the rooftop region for adequate boundary-layer stabilization against amplified TS-waves. The avoidance of such slightly adverse upper-surface rooftop pressure distributions on tapered swept- back wings entails a penalty on the cruise Mach number.
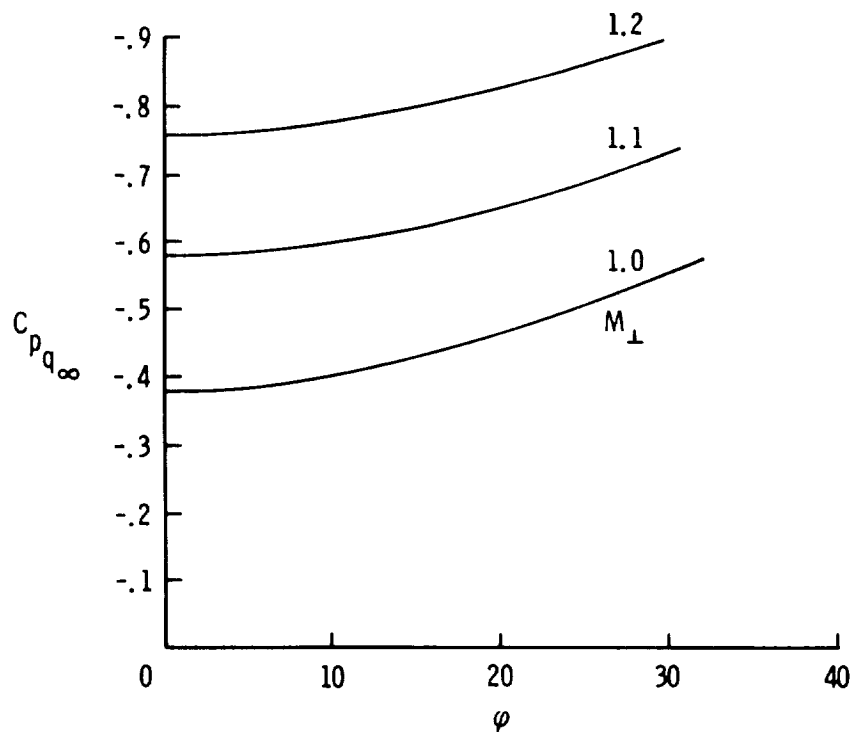
Figure 8

WING CHORD-REYNOLDS NUMBER CONSIDERATIONS

In addition to performance considerations, the design of a large LFC airplane is strongly influenced by all the many factors that affect suction laminarization. Therefore, since boundary-layer stability problems are alleviated at lower length Reynolds numbers and since the surface tolerances and roughness are inversely proportional to the unit Reynolds numbers, U_∞/ν , larger LFC airplanes should be designed such that performance optimization is compatible with the desire to alleviate the laminarization problems involved.

Since $Re_c = U_\infty C/\nu = 2\sqrt{w}\frac{\sqrt{(w/s)/(b^2/s)}}{a\mu C_L M}$ and $U = \frac{2(w/s)}{a\mu C_L M}$, it follows that Re_c is decreased by lowering the wing loading (W/s), raising the wing aspect ratio (b^2/s) and working with reasonably high cruise lift coefficients C_L, being easier possible with higher wing aspect ratios. Here, a is the velocity of sound, μ is the absolute viscosity of air, W is the airplane weight, s is the wing reference area, U_∞ is the freestream velocity, C is the mean-aerodynamic chord of the wing, ν is the kinematic viscosity of air, b is the wing span, and M is the Mach number. Thus the desire to reduce the induced drag-to-lift ratio $D_{ind.}/L = W/\pi q b^2$ (q is the dynamic pressure) for superior performance is well compatible with the desire to reduce Re_c.

INFLUENCE OF BOUNDARY-LAYER DISTURBANCES

For the design of a high subsonic speed LFC transport airplane the question arises concerning the initial disturbances introduced into the boundary layer. This is particularly important for LFC airplanes with extensive natural laminar flow in the flat rooftop area of the upper surface in the absence of suction (distributed suction along the entire chord highly stabilizes the boundary layer to allow correspondingly increased initial disturbances). With the atmospheric turbulence microscale generally much too weak to affect transition, the initial boundary-layer disturbances are generated primarily by the airplane and its propulsion system and possibly by suction-induced disturbances. As a result, it is particularly important to minimize the influence of propulsion noise by raising the airplane lift-to-drag ratio and avoiding propulsion noise in the frequency range of strongly amplified TS-disturbances. The present high bypass ratio fan engines (BPR $\approx$ 5 to 6) may not appear attractive for large LFC airplanes since their fan-tones and shock noise contain frequencies in the range of the strongly amplified TS-disturbances; the proposed super fans (BPR = 15 to 20) are much better in this respect since they rotate at relatively low subsonic tip speeds and allow substantial axial decaying of both the fan rotor pressure field and the many fan rotor-stator interference acoustic modes in the fan duct. Most of the fan tone noise is therefore generated at relatively low frequencies which are below the frequency range of strongly amplified TS-waves.

Turbulent fuselage boundary-layer noise may also contribute to initial boundary-layer disturbances. Turbulent fuselage boundary-layer noise of the dipole type generated by structural discontinuities such as fuselage bulkheads, etc., is more efficient sound radiator than quadruple-type boundary-layer noise (Ref. 5) and should, therefore, be avoided by designing the fuselage essentially as a continuous sandwich structure. The remaining quadruple-type fuselage boundary-layer noise is a rather inefficient sound radiator with relatively low frequencies.

PROS AND CONS OF SWEPT-FORWARD SC LFC WINGS

A swept-forward wing had been chosen in the area inboard of the external fuel pods for the large LFC airplanes discussed in this paper for several reasons:

1) As mentioned previously, the increasing sweep of the wing isobar from the wing leading to the trailing edge gives a more favorable chordwise pressure distribution for natural laminar flow in the region of the main wing-box structure, as compared to a swept-back wing.

2) The aerodynamic isobar sweep of a tapered swept-forward wing at the start of the rear pressure rise is larger than the wing structural sweep (especially with a steep rear pressure rise with suction or a slotted cruise flap,) and raises the aerodynamic span for a given structural span, and vice versa for a swept-back wing.

3) With the substantially reduced leading-edge sweep, both boundary-layer crossflow and leading-edge contamination problems (caused by flyspecks and atmospheric ice crystals) are greatly alleviated. As was found on the F94 LFC wing glove with its 10^0 swept leading edge (Ref. 2), laminar flow may even be possible in the presence of flyspecks at altitudes considerably below the airplane cruise altitude.

Disadvantages of swept-forward wings are wing divergence, excessive negative pressure peaks in the leading-edge region at the wing root, and spanwise boundary-layer crossflow at high C_L's near the wing root. For composite wings, wing divergence can be alleviated by properly aligning the spanwise wing bending fibers, sweeping back the wing outboard of the fuel pod, and actively deflecting the cruise flap and the active control surface of the fuel pod. The adverse aerodynamic behavior of the swept-forward wing in the wing root region can be alleviated by a suitable area-ruling of the fuselage and reducing the wing sweep near the root; this may be possible by thinning the inboard wing. (With the rapidly decreasing wing bending moments in the strut-braced inboard wing region, this is structurally possible). At the same time C_{D_∞} of this thinner inboard wing region is reduced somewhat to partially compensate for the strut parasite drag. With the forward sweep of the inboard wing thus reduced, spanwise boundary-layer crossflow near the wing root at higher C_L's is alleviated.

The rapid reduction of the inboard wing thickness also decreases the local Mach number of the wing upper surface in the region of the wing-strut intersection (the local flow is essentially 3-dimensional) and this allows a thicker wing in this structurally critical area where the moments are largest.

The outboard wing is particularly thin to minimize local wing sweep and improve high-speed buffeting near the wing tip where wing deflections are particularly large.

Variable camber leading edges were included in the design of this large LFC airplane to improve the low-speed characteristics of the X66 SC LFC airfoil with its relatively sharp leading edge. For take-off and especially landing, a slotted trailing-edge high-lift flap is assumed. Further design calculations have been conducted with similar SC LFC airfoils having a blunter leading edge, to further improve the high-lift characteristics at lower M_∞'s, this results in a penalty of about 0.004 to 0.005 in cruise Mach number.

APPROACHES TO INCREASE WING SPAN

Excessive structural weights associated with large span wings can be avoided by designing the wings to be supported by a wide-chord low-drag laminar strut. This reduces the wing bending and torsional moments and deformations. The reduced induced drag of the large span strut-braced wing by far compensates for the strut parasite drag.

A further increase in wing span and a reduction in induced drag can be achieved with an external, low-drag laminar-flow fuel nacelle located on the outer part of the wing and braced with laminar struts. These fuel nacelles reduce wing bending moments. Wing torsional deformations can be actively controlled by horizontal control surfaces at the rear of the fuel nacelle. The wing angle-of-attack at these nacelle locations should be kept at the same value as that at the wing root with the aid of suitable sensors. Excessive negative bending moments induced by these fuel nacelles during taxiing may be avoided by partially filling them on the ground and filling them up completely by redistributing fuel after take-off.

The wing span and aspect ratio can also be further increased with the use of advanced structural materials and actively lowering wing gust-, maneuver-, and dynamic loads as well as aeroelastic wing deformations; a full span cruise flap will permit this. The aeroelastic wing angle-of-attack changes induced by flap deflection can be largely compensated by deflecting the active horizontal control surfaces of the external fuel pods.

TOLLMIEN-SCHLICHTING (TS) INSTABILITY

With boundary-layer crossflow practically absent in the region of the upper-surface rooftop pressure distribution, the boundary layer must be stabilized essentially against amplified TS-waves by means of weak distributed suction applied form 5%- chord to 30% chord (non-dimensional suction massflow rates $C_q = 1.2 \times 10^{-4} at Re_c = 30 \times 10^6$, 23^0 sweep). Figure 9 presents the corresponding TS-growth rates using the COSAL computer program (Ref. 6). The stabilizing influence of compressibility on the growth of amplified TS-waves is crucial for high subsonic speed LFC airplanes. For a 23^0 swept SC LFC wing of the X66-type, the laminar-flow length Reynolds number at $M_\infty = 0.83$ is 2.5 times larger than in incompressible flow for the same TS-disturbance growth factor. Very substantial breaks in suction distribution are then possible in the flat rooftop region of the upper surface at cruise conditions.

COMPRESSIBLE T-S

T-S FREQ., Hz	n_{max}
o 2000.	4.745
□ 3000.	9.683
◇ 4000.	10.364
▵ 5000.	6.448
▵ 6000.	4.179
▵ 7000.	1.958
□ 8000.	2.043
o 9000.	1.988
◇ 10000.	.456

STABLE REGION

X/C
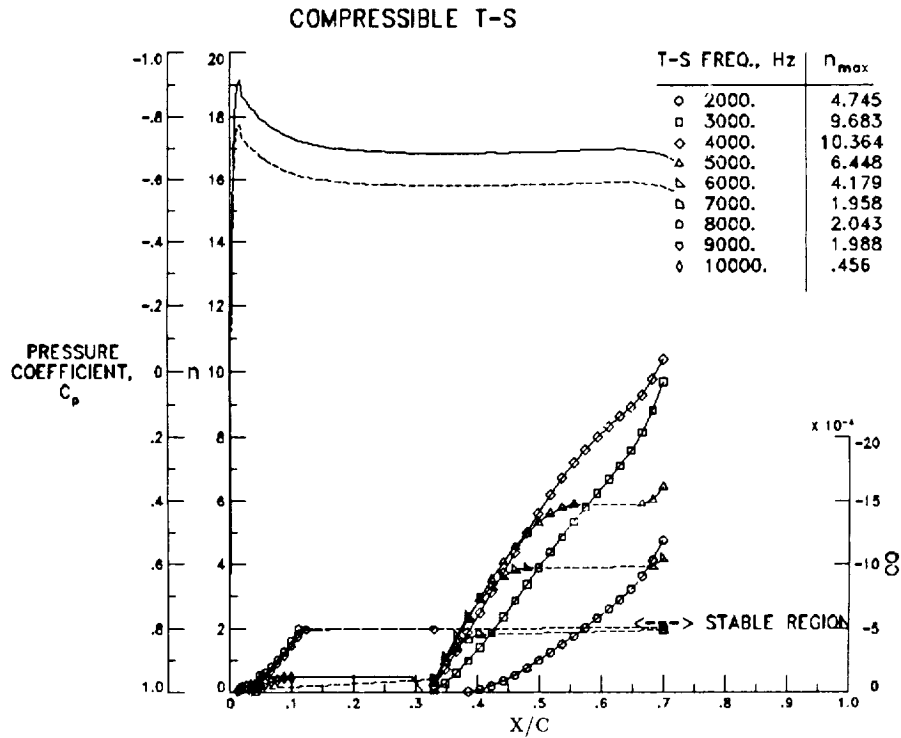
Figure 9

FUSELAGE LAMINARIZATION

Since the turbulent fuselage drag represents a large percentage drag contribution to an otherwise laminar LFC airplane, the question arises concerning the possible suction laminarization of the fuselage at high length Reynolds numbers, Re_L. Drag results obtained in the Ames 12-foot tunnel (Ref. 7) for the Northrop Reichardt LFC body of revolution (8 : 1 fineness ratio, 12-foot long) with minimum drag coefficient $C_{D_{min}} = 0.00026$ (based on body wetted area and including suction drag) are shown in Fig. 10. Drag reductions for this body were percentage-wise larger than for all-laminar flow wings tested at that time. The question then remains concerning the possible laminar flow Re_L − $values$ of an LFC fuselage in fight at high subsonic speeds. In view of the practically non-existent atmospheric turbulence microscale responsible for transition $(Re_{L_{Lamina}})$ obtained for the Reichardt LFC body may be possibly doubled in low-speed flight to 120×10^6. The stabilizing influence of compressibility on the growth of amplified TS-waves may again increase this to perhaps 200-240 million in flight at high subsonic cruising speeds.

For the present, relatively conservative example, a fully turbulent fuselage was assumed, accepting a 7% and 10% equivalent fuselage drag reduction by riblets (Ref. 8) and fuselage boundary-layer air propulsion (Ref. 9) in the rear part of the fuselage, respectively.
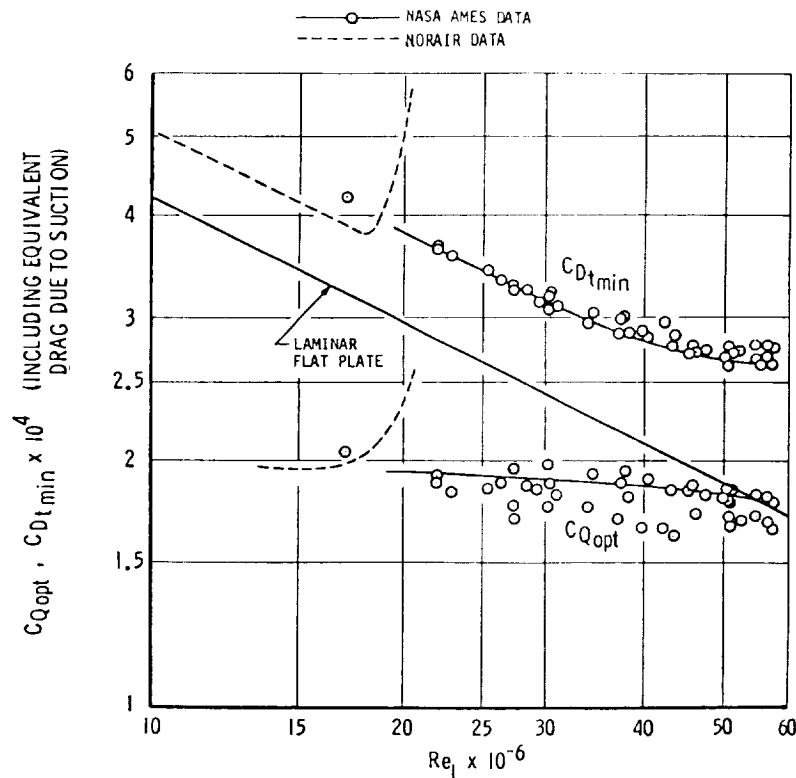
Figure 10

PROPULSION CONSIDERATIONS

Superfan-type bypass ratio 18 wing-mounted propulsion engines of about 18000 Kg take-off thrust were selected in the present study with an additional boundary-layer propulsion engine in the rear fuselage (thereby reducing the equivalent turbulent fuselage drag by about 10%) (Ref. 9). It is not clear whether to favor aft-mounted counter-rotating super fans with a direct drive or a geared front super fan. The aft fan may, in principle, allow a 3-spool gas generator with a correspondingly higher engine pressure ratio and thermodynamic efficiency. With the superfan generating essentially lower frequency noise below the range of amplified TS-waves, wing-mounted engines appear feasible for wing laminarization. Furthermore, extensive laminar flow by means of suitable geometric shaping and suction appears feasible on the external surfaces of the fan nacelles and even in the fan inlet up to the fan rotor. The parasite drag of these fan nacelles would then decrease drastically to narrow the difference in propulsive and overall efficiency between a superfan and a high-speed propeller. In addition, the superfan nacelle, located upstream of the wing, reduces the flow velocity in the area of the wing (area-rule considerations) to enable a correspondingly thicker wing in the area of the wing-strut juncture, thereby further reducing the performance gap between the superfan and high-speed turboprop.

SUCTION DRIVE

The airplane of Fig. 1 was designed with limited suction in the front part of the wing, tail surfaces, engine nacelles and struts. No suction was considered in the rear pressure rise areas on these surfaces. For these conditions, the suction massflow rates and suction power are sufficiently small such that the suction compressors can be driven mechanically from the main propulsion engines via a direct drive. In this manner the cruise thrust of the suction compressor is contributed at a particularly high propulsive- and overall efficiency. (Thermodynamically, when the LFC suction compressor system is part of the cruise propulsive system, the suction compressors should be driven by a thermodynamically highly efficient engine, i.e. it is basically wrong to drive the suction compressors with thermodynamically inefficient separate engines.) At lower flight speeds, the suction compressors may be geared down to reduce their power input.

AIRPLANE PERFORMANCE

In this study, 70% laminar flow was assumed on wing and tail surfaces, struts and fan nacelles of the airplane shown in fig. 11. Fully turbulent flow was assumed on the fuselage (6 meters diameter, 60 meters length). Split wing tips were chosen to reduce the induced drag by about 8% ($\kappa = 0.94$ was assumed as induced drag factor). Figure 11 shows L/D versus C_L of this airplane, with L/D = 39.4 at $C_L \approx 0.6$. In practice, C_L might be reduced somewhat to raise the cruise Mach number at a slight penalty in L/D.

For comparison, L/D of the same airplane is shown both with fully turbulent flow (L/D ≈ 27.5) as well as with fully laminar flow on the wings and tail surfaces, engine nacelles and struts by means of suction and various degrees of suction laminarization of the fuselage. Figure 11 shows a comparison of L/D and Re_c of the strut braced and a cantilevered wing on a LFC airplane ($b^2/S = 12$) versus C_L. The superior L/D performance and the substantially lower wing chord Reynolds numbers of the strut-braced design are obvious.

(A)
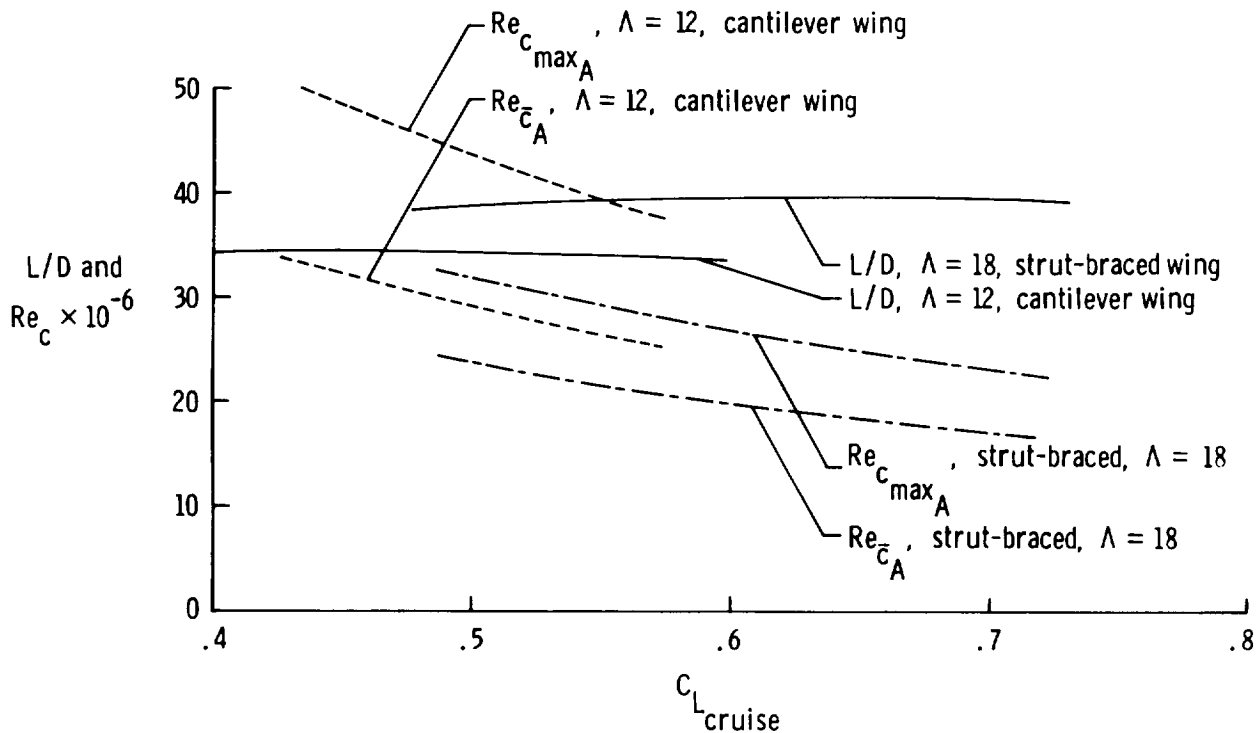
Figure 11

(B)

Figure 11

AIRPLANE RANGE

Assumptions

Take-off gross weight $W_o = 180000$ Kg,

$(L/D)_{average} = 37$,

spec. fuel consumption b $= 0.48$ kg/kg thrust at M $= 0.83$

i.e., $\eta_{overall} = 0.42$,

gross weight empty $= 0.38 \times$ take-off gross weight W_o,

Payload $= 50000$ Kg. $= 0.278\ W_o$,

$0.06\ W_o$ fuel reserves for take-off, climb, loitering. etc.

The unrefuelled range is R $= 21564$ Km $= 11606$ n. miles.

The all-out range without payload is about 68000 Km.

The same concepts can be applied with modifications to larger as well as smaller long range LFC transports.

CONCLUSIONS

M = 0.83 LFC transports, carrying large percentage payloads over a range of 20000 kilometers at cruise L/D's of 39 appear feasible with large span externally braced wings, external fuel pods, active controls, and 70% laminar flow on wing and tail surfaces, engine nacelles and struts, and a turbulent fuselage. To alleviate boundary-layer crossflow on the wing, the airfoils were designed for high M_∞'s (thereby reducing wing sweep) by undercutting the front and rear lower surface and selecting an extensive supersonic flat rooftop pressure-distribution on the upper surface with an upstream pressure minimum and a steep rear pressure rise. A slotted cruise flap improves the low drag $C_L - range$ and the rear pressure recovery. Weak suction from 0.05c to 0.30c appears adequate for 70% laminar flow on the upper wing surface.

A combination of a swept-forward inboard and a swept-back outer wing appears superior overall, especially for laminar flow and eliminating leading edge contamination probably caused by flyspecks and ice crystals. Wing divergence appears controllable by a combination of various methods.

Wing-mounted superfans with extensive laminar flow on their nacelles appear practical. Their dominant tone noise is below the frequency range of the most strongly amplified TS-waves.

REFERENCES

1. W. Pfenninger, "Some Results from the X-21 Program, Part I, Flow Phenomena at the Leading Edge of Swept Wings," Agardograph 97, Part IV, May 1965.

2. W. Pfenninger and E. Groth, "Low Drag Boundary Layer Suction Experiments in Flight on a Wing Glove of an F94A Airplane with Suction Through a Large Number of Fine Slots," Boundary Layer and Flow Control, G. V. Lachmann, Editor, Vol. 2, p. 981, 1961.

3. R. Whitcomb and L. Clark, "An Airfoil Shape for Efficient Flight at Supercritical Mach Numbers," NASA TM X-1109, July 1965.

4. F. Bauer, P. Garabedian, and A. Jameson, "Supercritical Wing Sections II," Springer-Verlag, No. 108, 1975.

5. P. M. Morse and K. U. Ingard, Theoretical Acoustics, McGRAW-HIll, 1968.

6. M. Malik, "COSAL - A Black Box Compressible Stability Analysis Code for Transition Prediction in 3-Dimensional Boundary Layers," NASA CR-165925, Contract NAS1-16919, May 1982.

7. L. W. Gross and W. Pfenninger, "Experimental and Theoretical Investigation of a Reichardt Body of Revolution with Low Drag Suction in the NASA Ames 12-Foot Pressure Wind Tunnel," Northrop Report NOR 63-46, BLC-148, 1963.

8. M. J. Walsh, "Turbulent Boundary Layer Drag Reduction Using Riblets," Presented at the AIAA 12th Aerospace Sciences Meeting, Orlando, Florida, January 1982. AIAA Paper No. 82-0169.

9. J. Ackeret, "Probleme des Flugzeng-antriels in Gegenwart u. Zukunft," Scjweoz Bauzeitung, 1938.

DEVELOPMENT FLIGHT TESTS OF
JETSTAR LFC LEADING-EDGE FLIGHT TEST EXPERIMENT

David F. Fisher
NASA Ames Research Center
Dryden Flight Research Facility
Edwards, California

Michael C. Fischer
NASA Langley Research Center
Hampton, Virginia

In 1973, fuel economy became more important with the sudden increased cost of fossil fuel due to the Arab oil boycott. This spurred NASA to initiate the ACEE (AirCraft Energy Efficiency) Program (ref. 1) that would seek out technologies that could be applied to aircraft and would save fuel. One technology in aerodynamics that had shown promise (refs. 2 to 9) is laminar flow control where a small portion of the boundary layer near the aircraft skin is removed through slotted or porous skin. It has been estimated that the drag of an aircraft could be reduced 25 to 40 percent (ref. 10) if the wing boundary layer was laminar instead of turbulent. However, laminar flow control had to be shown to be practical. Many of the problems or obstacles to making it practical, such as insect contamination, leading edge attachment line boundary layer, deicing, and suction, involve the wing leading edge. While some of the problems seemed to be solvable (refs. 11 and 12), they had not been incorporated into a single leading- edge design and flight-tested. These problems have been addressed in the JetStar Laminar Flow Control - Leading-Edge Flight Test (LFC-LEFT) Program described in references 10, 13, and 14; the program results are reported here and in references 15 and 16.

Laminar Flow Control
Leading-Edge Flight Test

ORIGINAL PAGE
BLACK AND WHITE PHOTOGRAPH
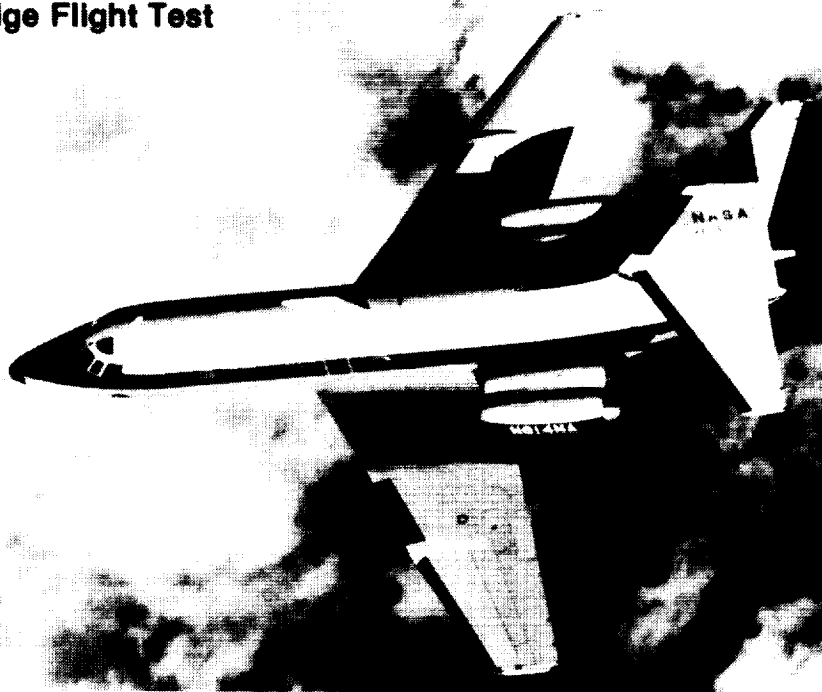
The overall objective of these flight tests on the JetStar airplane was to demonstrate the effectiveness and reliability of laminar flow control under representative flight conditions. One specific objective was to obtain laminar flow on the JetStar leading-edge test articles for the design and off-design conditions. The design point for the test articles was M = 0.75 at 38,000 ft and a lift coefficient of 0.3. Off-design points were to be tested from M = 0.7 to 0.8 at altitudes from 32,000 to 40,000 ft, which are representative of the speeds and altitudes that an LFC airplane of the 1990's will be flying. Another specific objective was to obtain operational experience on an LFC leading-edge system in a simulated airline service. This includes operational experience with cleaning requirements, the effect of clogging, possible foreign object damage, erosion, and the effects of ice particle and cloud encounters.

JetStar - Laminar Flow Control

Leading-Edge Flight Test

Overall objective

- Demonstrate the practicality and reliability of laminar flow control leading-edge systems under representative flight conditions

Specific requirements

- Obtain laminar flow on leading-edge test article for design and off-design conditions

- Obtain operational experience
    - Clogging and cleaning requirements
    - Foreign object damage
    - Erosion
    - Ice particle effects

The approach taken to achieve these objectives was to test alternative leading-edge laminar flow control concepts on each wing. Each concept would modify a spanwise section of a JetStar leading edge to include laminar flow control, insect protection, and deicing capability. One leading-edge test article built by the Lockheed Georgia Company uses a slotted skin, while the other test article built by Douglas Aircraft Company uses a porous skin.

At the start of the design of the test articles, NASA and the two contractors agreed that both articles would have the same airfoil shape. The shape agreed upon would have a peak local Mach number of 1.1 for the design test conditions of M = 0.75 at an altitude of 38,000 ft. The leading-edge sweep of the test articles is 30 deg, and each has a span of 61.25 in. Design studies indicated that suction would be needed to have laminar boundary layer flow over the article at design conditions.

- **Modify spanwise section of wing leading edge to include laminar flow control, insect protection, and deicing**
- **Compare alternative concepts**
- **Conduct flight research and airline simulation flights**
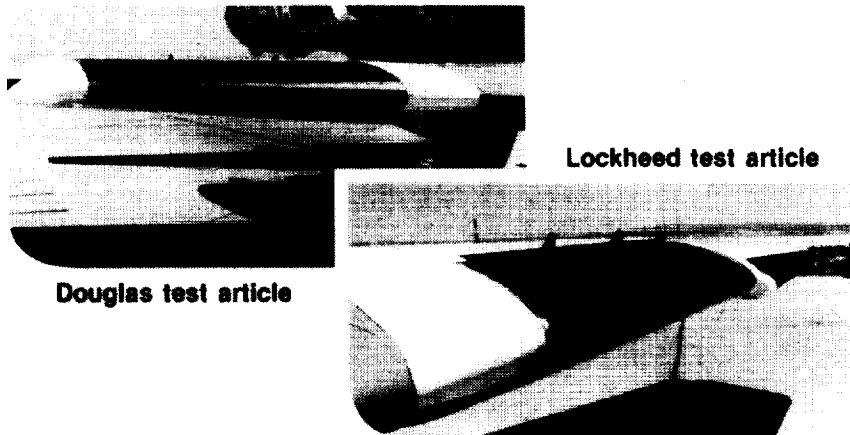
Lockheed test article

Douglas test article

The JetStar airplane is a business executive jet originally designed to carry 8 to 10 passengers. The aircraft was extensively modified for these flight tests. The auxiliary fuel tanks normally mounted midspan on each wing were removed, and the gap left was filled by leading-edge test articles. Suction tubes from the test articles were routed through the wing leading edges into the cabin of the aircraft to three large plenums or chamber valves. From the chamber valves, the air was then manifolded together and routed aft through the pressure bulkhead to the suction pump. Other major changes to the aircraft included the installation of real-time data and control consoles in the cabin and the cleaning liquid tanks in the aft fuselage.

JetStar LEFT Configuration
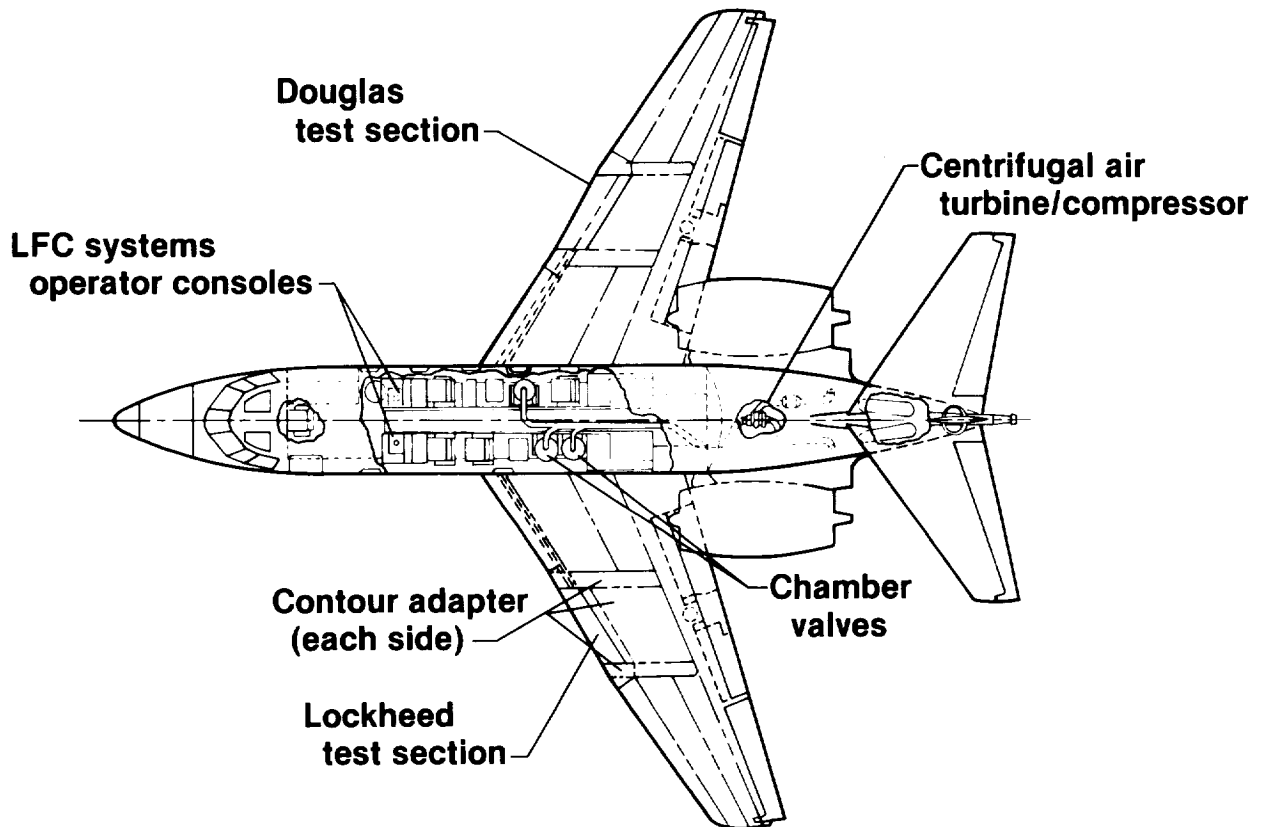
The test article built by Lockheed Georgia Company is of sandwich construction, comprised of graphite-epoxy face sheets with Nomex (E.I. du Pont de Nemours & Co.) core. The suction surface was formed by cutting twenty-seven 0.004-in spanwise slots on the upper and lower surface. The low-energy surface boundary layer is pulled through these slots into the slot duct. Metering holes were drilled through the slot duct and the outer face sheet in the collector duct. These approximately 0.030-in diameter holes are located on 0.20-in centers. From the collector duct, the air passes through the collector duct outlet holes. These 0.189-in-diameter holes are spaced at approximately 6-in intervals along the surface of the active slot surface. A 60/40 mixture of propylene glycol methyl ether (PGME) and water is expelled through eight of the slots at the leading edge to form a sheet of fluid over the test article for protection from insects and ice.

- **Suction on upper and lower surface**

- **Suction through spanwise slots**

- **Liquid expelled through slots for protection from insects and icing**

122
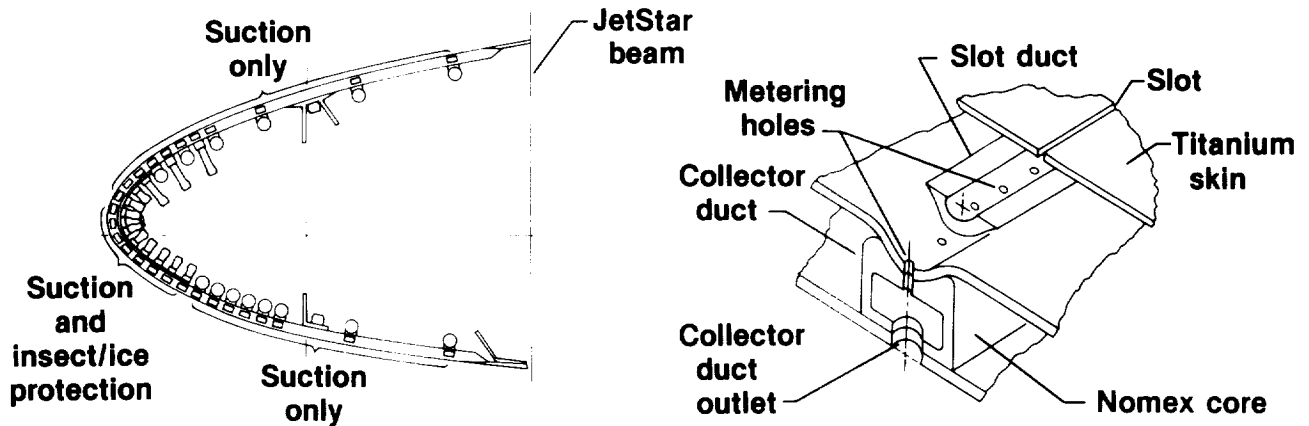
Suction was applied only to the upper surface of the Douglas test article. The low-energy boundary layer is drawn through a perforated titanium skin into 15 spanwise flutes. The 0.0025-in holes are drilled with an electron beam and are spaced 0.035-in apart. A leading-edge shield is extended at takeoff and landing for protection from insects. Nozzles behind the shield supplement the shield by spraying PGME on the test article. Protection from ice was provided by extending the shield and secreting a glycol fluid through a porous metal inset at the shield leading edge. The ice protection system can be supplemented by the spray system behind the shield.

- **Suction on upper surface only**
- **Suction through electron-beam-perforated skin**
- **Leading-edge shield extended for insect protection**
- **Deicer insert on shield for ice protection**
- **Supplementary spray nozzles for protection from insects and ice**
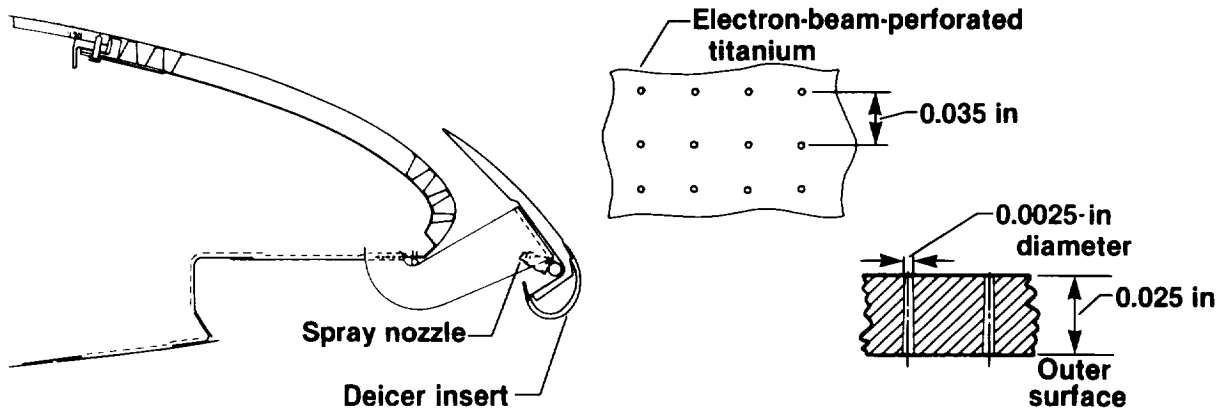
The JetStar airplane had several new systems installed for the LEFT Program similar to those proposed by the contractors for a future Laminar Flow Transport (refs. 17 to 19). The operation of these systems is as follows.

At takeoff, the PGME-water liquid is turned on to protect the Lockheed leading edge from insect contamination. The Douglas test article deploys a leading-edge shield supplemented with PGME-water spray. The secondary purge system, which uses the cabin pressurization system, provides a positive differential pressure in the suction flutes to prevent fluid from entering. At 1000 ft above ground level (AGL), the liquid is turned off and the secondary purge is used to clear the Lockheed suction lines, ducts, and slots. The shield is retracted at 4000 ft AGL. From 12,000 to 23,000 ft, purge air is supplied by the emergency pressurization system. The suction pump, a modified AiResearch turbocompressor originally designed for the air-conditioning system on the Boeing 707 airplane, is started at 20,000 ft. Suction is turned on at the cruise altitude.

LEFT Operations and In-Flight Leading Edge Washing

	Lockheed	Douglas
Takeoff	Liquid on	Shield extended Liquid on Secondary purge on
1,000 ft AGL	Liquid off Secondary purge on	Liquid off Secondary purge on
4,000 ft AGL		Retract shield
12,000 ft	Secondary purge off Primary purge on	Secondary purge off Primary purge on
20,000 ft	Suction pump start	Suction pump start
23,000 ft	Primary purge off	Primary purge off
32,000 ft	Beginning of suction on test article	Beginning of suction on test article
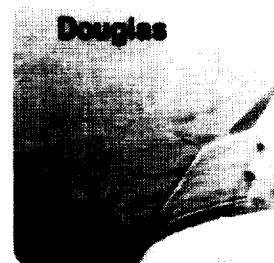
PGME-water liquid sprayed on leading edge through nozzles on shield

PGME-water liquid expelled through leading edge slots

INSTRUMENTATION

Chordwise rows of static pressure orifices were installed on each test article to measure the test article pressure distribution. A chordwise row of hot films was used to detect transition on the Douglas test article. A spanwise row of surface pitots at approximately 13-percent chord was calibrated to determine the extent of laminar flow.

Mass flows and suction distributions for each flute and slot were determined using sonic nozzles located in the chamber valves.

A pylon-mounted Knollenberg probe on the top of the airplane was used to count and size moisture and ice particles during flight. A charge patch on the leading edge of the pylon made a related measurement by detecting the static electric charge built up when flying through the particles. This system is described in further detail in reference 20.

Other miscellaneous pressures and temperatures were measured to monitor the operation and health of the suction pump and other leading-edge systems as well as basic aircraft parameters. These measurements were displayed in real time on the operator control consoles in the airplane cabin.

Surface pitots

Individual mass flow measurements

Test article

Surface pressure

Hot films

Inboard

12 percent x/c

Fairing

Surface pitots

65 percent x/c

Rear spar
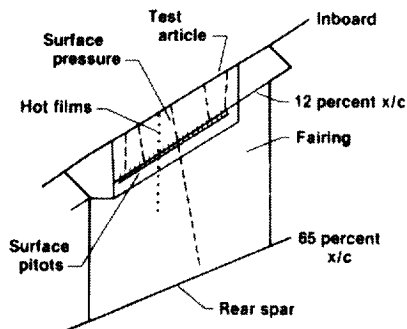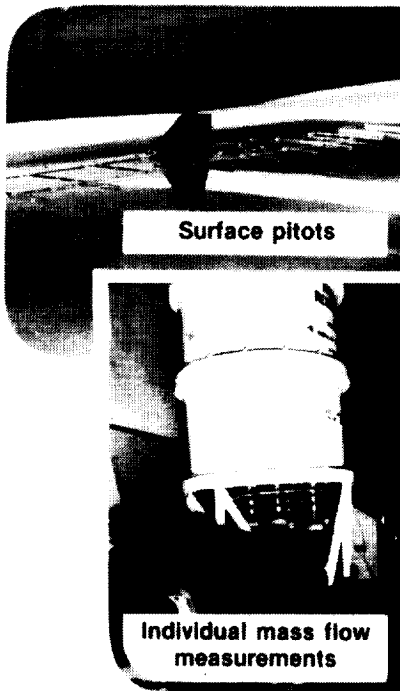
Measurements and CRT displays

- Aircraft and flight parameters

- System pressures and temperatures

- Mass flows and suction distributions

- Ice particle flux and aircraft charge

- Boundary-layer monitoring
    - Hot films
    - Pitots

- Surface pressure distributions

Real-time displays on aircraft

Knollenberg probe and charge patch

Static pressure orifices
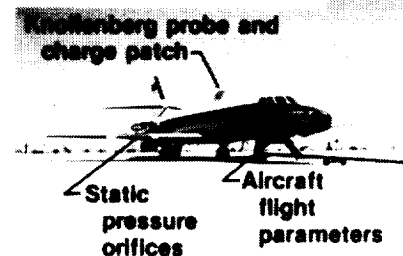
Aircraft flight parameters

Transition was detected using a spanwise array of pitots located near the surface of the test article skin at x/c ~ 0.13. The probe height was positioned to be just outside the thin boundary layer when the boundary layer was laminar; for the thicker turbulent boundary layer, the probe would therefore be immersed in this boundary layer. A reference probe measuring the free-stream pressure was located nearby. Transition was determined by comparing the pressure from the spanwise pitots with the free-stream pressure. For laminar flow, differential pressure is nearly zero. For a turbulent boundary layer, the free-stream pressure is higher. These spanwise probes were calibrated for transition location by placing spanwise transition strips at known x/c locations on the test article.

Determination of Extent of Spanwise Laminar Flow From Pitot Data

Douglas Test Article; M = 0.75
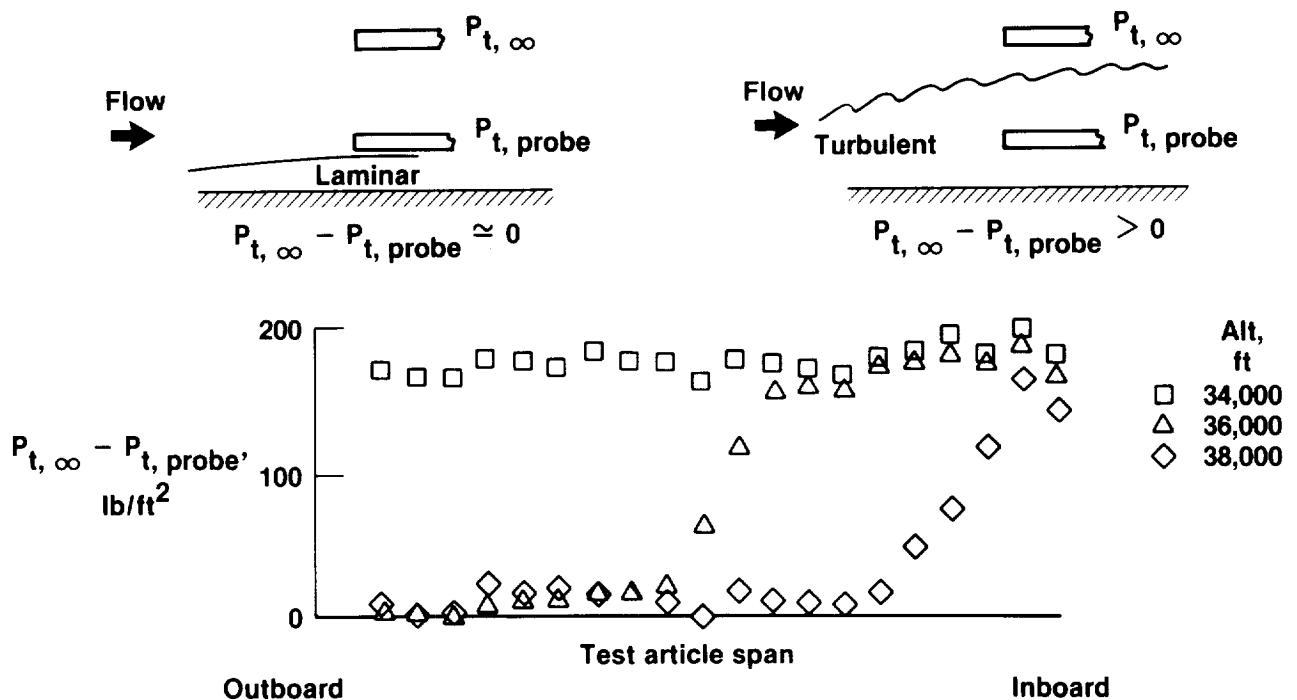
PRESSURE DISTRIBUTIONS

The pressure distributions measured in flight show the effects of varying Mach number between 0.705 and 0.786 at an altitude of 38,000 ft. The pressure distribution for the lowest Mach numbers had a steep suction peak with an adverse pressure gradient beginning at x/c = 0.04. The pressure distributions at the higher Mach numbers had a less steep suction peak with the adverse gradient delayed.

The variation of pressure distributions on the test articles as a function of altitude and lift coefficient C_L is shown. As the altitude and C_L increase, the pressure coefficients become more negative as expected. For comparison, the design pressure distribution is shown. While the local Mach number for the design case is slightly higher, M = 1.16 as compared to M = 1.12 for flight, the pressure gradients are similar.

Douglas Test Article; Midspan

M	C_L
□ 0.705	0.37
○ 0.725	0.35
◇ 0.747	0.33
△ 0.771	0.30
◻ 0.786	0.29

Alt = 38,000 ft
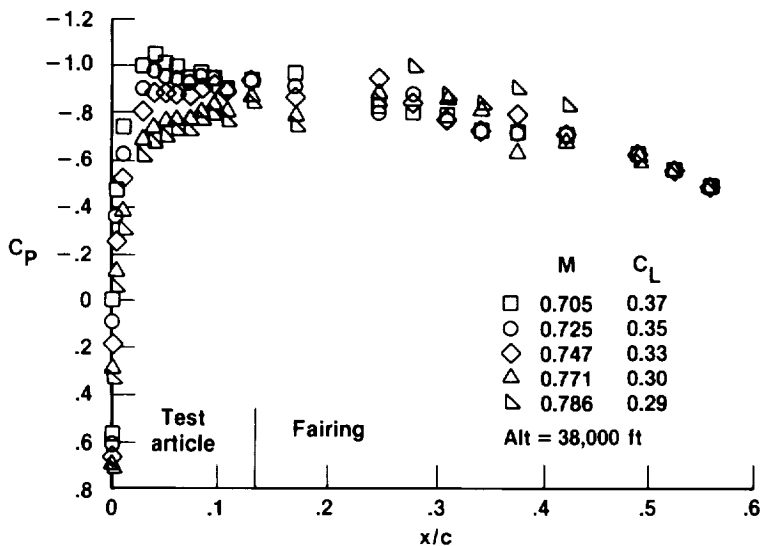
Variation with Mach number

	Alt, ft	C_L
○	32,118	0.24
□	34,175	0.26
△	36,181	0.27
◇	38,253	0.33
---	38,000	0.32

M = 0.75
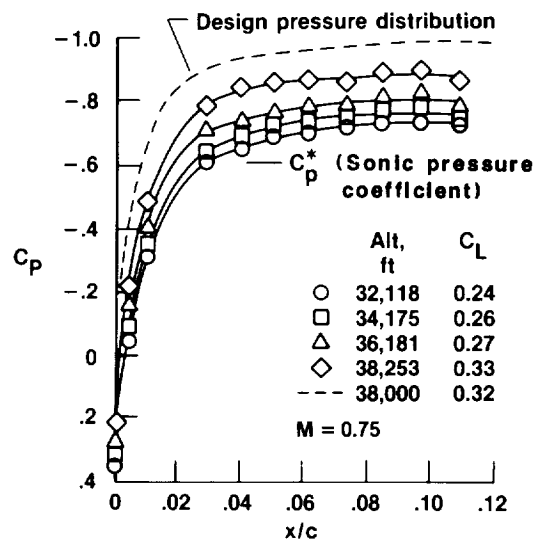
Variation with altitude

INITIAL FINDINGS – DOUGLAS TEST ARTICLE

For the nominal suction distribution used initially for the Douglas test article, a high degree of suction (suction coefficient C_q = 0.0009) was applied at the leading edge. After the first flute, the suction was reduced to C_q = 0.00065 to approximately s/c = 0.05 (ratio of surface length to chord length). From s/c = 0.05 to the test article trailing edge, a threshold level of C_q = 0.00016 was maintained.

The initial findings for the Douglas test article show the area of laminar flow on the test article as a function of Mach number. These data are derived from the 20 surface pitot probes at the test article trailing edge. Approximate transition locations were determined and laminar areas derived. This figure shows that the test points at the lowest speeds and highest altitudes (that is, the lowest Reynolds number) resulted in the most laminar flow. Conversely, the data at the lowest altitudes and highest speeds (that is, the highest Reynolds numbers) resulted in the least laminar flow. At the design point, approximately 83 percent of the test article was laminarized. At the off-design point of M = 0.705 and 38,000 ft, 97 percent of the test article had laminar flow, whereas at M = 0.78 and 32,000 ft, this value was only 7 or 8 percent.

$$C_q = \frac{\text{mass flow}}{\text{density} \times \text{velocity} \times \text{area}}$$
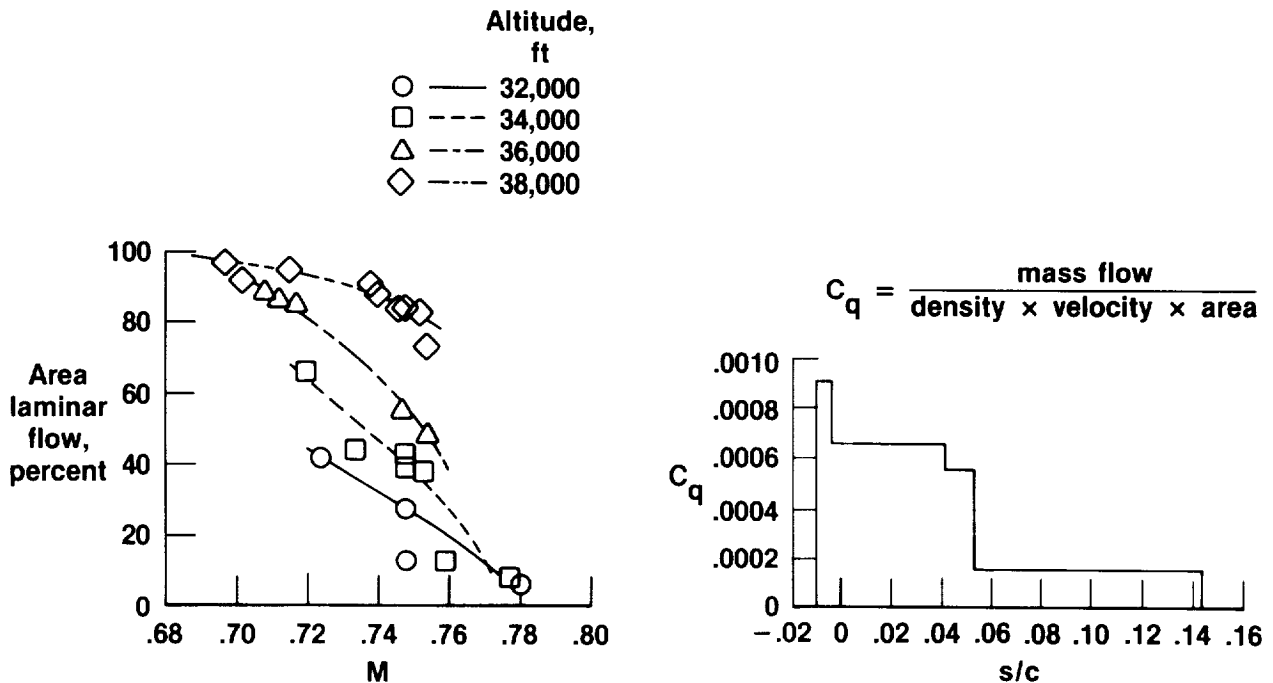
The spanwise transition location on the Douglas test article moved from inboard to farther outboard as the altitude was reduced and the Reynolds number was increased. The initial findings from the Douglas test article have been replotted as a function of momentum thickness Reynolds number, Re_θ. As Re_θ was reduced to values to near the X-21 criteria of 100, the extent of laminar flow approached 100 percent. This suggests that the attachment line boundary layer was traveling outboard along the wing leading edge and caused the flow on the test article to transition from laminar to turbulent flow. The X-21 criteria indicate that if $Re_\theta < 100$, the turbulent boundary layer from the fuselage and inner wing will not travel along the leading edge but will be swept back over or under the wing.

Evidence of Spanwise Contamination
Douglas Test Article; Initial Fairing

	Alt,ft	M
O	32,000	0.724 to 0.780
□	34,000	0.720 to 0.777
△	36,000	0.708 to 0.754
◇	38,000	0.697 to 0.748

$$Re_\theta \approx \sqrt{\frac{.407 \sin\lambda}{\cos\lambda}} \sqrt{Re_\infty \text{ LE radius}}$$

Flow

M = 0.75

Transition
32,000 ft
$Re_\theta = 122$

Transition
38,000 ft
$Re_\theta = 110$

Transition
36,000 ft
$Re_\theta = 117$
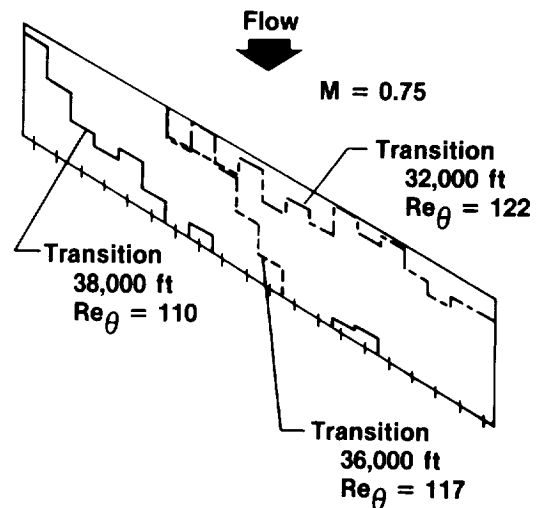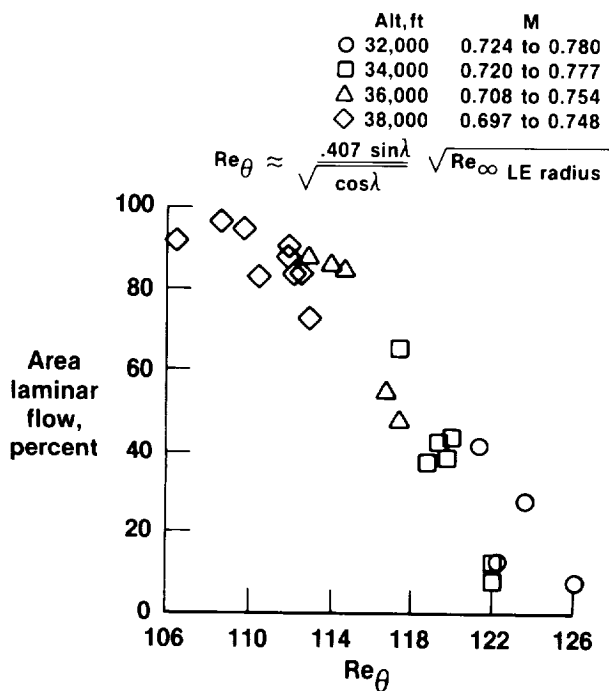
WOOD GASTER BUMP - DOUGLAS TEST ARTICLE

During tests with a half-span swept laminar flow control wing in the wind tunnel and in flight on a Lancaster bomber, Gaster (ref. 21) developed a small protrusion or leading-edge bump to alleviate this turbulent attachment line boundary-layer problem. A similar bump made of wood was attached and faired in at the approximate attachment line of the Douglas test articles as shown. The results of this modification using the same suction distribution as previously are also shown. At an altitude of 32,000 ft and M = 0.72 to 0.75, the test article was completely laminar across the span. The data from 34,000 and 36,000 ft show the test article to be at least 95-percent laminar. A slight degradation was noted as the Mach number was increased. The data from these altitudes show a marked improvement compared to the initial findings. The data at 38,000 ft with the wood Gaster bump show some improvement compared to the initial fairing. At the design point, M = 0.75 at a 38,000-ft altitude, about 90 percent of the surface was laminar as compared with 83 percent with the original fairing. However, at 40,000 ft, the data with the wood Gaster bump had less laminar flow than the initial findings at 38,000 ft.
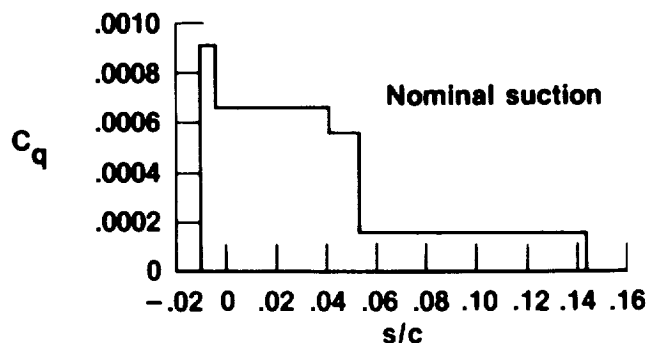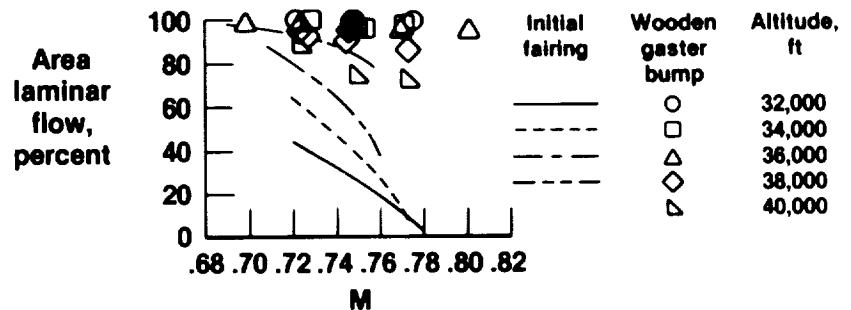
WOOD GASTER BUMP - LOCKHEED TEST ARTICLE

A similar wood leading-edge bump was installed on the Lockheed test article. The suction distribution on the Lockheed test article differs from the Douglas suction distribution in that the Lockheed test article used less suction at the leading edge. With the wood leading-edge bump, approximately 97 percent of the surface was laminarized at M = 0.725 and an altitude of 32,000 ft. However, at M = 0.775, the area of laminar flow was reduced to 74 percent. At the higher altitudes, the area of laminar flow ranged from 70 to 90 percent, with most of the data below 80 percent. At the design point, M = 0.75 at a 38,000-ft altitude, approximately 75 percent of the test article was laminarized.
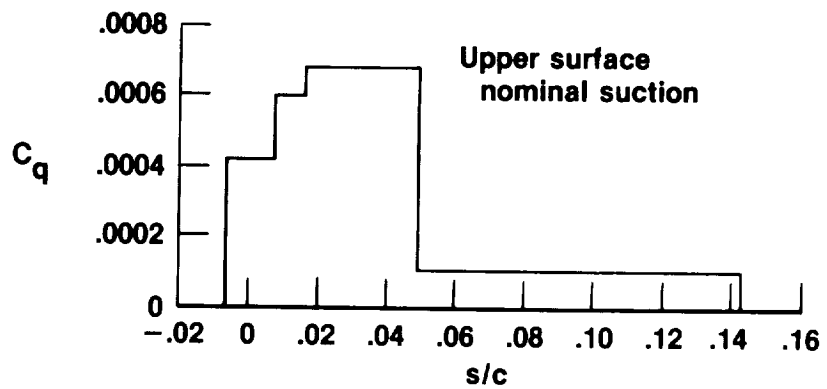
SHARP AND ROUNDED LEADING-EDGE NOTCHES

In preparation for the simulated airline service flights, it was believed that more permanent integral leading-edge bumps were needed, and also that their performance of achieving laminar flow on the test articles could be improved.

The first approach tried was to modify the inboard fairings with a notched leading edge that would divert the turbulent attachment line boundary layer at the leading edge over or under the wing. Both a sharp notch and a rounded notch were tested. The test results of both notches showed little or no improvement over the initial fairings; the notches were much worse than the wood Gaster bumps.

Sharp
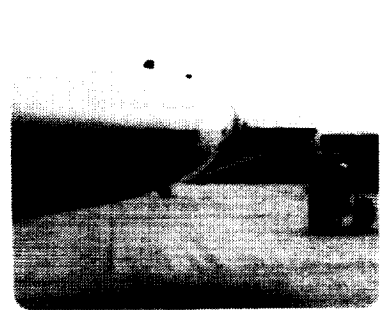
Rounded

Although the depth of the notch was approximately the height of the wood Gaster bumps, the notches did not achieve the same favorable effect. One difference between the Gaster bumps and the notches was the local leading-edge radius. The notches had the same leading-edge radius as the initial fairing (about 2.0 in), whereas the Gaster bumps had a much smaller radius, about 1.0 in. The smaller leading-edge radius reduced the momentum thickness Reynolds number Re_θ from about 128 for M = 0.78 at an altitude of 32,000 ft to about 90, which is well below the X-21 criteria of 100 and corresponds to Gaster's own criteria of 90. The notches inboard on the Douglas and Lockheed test articles were then modified into an integral notch-bump to reduce the leading-edge radius to ~ 1.0 in.

Douglas Test Article
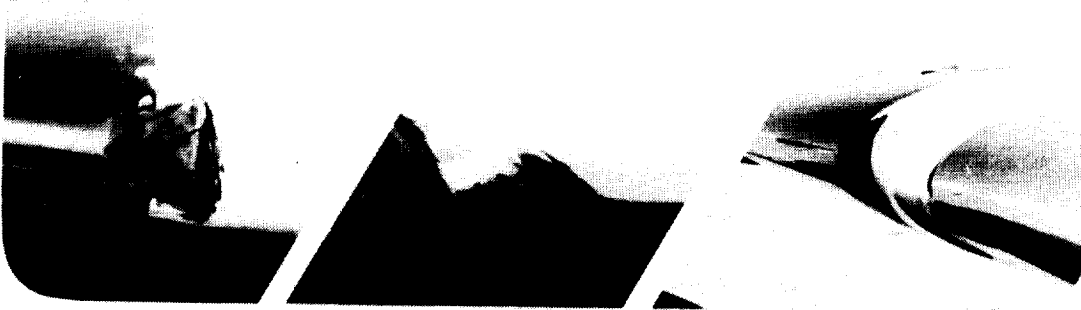
Lockheed Test Article
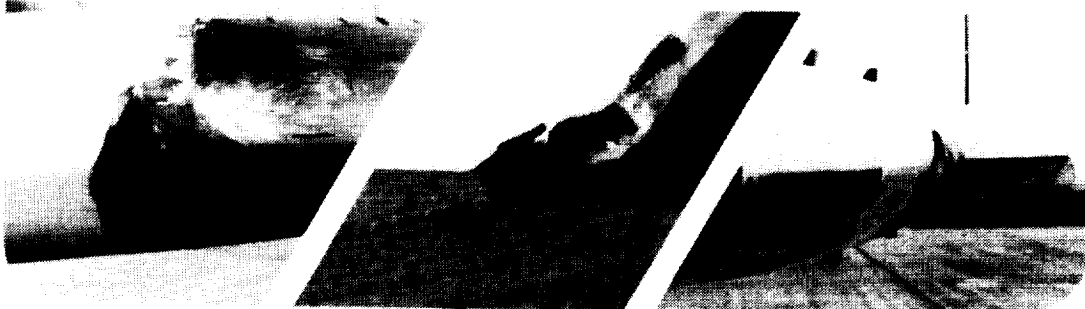
DOUGLAS TEST ARTICLE RESULTS WITH LEADING-EDGE NOTCH-BUMP

The results of the data for the notch-bump are compared with those for the wood Gaster bump. At all altitudes, the Douglas test article with the notch-bump modification showed as much or more laminar flow as with the wood Gaster bump. The suction distribution had been modified at this time, as shown, to provide increased suction in the aft flutes. This allowed the test article to achieve nearly fully laminar flow over the entire test article at the conditions tested. At the design test condition, $M = 0.75$ and an altitude of 38,000 ft, the test article was 96-percent laminar.
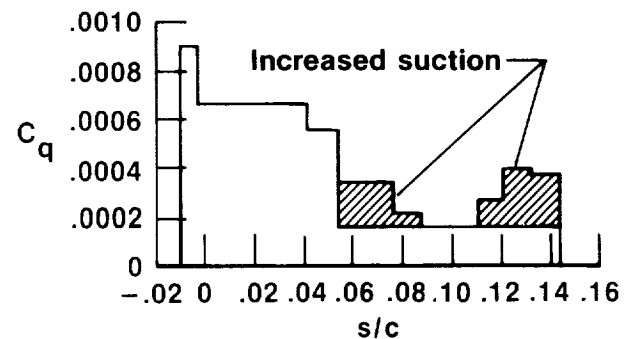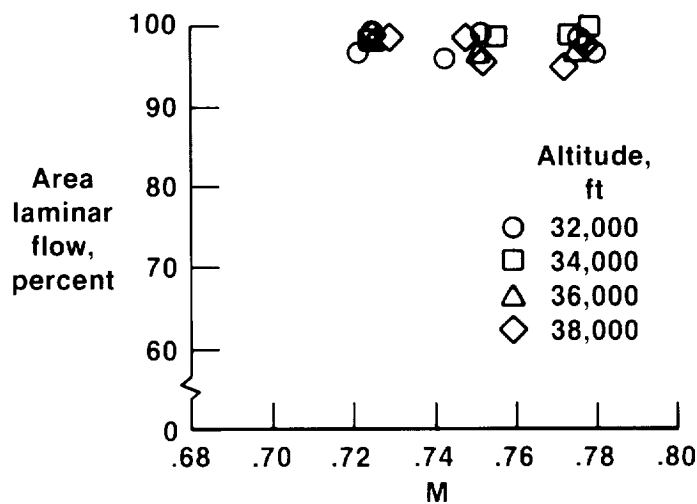
LOCKHEED TEST ARTICLE RESULTS WITH LEADING-EDGE NOTCH-BUMP

The Lockheed test article with the leading-edge notch-bumps did not maintain laminar flow as consistently as the Douglas test article. Near the design conditions, the test article surface varied between 80- and 94-percent laminar. At other Mach numbers and altitudes, the data were also scattered. These results are probably the effect of the manufacturing problems encountered in making the slotted test article, which caused uneven suction, surface waviness, and blocked slots.
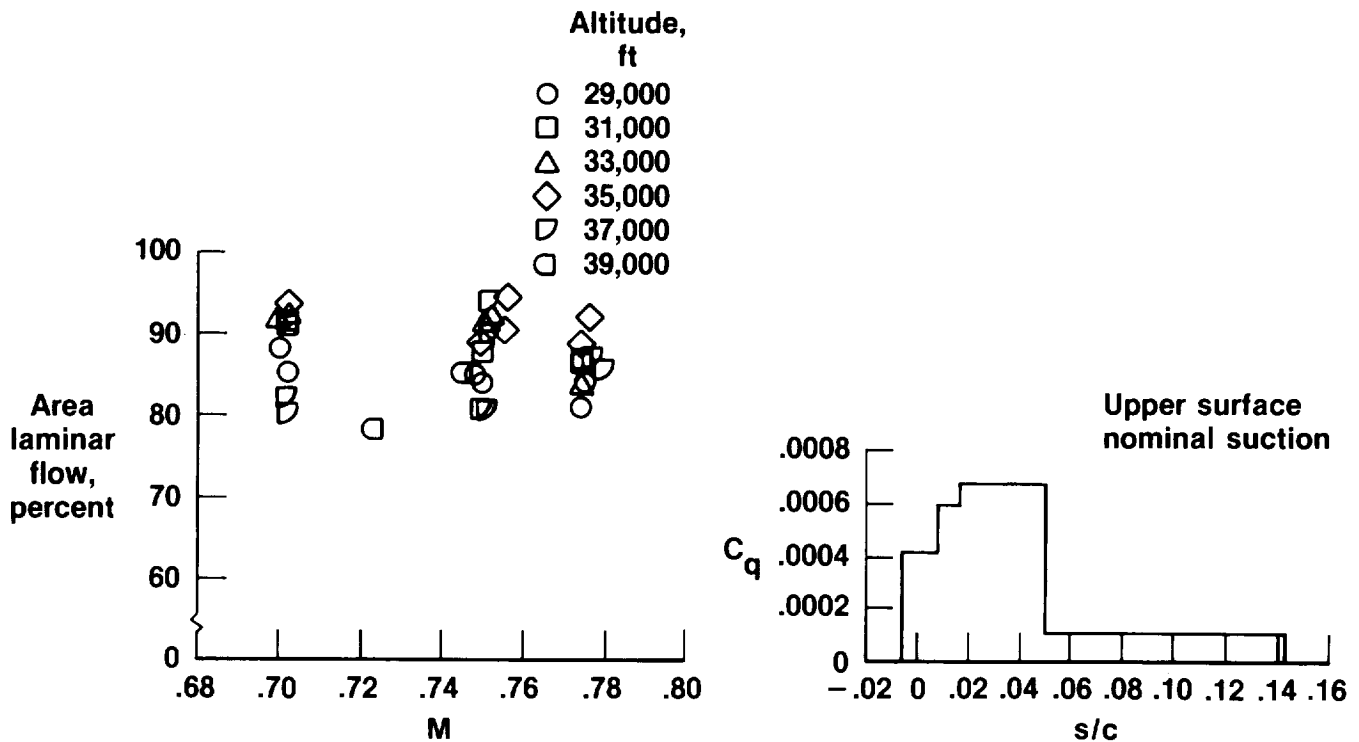
LOW-ALTITUDE RESULTS OF DOUGLAS TEST ARTICLE WITH NOTCH-BUMP

Additional testing of the Douglas test article at low altitude was conducted to determine if the test articles could be laminarized during the climb or descent portion of the flight. Tests were conducted at altitudes of 10,000, 15,000, 20,000, and 25,000 ft at three Mach numbers. Sample pressure distributions are shown. At the lowest Mach number and the highest angle of attack, a suction peak occurs in the pressure around 2 percent chord, followed by an adverse pressure gradient. At the highest Mach numbers and lowest angle of attack, a favorable gradient was present to approximately 7.5 percent chord. For these tests, because an LFC transport would probably use fixed valve settings, the same needle valve positions as for the design point were used. Even with this nonideal suction, the test article was approximately 90-percent laminar.

	M	Altitude, ft	C_L
O	0.453	19,900	0.38
□	0.550	19,900	0.26
△	0.656	19,900	0.18

	Altitude, ft
O	10,000
□	15,000
△	20,000
◇	25,000
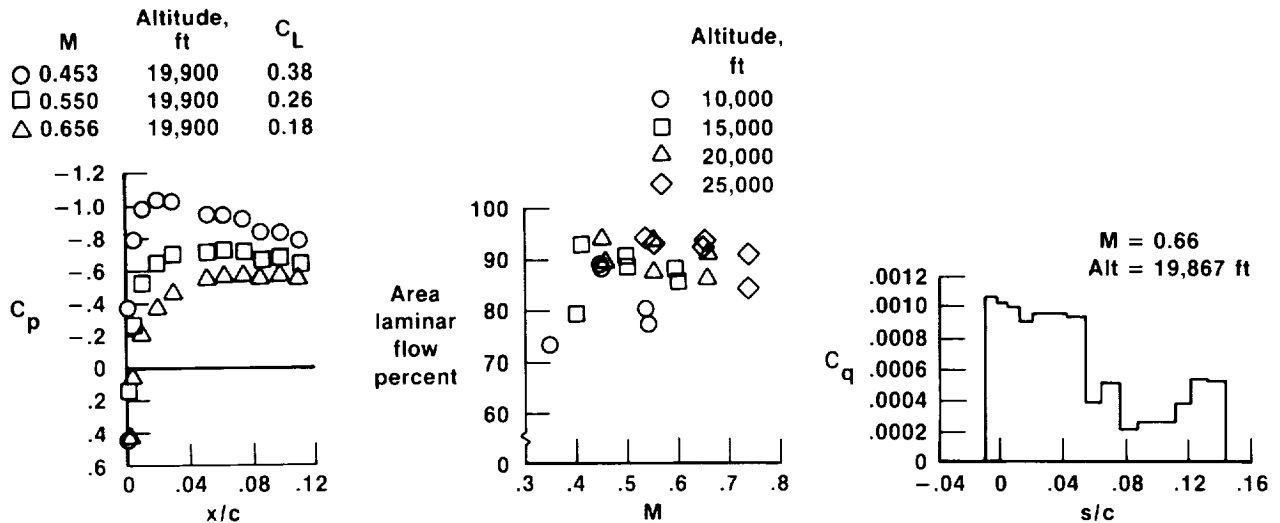
EFFECT OF CLOUDS AND ICE PARTICLES ON LAMINAR FLOW

During the flight tests of the leading-edge test articles, flight through clouds and ice particles at high altitude occurred. The results of these encounters are shown. Laminar flow on the test article was lost while encountering the clouds and ice particles but was restored immediately upon leaving the clouds and ice particles. This agrees with ice particle data obtained on the X-21A aircraft (ref. 8).

Douglas Test Article; M = 0.76, and 34,200 ft. Altitude

Inboard

Flow

Time = 0 sec
97-percent laminar flow

Time = 8 sec
43-percent laminar flow

Time = 4 sec
66-percent laminar flow

Time = 18 sec
17-percent laminar flow
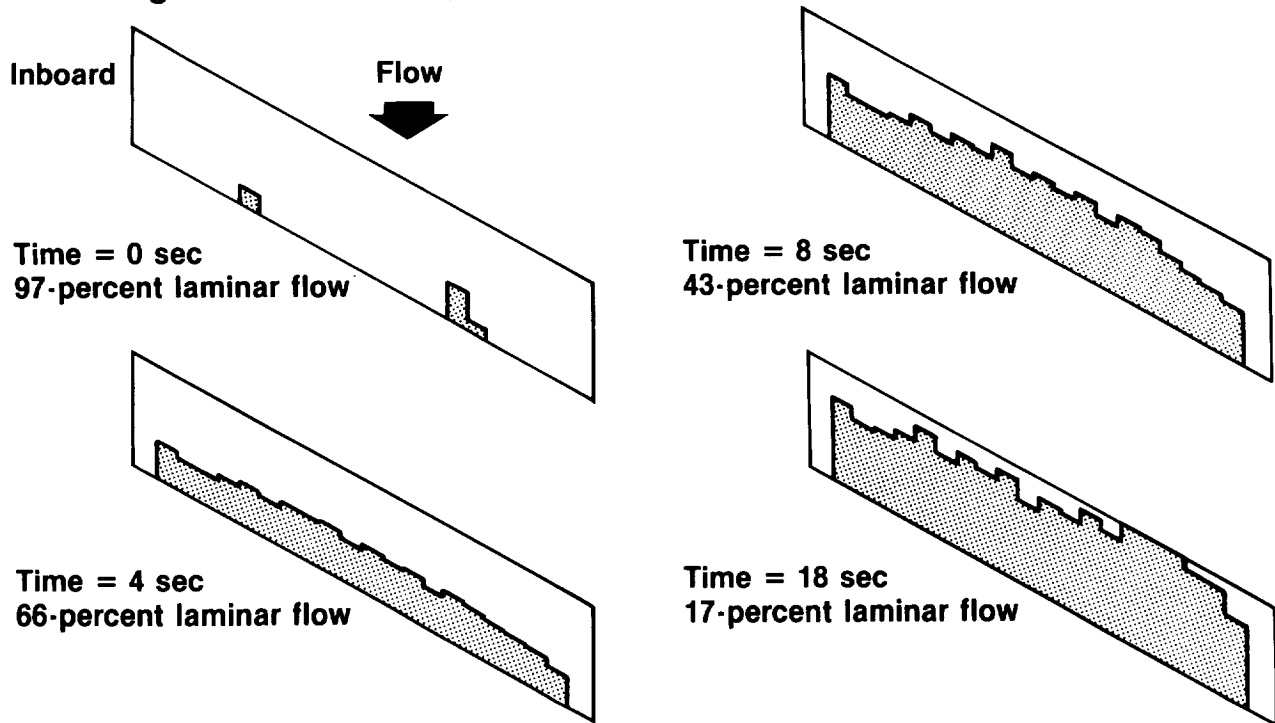
CONCLUDING REMARKS

The JetStar LFC Leading-Edge Flight Test Program development flights gave the following results:

1. The Douglas and Lockheed leading-edge test articles have been successfully installed and systems operated.

2. Attachment line contamination was present with the initial inboard fairings. Gaster bumps or leading-edge notch-bumps were effective in solving this problem by reducing the leading-edge momentum thickness Reynolds number to 90 or less.

3. The Douglas test article with the leading edge notch-bump configuration was 96-percent laminarized at the design point. In addition, the article was at least 95-percent laminarized for M = 0.72 to 0.78 and altitudes of 32,000 to 38,000 ft. Laminar flow on the Lockheed test article with the leading-edge notch-bump was inconsistent. Near the design point, the test article was laminarized from 80 to 94 percent.

4. Laminar flow was lost while encountering clouds or ice particles but was regained to previous levels after leaving the clouds or ice particles.

- ## Two LFC leading-edge test articles have been successfully installed and operated

- ## Attachment line contamination problem was solved using Gaster bumps and notch-bumps

- ## Douglas test article was nearly fully laminarized at the test conditions. Lockheed test article was laminarized from 80 to 94 percent at the design conditions

- ## Laminar flow was lost on test articles during encounters with clouds and ice particles. Laminar flow was immediately regained after exiting the cloud or particles

REFERENCES
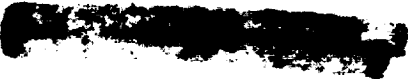
1. Povinelli, F.P.; Klineberg, J.M.; and Kramer, J.J.: Improving
   Aircraft Energy Efficiency, Astronaut. and Aeronaut. (AIAA),
   vol. 14, no. 2, Feb. 1976, pp. 18-31.

2. Tollmien, W.: Uber die Entsehung der Turbulenz. Mitteilung,
   Nachr. Wiss. Gottingen, Math. Phys. Klasse, 1929, pp. 21-44;
   Engl. transl. in NACA TM-609, 1931.

3. Schlichting, H.: Zur Enstehung der Turbulenz. Phys. Klasse, 1933,
   pp. 182-208; see also ZAMM, vol. 13, 1933, pp. 171-174.

4. Schubauer, G.B.; and Skramstad, H.K.: Laminar Boundary Layer
   Oscillations and Stability of Laminar Flow. National Bureau of
   Standards Research Paper 1772 (Reprint of a classified NACA
   Report first published in April 1943, and later released as NACA
   Wartime Report W-8), and J. Aero. Sci., vol. 14, no. 2, 1947, pp.
   69-78.

5. Groth, E.E.; Carmichael, B.H.; White, R.C.; and Phenninger, W.:
   Low Drag Boundary Layer Suction Experiments in Flight on the Wing
   Glove of a F94-A Airplane-Phase II: Suction Through 69 Slots.
   NAI-57-318, BLC-94, Northrop Aircraft Corp., Inc., 1957.

6. Antonatos, P.P.: Laminar Flow Control - Concepts and Applications.
   Astronaut. and Aeronaut. (AIAA), vol. 4, no. 7, July 1966, pp.
   32-36.

7. Nenni, J.P.; and Gluyas, G.L.: Aerodynamic Design and Analysis on
   an LFC Surface. Astronaut. and Aeronaut. (AIAA), vol. 4, no. 7,
   July 1966, pp. 52-57.

8. Whites, R.C.; Sudderth, R.W.; and Wheldan, W.G.: Laminar Flow
   Control on the X-21. Astronaut. and Aeronaut. (AIAA), vol. 4,
   no. 7, July 1966, pp. 38-43.

9. Pfenninger, W.; and Reed, V.D.: Laminar-Flow Research and
   Experiments. Astronaut. and Aeronaut. (AIAA), vol. 4, no. 7,
   July 1966, pp. 44-50.

10. Hefner, Jerry N.; and Wagner, Richard C.: Laminar Flow Research
    Applicable to Subsonic Aircraft. Presented at the International
    Symposium on Aeronautical Science & Technology of Indonesia,
    Jakarta, Indonesia, June 24-27, 1986. (Available as A86-50269).

11. Peterson, John B., Jr.; and Fisher, David F.: Flight Investigation
    of Insect Contamination and Its Alleviation. CTOL Transport
    Technology - 1978, NASA CP-2036, 1978, pp. 357-373.

12. Fisher, D.F.; and Peterson, J.B., Jr.: Flight Experience on the
    Need and Use of Inflight Leading Edge Washing for a Laminar Flow
    Airfoil. AIAA-78-1512, Aug. 1978.

13. Wagner, R.D.; and Fischer, M.C.: Developments in the NASA
    Transport Aircraft Laminar Flow Program. AIAA-83-0090, Jan.
    1983.

14. Fischer, M.C.; Wright, A.S., Jr.; and Wagner, R.D.: A Flight Test
    of Laminar Flow Control Leading-Edge Systems, NASA TM-85712,
    1983.

15. Montoya, Lawrence C.; and Maddalon, Dal V.: Suction
    Discontinuities in LFC Leading-Edge Surfaces. Presented at NLF
    and LFC Research Symposium, Langley Research Center, Hampton, VA,
    Mar. 16-19, 1987.

16. Maddalon, D.V.; Fisher, D.F.; Jennett, L.M.; and Fischer, M.C:
    Simulated Airline Service Experience With LFC Leading Edge
    System. Presented at NLF and LFC Research Symposium, Langley
    Research Center, Hampton, VA, Mar. 16-19, 1987, NASA CP 2487,
    pp. 195-218.

17. Evaluation of Laminar Flow Control Systems Concepts for Subsonic
    Commercial Transport Aircraft, Final Report. NASA CR-159251,
    1983.

18. Evaluation of Laminar Flow Control Systems Concepts for Subsonic
    Commercial Transport Aircraft: Studies and Analyses Report –
    Validator Aircraft Concepts Study. SAR-1042-2, Lockheed-Georgia
    Co., 1980.

19. Evaluation of Laminar Flow Control Systems Concepts for Subsonic
    Commercial Transport Aircraft. NASA CR-158976, 1978.

20. Davis, Richard E.; Fischer, Michael C.; Fisher, David F.; and
    Young, Ronald: Cloud Particle Effects on Laminar Flow in the
    NASA LEFT Program: Preliminary Results. AIAA-86-9811, Apr.
    1986.

21. Gaster, M: A Simple Device for Preventing Turbulent Contamination
    on Swept Leading Edges. Royal Aero. Soc. J. Technical Notes, vol.
    69, Nov. 1965, pp. 788-789.

THE RIGHT WING
OF THE
L.E.F.T. AIRPLANE

Arthur G. Powell
Douglas Aircraft Company
McDonnell Douglas
Long Beach, California

ABSTRACT

The NASA Leading-Edge Flight Test (L.E.F.T.) program addressed the environmental issues which were potential showstoppers in the application of Laminar Flow Control (LFC) to transport aircraft. These included contamination of the LFC surface due to dirt, rain, insect remains, snow, and ice, in the critical leading-edge region. As part of NASA contract NAS1-16220, Douglas Aircraft Company designed and built a test article which was mounted on the right wing of the NASA C-140 Jetstar aircraft. (The Lockheed test article, installed on the left wing, will not be discussed in this paper.) The Douglas test article featured a retractable leading-edge high-lift shield for contamination protection and suction through perforations on the upper surface for LFC.

Following a period of developmental flight testing, the aircraft entered simulated airline service, which included exposure to airborne insects, heavy rain, snow, and icing conditions both in the air and on the ground. During the roughly 3 years of flight testing, the Douglas test article has consistently demonstrated laminar flow in cruising flight.

This paper briefly summarizes the Douglas experience with the L.E.F.T. experiment, with emphasis on significant test findings. The following items are discussed:

- Test article design and features.

- Suction distribution.

- Instrumentation and transition point reckoning.

- Some problems and fixes.

- System performance and maintenance requirements.

- Conclusions.

FOREWORD

This paper highlights the design and analyses detailed in References 1 and 2, performed by the Douglas Aircraft Company, McDonnell-Douglas Corporation, under the NASA contract entitled, "Laminar Flow Control Leading-Edge Glove Flight Test Article Development." The program was administered through Langley Research Center under the direction of NASA Laminar Flow Control project manager, Mr. R. D. Wagner. The L.E.F.T. project technical manager was Mr. M. C. Fischer, and more recently, Mr. D. V. Maddalon.

Flight testing was conducted by NASA Ames/Dryden Flight Research Facility staff. The flight test project manager was Mr. R. S. Baron, and more recently, Ms. J. L. Baer-Riedhart. The principal investigator was Mr. D. F. Fisher, and more recently, Mr. L. C. Montoya. Special thanks goes to Mr. J. A. Thelander at Douglas, who patiently analyzed the data.

The ultimate acceptability of laminar flow technology to airplane operators depends critically on the level of additional maintenance required and the ability to achieve laminar flow reliably on a daily basis. Surface erosion and contaminant accretion are known to be almost exclusively confined to the wing leading-edge region. This region is the most critical for wing laminarization.

The NASA Leading-Edge Flight Test was conceived as a critical test of LFC contamination-avoidance technologies. Douglas Aircraft Company (DAC), under contract to NASA, designed and built a leading-edge test article which was flown on the starboard wing of NASA's C-140 Jetstar aircraft (Figure 1). The DAC test article featured a retractable leading-edge high-lift shield for contamination protection, and suction through perforations on the upper surface for laminar flow control.

Earlier DAC system studies suggested that a high-lift shield, deployed from the wing undersurface, could protect the LFC leading edge from airborne contamination and allow higher lift coefficients for takeoff and landing. Although the shield may prevent lower surface laminarization, the reduction in wing size allowed by the higher maximum lift coefficient, along with the simplification of the LFC suction systems, makes this a favorable trade.
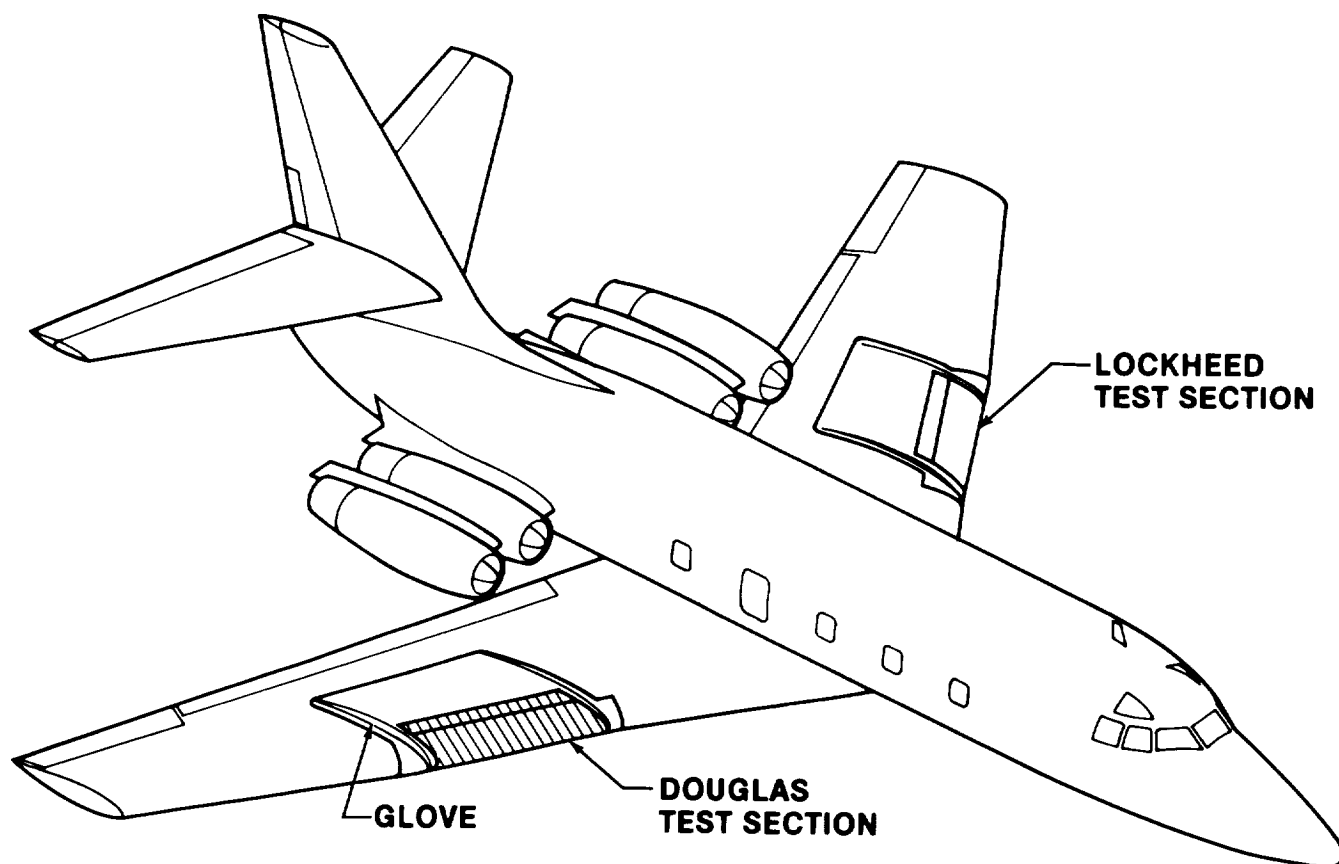
FIGURE 1. NASA JETSTAR AIRPLANE

The test article and glove were designed to give a chordwise pressure distribution that would be representative for both surfaces of a full-chord LFC wing. Douglas and Lockheed worked together to arrive at a suitable glove shape. The proximity of the engine nacelles caused a perturbation to the glove pressure distribution, which was accounted for by incorporating incremental nacelle pressures from a high-speed wind tunnel test of the LFC configuration. Figure 2 shows the test article planform, the changes to the wing geometry at the inboard and outboard glove stations, and the resulting chordwise pressure distribution in the glove midspan region.
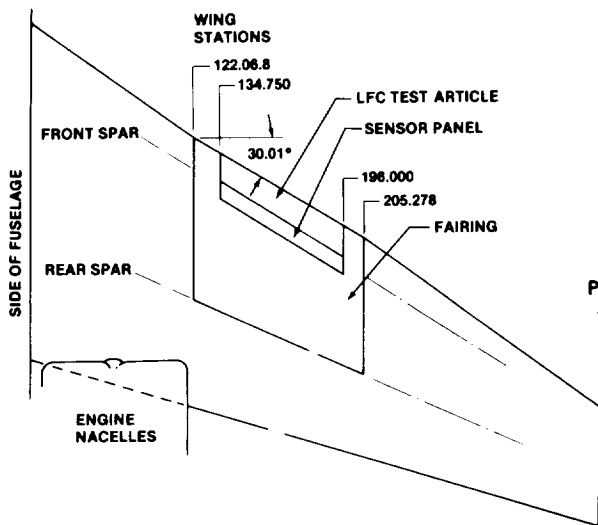
FIGURE 2A. JETSTAR LFC TEST ARTICLE PLANFORM
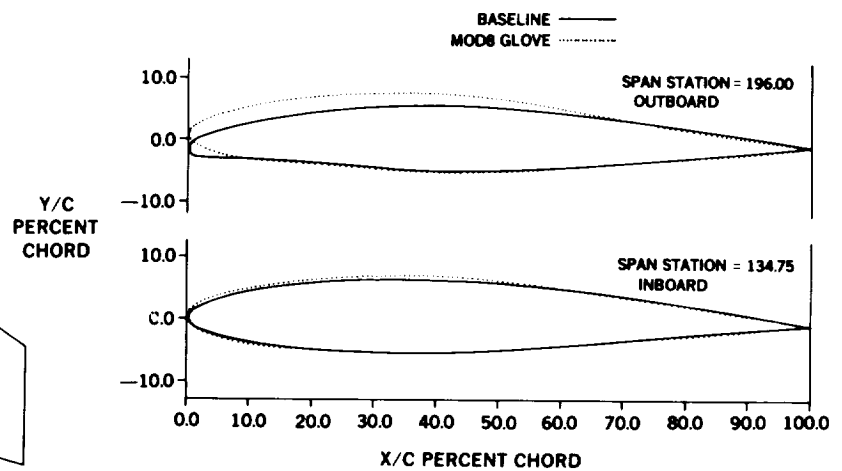
FIGURE 2B. COMPARISON OF JETSTAR AND LFC GLOVE DEFINING AIRFOIL SHAPES
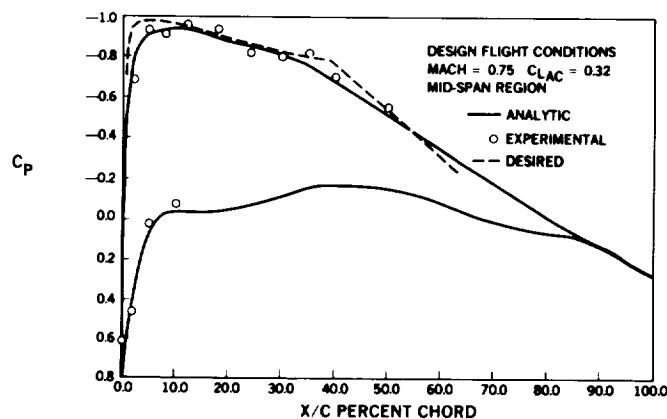
FIGURE 2C. COMPARISON OF PREDICTED DISTRIBUTION WITH JETSTAR MODEL TEST DATA AND DESIRED LFC PRESSURE DISTRIBUTION

145

The contamination-avoidance and ice-protection systems are shown in Figure 3. The primary component of these systems is the shield, which physically blocks contaminants from impacting on the leading edge. A propylene glycol methyl ether (PGME) spray system, located behind the shield, provides capability for de-icing after flight into icing conditions and was intended to augment the shield by wetting the LFC surface so any contaminants getting past the shield would not stick to it. (Despite its small size, the shield has proven so effective for contamination avoidance that the spray system was sealed off for summer operations.) Freezing-point depressant liquid (FPD) or rainwater is prevented from entering the perforated LFC surface by maintaining a small positive pressure differential across the porous surface. This is set by surface tension considerations at about 0.5 psi. Shield de-icing is provided by a woven stainless-steel insert on the shield leading edge which oozes FPD liquid.
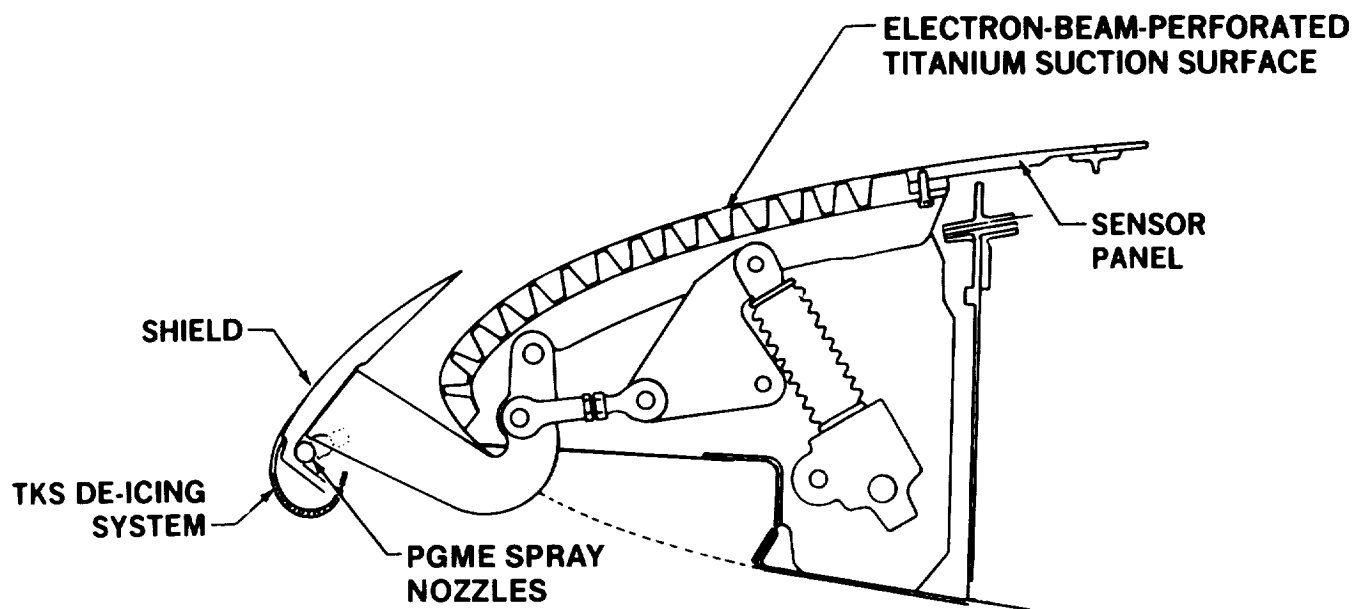
FIGURE 3. DOUGLAS CONTAMINATION-AVOIDANCE AND ICE-PROTECTION SYSTEMS

146

The NASA MARIA code (Reference 3) was found to be a convenient tool for evaluating the effectiveness of various trial suction distributions. Although the computations are done in an approximate way, and the code only computes the amplifications of zero-frequency cross-flow waves, it has the ability to quickly compute and present the amplifications of a wide spectrum of wavelengths. This allows the effects of many trial suction distributions to be viewed in a short time. The code also does an excellent job of identifying critical wavelengths for corroborative analyses using the SALLY or COSAL codes. Figure 4 illustrates the effectiveness of suction application at the attachment line (trial distribution Number 3). This result would not have been expected using the X-21 cross-flow transition criterion, but has been verified using the SALLY code and by test data. Trial distribution Number 3 became the basic suction distribution.

MARIA CROSS-FLOW STABILITY ANALYSIS
PARAMETRIC STUDY: BASELINE CONDITION (M = 0.75 $C_{L_{AC}}$ = 0.33 ALT = 38,000)
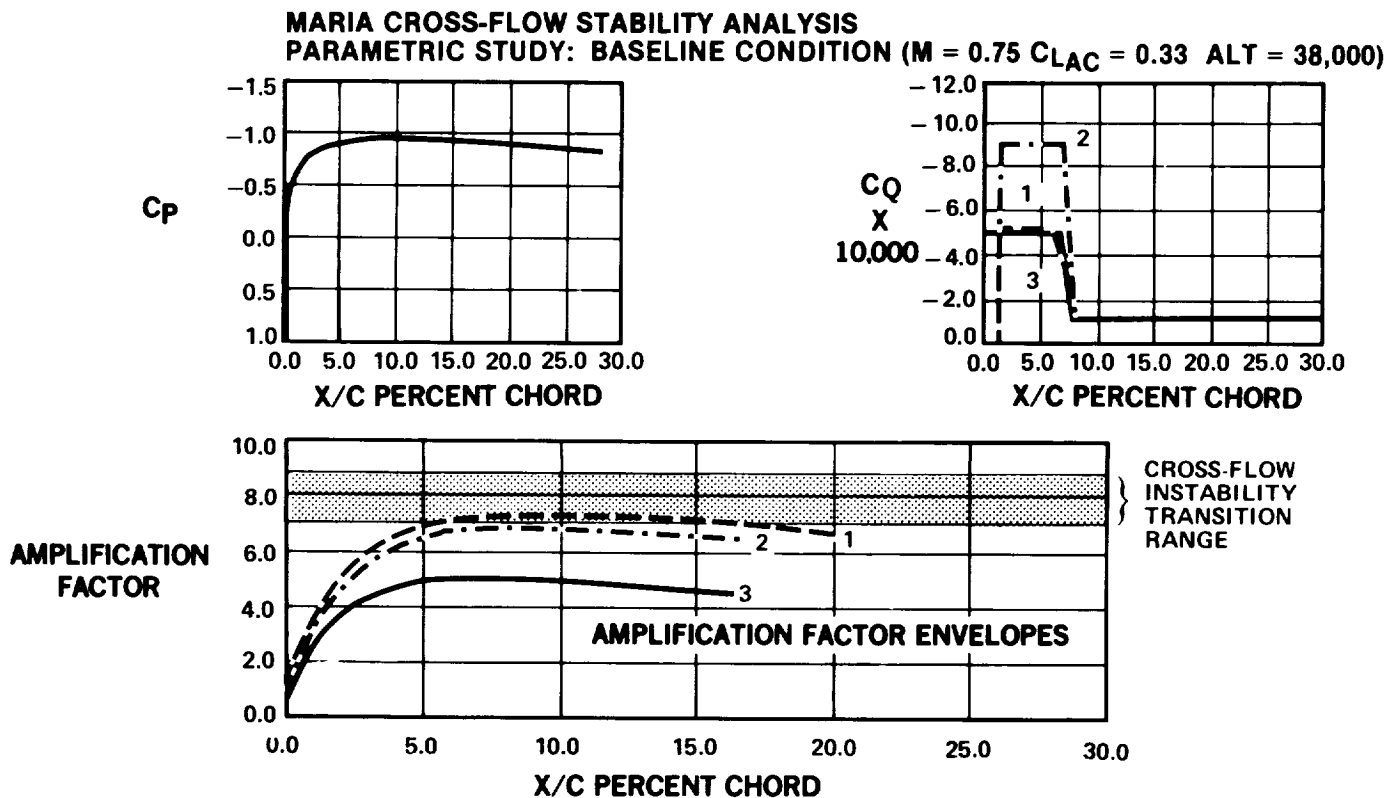
FIGURE 4. EFFECT OF SUCTION DISTRIBUTION ON CROSS-FLOW INSTABILITY

The basic and nominal suction distributions are shown in Figure 5. The basic suction distribution was developed based on MARIA and SALLY analyses of stationary cross-flow disturbance amplifications, taken at a computational station near the glove centerline. Cross-flow amplification factors were held at conservative levels of around five. Tollmien-Schlichting (T-S) amplifications were checked and found not to be critical. Using known external pressures and porous surface characteristics, required flute pressures were obtained. Analysis of spanwise and chordwise external pressure variations over the porous leading edge indicated the necessity of slightly higher suction levels in order to ensure that all span stations would have at least the basic suction levels. This defined the nominal suction distribution. The apparently higher suction level on flute Number 1 is only a consequence of the way in which the nonporous area is accounted for. The suction system was designed to allow at least a 50-percent oversuction capability from the nominal.
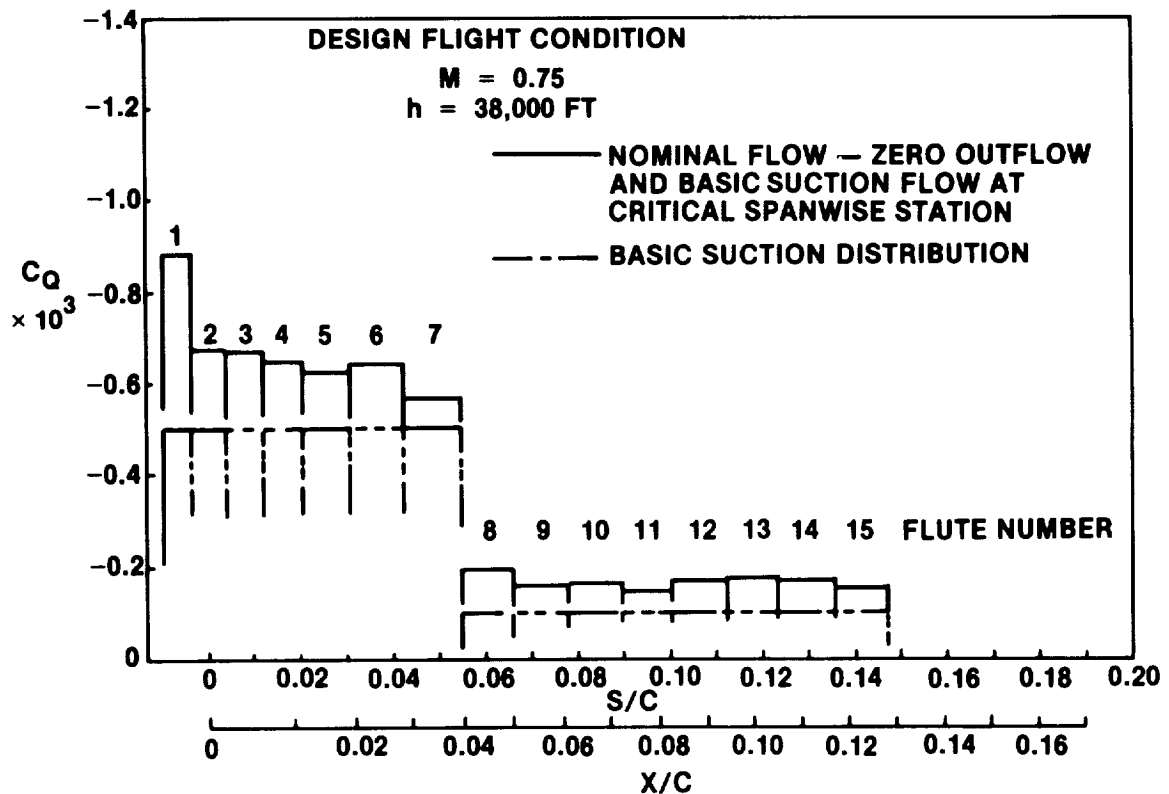
FIGURE 5. BASIC AND NOMINAL SUCTION DISTRIBUTIONS

The surface waviness criterion for the LFC leading edge was based on available X-21 results (Reference 4) and is shown in Figure 6 for M = 0.75, at 30,000- and 38,000-foot altitudes. Waviness measurements of the LFC leading-edge suction panel, after bonding the perforated titanium skin to the fiberglass substructure, are plotted in the figure. These measurements were all within the limits specified, and encompass the entire span of the suction panel. Observance of waviness criteria is a simplified approach to avoiding laminar separations, excessive growth of T-S waves, and critical amplification of Görtler vortices, which might not be accounted for otherwise. Aerodynamic and boundary layer stability analyses of the actual measured surface are the alternative.
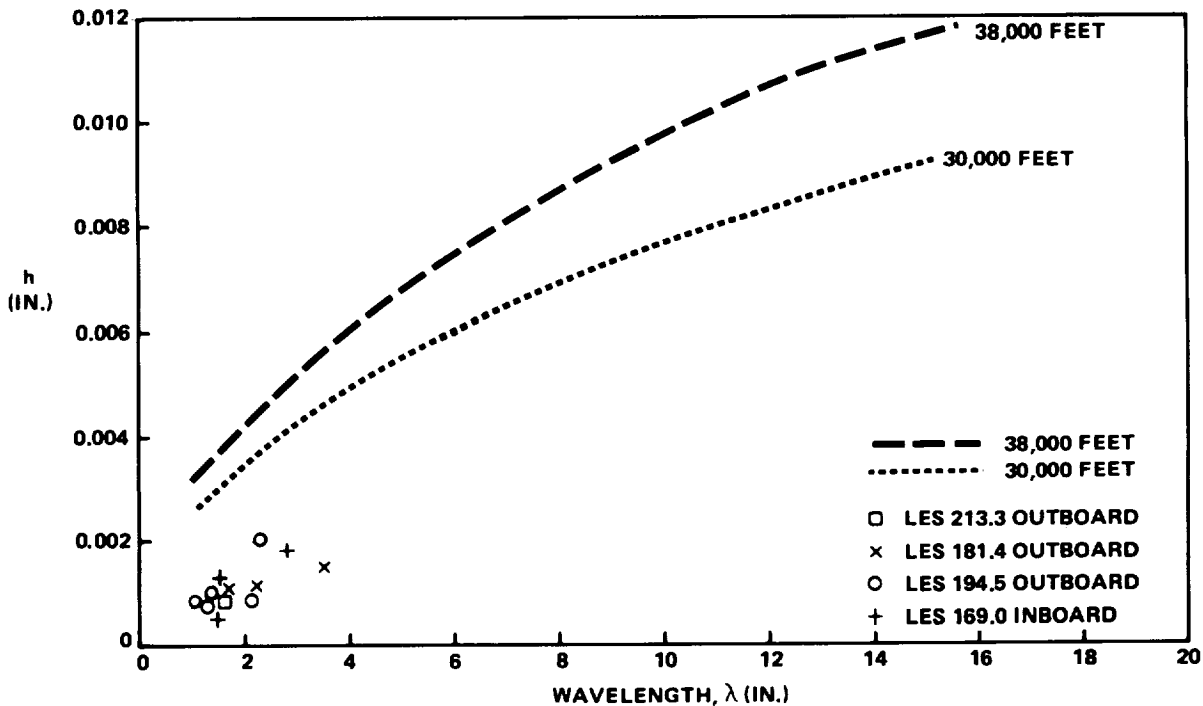
FIGURE 6. LFC FLIGHT TEST ARTICLE WAVINESS VERSUS MULTIPLE-WAVE CRITERION

149

The surface instrumentation layout is shown in Figure 7. It consists of three chordwise rows of static pressure taps, a leading-edge-normal row of hot film sensors, and a row of 20 boundary layer Pitot tubes mounted on a sensor panel just aft of the perforated LFC surface. It was important that the static pressure taps not trip the flow so the existing electron beam perforations were used where possible. The static pressure taps were placed in the inactive areas between the suction flutes. In locations where adhesive bonding had blocked the holes, a Number 80 drill was used, and was found sufficiently small so as to not disturb the flow. The centerline row consisted of 16 taps, and the two side rows had 8 taps each. The flute pressures were also monitored.
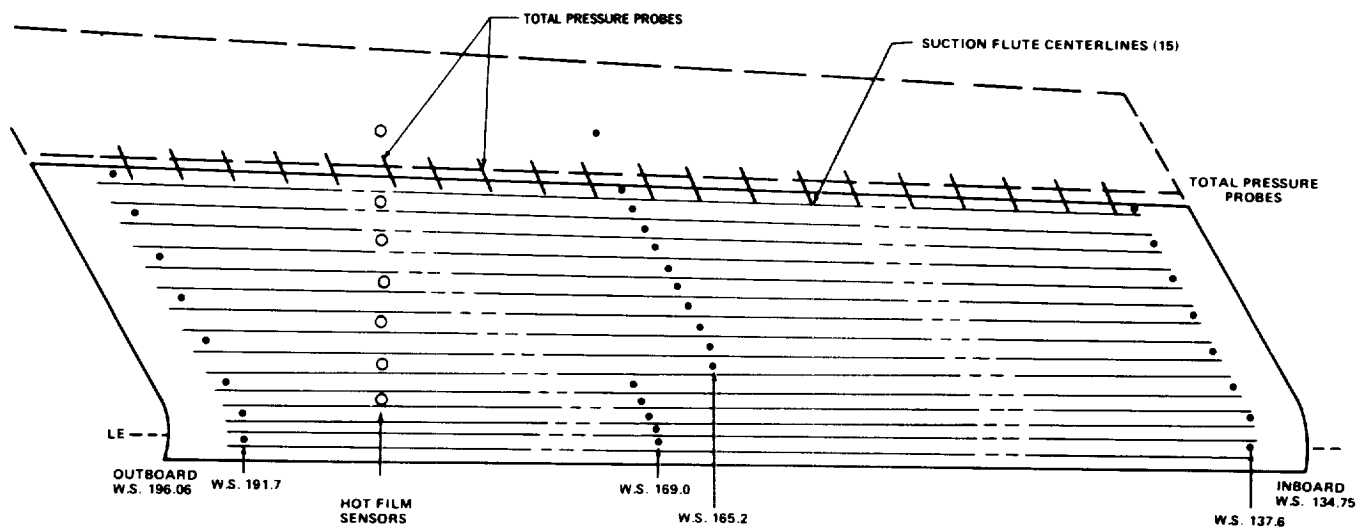
FIGURE 7. TEST ARTICLE SURFACE INSTRUMENTATION

150

A series of boundary layer Pitot tubes, mounted on the sensor panel aft of the suction surface, as shown in Figure 7, were used for determining whether or not the boundary layer is locally laminar, and for reckoning the transition point upstream. Two Pitot tubes located well above the boundary layer measured free-stream total pressure. Other tubes were located at 0.060 inch above the surface, just above a laminar boundary layer, but within a turbulent boundary layer. Total pressure deficit is used to determine transition location. Boundary layer computations were made, based on measured pressure distributions, for various altitudes at Mach 0.75 (Figure 8a) over a range of transition locations. A set of curves (Figure 8b) was constructed showing the total pressure deficit as a function of chordwise transition location for each altitude. Note that laminar separation is predicted for the 38,000- and 40,000-foot altitudes. This is due to a local compression in the chordwise pressure distributions near flutes 13 and 14 at these altitudes.
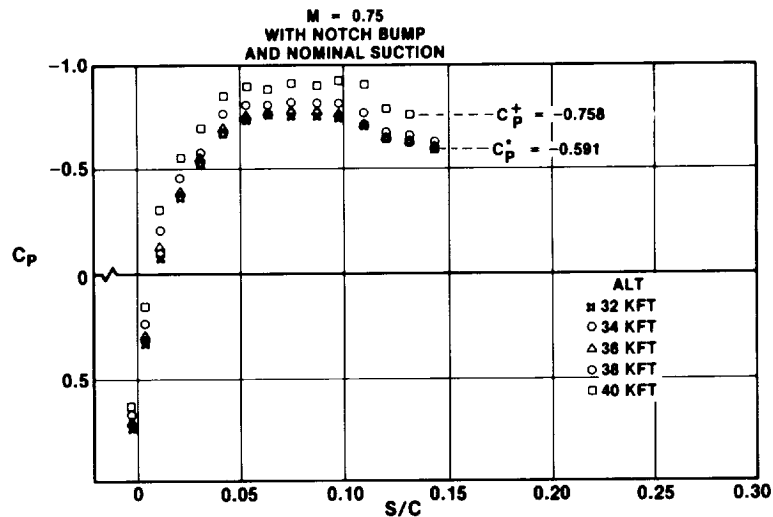
FIGURE 8A. MEASURED CHORDWISE PRESSURE DISTRIBUTIONS
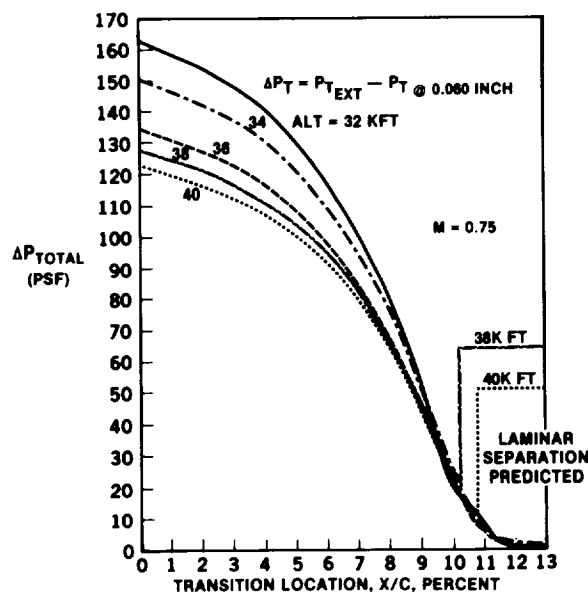
FIGURE 8B. PREDICTED BOUNDARY LAYER TOTAL PRESSURE DEFICIT VALUES

Figure 9 shows the boundary layer total pressure deficits on the test article for the first design-point test of the suction system. Except for a problem inboard, attributable to spanwise turbulence transfer along the attachment line onto the LFC test article, and a couple of small turbulent wedges, the test article succeeded in achieving laminar flow. The turbulent area inboard was later cured by the application of a passive turbulence diverter (Gaster bump or notch/bump). The pressure deficits further outboard occurred only at the higher altitude, where laminar separation was predicted.
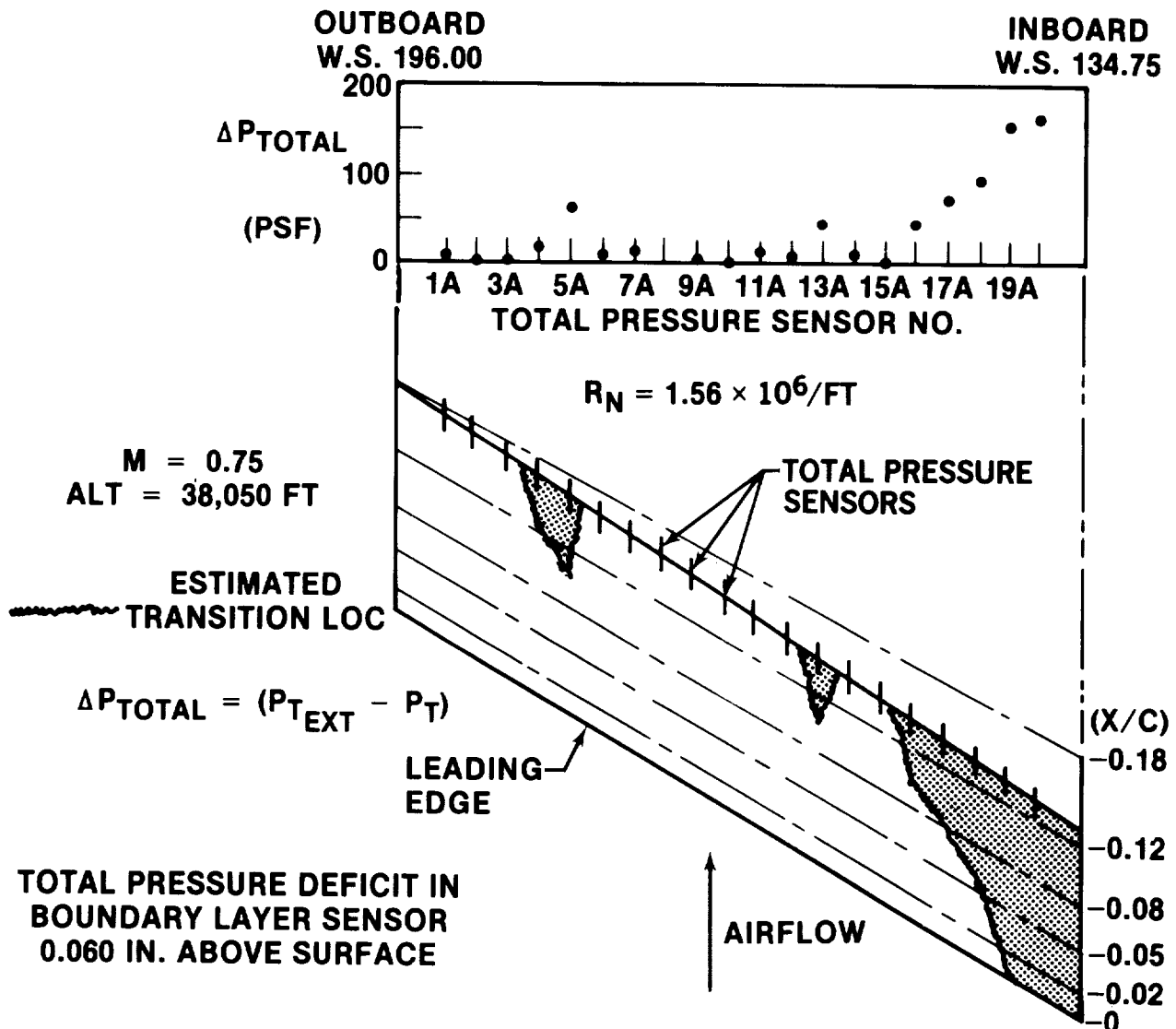
FIGURE 9. INITIAL TRANSITION PATTERN BEFORE INSTALLING NOTCH BUMP

A number of data points were taken at different flight conditions -- and different unit Reynolds numbers -- before the turbulence diverter was installed. The cases shown in Figure 10 are all for nominal suction. Of interest is the distance along the test article the turbulence was able to propagate at different unit Reynolds numbers. The attachment line momentum thickness Reynolds numbers are also shown in parentheses, and tend to confirm the lower critical value of around 100. The application of a turbulence diverter (notch/bump in this case) to the inboard end of the test article is seen to affect a cure. According to Reference 5, if the attachment line can be kept free of supercritical excrescences by the use of the shield, laminar flow is possible with attachment line momentum thickness Reynolds numbers up to approximately 240. Since the attachment line Reynolds number varies roughly with the square root of leading-edge radius, the successful functioning of the leading-edge shield as a protection device allows application of LFC to large aircraft.
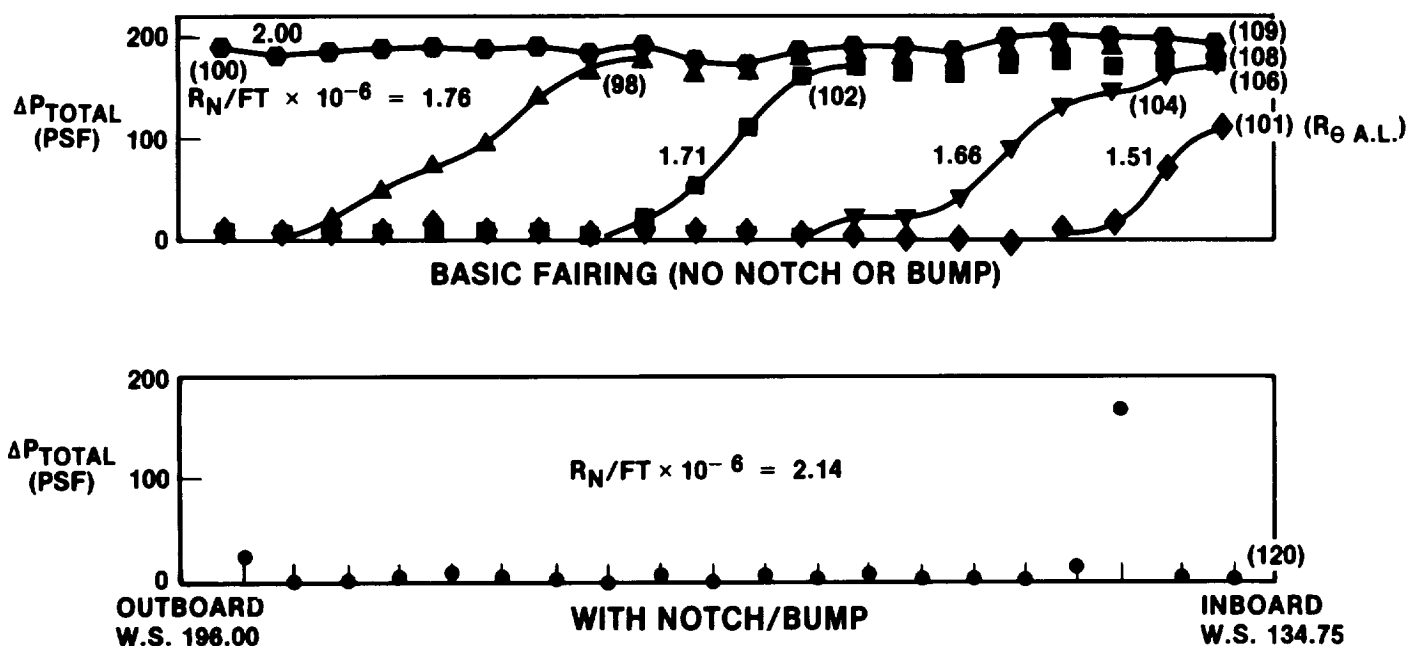
FIGURE 10. EFFECT OF R_N ON TURBULENCE TRANSFER AND NOTCH/BUMP EFFECTIVENESS

Figure 11 shows a matrix of test conditions varying with Mach number and altitude and showing the corresponding unit Reynolds numbers. To the left of the hatched bar, 100-percent laminar flow was achieved; to the right there was some reduction. It is obvious that this reduction was not caused by increasing Reynolds number or angle of attack and is consistent with being caused by an increasing shock tendency. This was also consistent with the previously discussed laminar separation predicted at higher altitudes and possibly by a local shock condition aggravated by the presence of the Pitot tube assembly and its mounting.
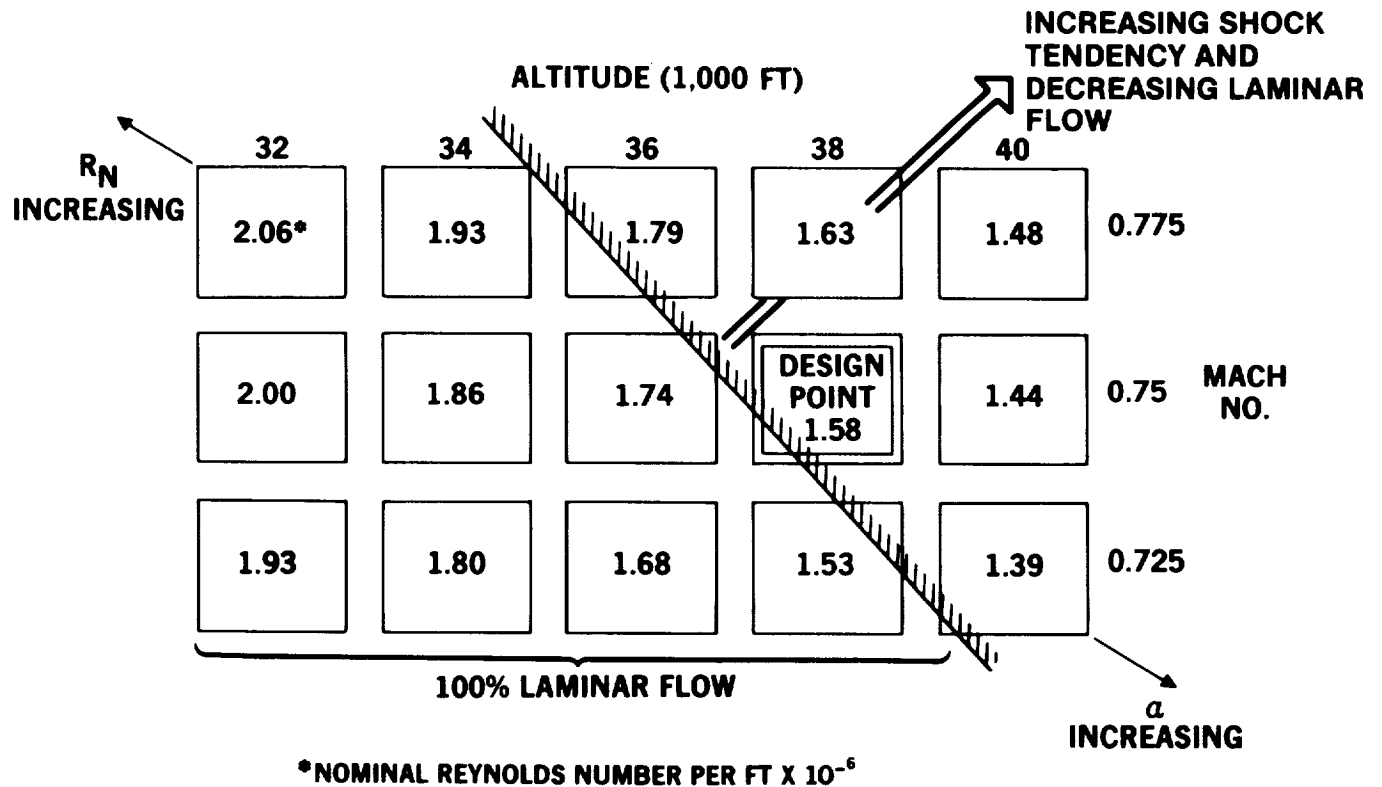
FIGURE 11. FLIGHT TEST MATRIX — SHOCK SENSITIVITY THRESHOLD

There has been concern expressed that high suction flow through a perforated surface might generate a disturbance sufficient to trip the boundary layer, due to vortices trailing off of each suction hole. These vortices are strongest at maximum suction. Suction, up to the level of choking the holes in the porous surface, was achieved when 150 percent of nominal suction flow was demonstrated at design-point flight conditions. For this flight the turbulence diverter was not yet installed, and the test point is within the region where the shock problem exists as shown in Figure 12. Flute Number 3 was choked, as evidenced by the low pressure ratio across the surface (less than 0.528) and the fact that increasing the total suction flow did not increase the suction coefficient. No adverse effect of the oversuction or even choking is seen; in fact, the oversuction has apparently reduced the extent of turbulence along the test article leading edge.

$$M = 0.75$$
$$\text{ALT} = 38,000 \text{ FT}$$
$$R_N/L = 1.52 \times 10^6/\text{FT}$$
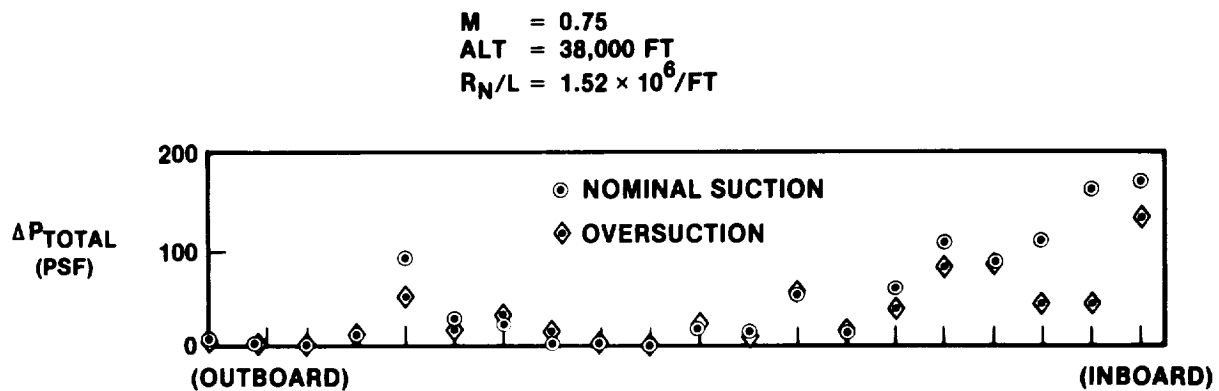
FIGURE 12. EFFECT OF OVERSUCTION AT DESIGN POINT

Goldsmith's single-row hole flow correlation (Reference 6) is the only guideline currently available for allowable hole parameters. Physically, the question of whether or not the boundary layer is tripped reduces to whether or not the trailing vortices created by the flow into the holes have an opportunity to interact in a destructive way before being damped out by viscosity. Transition is correlated to the equivalent disturbance-height Reynolds number, and a ratio of hole spacing to sucked streamtube height. The correlation is shown in Figure 13. The flute 3 choked-flow data point is shown. Since the boundary layer was not tripped, one can conclude that if a similar correlation curve exists for multiple hole rows, it lies to the right of the data point. It also appears highly probable that holes smaller than 0.0025 inch are not necessary.

**M = 0.75, h = 35,000 FT,
FLUTE NO. 3 CHOKED**

Δq = **VOLUME FLOW PER HOLE**

α = **CROSS-STREAM HOLE SPACING**

$\bar{h}$ = **CHARACTERISTIC HEIGHT OF SUCKED STREAMTUBE**

$\bar{V}$ = **CHARACTERISTIC VELOCITY OF SUCKED STREAMTUBE**

$$\bar{h} = \left[\frac{2\Delta q}{\alpha} \bigg/ \left(\frac{\partial u}{\partial y}\right)_{y=0} \right]^{1/2}$$

$$\bar{V} = \frac{\Delta q}{\alpha} \bigg/ \bar{h}$$

$$R_{ek} = \frac{\rho}{\mu} \frac{\Delta q}{\alpha} = \frac{\bar{V}\bar{h}}{\nu}$$
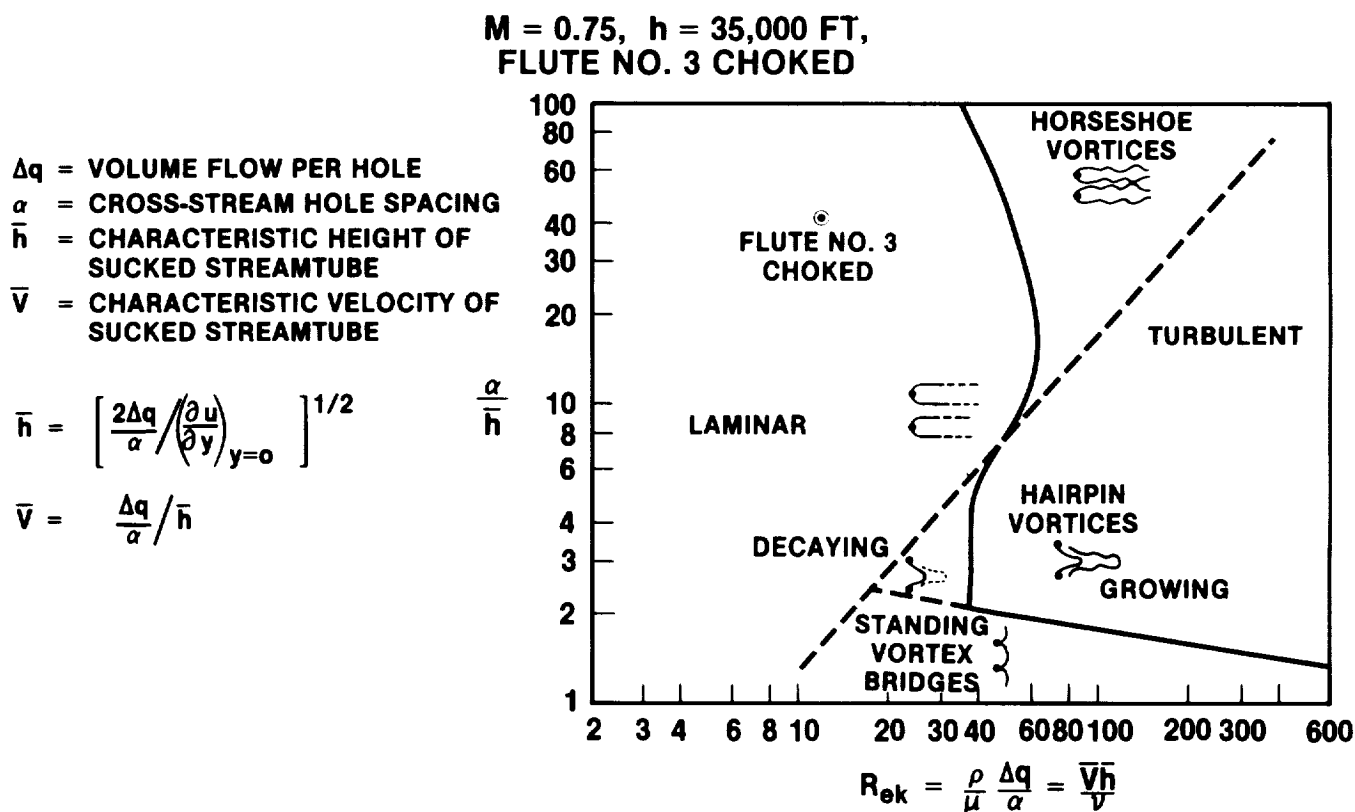
FIGURE 13. CHOKED PERFORATED SURFACE AND GOLDSMITH'S CORRELATION

The presence of atmospheric ice particles was detected by a charge plate which utilized the triboelectric effect (also responsible for carpet shock). The aircraft was flown through clouds and haze, which at cruise altitude consist of ice particles, and an excellent correlation was obtained between charge plate readings and laminar flow degradation or loss. Figure 14 is a typical result. Laminar flow was always recovered immediately upon exiting airspace where ice crystals were present. One interesting sidenote is that, in at least two instances, ice crystals apparently scoured away a supercritical deposited excrescence. A drop in boundary layer total pressure deficit at one station was observed as a result of an ice crystal encounter, indicating a recovery of laminar flow after the excrescence was removed.
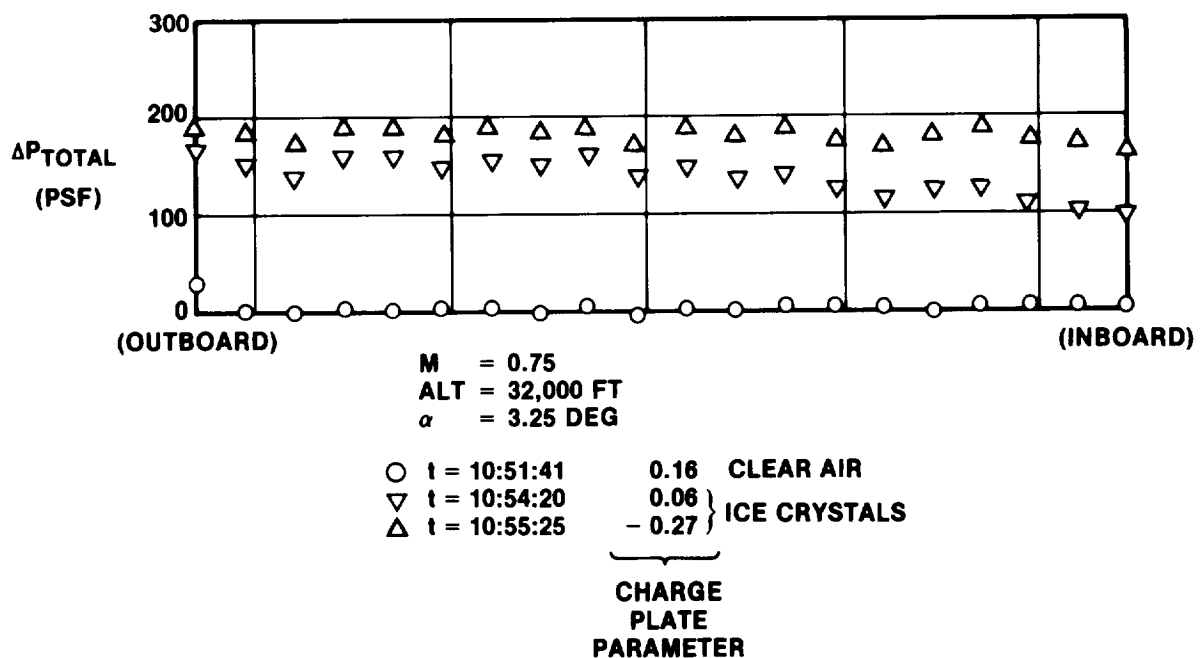
FIGURE 14. EFFECT OF ICE CRYSTAL ENCOUNTER

Following more than a year of developmental flight testing, the aircraft was placed into simulated airline service in order to test the effectiveness of the contamination-avoidance and ice-protection systems. This included operation in heavy rain and icing conditions, as well as operation in areas of heavy insect infestation. Despite this intentional exposure to the worst summer and winter conditions, the Douglas test article reliably achieved laminar flow. The performance of the Douglas system in 59 flights from 45 airports is summarized in Figures 15a and 15b.

CLEVELAND

PITTSBURGH

ATLANTA

HOME BASE

☐ ATLANTA
☐ PITTSBURGH
☐ CLEVELAND

DATE

JULY 85
SEPTEMBER 85
FEBRUARY 86

59 FLIGHTS TO 45 AIRPORTS
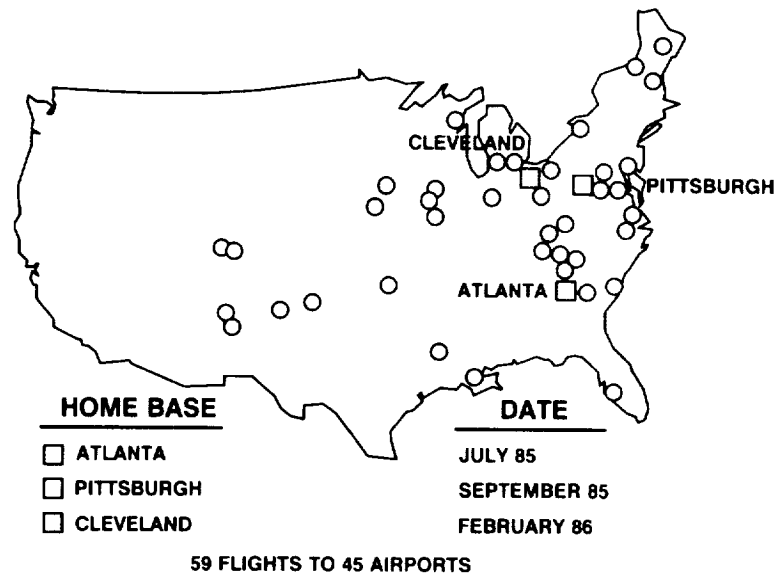
FIGURE 15A. SIMULATED SERVICE FLIGHT TESTS

- LFC ACHIEVED ON INITIAL TEST FLIGHT
- LFC RECOVERED IMMEDIATELY FOLLOWING
  FLIGHT THROUGH ICE CRYSTALS
- LFC OBTAINED RELIABLY THROUGHOUT SIMULATED
  AIRLINE SERVICE FLYING:
  - SUMMER CONDITIONS
    - AIRBORNE INSECT INFESTATION
    - HEAVY RAIN STORMS
  - WINTER CONDITIONS
    - OVERNIGHT EXPOSURE TO ICE AND SNOW
    - IN-FLIGHT ICING CONDITIONS
- NO DETERIORATION OF LFC POROUS SURFACE
  OR PERFORMANCE IN 3 YEARS OF FLIGHT TESTING

FIGURE 15B. SUMMARY OF DOUGLAS LFC LEADING EDGE PERFORMANCE
DURING JETSTAR FLIGHT TESTS

During the year-round simulated airline service, the aircraft was left out overnight in whatever conditions prevailed. Figure 16 shows the typical maintenance procedure for snow and ice removal, in this case after the aircraft was exposed to an overnight snow flurry in Cleveland. It is significant to note that 100-percent laminarization was routinely achieved with no additional maintenance required due to the presence of the Douglas LFC test article. The PGME spray system built into the shield was found to be unnecessary for contamination avoidance and was only used for de-icing. Detailed inspection of the perforated titanium surface after nearly three years of operation revealed no visible wear or erosion, and there has been no deterioration in performance.

ORIGINAL PAGE IS
OF POOR QUALITY
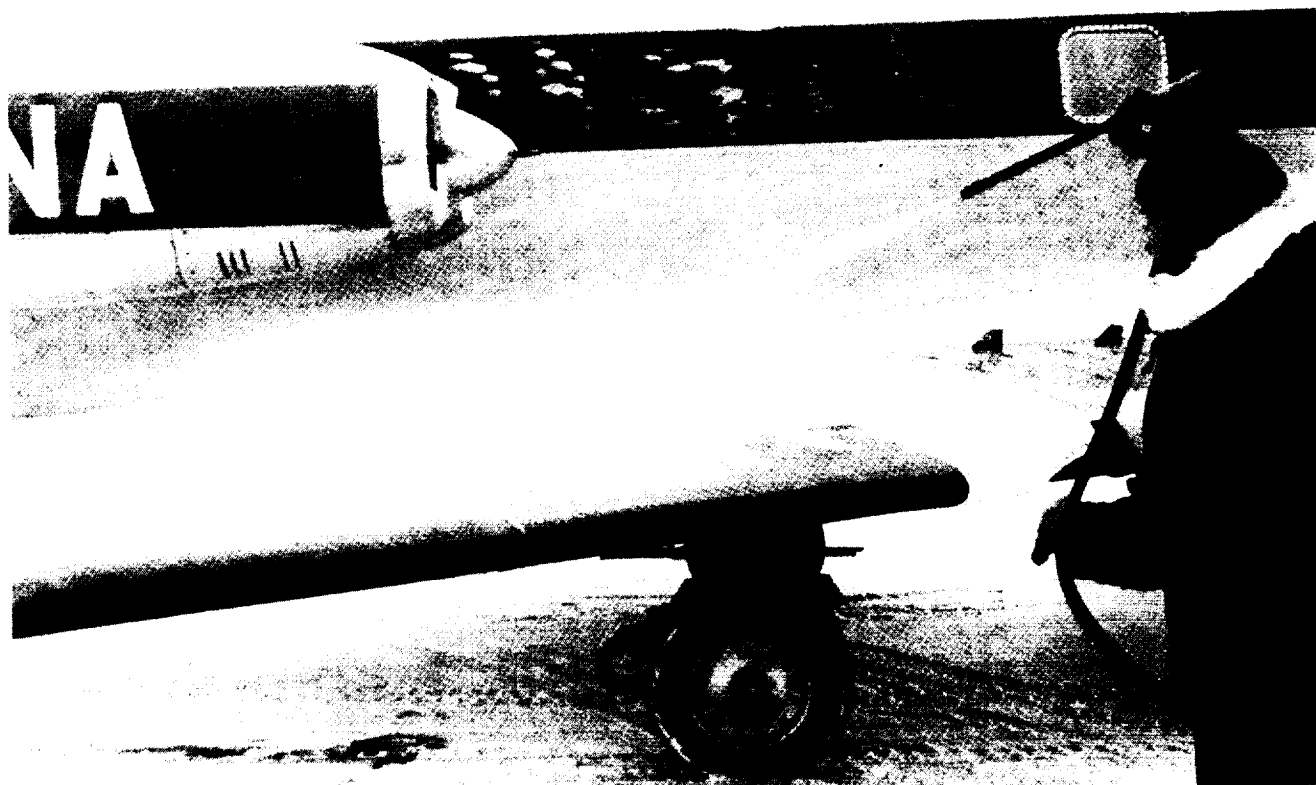
FIGURE 16. STANDARD SNOW AND ICE REMOVAL PROCEDURE

CONCLUSIONS

The results of this test program have been extremely encouraging. The success of the Douglas contamination-avoidance and ice-protection systems has established LFC as an attainable drag-reduction technology which would be acceptable to airplane operators. Principal conclusions are listed below.

1. The electron-beam perforated surface provided reliable laminar flow control.

2. The contamination-avoidance/ice-protection system was successful in protecting the LFC leading edge:

    a. The high-lift shield worked very well, despite its small size.

    b. Shield retraction at 5,000 feet AGL was sufficient to avoid insect contamination.

    c. The spray system was only needed for de-icing.

3. The Gaster-bump and notch/bump were successful in preventing the spanwise spread of turbulence along the attachment line.

4. Increasing the level of suction, even to the point of choking the holes, did not trip the boundary layer.

5. Some laminar flow is lost in ice particle encounters, but it is regained immediately in clear air.

6. No additional maintenance was required for the LFC system.

7. No degradation in the LFC surface or its performance was evident after 3 years of flight testing.

8. Laminar flow is attainable on a day-to-day operational basis regardless of environmental factors.

REFERENCES

1. Douglas Aircraft Company: Laminar Flow Control Leading-Edge Glove Flight Test Article Development. NASA CR 172137, November 1984.

2. Thelander, J. A.: Flight Test Data Analysis and Review, LFC Leading-Edge Flight Test Article Interim Report. MDC Report J3845, December 1985.

3. Dagenhart, J. R.: Amplified Cross-Flow Disturbances in the Laminar Boundary Layer on Swept Wings With Suction. NASA TP 1902, November 1981.

4. Carmichael, B. H.: Surface Waviness Criteria for Swept and Unswept Laminar Suction Wings. Northrop Report NOR-59-438, August 1959.

5. Bacon, J. W.; and Pfenninger, W.: Transition Experiments at the Front Attachment Line of a 45-Degree Swept Wing With a Blunt Leading Edge. AFFDL-TR-67-33, June 1967.

6. Goldsmith, J.: Critical Laminar Suction Into an Isolated Hole or a Single Row of Holes. Northrop Report NAI-57-529 or BLC-95, February 1957.

PERFORMANCE OF LAMINAR-FLOW LEADING-EDGE TEST ARTICLES
IN CLOUD ENCOUNTERS

Richard E. Davis, Dal V. Maddalon, and Richard D. Wagner
NASA Langley Research Center
Hampton, Virginia

BACKGROUND

MECHANISM FOR LOSS OF LAMINAR FLOW IN PARTICLES

The problem of cloud effects on LFC* aircraft was first noticed on the USAF X-21 program when, during flight testing at typical cruise conditions of M = 0.75 and 40,000 ft. altitude, it was observed that laminar flow was totally lost whenever the aircraft penetrated cirrus clouds, with horizontal visibilities estimated to be about 5,000-10,000 feet. Also, LFC performance was observed (ref. 1) to be partially degraded or erratic when penetrating light cirrus haze, even when the horizontal visibility was as much as 50 miles. (As will be described later in this paper, cirrus clouds, both thick and tenuous, are causing similar corresponding effects on the LEFT[+] JetStar aircraft). At these altitudes, cirrus clouds are composed mainly of ice crystals. These crystals have a detrimental effect on maintaining laminar flow, depending on their size and concentration (or flux as perceived by the aircraft). To explain the erratic LFC performance on the X-21, Hall (ref. 2) developed a theory to predict the effect of ice particle encounter on the maintenance of laminar flow. The theory postulated that ice particles entering the laminar boundary layer shed turbulent vortices; these vortices cause transition in the main flow (Fig. 1). As shown on the figure, the key factors which determine whether any given cloud encounter will cause total, partial, or negligible loss of laminar flow are the particle size, the particle concentration, and the particle's residence time in the boundary layer. Pfenninger (ref. 3) has suggested that wing sweep is also a key factor. The spanwise flow on a swept wing can lead to greater particle wake velocity defects, which promote increased turbulence production, and the increased effective chord results in higher particle residence time in the boundary layer.

---

*Laminar-flow control (LFC)
[+]Leading-Edge Flight Test (LEFT)

ICE PARTICLE DEGRADATION OF LAMINAR FLOW

Key parameters

● Particle size
● Particle flux or concentration
● Particle duration in boundary layer
● Particle Reynolds Number
● Airfoil L.E. geometry
● Wing sweep

Mechanism for laminar flow loss

● Some particles enter laminar boundary layer
● Wakes shed from particles become turbulent and trigger boundary-layer transition
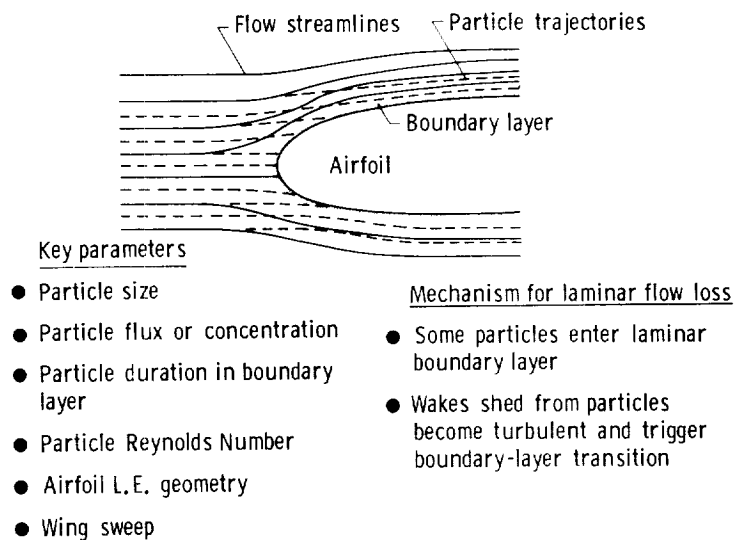
Figure 1

BACKGROUND

HALL CRITERIA FOR LOSS OF LAMINAR FLOW ON X-21

Hall's theoretical analysis considered only columnar ice crystals of length-to-diameter ratio 2.5, because that crystal form was assumed to be the predominant one. When the theoretical impingement dynamics of this type of particle on an elliptical approximation of the forward portion of the X-21 airfoil were considered, the results indicated that, for M = 0.75 and 40,000 ft. altitude, particles smaller than 4 micrometers (μm) in length will not impinge on the airfoil surface, but particles larger than about 50 μm will impinge at near free-stream velocity. If the particles are very small, i.e. shorter than 4 μm, aerodynamic forces predominate over inertia forces and most particles follow streamlines and few enter the boundary layer. As the ice particles become larger in size, they begin to penetrate the laminar boundary layer but do not cause a breakdown to turbulent flow until some critical size is attained. However, particles of this critical size must be present in a sufficiently large concentration in order to cause boundary-layer transition. Figure 2, from Hall's analysis, illustrates the above discussion for flight conditions of M = 0.75 and 40,000 ft. altitude. It should be noted that equivalent melted diameter, EMD, is chosen as the abscissa variable on the figure. It has been found that ice particles in cirrus clouds occur in several crystalline forms, and that the columnar variety is not necessarily the most numerous. (In any event, the regions on the figure pertain to columnar crystals). According to the analysis, for columnar ice particles with an EMD of less than 33 μm EMD, particle concentrations smaller than about 500 particles/m^3 produce no effect on maintaining laminar flow (LF)[region 2 of the figure]. As particle concentrations increase above about 500 particles/m^3 (for EMD greater than 33 μm), there is an increasingly detrimental effect on laminar flow (regions 3 and 4 of the figure).

It should be emphasized that the critical values of ice-particle size and concentration level depicted in Figure 2 pertain only to the X-21 aircraft, at M = 0.75 and 40,000 ft. altitude. For any aircraft, the critical values and the extent of the four regions just discussed are functions of airfoil leading-edge shape and sweep angle, and of aircraft airspeed and altitude. The critical values and extent also depend on the particle shape. All these factors affect the number of ice particles penetrating the boundary layer. One of the goals of the LEFT experiment is to develop, through operational experience, plots such as those of Figure 2 showing the regions for the JetStar aircraft. These may allow a limited validation of the Hall theory developed for the X-21, and allow its extension to other aircraft. Further discussion on these aspects may be found in reference 4.

PREDICTED LAMINAR FLOW DEGRADATION

40 000 ft, M = 0.75, X-21
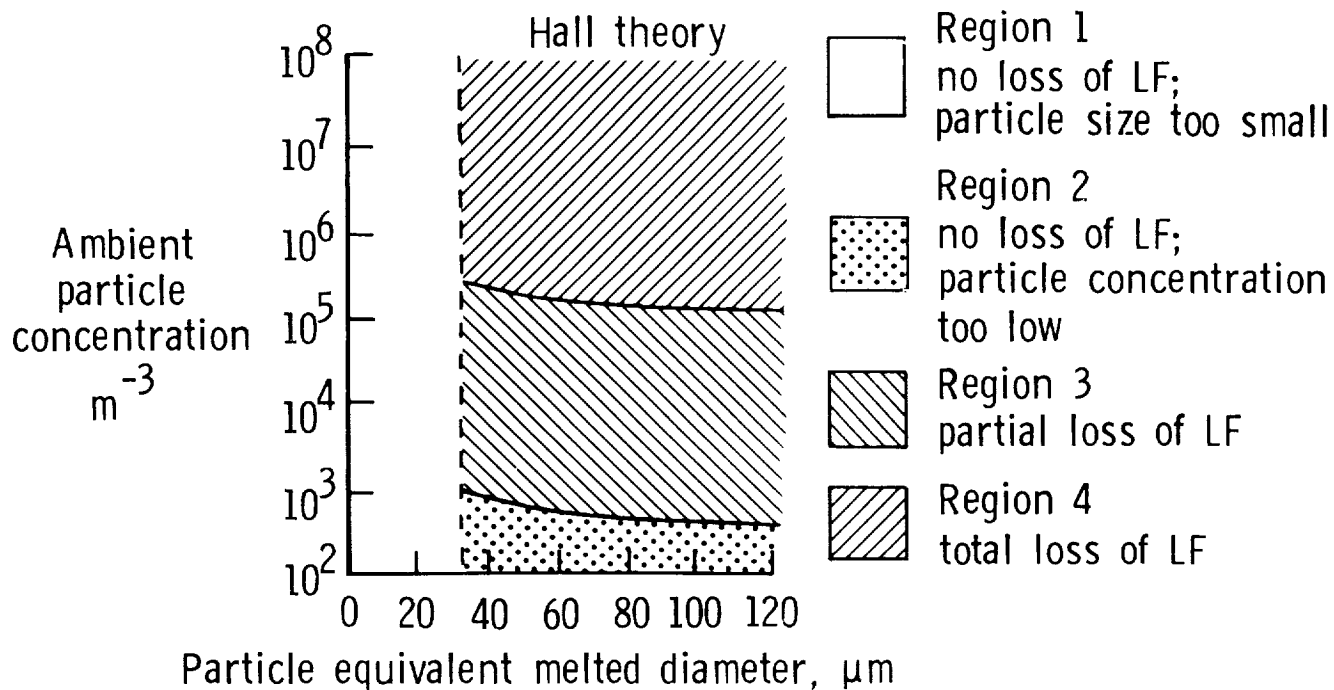
Figure 2

The objectives of our investigation are summarized in figure 3.

- Evaluate instruments for detecting conditions detrimental to laminar flow (LF)

- Measure cloud/haze particle environment and aircraft charge on all LEFT flights

- Correlate laminar flow extent on both leading-edge test articles with particle environment and aircraft charge

- Analyze data by statistical methods, for significant effects and relationships

- Validate the "Hall criteria", if possible

- Obtain statistical data on the probability of encountering clear air, haze or cloud

Figure 3

The meteorological instrumentation for measuring the ambient atmospheric particle environment during flights of the JetStar LEFT program consists of two instruments mounted on a pylon extending dorsally from the JetStar fuselage, as shown on Figure 4. The two instruments are a well-proven cloud particle spectrometer, commonly known as a Knollenberg probe, and an experimental particle detector based on a triboelectric (frictional) charge-exchange principle. Both instruments measure the free-stream particle environment, well away from any fuselage-induced concentration effects. A comprehensive description of both instruments may be found in reference 4; an abbreviated description is given next.
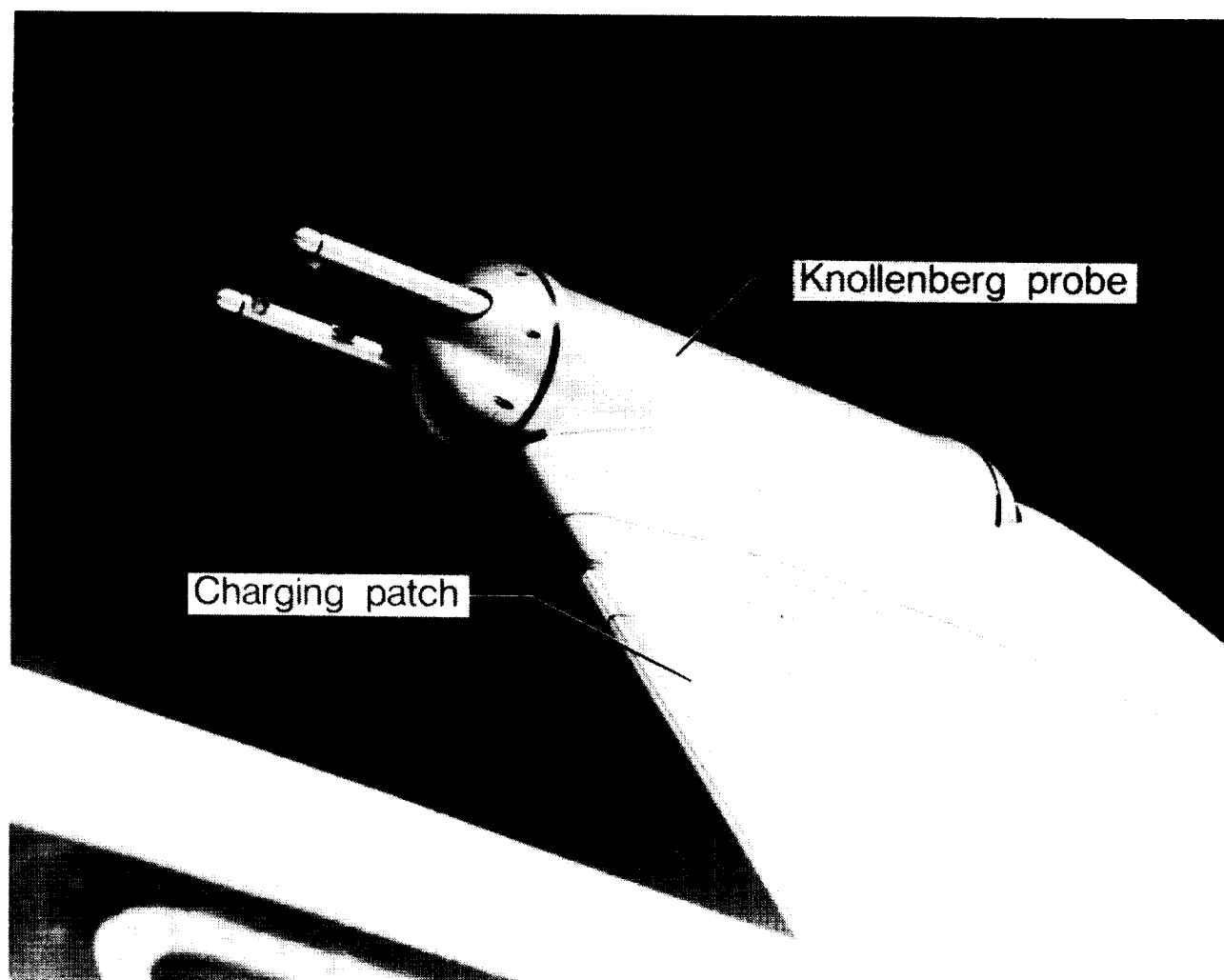
Figure 4

INSTRUMENTATION

CLOUD PARTICLE SPECTROMETER (KNOLLENBERG PROBE)

A Particle Measuring Systems (PMS), Inc. model OAP-230X Optical Array Cloud Droplet Spectrometer Probe; mounted atop the pylon in a cylinder (Fig. 4) is used as a "truth" instrument to measure the spectra (number density versus particle size) of cloud and other particles encountered on the LEFT missions. Figure 5 shows (a) the principle of operation, (b) a diagram of the probe's optical system, and (c) a photograph of the probe in its housing. Part (a) is a snapshot view of a particle passing transversely through the laser beam with the free-stream velocity V_∞. While within the beam, the particle's cross section casts a shadow which is imaged on the elements in the photodiode array. From the number of elements shadowed at any instant, an estimate of the particle's transverse dimension is obtained. The OAP-230X measures particles in 30 size bins between 20 and 600 μm effective size, with a bin resolution of 20 μm. The instrument is designed to provide measurements in all 30 size channels at 100 m sec^{-1} (194 knots) free-stream velocity; because the JetStar flies at approximately 500 kt. (258 m sec^{-1}), however, measurements in the first two size channels, 20-40 and 40-60 μm, are not obtained, but measurements of particles sized between 60 and 600 μm are obtained accurately. From Hall's (ref. 2) analysis, particles larger than 33 μm should affect laminar flow at 40,000 ft. and particles larger than 18 μm should effect laminar flow at 25,000 ft. altitude. Therefore, the probe will provide measurements of most of the particles that are predicted to affect LF, but not all. However, aerodynamic considerations, based on references 5 and 6 suggest that the other instrument (charging patch) is affected by particles down to 20 μm in size. Thus, the readings of both instruments taken together can be used to infer the total particle environment. This suggestion seems to be borne out by our operational experience, in which the charging patch indicates cloud encounters in about 4 percent more cases than does the probe. In most cases, however, both probe and patch indicate particles simultaneously.

OPTICAL ARRAY SPECTROMETER
(KNOLLENBERG PROBE)

Principle of operation
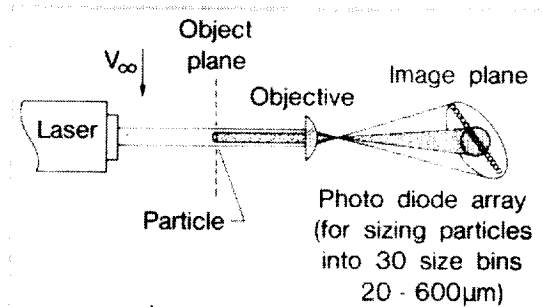
Probe optical system
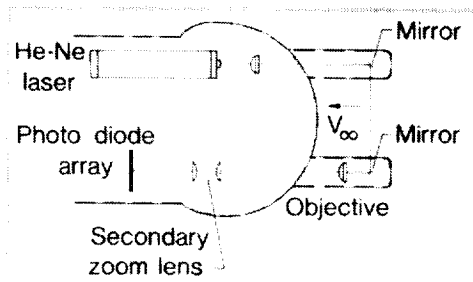
Probe in housing
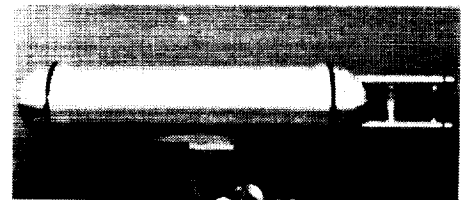
Figure 5

INSTRUMENTATION

CHARGING PATCH

As an aircraft encounters atmospheric particles, whether aerosols, volcanic dust, raindrops or ice crystals, its airframe becomes charged by a triboelectric (frictional) effect. A detailed description of the charging and discharging phenomena associated with aircraft is given in Reference 7. Therein, it is shown that the charge-discharge phenomenon is dependent upon several factors, discussed in the reference. The dependence is complex and cannot be completely described analytically; nevertheless, by electrically isolating part of the airframe as a "charging patch", the level of charging current on the patch may be monitored, and hopefully related to the ambient atmospheric particle environment. The use of charging patches has some precedence, in work in Europe and the USSR, as well as in the USA. Indeed, a charging patch was used on the X-21 aircraft (refs. 1 and 8), where it was found that a charge indication was usually correlated with a loss of laminar flow. NASA-Langley has refined the charging patch concept to the present application, mainly by increasing its sensitivity and using improved fabrication methods (ref. 9). Again, in the JetStar LEFT application, the charging patch is supported by the Knollenberg probe as a truth device. Hopefully through this two-instrument approach, the charging current behavior of this admittedly empirical device can be documented well enough to determine the suitability of the charging patch as a stand-alone cloud particle detector for LFC aircraft application.

METHOD OF CALCULATING THE AREAL PERCENTAGE
OF LAMINAR FLOW

As shown in Figure 6 for the port wing, looking aft from the Lockheed test article, an array ("rake") of 20 evenly spaced pitot tubes is mounted behind each leading-edge test article. These near-surface pitot tubes are mounted with their axes about 0.070 inch off the surface. Also, there are 5 stations where two additional probes are installed, at heights from the wing surface of 0.020 to 0.15 inches, and two stations with the pitots about 2.5 inches above the surface. Figure 7 illustrates how the pitot tube readings are used to detect the nature of the boundary layer. The near-surface pitots measure the near-surface total pressure (Pt, probe), and the reference pitots measure the reference pressure ($Pt_{,\infty}$). If laminar flow exists at the pitot tube, the boundary layer will be thin enough to pass under the tube, which will then register a pressure close to the reference pitot. But, if transition occurs ahead of the surface tube, the tube will be immersed in a turbulent boundary layer with much-reduced total pressure, so that ($Pt,\infty-Pt$, probe) is positive; the value of the pressure differential depends on where (chordwise) the boundary-layer transition occurs. A high pressure differential signifies that transition occurs near the leading edge; a lower value means that transition occurs further along the chord. A correlation of the chordwise location of flow transition and the pressure differential is shown in Figure 8; this correlation is based upon theoretical calculations with an assumed transition location and forced (transition strip) transition measurements. Figure 8 shows the curves used for the Douglas article, and the upper and lower surfaces of the Lockheed article. These curves can only be considered as approximations, and the predicted transition locations are, hence, only approximate at best, Rigorously, the correlation should be a function of several variables (e.g.: altitude, angle of attack, Mach number, span station), but qualitative results should be achievable with these simplified, one curve correlations. (The curves presented are for Mach 0.75 and 36,000 ft. altitude.) On Figure 8, the ratio $\Delta P/q$ is the ordinate, where ΔP is the measured pressure differential and q is the dynamic pressure. The abscissa is $(x/c)_{tr}$, or the fraction of chord at which transition takes place. Both leading-edge test articles extend to about 13 percent chord; the precise values are 0.137 for the Lockheed and 0.129 for the Douglas article.

When the $\Delta P/q$ values for all twenty near-surface pitots are calculated, and allowance is made for the spanwise spacing of the pitots (i.e., area weighting), the total percentage area of the article that is laminar may be estimated; (the estimate is made by summing parallelogram areas as in Figure 9. The figure shows an example from a point in Flight 1059 where it was calculated that 98.63 percent of the area of the Douglas upper article had laminar flow. (The shaded areas in the figure are turbulent.) In this paper, it is the areal percentage of laminar flow, that is analyzed for changes with the ambient cloud particle concentration or charging patch reading.

INSTRUMENTATION FOR MONITORING CONDITION OF BOUNDARY LAYER
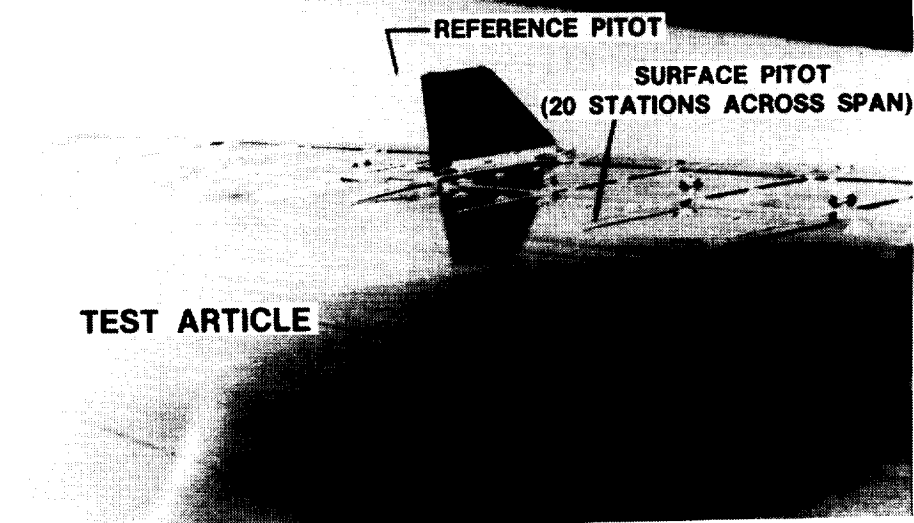
Figure 6

DETERMINATION OF SPANWISE EXTENT OF LAMINAR FLOW AT FRONT SPAR

Figure 7

173
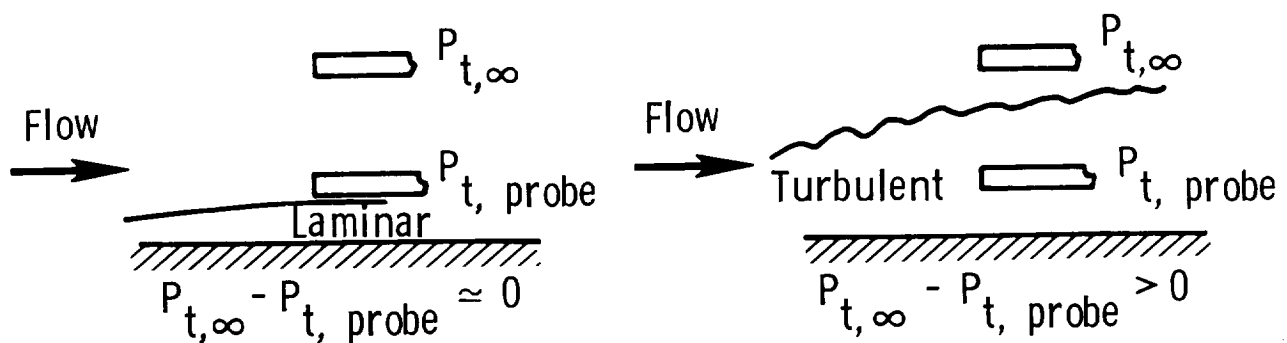
THEORETICAL CHORDWISE EXTENT OF LAMINAR FLOW

M = 0.75, 36000 ft

Lockheed, upper surface

Douglas

Lockheed, lower surface

$\frac{\Delta P}{q}$

$(X/C)_{tr}$

Criteria

$\frac{\Delta P}{q} \leq 0.09$: Laminar

$\frac{\Delta P}{q} > 0.09$: Transitional or turbulent

$(X/C)_{tr}$, max = 0.129 (Douglas)
= 0.137 (Lockheed)
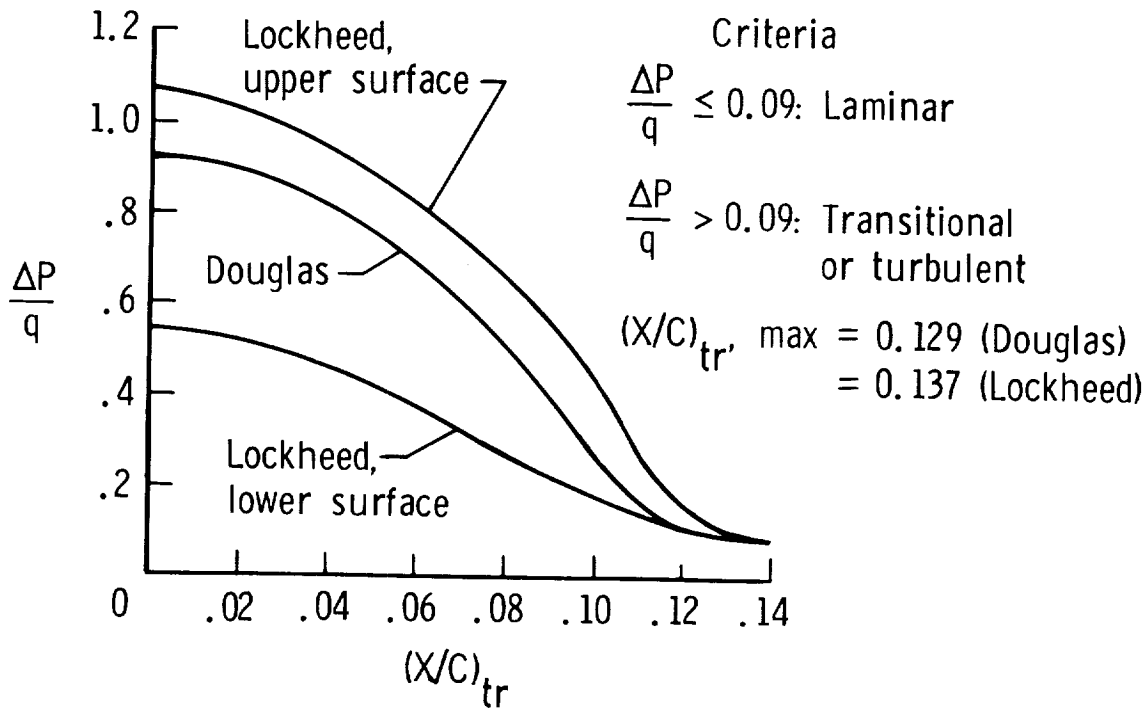
Figure 8

EXAMPLE OF CALCULATION
OF AREAL EXTENT OF LAMINAR FLOW

□ Flow laminar
■ Flow turbulent

Pitot tube

Douglas article
% laminar   98.63
Flight 1059
07 / 15 / 85
08:09:27
R 1.521×10^6
M_∞ 0.709
HP   36854 ft
Charge   -0.003 µa

Figure 9

174
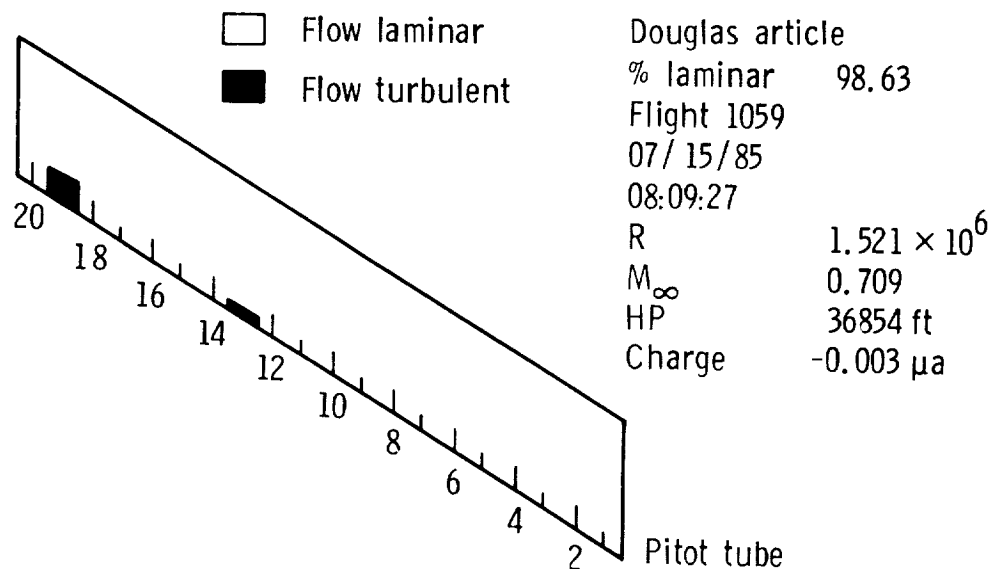
EXAMPLE OF CONCURRENT TRACES OF LAMINAR-FLOW PERCENTAGE AND PARTICLE PROBE AND CHARGING PATCH SIGNALS

Figure 10 shows an example of the concurrent time histories of laminar flow, on the Douglas and Lockheed articles, and of the signals from the particle probe and charging patch instruments. The data are taken from Flight 1099, which was chosen for discussion because it shows a progression from flight in clear air to a cloud encounter, to clear air again. The three panels of the figure show (a) the areal extent of laminar flow on the three test articles, (b) the charging patch current in microamperes (μa), and (c) the total number of particles registered by the particle probe (not the concentration) during each one-second sampling interval. The time traces begin at 9 hrs. 20 min. 00 sec. (0 sec on the figure) and extend 1000 seconds, or to 9 hrs. 36 min. 40 sec. At the beginning of the trace, the Douglas article is indicating 100 percent laminar flow to the front spar, the charging patch current is indicating a "clear air" reading of about -0.04 μa, and the particle count is zero. At about 750 seconds, the percentage of laminar flow decreases precipitously as a cloud element is encountered. An immediate change in the charge level takes place at the same time, and particle counts are noticed, also. This first cloud encounter is temporary, however, and the laminar-flow readings return to near clear air values at about 800 sec. Thereafter, a more sustained encounter with thicker clouds begins at about 830 seconds. Again, the results indicate simultaneous loss of LF, charge current increase, and an increase in the number of particles. The lowest levels of LF are reached at about 860-880 sec. (about 28 percent). At about 945 sec., the aircraft begins to exit the cloud, and charge and particle count are starting to decrease. By about 990 sec., clear air is again encountered.

The degree of LF on all articles changes simultaneously, and the particle count and charging patch readings are related to the degree of laminar flow that is present. The charging patch generally responds slightly before the particle counter does, and the particle counter ceases responding before the charging patch does. This is believed due to the fact that the charging patch responds to a wider range of particle sizes than does the particle counter and is also consistent with expected cloud behavior, with smaller particles and lower particle concentrations surrounding denser concentrations and larger particles. From comparison of the three figure panels, it is also evident that particles smaller than 60 μm definitely affect laminar flow, in addition to those 60 μm and larger in size.

Plots such as these were made for a large number of flights, and statistical analysis was performed, all of which led to the conclusion that both charging patch and particle probe readings can be useful as reliable indicators of the loss of laminar flow.

EXAMPLE OF CONCURRENCE OF SIGNALS
Flight 1099: 09:20:00 — 09:36:40 Local time

Percent LF

(a)

DAC
LAC-U
LAC-L

DAC — Douglas
LAC-U — Lockheed-upper
LAC-L — Lockheed-lower

Charging-
Patch
current, μa

(b)

Number
of
particles

(c)

Time

Time
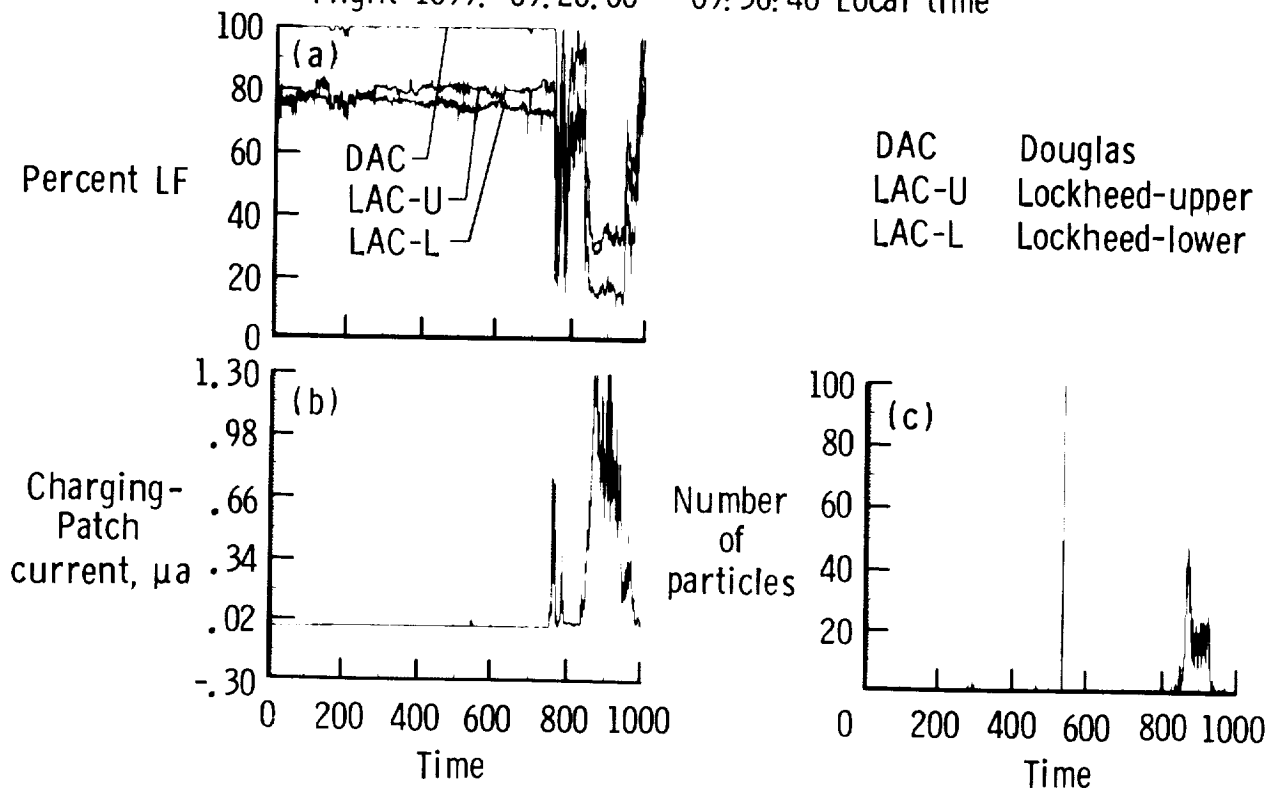
Figure 10

SUMMARY OF LAMINAR-FLOW PERFORMANCE AND METEOROLOGICAL ENVIRONMENT
ON SIMULATED AIRLINE SERVICE (SAS) FLIGHTS

Figure 11 gives a summary table of the laminar-flow performance and meteorological environment on the 13 Simulated Airline Service (SAS) flights analyzed to date. These particular flights were chosen from the total population of LEFT flights because the data tapes were already in hand, and these flights comprised a range of cloud encounter conditions for thoroughly evaluating the cloud detector instruments. The table lists for each flight: the altitude range, the average percentage of laminar flow (LF) on each article (Douglas, Lockheed upper surface and Lockheed lower surface) during cruise conditions, the cloud environment (percentage of time in clear air, haze, and cloud), the average and maximum values of particle concentration (m^{-3}) derived from the Knollenberg particle spectrometer, and the largest particle measured during the flight, in μm (micro-meters).

For this investigation, "haze" was defined as a total ambient particle concentration of less than 1000 m^{-3}, and "cloud" as an ambient concentration $\geq$ 1000 m^{-3}. "Clear air" is a particle count of zero. (Recall that only particles $\geq$ 60 μm in diameter are measured by the probe). The aircrew notes for missions 1061 and 1104 indicated possible icing on the pitot probes, so some laminar-flow results computed for those missions were not included in the LF analysis. Omitting these two missions, for the 11 SAS flights remaining in the sample, (with 20258 data points) the average LF performance of the Douglas article was 92.32 percent. For the Lockheed article, the average was 73.93 percent for the upper surface, and 69.56 for the lower surface. These average values give little inkling of the dramatic deviations that can occur. For instance, on some missions, the Douglas article indicated about 85 percent while the Lockheed article indicated about 10 percent LF.

As desired, cloud encounter environment varied over the 13 missions chosen for overall analysis. Minimum cloud encounter occurred on Flight 1082, where no particles at all were encountered, yielding a "clear air" figure of 100 percent. Maximum cloud encounter was obtained on Flight 1061 where the JetStar was in cloud for 58.60 percent of the time. The overall percentage of time in clear air, for all 13 missions, is 88.56 percent. The overall percentage for haze is 3.28 and that for clouds is 8.17. This average represents a disproportionate effect of Flight 1061, however, which had a heavy concentration of clouds. That flight represented conditions which undoubtedly would have been avoided (by altitude change, etc.) by the crew of an LFC transport. If Flight 1061 is removed from the sample, the resultant average percentages of time in clear air, haze and cloud for the remaining 12 flights are 92.81, 3.20, and 3.99, respectively, as given in the last line of the table. The combined figure for haze and cloud for the 12 flights is 7.19 percent, which is in good general agreement with our earlier estimate of 6 percent, which was based on an analysis of 1748 flights (6250 hours) of specially instrumented commercial aircraft data (Refs. 10 and 11). The fact that the JetStar number is a little higher is probably related to the fact that the 13 JetStar flights selected for analysis here were chosen because clouds were indeed encountered; in fact, there were several SAS flights where clouds were not encountered at all. Therefore, the figure of 7.19 percent is probably an upper bound on the likelihood of cloud encounter on an overall basis. Overall averages

C-3

for the sample, with data from Flights 1061 and 1104 removed (thus, leaving 11 flights) are included for completeness and for correlation with the overall LFC performance values in the second-to-last row of the table in figure 11.

Cloud particle environments penetrated by the aircraft ranged from the clear air condition of Flight 1082, through the small particle environments of Flights 1087 and 1104 (maximum particle sizes of 180 and 170 m, respectively), through the very thick clouds of Flight 1061, wherein particles up to 600 μm in size were encountered. Average particle concentrations ranged from 0 (Flight 1082) through the thin hazes of Flights 1059, 1060, 1087, and 1103, through the thicker hazes of clouds 1080, 1085, 1094, 1100, and 1104, through the cloud conditions of Flights 1081 and 1099, to the truly thick clouds of Flight 1061, (cf Fig. 11).

It is noted in Figure 11 that the average level of LF on the Douglas article for each flight is close numerically to the percentage clear air value for that flight. Also, the average level of LF is inversely related to the average particle concentration. This apparent agreement was confirmed by regression analysis, where it was found that: (% LF)$_{DAC}$ = 30.26 + 0.669 x (% clear air) with a correlation figure of 0.926, for the sample, excluding Flights 1061 and 1104.

LAMINAR FLOW PERFORMANCE AND METEOROLOGICAL ENVIRONMENT
ON THE THIRTEEN SAS+ FLIGHTS ANALYZED

MISSIONS:		LFC PERFORMANCE: LF %			CLOUD ENVIRONMENT % TIME IN:			PARTICLE ENVIRONMENT CONC., m^{-3}		SIZE (μm)
FLIGHT	ALTS.(kft)	DAC	LAC UPPER	LAC LOWER	CLEAR AIR	HAZE*	CLOUDS*	AVERAGE	MAX	MAX
1059	32.7-36.9	93.51	83.82	80.25	90.23	5.57	4.21	1.07E2	5.70E3	240
1060	32.7-36.8	93.75	84.59	70.93	94.77	2.90	2.32	1.10E2	1.84E4	300
1061	28.7-32.9	56.47	49.78	**	37.16	4.24	58.60	2.29E5	2.20E6	600
1080	30.7-32.7	91.42	66.01	68.13	91.04	3.82	5.15	2.89E2	2.91E4	440
1081	32.7	89.07	59.03	64.72	94.91	11.29	3.95	8.15E3	3.50E5	600
1082	28.7-32.8	97.96	87.70	79.26	100.00	0.00	0.00	(no particles encountered)		
1085	30.8-32.8	96.74	72.76	70.57	97.55	0.76	1.69	1.97E2	1.69E5	400
1087	26.2-34.7	96.02	79.47	77.34	99.05	0.85	0.10	7.00E1	1.29E5	180
1094	32.5-32.8	86.28	72.61	64.62	84.37	5.89	9.75	3.16E2	8.88E3	440
1099	30.6-34.7	86.24	72.88	65.17	83.51	9.08	7.41	8.66E3	3.60E5	600
1100	22.5-35.7	84.90	51.41	42.78	81.56	8.79	9.64	3.98E2	1.72E4	320
1103	34.7-34.8	97.97	84.95	80.74	99.43	0.28	0.28	1.00E1	3.78E3	200
1104	27.4-34.7	**	**	**	93.78	1.47	4.77	2.57E2	3.03E4	170

* HAZE   CONC. < 1.0E3m^{-3}; CLOUD $\geq$ 1.0E3 m^{-3}
** POSSIBLE ICING ON PITOT PROBES

MISSIONS		LFC PERFORMANCE			CLOUD ENVIRONMENT					
OVERALL (ALL 13 FLTS.)		____	____	____	88.56	3.28	8.17			
OVERALL (LESS 1061, 1104)		92.32	73.93	69.56	92.69	3.42	3.89			
OVERALL (LESS 1061)		____	____	____	92.81	3.20	3.99			

+Simulated airline service (SAS)

Figure 11

OVERALL PERFORMANCE OF BOTH LEADING-EDGE TEST ARTICLES

Figure 12 presents the overall degree of laminar flow performance for both Douglas and Lockheed leading-edge test articles, obtained in eleven representative SAS (Simulated Airline Service) flights over the altitude range given in Figure 11. A sample of 20258 data points (5.63 hrs. data) was included in the analysis. The results are plotted on probability paper (which accounts for the non-uniform demarcation of the ordinate) and are presented in the form of cumulative probability distributions. All meteorological conditions are included in the sample. (Separate breakouts by clear air, haze and clouds, and by ambient particle concentration are given in subsequent figures). In explanation, the ordinate gives the probability, in percent, that the extent of laminar flow on the article (i.e. back to the front spar) equals or exceeds the abscissa value. Three curves are given, one for the Douglas article, and one each for the upper and lower wing leading-edge surfaces of the Lockheed article. In an example, it is seen from the figure that the probability that the degree of laminar flow on the Douglas article equals or exceeds 30 percent is about 98 percent. Similarly, the probability of achieving or exceeding 70 percent (P> 70%) is about 89 percent, P(> 90%) = 84 percent, P(> 95%) = 82 percent and P(> 99%) = 63 percent. It may be inferred that the probability of achieving less than 30 percent LF was less than 2 percent; this means that this article was almost always (98 percent of the time) experiencing a degree of LF $\geq$ 30 percent.

Similar deductions can be made from the cumulative frequency plots for the Lockheed upper and lower surfaces. The Lockheed upper surface experienced at least 30 percent LF 96 percent of the time, but achieved $\geq$ 99 percent only about 2.5 percent of the time (versus 63 percent of the time, for the Douglas article). For the lower surface of the Lockheed article, the probability of exceeding a given degree of laminar flow is somewhat less than that for the upper surface, because of the more adverse chordwise pressure gradient on the lower surface.

To provide additional information, the average values of LF for the 20258 data point ensemble are plotted as solid symbols on the figure. The average values are 92.3 percent for the Douglas article, 74 percent for the upper surface of the Lockheed article and 70 percent for the Lower surface of the Lockheed article. An arrow is placed on the ordinate to denote the median (50th percentile) point. Reading across from this point, the median values are: Douglas article > 99 percent; Lockheed upper > 80 percent; Lockheed lower > 74.5 percent.

Another depiction of the same data is given as Figure 13, which is a histogram plot of the percentage of cases with a given degree of LF. For example, in the band with > 99 percent LF, it is again seen that about 63 percent of the cases for the Douglas article lay in this category, versus only about 2.5 percent for the Lockheed article, both for its upper and lower surfaces.

Finally, it should be mentioned that 92.7 percent of the cases in this 11-flight data sample were obtained in clear air, 3.4 percent in haze, and 3.9 percent in cloud.

EXTENT OF LAMINAR FLOW ON TEST ARTICLES
IN ELEVEN FLIGHTS IN SIMULATED AIRLINE SERVICE

20258 data points total

Probability of exceeding abscissa value, percent

O——O Douglas
□---□ Lockheed upper
◇---◇ Lockheed lower
Solid = LF avg value
Arrow = median

Meteorological conditions:
92.7% clear air
3.4% haze
3.9% cloud

Extent of laminar flow to front spar, percent
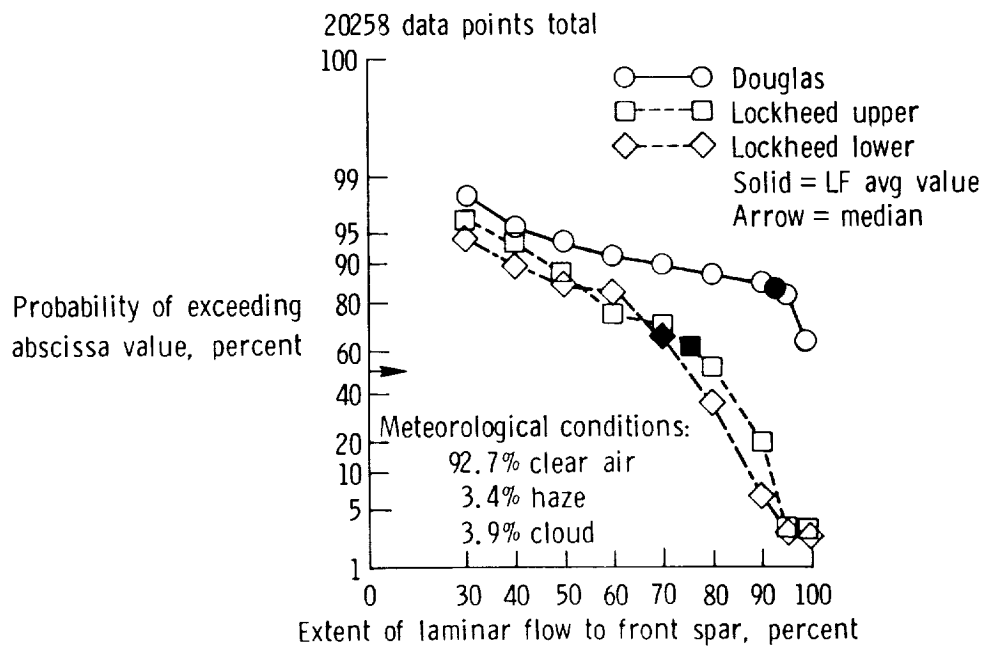
Figure 12

HISTOGRAM PLOT:
DISTRIBUTION OF LF OBSERVATIONS OBTAINED
IN ELEVEN SIMULATED AIRLINE SERVICE MISSIONS

All 20258 data points included

□ Douglas

▨ Lockheed upper surface

▦ Lockheed lower surface

Percentage of cases

50-60   60-70   70-80   80-90   90-95   95-99   >99

Extent of LF to front spar, percent

Figure 13

180
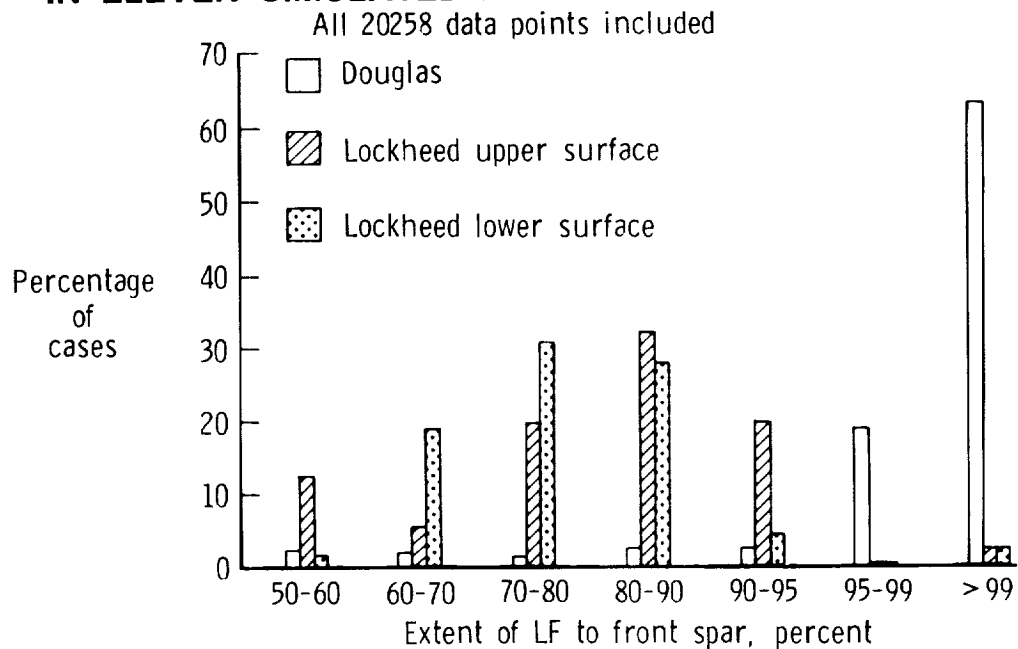
PERFORMANCE OF DOUGLAS ARTICLE IN CLEAR AIR, HAZE, AND CLOUDS

Figure 14 presents a series of cumulative probability distribution plots describing the LF performance of the Douglas leading-edge test article in clear air, haze, and clouds separately, as well as overall. (The overall plot is the same as that presented on Figure 12). For this investigation, "clear air" is arbitrarily defined as a total ambient particle concentration of 0, as measured by the Knollenberg probe particle spectrometer. "Haze" is defined as a non-zero total concentration of < 1000 m^{-3}, and "cloud" as an ambient concentration > 1000 m^{-3}. Only plots for the Douglas article are presented, because only that article showed a high probability of achieving a high level of laminar flow, in clear air conditions. (This is felt to be the result of surface imperfections in the Lockheed article, rather than to any intrinsic lack of merit of the slotted [versus porous] concept).

The results for clear air show that there is a 98.8 percent probability of achieving at least 30 percent LF, a 91 percent probability of $\geq$ 90 percent LF and a 78 percent probability of achieving $\geq$ 99 percent LF.

The results for haze show a marked decrease in probability of achieving a given degree of LF, compared to that in clear air. The results in cloud show a further marked decrease. Both decreases were found to be statistically significant. Thus, the X-21 experience is verified on statistical grounds, for the first time. The cumulative probability values for comparison to the clear air values stated above are, for haze: $P(\geq 30\%) = 96$ %, $P(\geq 90\%) = 13\%$, and $P(\geq 99\%) = 6.2\%$. For cloud, the values are: $P(\geq 30\%) = 78\%$, $P(\geq 90\%) = 6\%$, $P(\geq 99\%) = 5.8\%$. The overall plot is nearer the clear air plot than to any of the other curves; this merely reflects the fact that the preponderance of observations was obtained in clear air conditions.

Just as on figure 12, the average values of LF have been plotted as solid symbols. The average value is 96.3 percent for clear air, 62.5 percent in haze, and 45.2 percent in cloud. The overall value, 92.3 percent, is the same as that shown on figure 12. The median values are 99 percent in clear air, 61 percent in haze and 38.2 percent in cloud.

From the above results, there can remain no doubt that encounter with haze and cloud conditions causes a significant effect on the degree of LF performance of the Douglas article. The results for the Lockheed article, not presented here, show a similar marked effect.

EXTENT OF LAMINAR FLOW ON DOUGLAS TEST ARTICLE, DURING ELEVEN FLIGHTS IN SIMULATED AIRLINE SERVICE
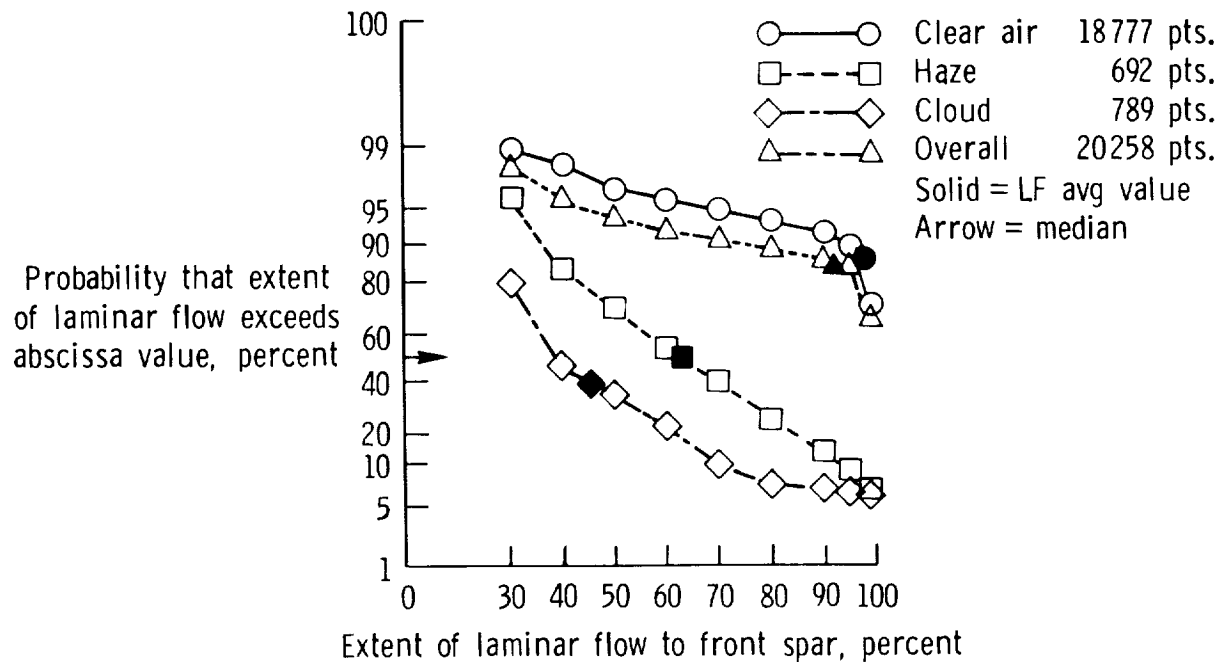
Figure 14

Figure 15 is another series of cumulative probability distribution plots. This time, a separate plot is presented for each range of total particle concentration in m^{-3}. The plot for zero concentration is the clear air plot from figure 14, and the overall plot is also common to that on figures 12 and 14.

A marked decrease in the probability of exceeding a given extent of laminar flow is observed, when the ambient concentration increases from zero to a thin haze value of 100-250 m^{-3}. As particle concentration increases further to thicker hazes, a continued decrease in probability is observed. As cloud level concentrations are achieved (≥ 1000 m^{-3}), the degree of probability decrease is hastened. The curves presented here account for 99 percent of all the data. At still higher concentrations occurring in the remaining one percent of cases, the data (not presented here for the sake of clarity) show that further decreases occur. As before, solid symbols denote the average values of LF-in this case, average values for each level of total particle concentration.

EFFECTS OF TOTAL PARTICLE CONCENTRATION ON EXTENT OF LAMINAR FLOW ON DOUGLAS TEST ARTICLE
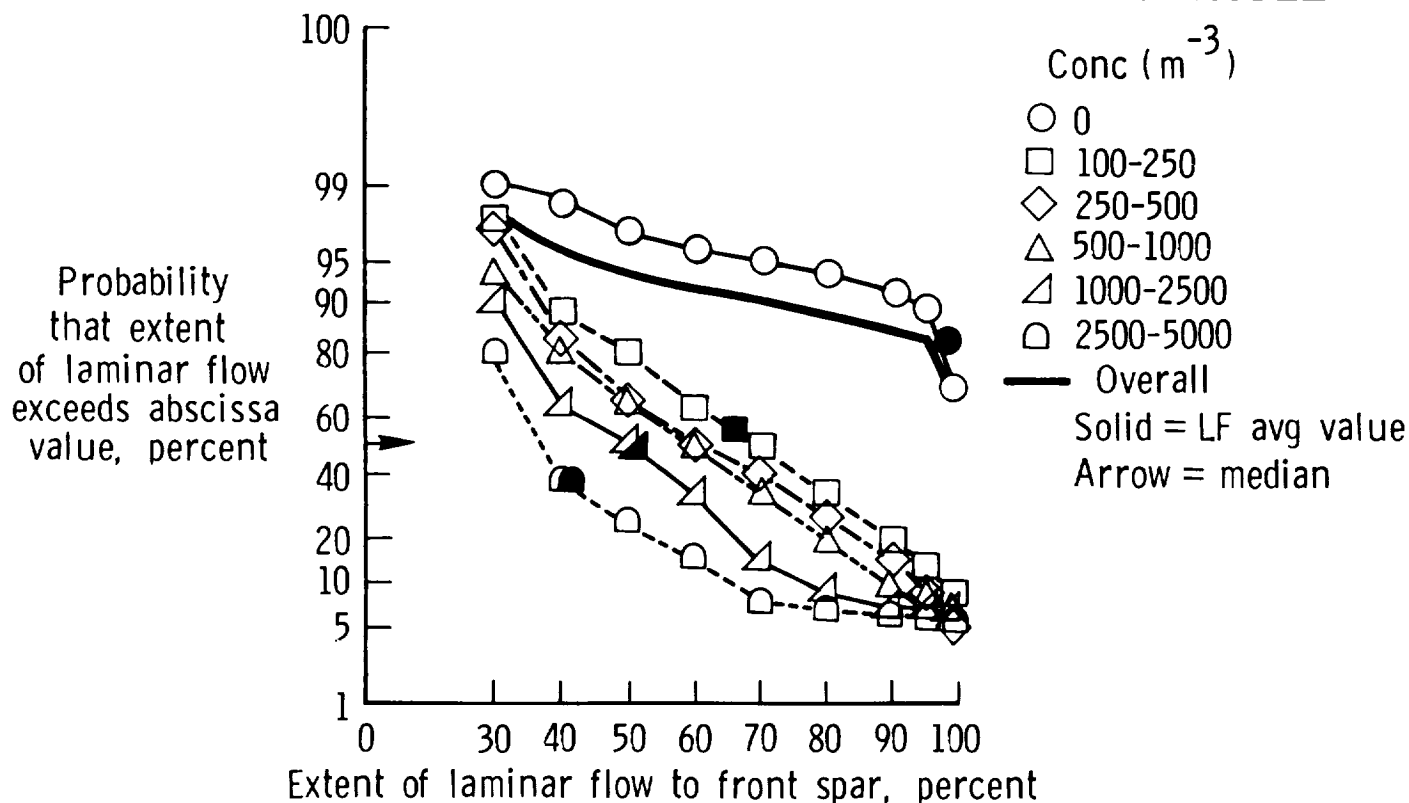
Figure 15

VALIDATION OF HALL CRITERIA WITH JETSTAR DATA

As previously mentioned, one of the goals of our investigation was to attempt to validate the Hall criteria, originally developed to explain LF loss on the X-21 aircraft, with data from the LEFT program. The Hall criteria were presented earlier (Fig. 2). Figure 16, presented below, is a copy of the Hall criteria in Figure 2, overlaid with observations of particle concentrations and values of the concurrent degree of LF loss, computed as described earlier, for Flight 1061, where many clouds were encountered, with a large range of particle concentrations. Particle concentrations computed from Knollenberg probe data were plotted for laminar-flow values lying in three arbitrarily chosen distinct ranges of LF on the Douglas article: 25-35 percent, 75-85 percent, and greater than 85 percent. Several distinct sampling times were chosen at random for each of these ranges, so that 30 times were chosen, overall.

From study of figure 16, it is evident that the range of concentrations corresponding to the 25-35 percent LF range is considerably higher than that for the 75-85 percent range. The range 85-100% had, for the most part, no particles at all observed, so the preponderance of observations lay at the bottom of the figure, within Hall region 2 of fig. 2 where it is predicted that LF will not be lost. However, there were some observations of high LF lying in Hall region 3 (of Fig. 2), which is the region of partial LF loss. These observations are believed consistent, however, with the fact that a high but not 100% reading of LF over the leading-edge test article is very probably associated with a lower overall chordwise percentage of LF.

As cautioned earlier, only a limited degree of validation of the Hall criteria may be possible, because airfoil shape, altitude, and Mach number conditions are different from those for which the Hall figure was derived. JetStar LF is measured to only about 13 percent, rather than full-chord. Nevertheless, the data do seem to show "Hall criteria-like" behavior, in that increasing particle concentrations do lead to progressively smaller degrees of laminar flow. Therefore, it is concluded that the Hall criteria seem to be consistent with JetStar observations, and that the criteria are validated qualitatively.

184

EXAMPLE OF VALIDATION OF "HALL CRITERIA"
Flight 1061
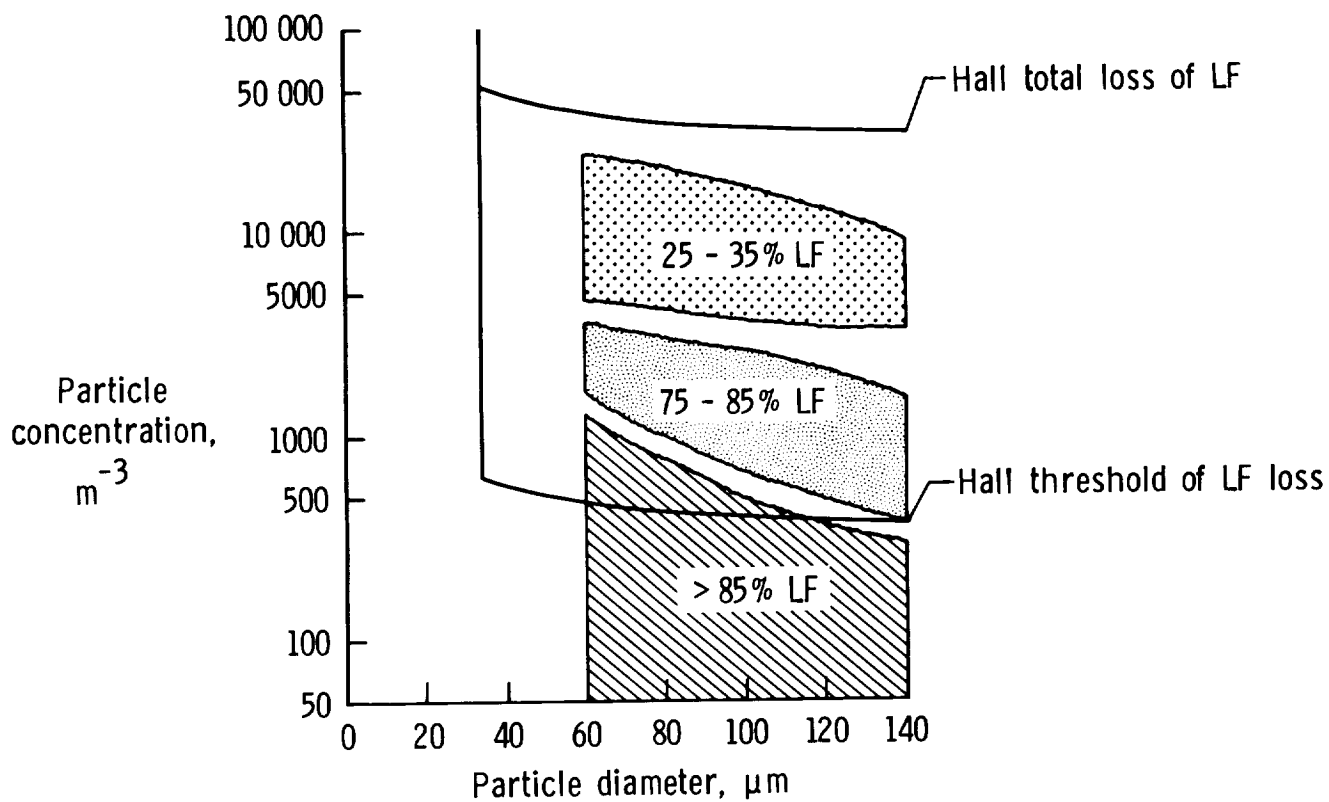
Figure 16

Figure 17 is another cumulative probability distribution, which shows the probability of obtaining a total ambient particle concentration which equals or exceeds the abscissa value. The solid curve represents the distribution from 12 SAS missions with 22837 data points. Data from Flight 1061 was not included in this curve, because the percentage of time in cloud on that flight was very high (58.60 percent) and represented a condition which undoubtedly would have been avoided by the aircrew of an LFC transport by using flight management procedures (change of altitude or rerouting). All the other flights constituted conditions into which an LFC aircraft would conceivably have been flown. Nevertheless, for completeness, results with Flight 1061 included are also presented on the figure, as the dashed curve.

Viewing the solid curve results, it is seen that an ambient particle concentration of 100 m^{-3} is attained or exceeded in only about 7 percent of cases. Clouds (concentration $\geq$ 1000 m^{-3}) were encountered on only about 4 percent of cases. From this plot, it might be inferred that the aircraft encountered essentially clear air conditions some (100 -7) or 93 percent of the time. This figure is consistent with earlier estimate of about 6 percent, obtained both in the X-21 project (ref. 1) and in our earlier empirical estimates, based on the analysis of GASP data (ref. 11). Also, the 93 percent figure is very close to the average amount of LF on the Douglas article, shown to be 92.32 percent. From this comparison, it might be inferred, as a general rule, that the average level of LF experienced on a flight is equal to the percentage of time spent in "clear-air" on the flight, for a well-performing test article.
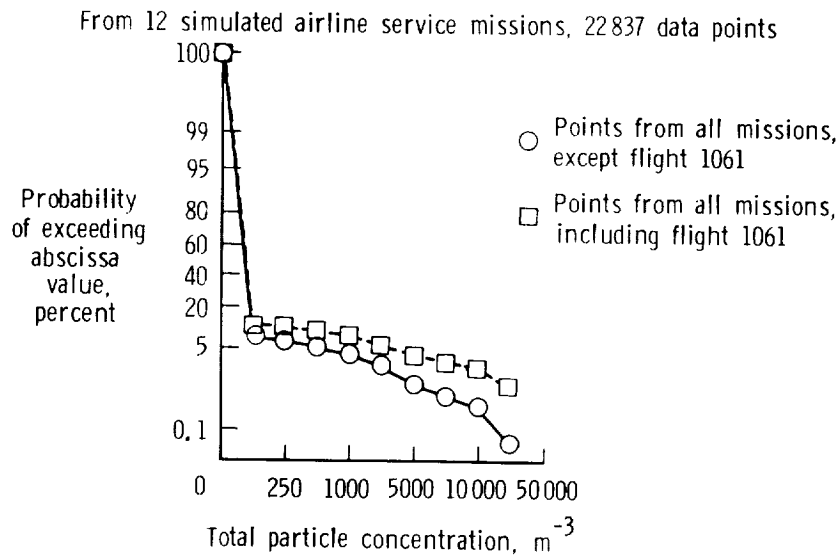
Figure 17

PHOTOGRAPHS OF HAZE CONDITIONS, WITH VARIOUS DEGREES OF LF LOSS

The need for onboard instrumentation for discerning the presence of ambient particle concentrations is sometimes questioned. True cloud conditions are, of course, visible in daylight, but the presence of haze may be difficult to discern, particularly if observer-Sun angles are unfavorable. Also, it is frequently difficult to assess ambient haze and cloud conditions at night. As an example of questionable haze conditions, figure 18 shows two photographs from Flight 1099 (this flight was discussed previously in connection with Figure 10). Both pictures were taken by the JetStar aircrew, while looking out of the port side of the aircraft, with the Sun behind the camera; the port wing is apparent in each photograph. A "haze" condition is apparent at about the elevation level of the wingtip. Photo A was taken at 9:24:00 local time (corresponding to the 240-second mark on Figure 10). Photo B was taken at 9:33:00 (corresponding to the 780-second mark on Figure 10).

When the first photograph (panel a) was taken, the Douglas article was indicating 100 percent LF. During the second photograph (panel b) the degree of LF was 80 percent. Yet, the difference in haze conditions between the two photographs is not very apparent. For conditions such as these, an instrument which indicates the presence of cloud or haze particles would be most useful.

9:24:00 local time, 100% LF

(A)

Figure 18

HAZE CONDITIONS ON FLIGHT 1099

9:33:00 local time, 80% LF

(B)

Figure 18

COMPARISON OF PARTICLE PROBE AND CHARGING PATCH AS DIAGNOSTIC INSTRUMENTS FOR LFC AIRCRAFT

The table shown in Figure 19 presents a comparison of the performance of the Knollenberg probe particle spectrometer and the charging patch for detecting conditions favorable or unfavorable to the maintenance of laminar flow. The evaluation is based on the sample of eleven simulated airline service flights discussed previously (20258 data points).

A two-level reading approach was adopted for simplicity. For the probe, the levels are (1) a total particle count of zero, presumably related to a clear air condition in the ambient, and (2) a non-zero particle count, obviously related to the presence of clouds, haze, etc. For the charging patch, the two levels are: (1) a "zero-range", chosen empirically to be associated with a minimum particle count reading from the probe, and (2) a "non-zero" range, comprising readings outside the zero range. The zero range was determined to be from -0.05 to 0.00 μa (microamperes).

In an example use of the table, a particle probe reading of zero is associated with a $\geq$ 90 percent extent of laminar flow on the Douglas article 90.36 percent of the time. If the particle probe reading is non-zero, there is only a 9.72 percent chance of there being $\geq$ 90 percent laminar flow. Thus, the two levels discriminate effectively between LF-favorable and LF-unfavorable conditions.

Continuing the same example, if the charging patch is used as the diagnostic instrument, a "zero-range" reading is associated with a $\geq$ 90 percent level of LF 92.74 percent of the time. A non zero-range reading is associated with this level of LF only 21.99 percent of the time. Thus, an effective discrimination is again made.

In performing a series of comparisons in this way, it is seen that the two devices give comparable performance, with the charging patch giving slightly more reliable indications of clear air conditions, and the particle probe giving more reliable indications of conditions for loss of LF. This is explained easily by noting that the particle probe is sensitive only to particles 60 μm and larger in diameter, whereas the patch responds to smaller particles as well. These smaller particles do, however, also affect LF, so it is not surprising that a zero-range reading is a better indicator of LF-favorable conditions than is a zero particle count reading. In un-clear conditions, the results are reversed. The reason for this is that a non-zero particle probe reading is indeed associated with the presence of larger particles which more effectively degrade LF than do the smaller ones, whereas a non-zero charge patch reading may result, in part, from the more numerous smaller particles which do not have as marked an impact on LF. Therefore, the non-zero range probabilities of achieving a given level of LF are somewhat larger than those for the non-zero probe probabilities, at the same level of LF. Nevertheless, the non-zero range patch probabilities are still low enough to indicate that the two-level charging patch device provides an effective discrimination between LF-favorable and LF-unfavorable conditions. For this reason, the patch is favored over the particle probe, due to its low cost and simplicity.

COMPARISON OF PARTICLE PROBE AND CHARGING PATCH AS DIAGNOSTIC INSTRUMENTS FOR LFC AIRCRAFT

PROBABILITY OF ACHIEVING DESIRED EXTENT OF LAMINAR FLOW ON DOUGLAS ARTICLE, PERCENT

DESIRED EXTENT OF LAMINAR FLOW, PERCENT	PARTICLE PROBE READING		CHARGING PATCH READING	
	0	≠0	IN "ZERO RANGE"*	NOT IN "ZERO-RANGE"
≥30	98.90	86.50	98.88	91.77
≥40	98.28	62.39	98.52	74.55
≥50	96.85	50.00	97.40	63.40
≥60	95.48	35.79	96.39	51.29
≥70	94.27	23.43	95.54	40.35
≥80	92.93	15.06	94.47	32.67
≥90	90.36	9.72	92.74	21.99
≥95	87.76	7.78	91.01	13.21
≥99	67.55	6.14	70.60	5.99

*"ZERO-RANGE = -0.05 → 0.00 μA
NOTES: 1. 20258 DATA POINTS IN SAMPLE, FROM 11 SAS FLIGHTS
       2. PARTICLE PROBE COUNTS PARTICLES 60 μM DIAMETER AND LARGER

Figure 19

Conclusions and summary comments regarding our investigation of the thirteen JetStar simulated airline service flights so far analyzed are given in figure 20.

LEFT program results

- An extensive data bank of concurrent measurements of laminar flow (LF), particle concentration, and aircraft charging state has been gathered for the first time.

- From this data bank, 13 flights in the simulated airline service (SAS) portion have been analyzed to date. A total of 6.86 hours of data at one-second resolution have thereby been analyzed.

- An extensive statistical analysis, for both leading-edge test articles, shows that there is a significant effect of cloud and haze particles on the extent of laminar flow obtained.

- ~ 93 percent of data points simulating LFC flight were obtained in clear air conditions; ~ 7 percent were obtained in cloud and haze. These percentages are consistent with earlier USAF and NASA estimates and results.

- The "Hall" laminar flow loss criteria have been verified qualitatively.

- Larger particles and higher particle concentrations have a more marked effect on LF than do small particles.

- A particle spectrometer or a charging patch are both acceptable as diagnostic indicators of the presence of particles detrimental to laminar flow.

Figure 20

avg	average
conc.	concentration
DAC	Douglas Aircraft Company
EMD	Equivalent Melted Diameter (of ice particle)
GASP	Global Atmospheric Sampling Program
HP	pressure altitude
LAC	Lockheed Aircraft Corporation
LAC-L	lower surface of Lockheed article
LAC-U	upper surface of Lockheed article
L.E.	Leading Edge
LEFT	Leading-Edge Flight Test
LF	Laminar Flow
LFC	Laminar-Flow Control
M	free-stream Mach number
P ( )	probability of ( )
PMS	Particle Measuring Systems, Inc.
$P_{t, probe}$	total pressure, measured at near-surface pitot probe
$P_{t,\infty}$	free-stream total pressure
q	dynamic pressure
R	Reynolds number
SAS	Simulated Airline Service
V_∞	free-stream velocity
ΔP	measured pressure differential
μa	microampere = 1×10^{-6} ampere
μm	micrometer = 1×10^{-6} m

192

REFERENCES

1. Whites, R. C.; Sudderth, R. W.; and Wheldan, W. G.: Laminar Flow Control
    on the X-21. Astronautics and Aeronautics, (AIAA), Vol. 4, No. 7, July
    1966.

2. Hall, G. R.: On the Mechanics of Transition Produced by Particles Passing
    Through an Initially Laminar Boundary Layer and the Estimated Effect on
    the LFC Performance of the X-21 Aircraft. Northrop Corp., October 1964.

3. Pfenninger, W: Design Considerations of Long-Range and Endurance LFC
    Airplanes with Practically All Laminar Flow. NASA Joint Institute for
    Advancement of Flight Sciences. Aug. 1982.

4. Davis, R. E.; and Fischer, M. C.: Cloud Particle Effects on Laminar Flow
    in the NASA LEFT Program: Preliminary Results. AIAA Paper 86-9811, 1986.

5. Dorsch, R. G.; Brun, R. J.; and Gregg, J. L.: Impingement of Water
    Droplets on an Ellipsoid With Fineness Ratio 5 in Axisymmetric Flow. NACA
    TN 3099, March 1954.

6. Brun, R. J.; and Dorsch, R. G.: Impingement of Water Droplets on an
    Ellipsoid With Fineness Ratio 10 in Axisymmetric Flow. NACA TN 3147, May
    1954.

7. Imyanitov, I. M.: Aircraft Electrification in Clouds and Precipitation.
    (Edited Translation of "Elektrizatsiya Samoletov v Oblakakh Osadkakh",
    1970, pp. 1-211). Report FTD-HC23-544-70, U.S. Air Force, April 1971.

8. Mee, T. R.: An Investigation of Atmospheric Factors that May Affect
    Laminar Flow Control. Report MRI-64-R212A, Meteorology Research, Inc.
    Altadena, California, December 1964.

9. Campbell, R. E.; and McPherson, J. P.: Cloud Particle Detector. NASA Tech
    Brief LAR 13137, 1983.

10. Jasperson, W. H.; Nastrom, G. D.; Davis, R. E.; and Holdeman, J. D.: GASP
    Cloud-and Particle Encounter Statistics, and Their Application to LFC
    Aircraft Studies (2 vols.). NASA TM 85835, October 1984.

11. Jasperson, W. H.; Nastrom, G. D.; Davis, R. E.; and Holdeman, J. D.: GASP
    Cloud Encounter Statistics: Implications for Laminar Flow Control
    Flight. J. of Aircraft, Vol. 21, No. 11, November 1984, pp. 851-857.

|

SIMULATED AIRLINE SERVICE EXPERIENCE WITH LAMINAR-FLOW CONTROL LEADING-EDGE SYSTEMS

Dal V. Maddalon*, David F. Fisher**,
Lisa A. Jennett**, and Michael C. Fischer*
*NASA Langley Research Center
Hampton, Virginia
**NASA Dryden Flight Research Facility
Edwards, California

SUMMARY

Achieving laminar flow on the wings of a commercial transport involves difficult problems associated with the wing leading edge. The NASA JetStar Leading Edge Flight Test Program has made major progress toward solution of these problems. Effectiveness and practicality of laminar-flow leading edge systems were proven under representative airline flight conditions. This was accomplished in a series of simulated airline service flights by modifying a JetStar aircraft with laminar-flow control leading-edge systems and operating it out of three commercial airports (Atlanta-Hartsfield, Greater Pittsburgh International, and Cleveland-Hopkins International) as an airline would under actual air traffic conditions, bad weather, and insect infestations. About 62 flights to 33 domestic airports were made during severe summer and winter weather.

Two different leading-edge test articles were flown. One used suction through approximately 1 million 0.0025 inch diameter electron-beam perforated holes in titanium skin to maintain laminar flow on the test article upper surface. A Krueger-type flap served as a protective shield against insect impact. The test article also contained cleaning, deicing, and purging systems. The second test article used suction through 27 narrow spanwise slots (about 0.004 inch wide) on both upper and lower titanium surfaces.

LEFT JETSTAR SIMULATED AIRLINE SERVICE

The **JetStar** Leading Edge Flight Test (LEFT) aircraft is shown in figure 1 being serviced during the Simulated Airline Service (SAS) flight test segment based at Pittsburgh, September 13, 1985. The objective of the SAS program was to obtain operational data on practical laminar-flow control (LFC) leading-edge systems in the commercial airline environment. Summaries of laminar-flow control definition studies are available in references 1-5. References 6-9 provide complete descriptions of the LEFT test articles development program. LFC structural design details are given in references 10-13. Meteorological data are summarized in references 14-16.

OBJECTIVE: OBTAIN OPERATIONAL DATA ON LFC LEADING EDGE SYSTEMS IN THE COMMERCIAL AIRLINE ENVIRONMENT
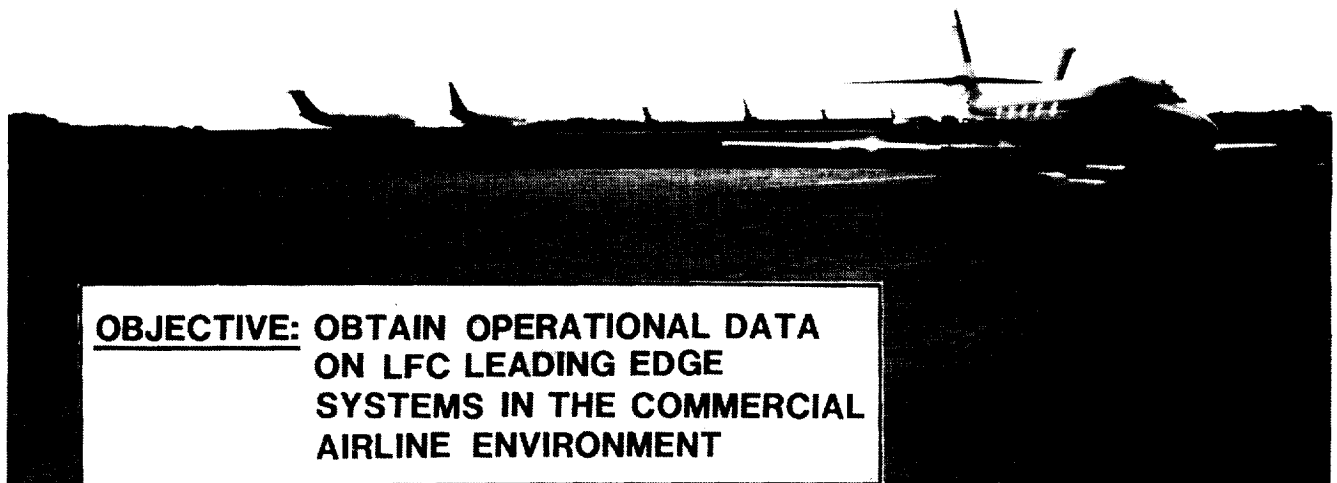
Figure 1

During the simulated airline service, one to four flights per day were made from three "home base" United States airports (Atlanta, Pittsburgh, and Cleveland). From these three major airports, a total of 62 SAS flights to 33 airports were made (figure 2). Seasonal data were obtained with the Atlanta flights in July, the Pittsburgh flights in September, and the Cleveland flights in February. Thus, the weather conditions experienced varied from extreme summer to severe winter. The SAS flights were preceded by flight tests designed to shake-out the airplane and its systems, and to determine a nominal suction level for the SAS flights (ref. 9). In addition, a precursor airline type flight series was made throughout the western United States for which the JetStar was based at the NASA Ames/Dryden Flight Research Facility (ref. 9). Thus, the SAS and the associated Dryden based flights fairly simulated airline service throughout the domestic United States.

HOME BASE	DATE	FLIGHTS
☐ ATLANTA	JULY 85	BASED AT 3 MAJOR AIRPORTS
■ PITTSBURGH	SEPT. 85	FLOWN IN/OUT 33 AIRPORTS
▨ CLEVELAND	FEB. 86	62 FLIGHTS MADE
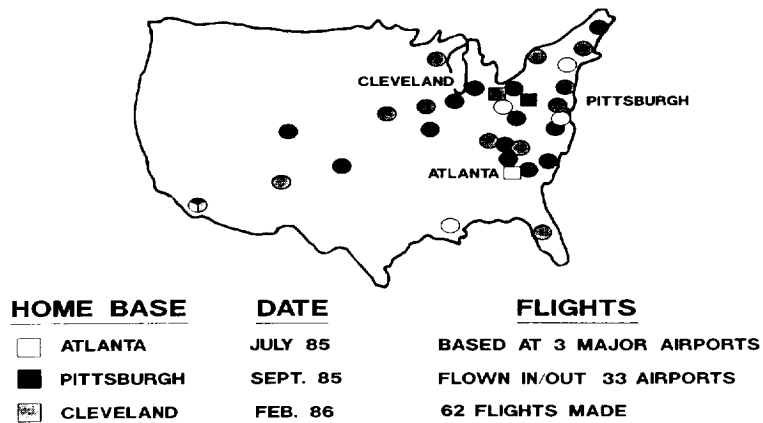
Figure 2

A summary of the SAS flight number, date of flight, airport, and cruise time is provided in figure 3. More than 39 hours of cruise data were obtained. Block time was over 60 hours.

BASE	FLIGHT	DATE	FROM	TO	CRUISE TIME, HRS
ATLANTA	1059	07/15/85	EDW	AMA	0.64
(13 FLIGHTS)	1060	07/15/85	AMA	BAD	0.43
	1061	07/15/85	BAD	ATL	0.47
	1062	07/16/85	ATL	STL	0.82
	1063	07/16/85	STL	ATL	0.36
	1064	07/17/85	ATL	CLE	0.50
	1065	07/17/85	CLE	SPI	0.73
	1066	07/17/85	SPI	ATL	0.60
	1067	07/18/85	ATL	MSY	N.A.
	1068	07/18/85	MSY	ATL	N.A.
	1069	07/20/85	ATL	ORF	0.38
	1070	07/20/85	ORF	ATL	0.37
	1071	07/22/85	ATL	LFI	0.49
PITTSBURGH	1079	09/09/85	EDW	DEN	0.95
(26 FLIGHTS)	1080	09/09/85	DEN	STL	0.83
	1081	09/09/85	STL	PIT	0.47
	1082	09/10/85	PIT	BOS	0.50
	1083	09/10/85	BOS	PIT	0.55
	1084	09/11/85	PIT	ORD	0.33
	1085	09/11/85	ORD	CHA	0.47
	1086	09/11/85	CHA	PIT	0.40
	1087	09/12/85	PIT	BNA	0.62
	1088	09/12/85	BNA	CLE	0.50
	1089	09/12/85	CLE	PIT	0.53
	1090	09/13/85	PIT	CHS	0.52
	1091	09/13/85	CHS	DCA	0.39
	1092	09/13/85	DCA	PIT	0.52
	1093	09/14/85	PIT	DET	0.41
	1094	09/14/85	DET	PIT	0.64
	1095	09/16/85	PIT	BGR	0.67
	1096	09/16/85	BGR	JFK	0.33
	1097	09/16/85	JFK	RDU	0.43
	1098	09/16/85	RDU	PIT	0.50
	1099	09/17/85	PIT	AZO	0.51
	1100	09/17/85	AZO	PIT	0.50
	1101	09/18/85	PIT	STL	0.80
	1102	09/18/85	STL	OKC	0.60
	1103	09/18/85	OKC	ABQ	0.53
	1104	09/18/85	ABQ	EDW	0.70
CLEVELAND	1131	02/19/86	EDW	AMA	1.17
(23 FLIGHTS)	1132	02/19/86	AMA	SPI	0.99
	1133	02/19/86	SPI	CLE	0.56
	1134	02/20/86	CLE	ATL	0.66
	1135	02/20/86	ATL	ACY	1.07
	1136	02/20/86	ACY	CLE	0.63
	1137	02/21/86	CLE	BOS	0.62
	1138	02/22/86	BOS	CLE	1.03
	1139	02/24/86	CLE	TYS	0.59
	1140	02/24/86	TYS	TPA	0.75
	1141	02/24/86	TPA	BNA	0.97
	1142	02/24/86	BNA	CLE	0.62
	1143	02/25/86	CLE	GRB	0.65
	1144	02/25/86	GRB	LOU	0.53
	1145	02/25/86	LOU	CLE	0.76
	1146	02/26/86	CLE	BTV	0.73
	1147	02/26/86	BTV	LFI	0.81
	1148	02/26/86	LFI	CLE	0.75
	1149	02/27/86	CLE	RIC	0.85
	1150	02/27/86	RIC	CLE	0.83
Total Cruise	1151	02/28/86	CLE	DSM	0.96
Time Hours = 39.08	1152	02/28/86	DSM	DEN	1.11
	1153	02/28/86	DEN	EDW	1.45

Figure 3

JETSTAR FLIGHT SCHEDULE

An example of the Jetstar flight schedule for February 24, 1986, during the Pittsburgh based simulated airline service, is presented in figure 4. Four airline-type flights were made on this day. Aircraft turn-around time was about 1.5 hours. Flights included airline simulation of service during peak traffic hours.

FLIGHT	DATE	TIME	LOCATION	WEATHER
1139	2/24/86	8:32 AM 9:46 AM	CLEVELAND, OH KNOXVILLE, TN	26° F, OVERCAST
1140	2/24/86	10:42 AM 12:05 PM	KNOXVILLE, TN TAMPA, FL	41° F, RAIN
1141	2/24/86	1:04 PM 2:42 PM	TAMPA, FL NASHVILLE, TN	70° F, SCATTERED CLOUDS
1142	2/24/86	3:25 PM 4:41 PM	NASHVILLE, TN CLEVELAND, OH	40° F, OVERCAST

Figure 4

The LEFT JetStar SAS flights were made as similar to commercial transport airplane operation as was possible (figure 5). This included scheduled take-offs and landings; queuing up with commercial airliners; use of air traffic control of vector, altitude, and speed; operation at various times of day including peak traffic hours; before, during, and after flight exposure to the same atmospheric conditions as experienced by the transport airplanes; and overnight outdoor parking. LFC systems were operated in a "hands-off" mode with no adjustments permitted during flight (i.e. the same suction control settings were used for all flights). The LFC suction system was operated in an on/off mode.

GROUND RULES

- **OPERATED LIKE AIRLINE WOULD**
    - **SCHEDULED DISPATCH**
    - **QUEUE UP WITH OTHER AIRLINES**
    - **ATC SYSTEM**
    - **PEAK TRAFFIC HOURS**

- **OVERNIGHT APRON PARKING**

- **EXPOSED TO ELEMENTS**

- **ON/OFF LFC SYSTEMS OPERATION**

Figure 5

EVALUATION OF LFC SYSTEMS

Five laminar flow control systems were used on the LEFT JetStar aircraft and evaluated during the simulated airline service flights. These five systems are the suction, high-lift/shield, wetting, purge, and anti-icing systems (figure 6). The suction system removes a small amount of the laminar boundary layer through either surface perforations or slots. This controls growth of boundary layer disturbances and thus delays transition of the boundary layer from laminar to turbulent flow.

The suction surfaces include both a perforated and a slotted test article, one on each wing. The perforated suction surface test article, designed and built by the Douglas Aircraft Company (DAC), maintains laminar flow on the upper surface of the right wing to the front spar (ref. 7). The front spar is located at about 14 percent chord. Suction is obtained through approximately 1 million 0.0025 inch diameter electron-beam drilled holes in titanium skin. A retractable Krueger-type shield is used as the primary insect contamination avoidance device, and provides line-of-sight protection against insect impingement. Normally, the shield would also serve as a high-lift leading-edge device. For this flight program, however, safety considerations dictated that the shield be deliberately designed for very little high lift production. The supplemental freezing-point depressant, Propylene Glycol Methyl Ether (PGME), sprayed on the wing upper surface from nozzles mounted underneath the shield, wets the suction surface and provides additional protection against insect adhesion and icing. When no insects are present, as at Cleveland in the winter, neither the shield nor the wetting system is needed for insect protection. Anti-icing systems were evaluated during the Cleveland service.

The slotted suction surface test article, built by the Lockheed-Georgia Company (LAC), is designed to maintain laminar flow to the front spar on both upper and lower wing suction surfaces and therefore has no leading edge shield (ref. 6). Suction is attained through 27 spanwise slots about 0.004 inch wide. Wetting the wing leading edge region with the freezing-point depressant (ejected through surface slots during insect encounters) is the means used for preventing insect accumulation (refs. 1, 2). This fluid system also provides the anti-icing function.

To prevent clogging of the perforations or surface slots by the wetting fluid, both concepts require a purging system that clears the LFC passages by pressurizing the subsurface and thus removing the PGME fluid from the LFC ducts and surface.

Operational experience with these five LFC systems was obtained at varying geographical location, season, cruise altitude, and speed.

	ATLANTA	PITTSBURGH	CLEVELAND
SUCTION	YES	YES	YES
HI-LIFT/SHIELD	YES	YES	NO
WETTING	YES	YES	NO
PURGE	YES	YES	YES
ANTI-ICING	NO	NO	YES

Figure 6

DOUGLAS INSECT/ICE PROTECTION SYSTEM IN FLIGHT

The Douglas perforated test article insect and ice protection system in flight use is shown in figure 7. In the Douglas concept for a full wing (ref. 2), laminar flow is attained only on the upper surface which contributes nearly two-thirds of the wing friction drag and thus two-thirds of the potential net drag reduction. Elimination of the lower surface suction systems and the associated stringent LFC surface smoothness requirements then permits use of the Krueger-type leading edge insect protection shield and high lift device stored in the lower surface of the leading edge during cruise. Spray nozzles are mounted on the Krueger underside to supplement, if needed, the insect protection capability of the shield, or to provide the PGME freezing-point depressant fluid for leading edge anti-icing. A system for purging fluid from the suction flutes and surface perforations is also provided. Shield leading edge anti-icing is obtained through use of a commercially available system manufactured by TKS, Ltd.

Figure 7

203

The Lockheed slotted test article insect and ice protection system in flight use is shown in figure 8. Laminar flow is obtained on both top and bottom surfaces (refs. 1,6). Six slots in the leading edge region provide the fluid film for both insect protection and anti-icing. To purge this fluid, pressurized air is forced through the slots during climbout after which these slots are also used for suction to laminarize the boundary layer.
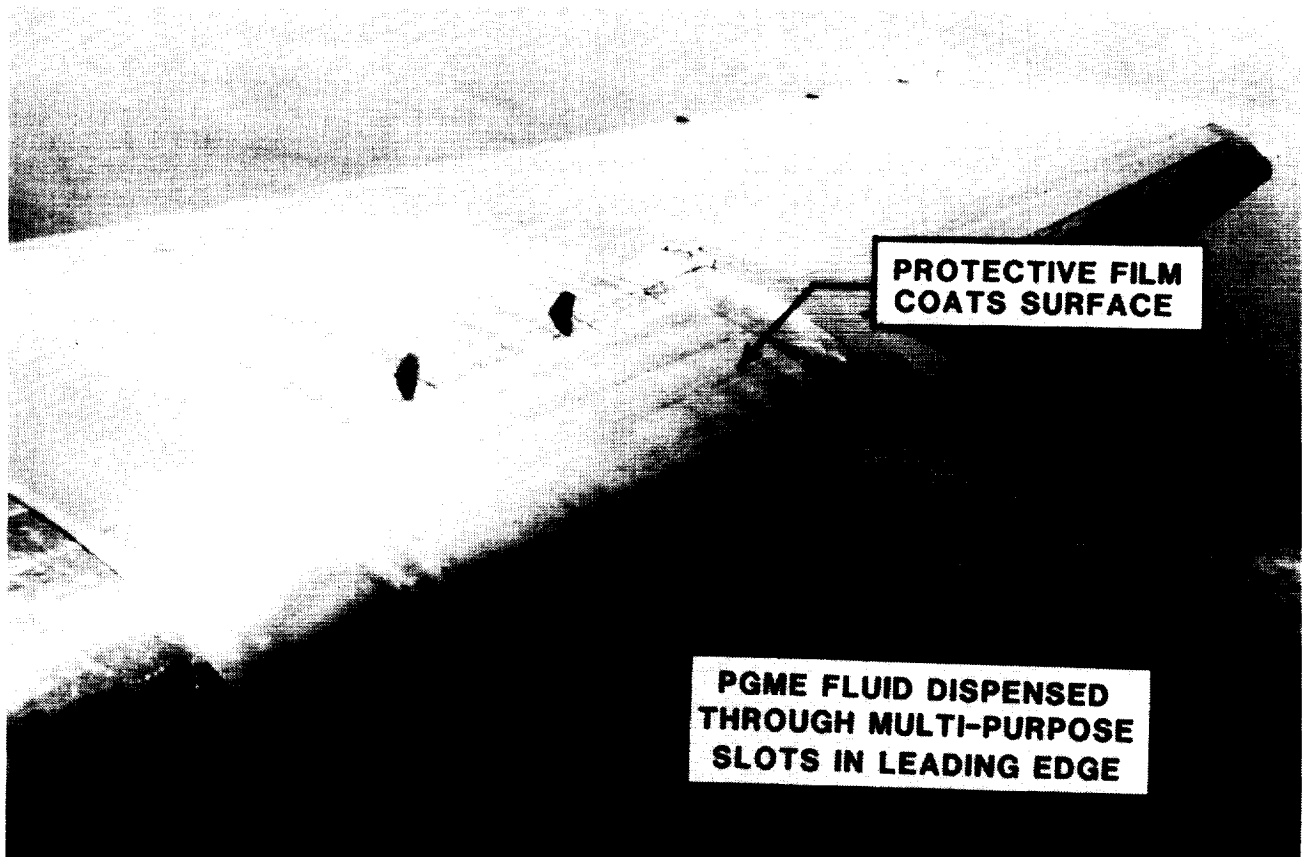
Figure 8

ORIGINAL PAGE IS
OF POOR QUALITY

Figure 9 indicates how bad insect deposits can be during a flight descent in other than winter conditions. Flight 1083 was made September 10, 1985, from Boston to Pittsburgh. Insects accumulated on the Lockheed test article during descent only when the anti-contaminant fluid was not ejected. Simple cleaning of the slotted test article leading edge region with a damp cloth was therefore necessary before every non-winter SAS flight. The anti-contaminant fluid was almost 100% effective in eliminating insect contamination on the slotted test article in takeoff and climb.

The Krueger shield on the Douglas test article could be used during descent as well as ascent and was almost completely effective in eliminating bug hits. The occasional insect deposits that did occur at the inboard end of the shield would be eliminated with a more effective design. The Atlanta SAS flights showed that the perforated article did not have to be cleaned after each flight. Beginning with Flight 1071, therefore, the perforated test article was not cleaned before each flight. It was also noticed that insect debris tended to erode away with time, and that passing through cloud cover allowed a natural washing of the surface. Partway through the Pittsburgh simulated service, it was found that the shield alone was sufficient to protect the perforated test article from insects. Use of the anti-contaminant fluid was discontinued from that point onward; a definite need for supplemental anti-contaminant spray, therefore, could not be established - provided the configuration includes a properly designed insect protection/high-lift device. The perforated article took only 5 insect hits during the entire simulated airline service flights; all 5 hits were inboard near the locations shown in figure 9.

Should the suction surfaces eventually clog after long service, the test articles can be steam-cleaned (ref. 2). This cleaning method was demonstrated on one occasion after months of flight testing at Ames-Dryden, even though no change in surface porosity, evidence of clogging, or need for cleaning was evident as a result of flight service. The entire simulated airline service flight program was conducted over a period of 7 months with no need for steam cleaning.
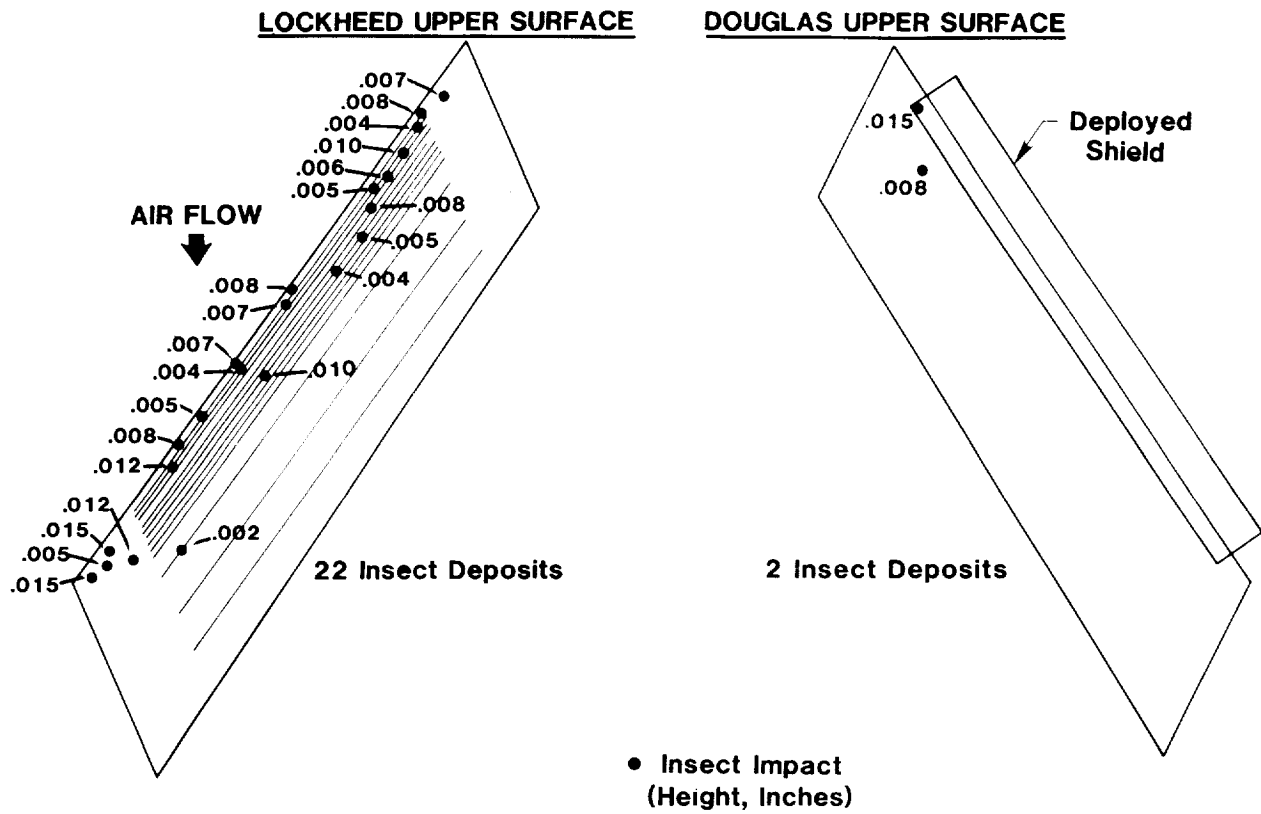
Figure 9

SIMULATED AIRLINE SERVICE WINTER CONDITIONS

Figures 10-12 show the severe snow and ice accumulation on the airplane after it was left out overnight during winter conditions in the simulated service flights based at Cleveland during February, 1986.

Figure 10

ORIGINAL PAGE
BLACK AND WHITE PHOTOGRAPH
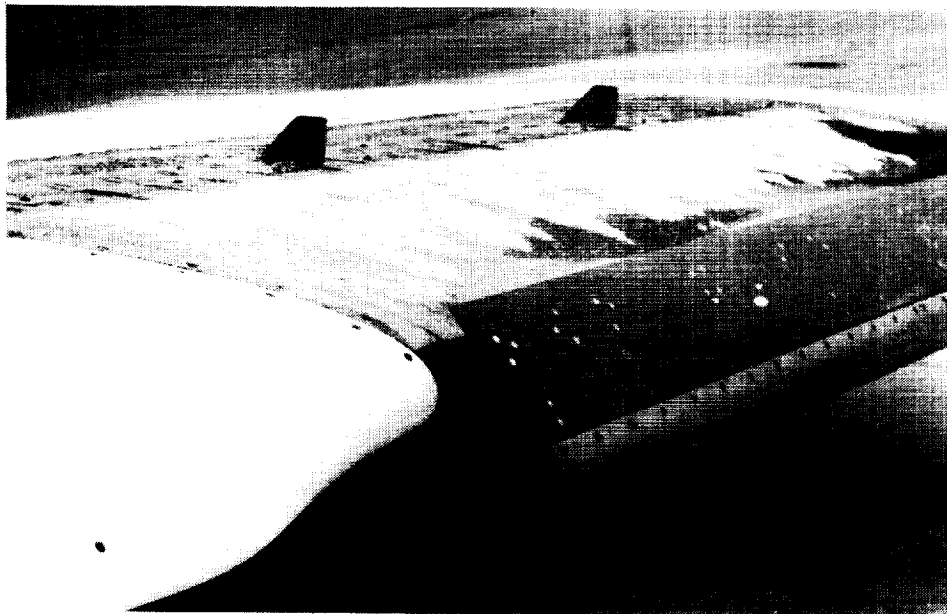
Figure 11

Figure 12

Ground deicing of the LFC test articles was no more difficult than normal deicing of commercial transports. Snow and ice accumulation was easily eliminated with the hand-held deicing equipment shown in figure 13. This photo was taken before takeoff from Cleveland, February 21, 1986. Use of the anti-icing fluid on the test articles in flight was previously shown in figures 7 and 8.

ORIGINAL PAGE IS
OF POOR QUALITY

Figure 13

ORIGINAL PAGE
BLACK AND WHITE PHOTOGRAPH

Results shown in figure 14 indicate long periods of steady amounts of laminar flow in clear air. Figure 14 also shows a large forward movement in transition location and consequent loss of laminar flow when flying through clouds (see t = 28 and 30 min.). The data are from flight 1135 from Atlanta to Atlantic City on February 20, 1986. Cloud penetration is indicated by an increase in airplane electrical charge as measured by the charge patch instrument mounted on the leading edge of the plyon. The plyon is located on the top of the JetStar fuselage. Charge indicator results were correlated with ice particle measurements using the Knollenberg probe mounted on top of the plyon. Detailed meteorological results on laminar flow loss in clouds and statistics on cloud occurrence are presented in the companion paper by Davis (ref. 16). When the aircraft emerged from these clouds, laminar flow is regained almost instantaneously (t = 32 min.).
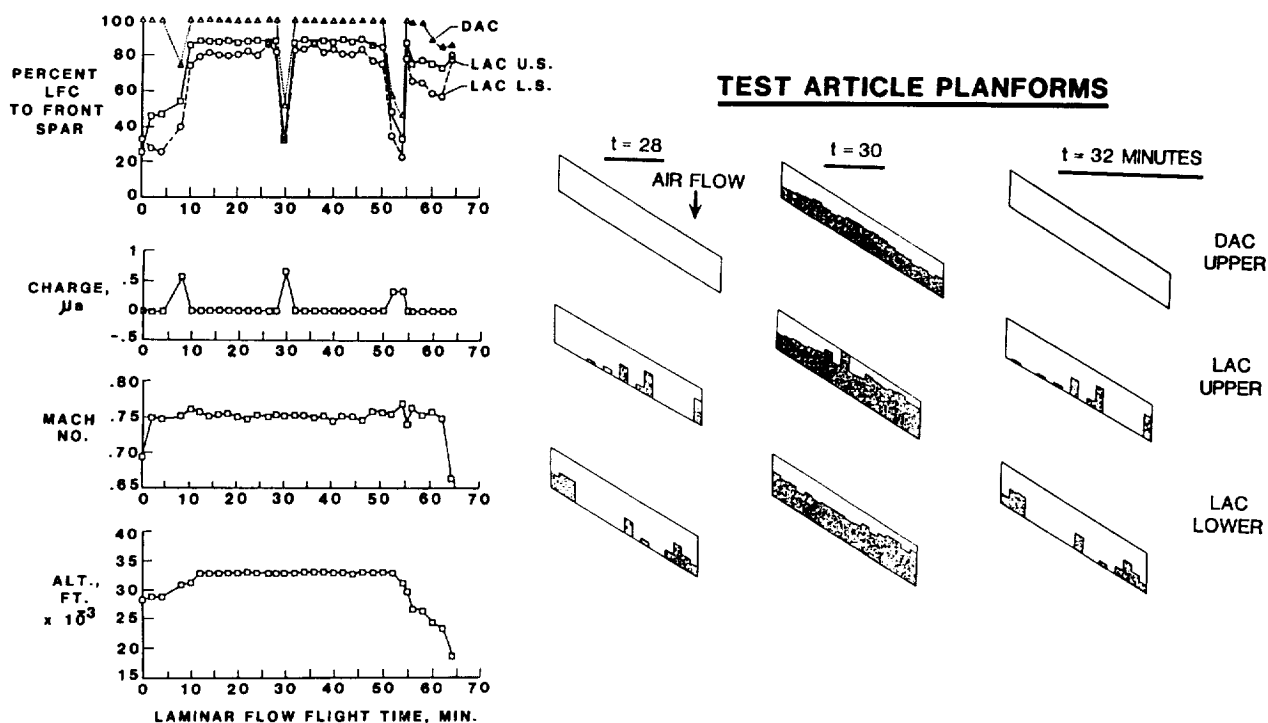
Figure 14

Extensive flight tests were made using LFC systems located in the JetStar aircraft's leading edge region at flight conditions representative of transport airplanes in a commercial airline operational environment. LFC systems evaluated included the suction surface and ducting, insect protection, and anti-icing. A summary of the results is presented in figure 15. All operational experience was positive. No dispatch delays were encountered due to the LFC systems. There was no need to adjust suction system controls throughout the test range of cruise altitude, Mach number, and lift coefficient. Both insect anti-contaminant systems were effective in alleviating insect deposits. Non-use of the spray system on the Lockheed article during descent necessitated leading-edge cleaning between flights. Results also indicated that the supplemental spray for insect protection is not necessary for LFC transport airplanes equipped with the insect shield/high-lift device. Both anti-icing systems were effective in flight, and ground deicing was not exacerbated by the LFC systems. The system for purging the anti-contaminant/anti-icing fluid from air passages operated satisfactorily. During the simulated service in Atlanta, while on the ground the aircraft was exposed to a heavy rain of over 1.5 in. in a short time. The next day it was found that rainwater which had seeped into the LFC ducts could be successfully purged from the test article during climbout. Such results have established a preliminary maintenance and reliability data base for these LFC systems.

	PERFORATED	SLOTTED
DISPATCH RELIABILITY	GOOD	GOOD
HANDS-OFF SUCTION SYSTEM	YES	YES
ANTI-CONTAMINATION SYSTEM	SHIELD EFFECTIVE, W & W/O SPRAY	WETTING ON T.O. EFFECTIVE
LE CLEANED BETWEEN FLIGHTS	NO	YES
TEST ARTICLES/AIRCRAFT DEICED	YES	YES
ANTI-ICING SYSTEM	EFFECTIVE	EFFECTIVE
PURGE SYSTEM	EFFECTIVE	EFFECTIVE

Figure 15

211

Fabrication difficulties with the slotted test article internal suction system and external surface quality (ref. 5) limited the extent of laminar flow attained on this article to less than that attained by the perforated article (fig. 16). Further development of fabrication techniques for the slotted concept is therefore required. Because data were taken at one second intervals, detailed analysis is possible. Based on 20,258 data points measured during 11 flights (ref. 16), the extent of laminar flow attained on the perforated article exceeded 96 percent (cruise average to the front spar), versus 78 percent for the upper surface of the slotted article[*] (fig. 16). An improved surface quality on the slotted article would be expected to result in as much laminar flow as was achieved with the perforated article. Partway through the Pittsburgh simulated airline service flights, the LFC systems were used during climb and descent, as well as for cruise, and laminar flow was obtained on both test articles to altitudes as low as 10,000 feet. The amount of laminar flow achieved under these conditions was not as great as in cruise but these flights conclusively demonstrated that laminar flow could be achieved during transient flight altitudes and Mach numbers. As expected, laminar flow was lost during flight through clouds. Approximately 7 percent of the 20,258 data points were taken in clouds; this time-in-cloud result for the domestic United States is close to the time-in-cloud result of 6 percent determined as a result of a world-wide data analysis (ref. 15). No attempt was made to utilize altitude flight management in order to avoid clouds; such management would be expected to reduce the amount of time spent-in-cloud. With the exception of the inboard end of the Krueger shield, both systems for alleviation of insect deposits were effective. If the wetting anti-contamination system on the Lockheed slotted article was not used during descent, surface cleaning of the leading edge region was required before the next flight.

---

[*]The Lockheed slotted lower surface attained 73 percent laminar flow to the front spar (cruise average). Otherwise, the slotted lower surface results were the same as for the upper.

TEST ARTICLE LFC PERFORMANCE (UPPER SURFACE)

	PERFORATED LEADING-EDGE	SLOTTED LEADING-EDGE
*CLEAR AIR, CRUISE AVERAGE	~ 96% L.F. (TO FRONT SPAR)	~ 78% L.F. (TO FRONT SPAR)
CLEAR AIR, CLIMB OR DESCENT	LAMINAR FLOW TO 10,000 FT.	LAMINAR FLOW TO 10,000 FT.
CLOUDS/ICE PARTICLES	LOST LAMINAR FLOW	LOST LAMINAR FLOW
*TIME IN CLOUDS	~ 7%	~ 7%
TEST ARTICLE BUG HITS 62 FLIGHTS	~ 5	MANY (ON LANDING)

* BASED ON 11 FLIGHTS (20,258 DATA POINTS)

Figure 16

213

Simulated airline service flight test results are summarized in figure 17.

- **LAMINAR FLOW OBTAINED AFTER EXPOSURE TO HEAT, COLD, HUMIDITY, INSECTS, RAIN, FREEZING RAIN, SNOW, AND ICE**

- **"HANDS-OFF SUCTION CONTROLS" FLIGHTS RESULTED IN COMPLETE LAMINAR FLOW OF PERFORATED LEADING-EDGE TEST ARTICLE (10,000 FT. TO 38,000 FT.)**

- **LAMINAR FLOW MAINTAINED DURING MODERATE TURBULENCE**

- **LAMINAR FLOW LOST IN CLOUDS**

- **HI-LIFT SHIELD WITHOUT FLUIDS PREVENTED INSECT CONTAMINATION**

- **INSECT ALLEVIATION SYSTEMS WERE EFFECTIVE AND LEADING EDGES DID NOT REQUIRE CLEANING BETWEEN FLIGHTS UNLESS THESE SYSTEMS WERE NOT USED**

- **CONVENTIONAL GROUND ANTI-ICING EQUIPMENT SUFFICIENT FOR ICE/SNOW REMOVAL**

Figure 17

The first JetStar leading edge flight test was made November 30, 1983.
The JetStar has now been flown for more than 3 years. The titanium leading
edge test articles today remain in virtually the same condition as they were
in on that first flight. No degradation of laminar flow performance has
occurred as a result of service. The JetStar simulated airline service
flights have demonstrated that effective, practical leading edge systems are
available for future commercial transports. Specific conclusions based on the
results of the simulated airline service test program are summarized in figure
18.

- **LFC SYSTEMS PERFORMANCE WAS PROVEN EFFECTIVE DURING SIMULATED AIRLINE SERVICE**

- **SIMULATED SERVICE REVEALED NO OPERATIONAL PROBLEMS WITH LFC SYSTEMS AND NO SPECIAL MAINTENANCE REQUIREMENTS WERE UNCOVERED**

- **LEFT JETSTAR PROGRAM HAS ESTABLISHED THE PRACTICALITY OF BASELINE DESIGNS FOR LEADING EDGE LFC SYSTEMS FOR FUTURE COMMERCIAL TRANSPORT AIRCRAFT**

Figure 18

alt	altitude, feet
ATC	Air Traffic Control
DAC	Douglas Aircraft Company
FT	Feet
LAC	Lockheed Aircraft Company
LE	Leading Edge
LEFT	Leading-Edge Flight Test
LF	Laminar Flow
LFC	Laminar-Flow Control
NA	Not Available
PGME	Propylene Glycol Methyl Ether
SAS	Simulated Airline Service
t	time, minutes
TO	Takeoff
w	with
wo	without
μa	charge patch current, microamperes = 1 x 10E-06 ampere

Airports

ABQ	Albuquerque, New Mexico
ACY	Atlantic City, New Jersey
AMA	Amarillo, Texas
ATL	Atlanta, Georgia
AZO	Kalamazoo, Michigan
BAD	Barksdale, Louisiana
BGR	Bangor, Maine
BNA	Nashville, Tennessee
BOS	Boston, Massachusetts
BTV	Burlington, Vermont
CHA	Chattanooga, Tennessee
CHS	Charleston, West Virginia
CLE	Cleveland, Ohio
DCA	Washington, DC
DEN	Denver, Colorado
DET	Detroit, Michigan
DSM	Des Moines, Iowa
EDW	Edwards Air Force Base, California
GRB	Green Bay, Wisconsin
JFK	New York, New York
LFI	Langley Research Center, Hampton, Virginia
LOU	Louisville, Kentucky
MSY	New Orleans, Louisiana
OKC	Oklahoma City, Oklahoma
ORD	Chicago, Illinois
ORF	Norfolk, Virginia
PIT	Pittsburgh, Pennsylvania
RDU	Raleigh-Durham, North Carolina
RIC	Richmond, Virginia
SPI	Springfield, Illinois
STL	St. Louis, Missouri
TPA	Tampa, Florida
TYS	Knoxville, Tennessee

REFERENCES

1. Sturgeon, R. F.; et al.: Evaluation of Laminar Flow Control System Concepts for Subsonic Commercial Transport Aircraft. NASA CR-159253, 1980.

2. Douglas Aircraft Co. Staff: Evaluation of Laminar Flow Control System Concepts for Subsonic Commercial Transport Aircraft. NASA CR-159251, 1983.

3. Wagner, R. D.; Maddalon, D. V.; and Fischer, M. C.: Technology Developments for Laminar Boundary Layer Control on Subsonic Transport Aircraft. AGARD Conference Proceedings No. 365, Improvement of Aerodynamic Performance Through Boundary Layer Control and High Lift Systems, 1984.

4. Braslow, A. L.; and Fischer, M. C.: Design Considerations for Application of Laminar Flow Control Systems to Transport Aircraft. AGARD Report No. 723, Aircraft Drag Prediction and Reduction. Rhode-St. Genese, Belgium, August, 1985.

5. Maddalon, D. V.; and Wagner, R. D.: Laminar Flow Aircraft Certification. NASA CP 2413, 1986.

6. Etchberger, F. R.: Laminar Flow Control Leading Edge Glove Flight - Aircraft Modification Design, Test Article Development, and Systems Integration. NASA CR-172136, 1983.

7. Douglas Aircraft Co. Staff: Laminar Flow Control Leading Edge Glove Flight Test Article Development. NASA CR-172137, 1984.

8. Fischer, M. C.; Wright, A. S., Jr.; and Wagner, R. D.: A Flight Test of Laminar Flow Control Leading-Edge Systems. NASA TM-85712, 1983.

9. Fisher, D. F.; and Fischer, M. C.: The Development Flight Tests of the Jetstar LFC Leading-Edge Flight Experiment. NASA CP 2487, pp. 117-140. December 1987.

10. Lineberger, L. B; et al.: Development of Laminar Flow Control Wing Surface Composite Structures. NASA CR-172330, 1984.

11. **Lineberger, L. B.: Structural Tests and Development of a Laminar Flow Control Wing Surface Composite Chordwise Joint. NASA CR-172462, 1984.**

12. Douglas Aircraft Company: Development of Laminar Flow Control Wing Surface Porous Structure. NASA CR-172424, 1984.

13. Fischler, J. E.; et al.: Laminar Flow Control Perforated Wing Panel Development. NASA CR-178166, 1986.

14. Davis, R. E.; and Fischer, M. C.: Cloud Particle Effects on Laminar Flow in the NASA LEFT Program: Preliminary Results. AIAA Paper 86-9811, 1986.

15. Jasperson, W. H.; Nastrom, G. D.; Davis, R. E.; and Holdeman, J. D.: GASP Cloud-and-Particle Encounter Statistics, and Their Application to LFC Aircraft Studies (2 vols.). NASA TM 85835, October, 1984.

16. Davis, R. E.; Maddalon, D. V.; and Wagner, R. D.: Performance of Laminar Flow Leading Edge Test Articles in Cloud Encounters. NASA CP 2487, pp. 163-193. December 1987.

STABILITY THEORY APPLICATIONS TO
LAMINAR-FLOW CONTROL

Mujeeb R. Malik
High Technology Corporation
Hampton, VA

APPLICATION OF STABILITY THEORY TO LAMINAR FLOW CONTROL

In order to design LFC[*] configurations, one needs reliable methods for boundary-layer transition prediction. Among the available methods, there are correlations based upon R_θ, shape factors, Görtler number and crossflow Reynolds number. These correlations derived from experimental information have limited scope. The most advanced transition prediction method is based upon linear stability theory in the form of the e^N method which has proven to be successful in predicting transition in two- and three-dimensional boundary layers and, in particular, studying the sensitivity of boundary-layer transition to various control parameters such as pressure gradient, suction, and wall temperature.

---

*Laminar-flow Control (LFC).

- LFC — DELAY OF BOUNDARY-LAYER TRANSITION USING MEANS SUCH AS PRESSURE GRADIENT, SUCTION, WALL TEMPERATURE, ETC.

- NEED FOR TRANSITION PREDICTION METHODS

- AVAILABLE METHODS

    - CORRELATIONS BASED UPON R_θ , SHAPE FACTORS, GÖRTLER NUMBER, CROSSFLOW REYNOLDS NUMBER, ETC.

    - PREDICTION METHODS BASED UPON BOUNDARY-LAYER STABILITY THEORY

EVOLUTIONARY PATHS IN LAMINAR/TURBULENT TRANSITION

There are various stages involved in the transition process. External disturbances in the form of freestream vorticity, sound, entropy spots, surface roughness and surface vibrations get internalized in the boundary through a process known as 'receptivity' -- a phrase first coined by Morkovin (Ref. 1). These internalized small disturbances begin to grow past a critical Reynolds number. At first the disturbances grow exponentially (according to linear theory) in the form of Tollmien-Schlichting (T-S), Görtler or crossflow waves until nonlinearity sets in and then secondary and perhaps tertiary instabilities in the flow cause transition. We are beginning to understand more and more about receptivity and nonlinear stages now. We know, for example, that flow nonhomogeneities play an important role in receptivity process (Refs. 2-5). In recent years, considerable progress has been made in understanding nonlinear stages of transition process (Refs. 6-10). More advances will certainly be made both in the field of receptivity and nonlinear breakdown mechanism. But transition essentially depends upon the disturbance environment and it is the lack of detailed quantitative characterization of the disturbance environment that we will always have to rely upon empirical information for transition prediction in practical situations.

Transition may also take place through nonlinear mechanisms by passing the usual linear mechanism. An example is the swept attachment line boundary layer which exhibits subcritical transition (Ref. 11). However, if the initial disturbance level is kept low the linear process (exponential growth) is, in general, involved and its extent (in terms of distance along the body and total amplification) is quite large in comparison with the nonlinear process and this essentially leads to the success of the e^N method.

It is at the linear state that control, whether 'passive' (through boundary layer modification) or 'active' (through disturbance cancellation) is possible. Though some CFD studies indicate possibility of control at nonlinear stages too (Ref. 12). An LFC designer, however, ought to be conservative and keep the amplitudes low.

EVOLUTIONARY PATHS IN LAMINAR/TURBULENT TRANSITION

EXTERNAL DISTURBANCES

FREESTREAM VORTICITY
FREESTREAM SOUND
FREESTREAM ENTROPY SPOTS
SURFACE ROUGHNESS
VIBRATIONS

RECEPTIVITY

SLOW LINEAR AMPLIFICATION

T-S INSTABILITY
GÖRTLER INSTABILITY
CROSSFLOW INSTABILITY

OPERATION MODIFIERS

MEAN BOUNDARY LAYER PROPERTIES	DISTURBANCE PROPERTIES
$P(x)$	ACTIVE
T_w/T_R	CONTROL
$\dot{M}$	
CURVATURE	HEATING OR
WAVINESS	COOLING
ROUGHNESS	MASS
ANGLE OF ATTACK	TRANSFER,
LEADING EDGE	ETC. TO
SWEEP	CANCEL
ROTATION	DISTURBANCE

BYPASSES
3-D NONLINEAR
SPACE TIME
DISTURBANCES

SECONDARY AND TERTIARY INSTABILITIES

TURBULENCE

THE e^N METHOD FOR TRANSITION PREDICTION

The e^N method was first used by A.M.O. Smith in 1952* (Ref. 13) for Görtler instability on concave surfaces, though the work remained classified and was not published until 1955 (Ref. 14). By that time, both Smith and van Ingen (Ref. 15, 16) independently had shown that, for two-dimensional flows, the e^N method could correlate low disturbance experimental data with N approximately 9 and the method came to be known as the e^9 method.

The necessary steps involved in application of the e^N method are: (1) computation of mean boundary layer profiles accurately, (2) computation of linear amplification rate by an "appropriate stability model," and (3) integration of the growth rate from onset of instability x_0 to transition initiation location x_T. The value of the integral is equal to the exponent in e^N and is commonly known as the "N factor."

● CALCULATE MEAN BOUNDARY—LAYER PROFILES

● CALCULATE LINEAR AMPLIFICATION RATE BY USING "APPROPRIATE STABILITY MODEL"

● TRANSITION OCCURS WHEN DISTURBANCES IN THE BOUNDARY LAYER ARE FIRST

AMPLIFIED BY A FACTOR e^N, WHERE

$$N = \ln(A/A_0) = \int_{x_0}^{x_T} (\text{LINEAR AMPLFICATION RATE}) \, dx$$

(SMITH, 1952)

*Smith, A.M.O.: Design of the DESA-2 Airfoil. Douglas Aircraft Co., ES17117, AD143008, 1952. (Reference 13 mentions 1952 reference.)

REVIEW OF LINEAR STABILITY THEORY

The first question one asks is: "What is the ´appropriate stability model´ for computation of the linear growth rates?" The simplest of the model is the Orr-Sommerfeld equation, which is a fourth-order ordinary differential equation in the disturbance stream function ϕ derived from the Navier-Stokes equation written in the cartesian coordinates x,y,z, where y is the normal boundary layer coordinate and x and z are in the plane parallel to the surface. In deriving this equation it is assumed that mean flow profiles such as U in the direction of X and W in the direction of Z are functions of y only. This is the well-known ´parallel flow´ assumption. The disturbance is assumed to have a waveform with wave numbers α, β in x and z directions respectively and ω is the disturbance frequency.

We have an eigenvalue problem, given by the dispersion relation, meaning that nontrivial solution of the Orr-Sommerfeld equation exists only for certain combinations of α, β, and ω. In general, α, β, ω can all be complex. However, we can talk in terms of temporal or spatial theories where either $e^{-\alpha_i x - \beta_i z}$ or $e^{\omega_i t}$ is set to unity. The Orr-Sommerfeld equation is a model equation for T-S or crossflow disturbances in incompressible flows.

● ORR-SOMMERFELD EQUATION (INCOMPRESSIBLE FLOW)

$$\left(\frac{d^2}{dy^2} - (\alpha^2 + \beta^2)\right)^2 \phi = iR\left[(\alpha U + \beta W - \omega)\left\{\frac{d^2}{dy^2} - (\alpha^2 + \beta^2)\right\}\phi - (\alpha U'' + \beta W'')\right]$$

B. C. $\phi(0) = \phi'(0) = 0;$ $\phi = 0,$ $\phi' = 0$ WHEN $y = \infty$

- DERIVED FROM NAVIER-STOKES EQUATION USING PARALLEL FLOW ASSUMPTION AND BY ASSUMING

$$u(x,y,z,t) = U(y) + \phi_y(y)e^{i(\alpha_r x + \beta_r z - \omega_r t)}e^{-\alpha_i x - \beta_i z}e^{\omega_i t}$$

- EIGENVALUE PROBLEM: $\omega = \omega(\alpha, \beta)$

- TEMPORAL THEORY

- SPATIAL THEORY

224

LINEAR STABILITY THEORY (CONCLUDED)

When effects of curvature (body or streamline) are important, as in the Görtler problem, then the governing equations become sixth-order.

The governing equations for compressible stability with or without curvature are, in general, eighth-order. There, for hypersonic flows, one needs to worry about real gas effects. Some recent calculations (Ref. 17) at Mach 10 show their significance.

Boundary layer flows, in general, are nonparallel. For comparison with stability experiments on quantities such as disturbance eigenfunctions and growth rates, it is advisable to use nonparallel stability theory (Ref. 18). Since the e^N method is essentially a correlation with experimental data, it is not necessary to use nonparallel theory for transition prediction purposes. Use of nonparallel theory, say for two-dimensional boundary-layer flows analyzed by Smith (Ref. 15), will simply shift the value of N from 9 to some other value (say 12) and the method would have been known as the e^{12} method.

- **SIXTH-ORDER SYSTEM (INCOMPRESSIBLE FLOW)**

    - EFFECT OF CURVATURE (BODY AND STREAMLINE)

    - EFFECT OF ROTATION

- **COMPRESSIBLE STABILITY**

    - EIGHTH-ORDER SYSTEM OF EQUATION

    - PHYSICAL AND TRANSPORT PROPERTIES (PERFECT OR REAL GAS)

- **NONPARALLEL STABILITY**

225

An example of a typical e^N calculation is provided in this figure. In reality disturbances develop in the form of ‾wave-packets,‾ but then questions regarding initial conditions and the origins of these packets arise. So for the e^N purposes, it is common to consider monochromatic waves. Calculations for a fixed frequency are performed and repeated for others. When a frequency first reaches an N factor of, say 10, transition is said to initiate. In this figure, for example, transition takes place at R of about 2500 where a frequency $F = .2 \times 10^{-4}$ first reaches $N = 10$. To compare experimental transition data, one could generate an N versus an F curve at the transition location, and the peak of such a curve then gives a relevant N factor.

10^0 SHARP CONE, $M_\infty = 1.5$

$$F = \frac{2\pi\nu_e}{U_e^2} f \ (Hertz)$$

$$R = (R_x)^{1/2}$$
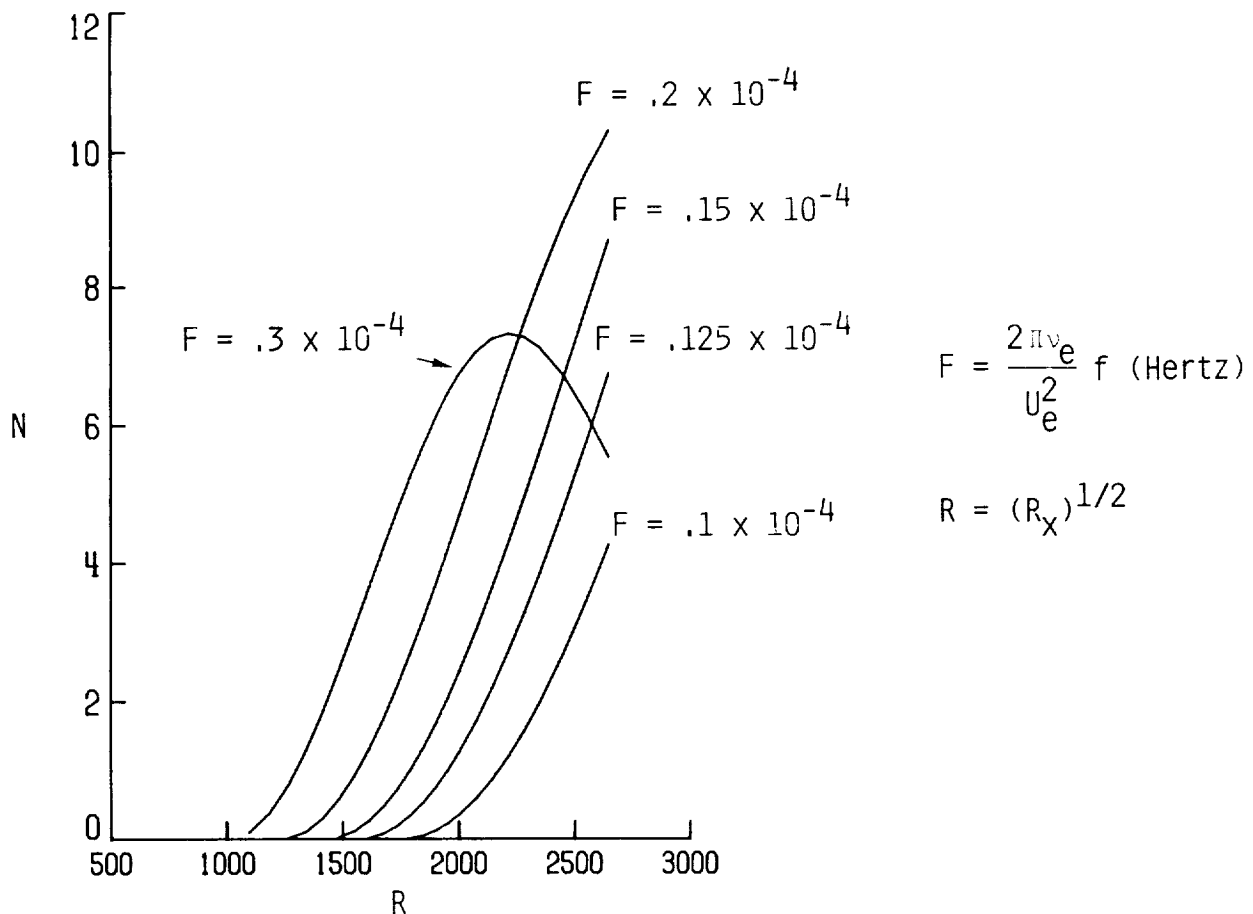
TRANSITION N FACTORS FOR QUIET TUNNEL AND F-15 CONE DATA

The N versus F curves have been generated for the experimental transition data listed in the table. These data are for 10° sharp cones from F-15 flight and the Mach 3.5 Langley quiet tunnel. Calculations are made using adiabatic wall conditions to closely match the experimental conditions. Eigenvalues are computed using the full eight-order system. Note that the peak of all the curves for the first six test cases listed in the table lie between about 9 and 11. So the e^N method (with N from 9-11) is successful in correlating with experimental transition data at Mach 1.2 to 3.5. For the last case (QT3) listed in the table, the N factor was calculated to be 6 at the last computational station indicating no transition. This is consistent with the experiment where flow was still laminar at the last measurement station and the cone was not long enough to have transition. External disturbances in these experiments are believed to be low — a necessary condition for the success of the e^N method. Correlation with experimental data from conventional supersonic wind tunnels would yield low values of N (2-4) since they have high level of freestream disturbances.

10° SHARP CONE

CASE I·D·	M_∞	U_e / ν_e $\times 10^6/m$	Re_{tr} $\times 10^6$
FL1	1·20	9·16	6·99
FL2	1·35	9·28	5·59
FL3	1·60	11·55	7·86
FL4	1·92	14·19	7·26
QT1	3·5	29·46	8·08
QT2	3·5	19·94	6·74
QT3	3·5	9·50	-
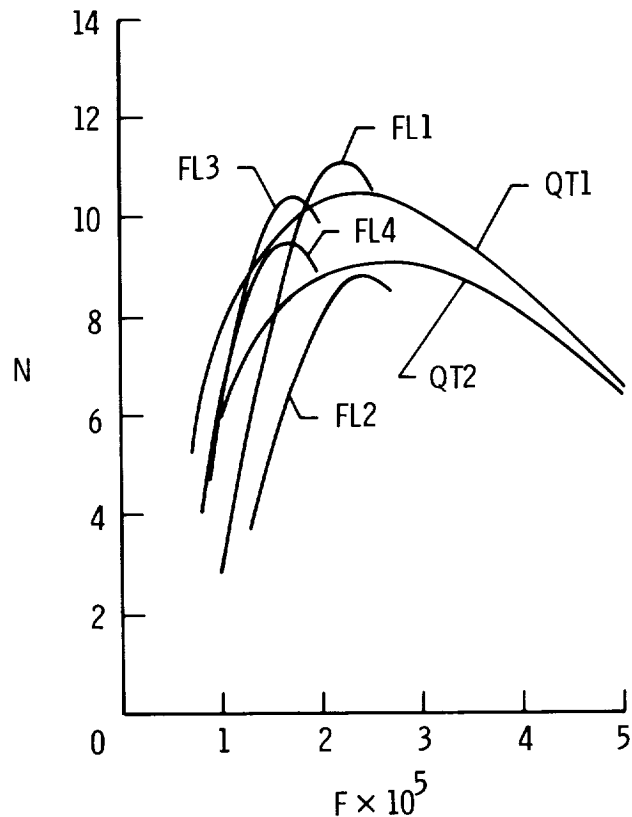
TRANSITION IN A BOUNDARY LAYER APPROACHING SEPARATION

When flow approaches separation, the validity of both the boundary-layer theory and the Orr-Sommerfeld equation becomes questionable. However, amplification rates become large due to the development of inflectional velocity profiles and any error committed by the e^N method in predicting transition becomes small in terms of surface distance. The figure presents results for the most amplified frequency in the boundary layer over the Beechcraft T-34C NLF glove. In the experiment (Ref. 19), transition took place at X/C = .44 and separation occurred at X/C = .45. At X/C = .44, the N factor is 12.8. N increases very rapidly beyond X/C = .4 due to inflectional streamwise velocity profiles (note that this is an unswept airfoil). If an N of 10 had been used to predict onset of transition in this experiment, a value of $(X/C)_{transition}$ = .42 will result as compared to .44 observed in the experiment.

BEECHCRAFT T-34C NLF GLOVE

$M = 0.27$, $R = 12.6 \times 10^6$, $C_L = 0.35$
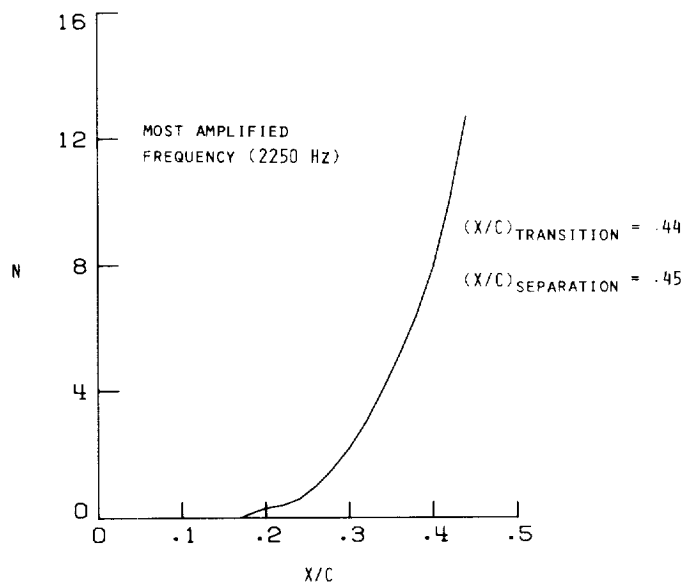
AMPLIFICATION OF GÖRTLER VORTICES ALONG A MACH 3.5 NOZZLE WALL

The question of Görtler or centrifugal instability has been a subject of controversy for many years. The attempts have been made to obtain a critical value of the Görtler number. It was pointed out by Hall (Ref. 20) that parabolic PDE´s need to be solved for this problem in which case neutral curves are not unique since they depend upon initial conditions. If one thinks of transition taking place at an N of 9-11, then the parameters that are involved which give such a growth are not significantly affected by the region of controversy (low wavenumber region) and computations may be made using parallel flow theory. We tested this for various quiet tunnel test runs where transition on the nozzle walls takes place due to the amplification of Görtler vortices. The transition location could be correlated in those cases with an N factor of 9-11 (see Ref. 21). The success of parallel flow theory implies that perhaps asymptotic theory will also be successful. In this figure, N factor results are presented for Mach 3.5 nozzle wall using parallel (Ref. 21) and asymptotic (Ref. 22) theories. Both theories give results that are quite close for design purposes. The asymptotic theory requires an order of magnitude less computer time since eigenvalue computations are not involved.

DISTANCE FROM THROAT, CM
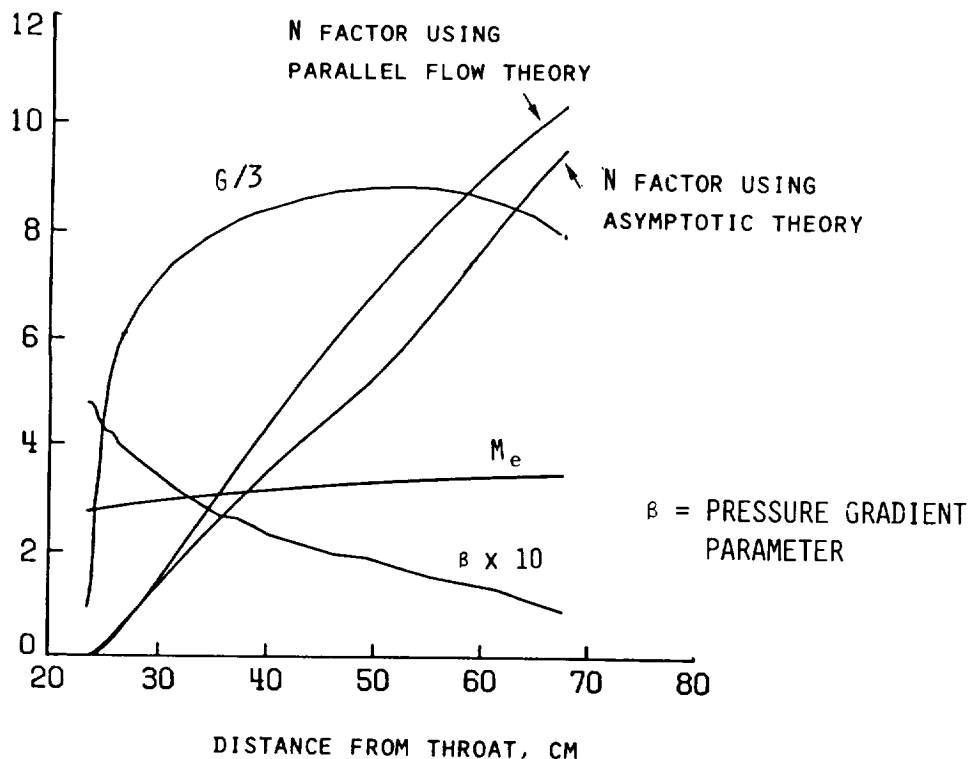
TRANSITION IN 3-D BOUNDARY LAYERS

Stability computations are very sensitive to the details of the mean boundary-layer profiles which, therefore, have to be computed accurately. Anything that affects boundary-layer profile shape also indirectly affects their stability. So, inviscid solution has to be accurately prescribed and should be free of any unwanted wiggles. Boundary-layer computation is a rather trivial matter for two-dimensional flows but this is certainly not the case for three-dimensional configurations. To date, almost all swept-wing computations have been done using conical similarity using computer codes similar to the one due to Kaups and Cebeci (Ref. 23). While comparing the stability calculations with experimental data, one has to know if the conical similarity assumption, which requires straight isobars, is valid. If spanwise pressure gradient is present, the computed crossflow and thus, the crossflow instability will be in error by an unknown magnitude.

- MEAN FLOW

  - INVISCID
    COMPUTED, EXPERIMENTAL

  - BOUNDARY LAYER
    FULLY 3-D, CONICAL ASSUMPTION

- STABILTIY EQUATIONS

  - EFFECT OF CURVATURE (BODY, STREAMLINE)

- UNSTEADY VERSUS STEADY DISTURBANCES NEAR THE LEADING EDGE

TRANSITION IN 3-D BOUNDARY LAYERS (CONTINUED)

In the stability of three-dimensional boundary layers, the question that immediately arises is how waves propagate in these boundary layers or the bottomline question ´how to compute N?´

One can start with spatial stability theory. There are five parameters: real parts of α, β, ω and imaginary parts of α, β. Two conditions are provided by the dispersion relation itself. Since we consider monochromatic waves, the real part of ω is also fixed. So, two more conditions need to be specified. Nayfeh (Ref. 24) and Cebeci and Stewartson (Ref. 25) independently derived a condition that the group velcoity ratio ought to be real. This fixes direction of growth. It seems reasonable to follow disturbances that grow the most, so the second condition is that the growth rate should be a maximum. This fixes the wave angle. However, this angle may vary as the boundary layer develops. By providing these conditions, all the arbitrariness in the problem has been eliminated and the N factor calculation may proceed.

- ● WAVE-PROPAGATION (OR HOW TO COMPUTE N?)

  - SPATIAL STABILITY

    5 PARAMETERS: REAL (α, β, ω); $Im(\alpha, \beta)$

    TWO CONDITIONS PROVIDED BY DISPERSION RELATION

    FOR FIXED REAL (ω), TWO CONDITIONS NEEDED

    NAYFEH (1979), CEBECI AND STEWARTSON (1979):

      (1) GROUP VELOCITY RATIO $(\omega_\beta/\omega_\alpha)$ IS REAL

      (2) MAXIMIZE GROWTH RATE $\sigma = -\alpha_i - \beta_i(\omega_\beta/\omega_\alpha)$

TRANSITION IN 3-D BOUNDARY LAYERS (CONCLUDED)

Alternatively one may use temporal stability. Now there are four parameters: real (α, β, ω) and imaginary part of ω or ω_i. Again, two conditions are provided by the dispersion relation. For fixed real ω, one can maximize ω_i to follow waves that amplify the most. When this maximum is computed, it turns out (and it can also be shown mathematically) that group velocity ratio is automatically real. One also needs group velocity transformations to obtain spatial growth rates for computation of N factors. This scheme is commonly referred to as the envelope method and is built in computer codes SALLY (Ref. 26) and COSAL (Ref. 27). N factor results from this approach have been found to be quite close to the ones obtained using the spatial approach outlined in the previous figure.

A third approach is the one that is commonly used by Boeing and is called the N_{CF}/N_{T-S} approach. In this approach, different methods of integration are used for crossflow and T-S waves. The crossflow waves are assumed always to be stationary and are subjected to the condition that the curl of the wavenumber vector vanishes - a condition that is strictly only true for conservative wave systems. A boundary layer is not considered to be such a system. The direction of growth is the same as the external streamline direction. The T-S waves, on the other hand, always orient themselves at some fixed angle with respect to the external streamline. The direction of growth is again taken as the external streamline. This approach then results in two sets of N factors, N_{CF} for crossflow disturbances and N_{T-S} for T-S waves as described above. The N factors are then correlated with experimental transition data on swept-back wings.

- TEMPORAL STABILITY

    4 PARAMETERS: REAL (α, β, ω); $Im(\omega)$

    FOR FIXED REAL (ω):

    (1) MAXIMIZE ω_i

    $\longrightarrow$ GROUP VELOCITY RATIO AUTOMATICALLY REAL

    (2) SPATIAL GROWTH RATE: $\sigma = \dfrac{\omega_i}{|V_g|}$; $V_g = \left(\dfrac{\partial \omega_r}{\partial \alpha} , \dfrac{\partial \omega_r}{\partial \beta} \right)$

- BOEING'S N_{CF}/N_{TS} APPROACH

    N_{CF}
        (1) IRROTATIONALITY OF WAVE NUMBER VECTOR
        (2) GROWTH IN THE DIRECTION OF EXTERNAL STREAMLINE

    N_{TS}
        (1) FIXED WAVE-ANGLE
        (2) GROWTH IN THE DIRECTION OF EXTERNAL STREAMLINE

232

N FACTORS FOR F-111 TEST CASE NO. 19

If one uses the first or the second approach and computes N factors for a range of frequencies without a priori labelling the waves as crossflow or T-S, then most often it turns out that N for the most amplified wave is around 9-11. An example, using the envelope method, is provided in this figure for F-111 Test Case No. 19 where the computed N factor is about 9. The corresponding Boeing calculation yields N_{CF} = 2.2 and N_{T-S} = 5.4. However, in cases where transition is closer to the leading edge and the c_p distribution is such that large growth takes place very near the leading edge, then the envelope method will give very high N's if curvature terms are not included in the analysis. The reason is that the correct stability equations do contain curvature terms but it is for simplicity that they are ignored. However, very near the leading edge both the body and streamline curvature have a dominant role and they ought to be in the governing equations. To make a convincing case for the importance of streamline and body curvature, we present two cases in the next two figures.

$$M = 0.83, \quad \Lambda = 16.1^{\circ}, \quad C_L = 0.379, \quad RE_C = 23.3 \times 10^6$$
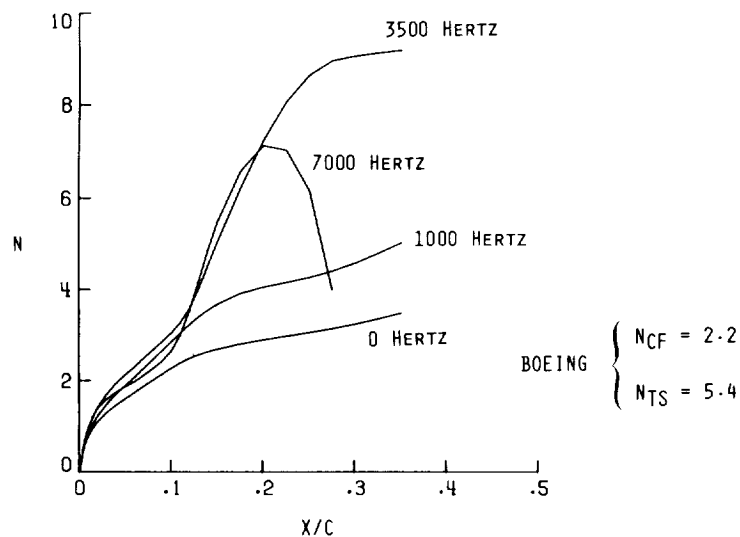
The first of these cases is the classical problem of a disk rotating in an otherwise quiescent ambient. The mean flow that develops on the disk has an exact solution to the Navier-Stokes equations and is also subjected to the crossflow instability and for that reason has long been used as a model problem for the swept leading-edge flow. Cebeci and Stewartson (Ref. 25) using the Orr-Sommerfeld equation as the stability model found that N comes out to be about 20. Their result suggested that perhaps the e^N method, which worked so well for two-dimensional flows, will not work for three-dimensional boundary layers. However, it was shown by Malik, Wilkinson, and Orszag (Ref. 28) that when the full sixth-order stability model is used, including the streamline curvature effects and Coriolis force (an effect present due to rotation), then N drops to about 11 which is in line with the 2-D values. The importance of the full sixth-order system was also demonstrated by the wavepacket computations of Mack (Ref. 29) for the Wilkinson-Malik disk experiment (Ref. 30). There, Mack noted that he could simulate all the fine details of the experiment only when he used the sixth-order system of Malik, Wilkinson, and Orszag.
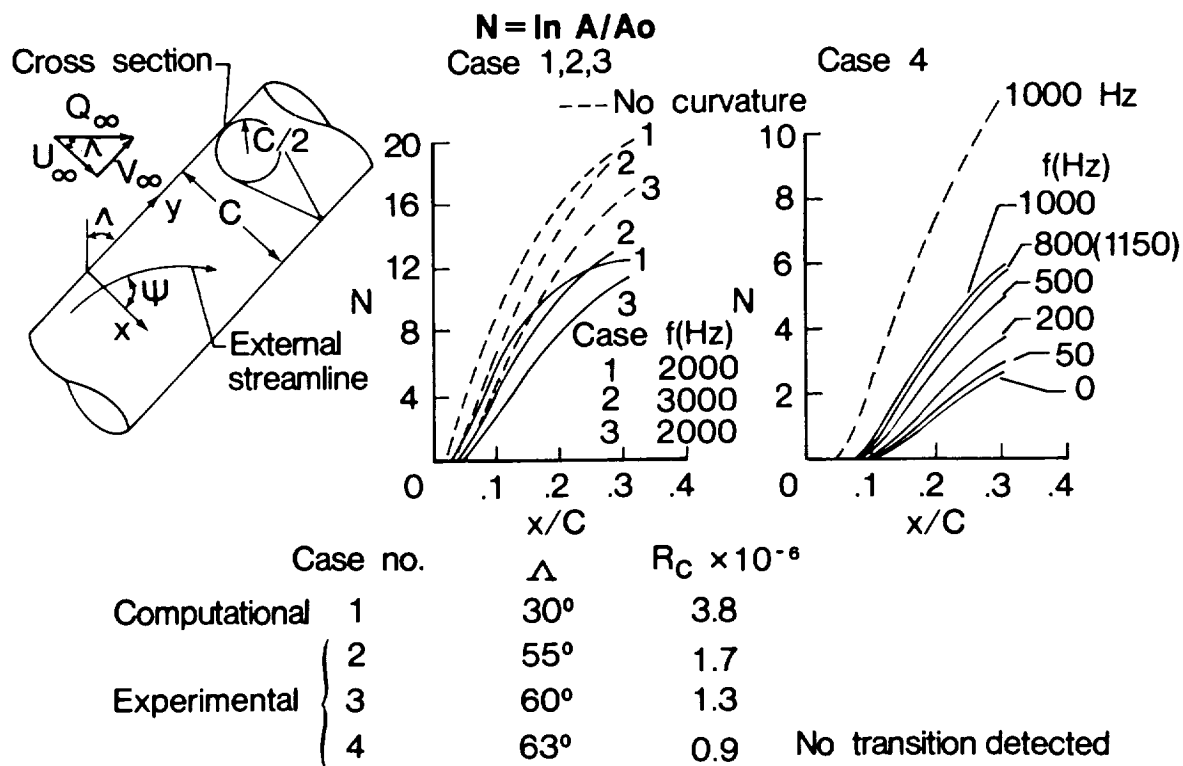
(a) Orr-Sommerfeld equation
(b) Sixth-order equation
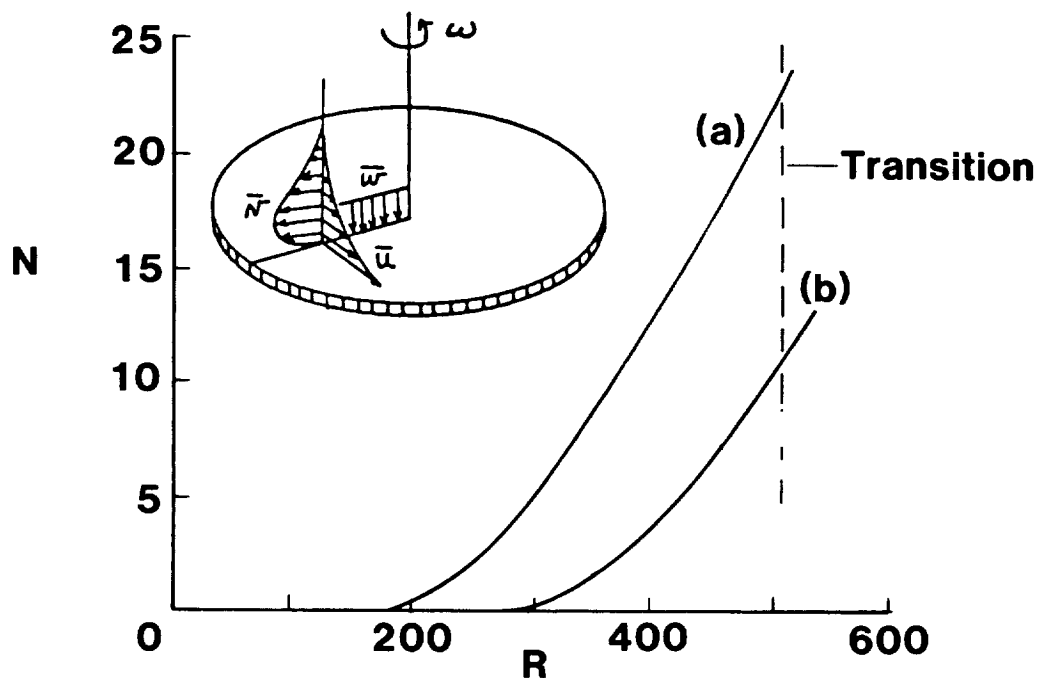
N FACTORS FOR SWEPT CYLINDER

Another case for the inclusion of curvature terms in the stability model may be made by considering the experiment of Poll (Ref. 31) on a swept cylinder which simulates the leading edge of a swept wing. For simplicity, let us concentrate on cases 3 and 4 in the figure. For case 3, when computations of the N factor are carried to the transition location without curvature terms, N factor is about 17. If the curvature terms (both body and streamline) are included, then N drops to around 11. The most amplified waves are not stationary, though the theory does predict the correct wavelength of the stationary disturbances measured from oil-flow photographs.

In case 4, flow was still laminar at the last measured station. Without curvature, an N above 10 is computed. With curvature, an N of 6 is computed indicating no transition. The most amplified wave in this computation was about 1000 Hertz. Poll, with a hot-wire, observed disturbances with a frequency of about 1050 Hertz. The unsteady disturbances have also been observed in the recent experiments of Bippes and Nitschke-Kowsky (Ref. 32.).

Case no.		Λ	$R_C \times 10^{-6}$
Computational	1	30°	3.8
Experimental	2	55°	1.7
	3	60°	1.3
	4	63°	0.9 No transition detected

CALIBRATION OF e^N METHOD FOR TRANSITION PREDICTION/LFC DESIGN

The list of cases where e^N works is quite long. This includes the work of A.M.O. Smith and others. The conclusions from these applications are that when the mean flow is correct and the linear stability equations include dominant physical effects, N is of O(9-11) for a low disturbance environment.

LOW-SPEED

- AXIS. (INCL. HEATING IN WATER, PRESSURE GRADIENT STABILIZATION)
- CONCAVE (GÖRTLER)
- ROTATING DISK
- 2-D WINGS (FLIGHT)
- 3-D (SWEPT WING, FLIGHT & W.T.)
- SWEPT L.E. REGION (CONVEX CURV. SURFACE AND IN-PLANE STREAMLINE CURV.)

HIGH-SPEED

- AXIS. (FLIGHT & W.T.)
- GÖRTLER
- SWEPT LEADING EDGE

CONCLUSIONS FROM THESE APPLICATIONS:

- WHEN LINEAR THEORY HAS CORRECT PHYSICS, THEN N $\sim$ O(9-11) FOR BACKGROUND DISTURBANCES OF O(.05%)

POSSIBLE STREAM/WALL DISTURBANCES CRITICAL TO BOUNDARY-LAYER TRANSITION

However, the list of things that can affect transition is also very long. For that reason, the e^N method is not a general method for transition prediction. However, it is applicable to LFC studies since there a designer will strive hard to minimize all kinds of disturbances in order to obtain long runs of laminar flow.

- ROUGHNESS
  - DISCRETE
  - DISCONTINUOUS
  - TWO-DIMENSIONAL
  - THREE-DIMENSIONAL
  - STEPS
  - GAPS
  - PARTICLE IMPACT/EROSION
  - CORROSION
  - LEAKAGE

- ACOUSTIC ENVIRONMENT
  - ATTACHED FLOW
  - SEPARATED FLOW
  - PROPULSION SYSTEM
  - VORTEX SHEDDING

- PARTICLES
  - ICE CLOUDS
  - RAIN
  - ALGAE
  - SUSPENSIONS
  - FAUNA (INSECTS, FISH, ETC.)

- WALL WAVINESS
  - TWO-DIMENSIONAL
  - THREE-DIMENSIONAL
  - SINGLE WAVE
  - MULTIPLE WAVE
  - DISTORTION UNDER LOAD

- SURFACE AND DUCT VIBRATION

- STREAM FLUCTUATIONS AND VORTICITY
  - PROPELLER WAKES
  - OCEAN SURFACE
  - BODY WAKES (FISH/AIRCRAFT)
  - HIGH SHEAR AREAS (WEATHER FRONTS/ JET STREAM EDGES/OCEAN CURRENTS)

- LFC SYSTEM-GENERATED DISTURBANCES
  - VORTEX SHEDDING (BLOCKED SLOTS, HOLES, PORES)
  - ACOUSTIC OR CHUGGING
  - PORE DISTURBANCES
  - NON-UNIFORMITIES

WAVE INTERACTION IN BOUNDARY LAYERS

The possibility of wave-interactions is a matter of great concern to an LFC designer. While there are many possible regions of interactions, only the cases where crossflow or Görtler is finite-amplitude and T-S is infinitesimally small will be discussed here. Reed (Ref. 33) developed a theory to compute such interactions on X-21 wing and showed that in the presence of finite-amplitude crossflow vortices, T-S waves are excited. The N factor for these T-S waves jumps from about 0.5 to 8.5 due to what is commonly known as ´double exponential growth´ (Ref. 34). However, it was pointed out by Malik (Ref. 35) that the excited waves have unphysically long wavelengths at finite Reynolds numbers. Later, Reed* did not find the explosive growth of T-S waves (observed in Ref. 33) in other swept-wing boundary layers.

An earlier theory by Nayfeh (Ref. 36) on Görtler/T-S interaction had shown a similar type of ´double exponential growth´ of T-S waves in the presence of finite-amplitude Görtler vortices. According to his theory, T-S waves with spanwise wavelength twice that of the Görtler wavelengths are excited. We have performed a computation to test the Görtler/T-S interaction of the type suggested by Nayfeh´s theory. This Navier-Stokes simulation is limited in scope since it uses periodic boundary conditions in the stream-wise direction; this implies a parallel boundary layer, which is a common practice for boundary-layer transition simulations on flat plates (Ref. 6 and Ref. 9). However, if the Görtler/T-S interaction is dominated by non-parallel effects, the computation will fail to capture it. Nayfeh (Ref. 36) mentioned that non-parallelism had little effect on the excited T-S wave.

---

*Reed, H., Arizona State University, private communication, 1986.

- CROSSFLOW/T-S INTERACTION

  - REED'S (1984) THEORY OF DOUBLE EXPONENTIAL GROWTH

  - CONCERN FOR HYBRID LAMINAR-FLOW CONTROL

- GÖRTLER/T-S INTERACTION

  - NAYFEH'S (1981) THEORY OF DOUBLE EXPONENTIAL GROWTH

  - CONCERN FOR LFC DESIGN OF CONCAVE SURFACES (QUIET TUNNEL)

# NAVIER-STOKES SIMULATION OF GÖRTLER/T-S INTERACTION IN A BOUNDARY LAYER

First, computation is made with the Görtler vortex having a 1% initial amplitude which is superposed on the Blasius flow. The Görtler vortex is noted as $(0,2\beta)$ mode in the figure. Also included in the initial conditions are two oblique T-S waves $(\alpha,\pm\beta)$ with amplitude of .1%. The figure presents energy in various modes as a function of time. For simplicity let us concentrate on the primary Görtler $(0,2\beta)$ mode and oblique T-S (α,β) mode. The T-S mode does not show any sign of strong instability. Towards the end of the computation, its growth rate actually drops slightly below the linear theory result. A notable feature in the figure is the strong growth of the first harmonic, i.e., $(0,2\beta)$ mode. This is consistent with the experiment of Aihara and Koyama (Ref. 37).

An error in Nayfeh's paper (Ref. 36) was found by Malik (Ref. 35). When corrected, Nayfeh* finds that the growth rates of the excited T-S waves are small. However, he maintains that strong excitation may take place at some other values of parameters α, β, R and G.

---

*Nayfeh, A. H., Virginia Polytechnic Institute and State University, private communication, 1987.

$$R = 950, \quad G_\theta = 7.5, \quad \alpha = .103, \quad \beta = .15$$

INITIAL AMPLITUDE OF GÖRTLER $(0, 2\beta)$ MODE = 1%
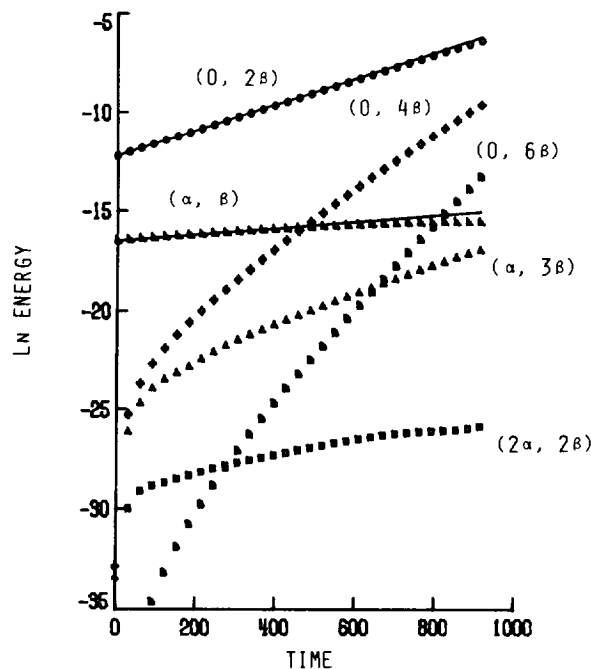
GÖRTLER/T-S INTERACTION WHEN GÖRTLER AMPLITUDE IS LARGE

Another calculation was made with a 2% initial amplitude for the Görtler vortex, and the solution was carried to longer times. The Görtler mode reaches an equilibrium state at which time the (α,β) mode grows fast but then other oblique modes (such as the $(2\alpha,2\beta)$ mode) also show strong instability. It should be pointed out that at this stage the amplitude of the fundamental has reached in excess of 30%. At these amplitudes interactions are not a concern for the LFC designer. However, we have not yet searched for possible interactions when both Görtler and T-S have about the same finite amplitude.

$$R = 950, \qquad G_\theta = 7.5, \qquad \alpha = .103, \qquad \beta = .15,$$

$$\text{INITIAL AMPLITUDE OF GÖRTLER } (0, 2\beta) \text{ MODE} = 2\%$$
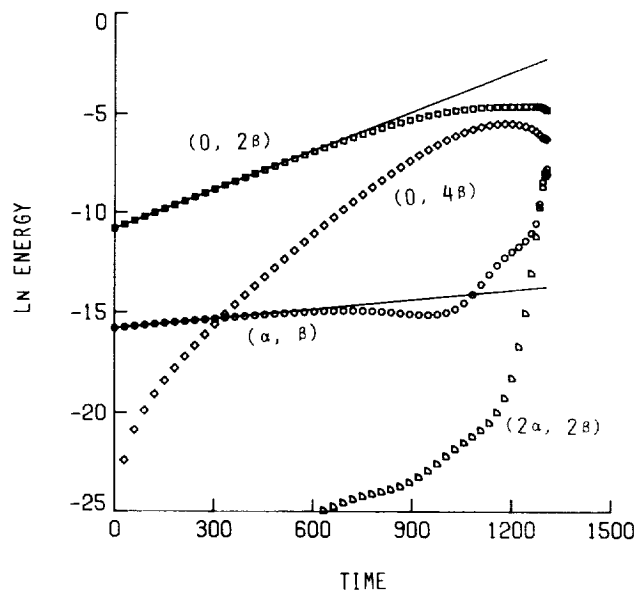
CONCLUSIONS

1. When transition occurs in a low-disturbance environment, the e^N method provides a viable design tool for transition prediction and LFC in both 2-D and 3-D subsonic/supersonic flows. This is true for transition dominated by either T-S, crossflow, or Görtler instability.

2. If Görtler/T-S or crossflow/T-S interaction is present, then the e^N will fail to predict transition. However, there is no evidence of such interaction at low amplitudes of Görtler and crossflow vortices.

REFERENCES

1. Morkovin, M. V.: Critical Evaluation of Transition From Laminar to Turbulent Shear Layers with Emphasis on Hypersonically Traveling Bodies, TR-68-149, March 1969, Air Force Flight Dynamics Laboratory, Wright-Patterson Air Force Base, OH.

2. Goldstein, M. E.: The Generation of Tollmien-Schlichting Waves by Long Wavelength Free-Stream Disturbances, Stability of Time Dependent and Spatially Varying Flows, (D. L. Dwoyer and M. Y. Hussaini, eds.), 1987, Springer-Verlag, New York, pp. 58-81.

3. Gapanov, S. A.: Excitation by Sound of Tollmien-Schlichting Waves in Supersonic Boundary Layer, Izv. Akad. Nauk SSSR Mekh. Zhidk. Gaza, June 8, 1983, pp. 59-66.

4. Nishioka, M.; and Morkovin, M. V.: Boundary Layer Receptivity to Unsteady Pressure Gradients: Experiments and Overview, J. Fluid Mech., Vol. 171, 1986, pp. 219-261.

5. Fedorov, A. V.: Excitation of Tollmien-Schlichting Waves by Acoustic Disturbances in a Compressible Boundary Layer, Laminar-Turbulent Transition, (V. V. Kozlov, ed.), IUTAM Symposium Novosibirsh 1984, Springer-Verlag, 1985, pp. 249-254.

6. Wray, A.; and Hussaini, M. Y.: Numerical Experiments in Boundary-Layer Stability, Proc. Roy. Soc. London, Series A, Vol. 392, April 1984, pp. 373-389.

7. Herbert, T.: Analysis of the Subharmonic Route to Transition in Boundary Layers, AIAA Paper No. 84-0009, 1984.

8. Singer, B. A.; Reed, H. L.; and Ferziger, J. H.: Effect of Streamwise Vortices on Transition in Plane-Channel Flows, AIAA Paper No. 87-0048, 1987.

9. Spalart, P. R.: Numerical Simulation of Boundary-Layer Transition, 9th International Conference on Numerical Methods in Fluid Dynamics, Proceedings, Paris, June 1984, pp.

10. Malik, M. R.: Numerical Simulation of Transition in a Three-Dimensional Boundary Layer, 10th International Conference on Numerical Methods in Fluid Dynamics, Proceedings, Beijing 1986 (F. G. Zhuang and Y. L. Zhu, eds.), Springer-Verlag, 1986, pp. 455-461.

11. Hall, P; and Malik, M. R.: On the Instability of a Three-Dimensional Attachment-Line Boundary Layer: Weakly Nonlinear Theory and a Numerical Approach, J. Fluid Mech., Vol. 163, 1986, pp. 257-282.

12. Kleiser, L.; and Laurien, E.: Numerical Investigation of Interactive Transition Control, AIAA Paper No. 85-0566, 1985.

13. Smith, A. M. O.: The Boundary Layer and I, <u>AIAA J.</u>, Vol. 19, 1981, pp. 1377-1385.

14. Smith, A. M. O.: On the Growth of Taylor-Görtler Vortices on Highly Concave Walls, <u>Quart. Appl. Math.</u>, Vol. 13, 1976, pp. 1039-1055.

15. Smith, A. M. O.; and Gamberoni, N.: Transition, Pressure Gradient and Stability Theory, Report No. ES-26388, Douglas Aircraft Company, El Segundo, CA, 1956.

16. Van Ingen, J. L.: A Suggested Semi-Empirical Method for the Calculation of the Boundary Layer Transition Region, University of Technology, Department of Aerospace Engineering, Report VTH-74, Delft, Holland, 1956.

17. Malik, M. R.: Prediction and Control of Transition in Hypersonic Boundary Layers, AIAA Paper No. 87-1414, 1987.

18. Nayfeh, A. H.; Saric, W. S.; and Mook, D. T.: Stability of Non-Parallel Flows, <u>Arch. Mech.</u>, 1974, pp. 401-406.

19. Obara, C. J.; and Holmes, B. J.: Flight-Measured Laminar Boundary-Layer Transition Phenomena Including Stability Theory Analysis, NASA TP-2417, April 1985.

20. Hall, P.: The Linear Development of Görtler Vortices in Growing Boundary Layers, <u>J. Fluid Mech.</u>, Vol. 130, 1983, pp. 41-58.

21. Chen, F. J.; Malik, M. R.; and Beckwith, I. E.: Instabilities and Transition in the Wall Boundary Layers of Low-Disturbance Supersonic Nozzles, AIAA Paper No. 85-1573, 1985.

22. Hall, P.; and Malik, M. R.: The Growth of Görtler Vortices in Compressible Boundary Layers, ICASE Report No. 87-46, July 1987.

23. Kaups, K.; and Cebeci, T.: Compressible Laminar Boundary Layers with Suction on Swept and Tapered Wings, <u>J. Aircraft</u>, Vol. 14, 1977, pp. 661-667.

24. Nayfeh, A. H.: Stability of Three-Dimensional Boundary Layers, <u>AIAA J.</u>, Vol. 18, April 1980, pp. 406-416.

25. Cebeci, T.; and Stewartson, K.: On Stability and Transition of Three-Dimensional Flows, <u>AIAA J.</u>, Vol. 18, April 1980, pp. 398-405.

26. Srokowski, A. J.: and Orszag, S. A.: Mass Flow Requirements for LFC Wing Design, AIAA Paper No. 77-1222, 1977.

27. Malik, M. R.: COSAL — A Black-Box Compressible Stability Analysis Code for Transition Prediction in Three-Dimensinal Boundary Layers, NASA CR-165925, May 1982.

28. Malik, M. R.; Wilkinson, S. P.; and Orszag, S. A.: Instability and Transition in Rotating Disk Flow, AIAA J., Vol. 19, 1981, pp. 1131-1138.

29. Mack, L. M.: The Stationary Wave Pattern Produced by Point Source on a Rotating Disk, AIAA Paper No. 85-0490, 1985.

30. Wilkinson, S. P.; and Malik, M. R.: Stability Experiments in the Flow over a Rotating Disk, AIAA J., Vol. 23, 1985, pp. 588-595.

31. Poll, D. I. A.: Some Observations of the Transition Process on the Windward Face of a Long Yawed Cylinder, J. Fluid Mech., Vol. 150, January 1985, pp. 329-356.

32. Bippes, H.; Nitschke-Kowsky, P.: Experimental Study of Instability Modes in a Three-Dimensional Boundary Layer, AIAA Paper No. 87-1336, June 1987.

33. Reed, H.: Wave-Interactions in Swept Wing Flows, AIAA Paper No. 84-1678, 1984.

34. Herbert T.; and Morkovin, M. V.: Dialogue on Bridging Some Gaps in Stability and Transition Research, Laminar-Turbulent Transition (R. Eppler and H. Fasel, eds.), Springer-Verlag, 1980, pp. 47-72.

35. Malik, M. R.: Wave-Interactions in Three-Dimensional Boundary Layers, AIAA Paper No. 86-1129, 1986.

36. Nayfeh, A. H.: Effect of Streamwise Vortices on Tollmien-Schlichting Waves, J. Fluid Mech., Vol. 107, 1981, pp. 441-453.

37. Aihara, Y.; and Koyama, H.: Secondary Instability of Görtler Vortices: Formation of Periodic Three-dimensional Coherent Structures, Trans. Japan Soc. Aero. Space Sci., Vol. 24, 1981, pp.78-94.

NONPARALLEL STABILITY OF BOUNDARY LAYERS

Ali H. Nayfeh
Department of Engineering Science and Mechanics
Virginia Polytechnic Institute and State University
Blacksburg, Virginia

Nonparallel Stability of Boundary Layers

The asymptotic formulations of the nonparallel linear stability of incompressible growing boundary layers are critically reviewed. These formulations can be divided into two approaches. The first approach combines a numerical method with either the method of multiple scales, or the method of averaging, or the Wentzel-Kramers-Brillouin (WKB) approximation; all these methods yield the same result. The second approach combines a multi-structure theory with the method of multiple scales. Proponents of the second approach have claimed that their approach is rational and the first approach is not rational. The first approach yields results that are in excellent agreement with all available experimental data, including the growth rates as well as the neutral stability curve. On the other hand, the second approach cannot even yield the neutral curve for the Blasius flow.

Introduction

This paper addresses the linear stability of incompressible growing boundary layers. For two-dimensional mean flows, the streamwise velocity component $U(x,y)$ is a function of the transverse coordinate y as well as the streamwise coordinate x. However, the rate of variation of U with respect to x (i.e., $\partial U/\partial x$) is small compared with the rate of variation of U with respect to y (i.e., $\partial U/\partial y$). Moreover, the transverse velocity component $V(x,y)$ is small compared with U and is a function of y as well as x. For three-dimensional flows, the velocity components $U(x,y,z)$ and $W(x,y,z)$ in the plane of the body are much larger than the transverse velocity component $V(x,y,z)$. Moreover, $\partial U/\partial x$, $\partial U/\partial z$, $\partial W/\partial x$, and $\partial W/\partial z$ are small compared with $\partial U/\partial y$ and $\partial W/\partial y$.

To determine the linear stability of a three-dimensional mean flow, we superimpose on it a small disturbance $u(x,y,z,t)$ $v(x,y,z,t)$, $w(x,y,z,t)$, and $p(x,y,z,t)$. Substituting the total flow into the Navier-Stokes equations, subtracting the mean-flow quantities, and linearizing the resulting equations, we obtain

$$\frac{\partial u}{\partial x} + \frac{\partial v}{\partial y} + \frac{\partial w}{\partial z} = 0 \tag{1}$$

$$\frac{\partial u}{\partial t} + U \frac{\partial u}{\partial x} + W \frac{\partial u}{\partial z} + v \frac{\partial U}{\partial y} + \frac{\partial p}{\partial x} - \frac{1}{R} \nabla^2 u$$
$$+ \left[u \frac{\partial U}{\partial x} + V \frac{\partial u}{\partial y} + w \frac{\partial W}{\partial z} \right] = 0 \tag{2}$$

$$\frac{\partial v}{\partial t} + U \frac{\partial v}{\partial x} + W \frac{\partial v}{\partial z} + \frac{\partial p}{\partial y} - \frac{1}{R} \nabla^2 v$$
$$+ \left[u \frac{\partial V}{\partial x} + v \frac{\partial V}{\partial y} + V \frac{\partial v}{\partial y} + w \frac{\partial V}{\partial z} \right] = 0 \tag{3}$$

246

$$\frac{\partial w}{\partial t} + U \frac{\partial w}{\partial x} + W \frac{\partial w}{\partial z} + v \frac{\partial W}{\partial y} + \frac{\partial p}{\partial z} - \frac{1}{R} \nabla^2 w$$

$$+ \left[u \frac{\partial W}{\partial x} + V \frac{\partial w}{\partial y} + w \frac{\partial W}{\partial z} \right] = 0 \tag{4}$$

where velocities, lengths, and time were made dimensionless using the free-stream velocity U_∞, a characteristic length δ, and a characteristic time δ/U_∞. Here, $R = U_\infty \delta/\nu$ is the Reynolds number. The boundary conditions are

$$u = v = w = 0 \quad \text{at} \quad y = 0 \tag{5}$$

$$u, v, w, p \to 0 \quad \text{as} \quad y \to \infty \tag{6}$$

The terms in the square brackets in Eqs. (2)-(4) are due to the growth of the boundary layer (nonparallel terms).

Parallel Problem

Considering the parallel problem, one neglects the terms in square brackets in Eqs. (2)-(4) and considers U and W to be functions of y only. Then, one seeks a normal mode solution of the form

$$u = \zeta_1(y)E, \quad v = \zeta_3(y)E, \quad w = \zeta_5(y)E, \quad p = \zeta_4(y)E \tag{7}$$

where

$$E = \exp\left[i(\alpha x + \beta z - \omega t) \right] \tag{8}$$

Substituting Eqs. (7) and (8) into Eqs. (1)-(6) and neglecting the terms in square brackets yields

$$i\alpha\zeta_1 + D\zeta_3 + i\beta\zeta_5 = 0 \tag{9}$$

$$i(\alpha U + \beta W - \omega)\zeta_1 + \zeta_3 DU + i\alpha\zeta_4 - \frac{1}{R}(D^2 - \alpha^2 - \beta^2)\zeta_1 = 0 \tag{10}$$

$$i(\alpha U + \beta W - \omega)\zeta_3 + D\zeta_4 - \frac{1}{R}(D^2 - \alpha^2 - \beta^2)\zeta_3 = 0 \tag{11}$$

$$i(\alpha U + \beta W - \omega)\zeta_5 + \zeta_3 DW + i\beta\zeta_4 - \frac{1}{R}(D^2 - \alpha^2 - \beta^2)\zeta_5 = 0 \tag{12}$$

$$\zeta_1 = \zeta_3 = \zeta_5 = 0 \quad \text{at} \quad y = 0 \tag{13}$$

$$\zeta_n \to 0 \quad \text{as} \quad y \to \infty \tag{14}$$

where $D = \partial/\partial y$. For a given U(y) and W(y), Eqs. (9)-(14) constitute an eigenvalue problem, which yields a dispersion relation of the form

$$\omega = \omega(\alpha,\beta,R) \tag{15}$$

A number of techniques have been developed for solving this eigenvalue problem. These include shooting techniques, finite-difference methods, Galerkin methods, and collocation techniques using Chebyshev or Jacobi polynomials.

For the case of a two-dimensional mean flow and a two-dimensional disturbance, $W = 0$, $\zeta_5 = 0$ and $\beta = 0$, and Eqs. (9)-(14) reduce to

$$i\alpha\zeta_1 + D\zeta_3 = 0 \tag{16}$$

$$i(\alpha U - \omega)\zeta_1 + \zeta_3 DU + i\alpha\zeta_4 - \frac{1}{R}(D^2 - \alpha^2)\zeta_1 = 0 \tag{17}$$

$$i(\alpha U - \omega)\zeta_3 + D\zeta_4 - \frac{1}{R}(D^2 - \alpha^2)\zeta_3 = 0 \tag{18}$$

$$\zeta_1 = \zeta_3 = 0 \quad \text{at} \quad y = 0 \tag{19}$$

$$\zeta_n \to 0 \quad \text{as} \quad y \to \infty \tag{20}$$

Equations (16)-(20) can be combined to yield the Orr-Sommerfeld equation

$$(i\alpha R)^{-1}(D^2 - \alpha^2)^2\zeta_3 = (U - c)(D^2 - \alpha^2)\zeta_3 - \zeta_3 D^2 U$$

$$\tag{21}$$

subject to the boundary conditions

$$\zeta_3 = D\zeta_3 = 0 \quad \text{at} \quad y = 0 \tag{22}$$

$$\zeta_3, D\zeta_3 \to 0 \quad \text{as} \quad y \to \infty \tag{23}$$

where $c = \omega/\alpha$. The neutral stability curve calculated using either Eqs. (16)-(20) or Eqs. (21)-(23) are in good agreement with available experimental data as shown in Figure 1.

Recently, Smith[1] claimed the above methods to be "irrational" and developed multi-structured theories for treating this problem. He used a result from an "irrational theory" for the Blasius flow to observe that "the typical wavelength of the neutrally stable modes on the lower branch increases proportionally to $Re^{1/8}$ as $Re \to \infty$" and concluded that disturbances at the lower branch vary on a streamwise length $O(Re^{-3/8})$ and a time scale $O(Re^{-1/4})$ and hence they are governed by a triple-deck structure. Consequently, he let

$$x = 1 + \varepsilon^3 X, \quad t = \varepsilon^2 T \tag{24}$$

and

$$u,v,p \propto E = \exp[i\theta(x) - i\Omega T] \tag{25}$$

where $\varepsilon = Re^{-1/8}$ and

$$\Omega = \omega_1 + \varepsilon\omega_2 + \varepsilon^2\omega_3 + \varepsilon^3 \ln\varepsilon \; \omega_{4L} + \dots \tag{26}$$

$$\frac{d\theta}{dX} = \alpha_1 + \varepsilon\alpha_2 + \varepsilon^2\alpha_3 + \varepsilon^3 \ln\varepsilon \; \alpha_{4L} + \dots \tag{27}$$

Then, he expanded the variables in the three decks as follows:

Main Deck

$$u = \left[u_1 + \varepsilon u_2 + \varepsilon^2 u_3 + \varepsilon^3 \ln\varepsilon \; u_{4L} + \dots\right]E \tag{28}$$

$$v = \left[\varepsilon v_1 + \varepsilon^2 v_2 + \varepsilon^3 v_3 + \varepsilon^4 \ln\varepsilon \; v_{4L} + \dots\right]E \tag{29}$$

$$p = \left[\varepsilon p_1 + \varepsilon^2 p_2 + \varepsilon^3 p_3 + \varepsilon^4 \ln\varepsilon \; p_{4L} + \dots\right]E \tag{30}$$

where

$$y = \varepsilon^4 Y, \quad Y = O(1)$$

Lower Deck

$$u = \left[U_1 + \varepsilon U_2 + \varepsilon^2 U_3 + \varepsilon^3 \ln\varepsilon \; U_{4L} + \dots\right]E \tag{31}$$

$$v = \left[\varepsilon^2 V_1 + \varepsilon^3 V_2 + \varepsilon^4 V_3 + \varepsilon^5 \ln\varepsilon \; V_{4L} + \dots\right]E \tag{32}$$

$$p = \left[\varepsilon P_1 + \varepsilon^2 P_2 + \varepsilon^3 P_3 + \varepsilon^4 \ln\varepsilon \; P_{4L} + \dots\right]E \tag{33}$$

where

$$y = \varepsilon^5 Z, \quad Z = O(1)$$

Upper Deck

$$u = \left[\varepsilon \bar{u}_1 + \varepsilon^2 \bar{u}_2 + \varepsilon^3 \bar{u}_3 + \varepsilon^4 \ln\varepsilon \; \bar{u}_{4L} + \dots\right]E \tag{34}$$

$$v = \left[\varepsilon \bar{v}_1 + \varepsilon^2 \bar{v}_2 + \varepsilon^3 \bar{v}_3 + \varepsilon^4 \ln\varepsilon \; \bar{v}_{4L} + \dots\right]E \tag{35}$$

$$p = \left[\varepsilon \bar{p}_1 + \varepsilon^2 \bar{p}_2 + \varepsilon^3 \bar{p}_3 + \varepsilon^4 \ln\varepsilon \; \bar{p}_{4L} + \dots\right]E \tag{36}$$

where

$$y = \varepsilon^3 \bar{y}, \quad \bar{y} = O(1)$$

To account for the nonparallel effects, Smith had to include the next term in each of the expansions in Eqs. (26)-(36).

Substituting the above expansions into the parallel part of the disturbance equations (1)-(4) and boundary conditions (5) and (6), dropping the terms in square brackets, putting W = 0, separating coefficients of like powers of ε, and solving the resulting 36 equations, one obtains expressions for u, v, and p in the different decks. Matching the resulting expressions provides asymptotic expansions for u, v, and p. For the neutral stability curve, Smith obtained

$$F_n = \omega_n = 0.995 \; R_\delta^{-3/2} \left[1 + 1.597 \; R_\delta^{-\frac{1}{4}} + 10.02 \; R_\delta^{-\frac{1}{2}} \right.$$

$$\left. + 0.988 \; R_\delta^{-3/4} \ln R_\delta + \ldots \right]$$

where

$$R_\delta = 1.7208\sqrt{xRe}$$

This expression is in fair agreement with the lower branch of the neutral stability curve for large Re. However, its accuracy deteriorates as Re decreases. In fact, it does not predict a minimum critical Reynolds number.

Bodonyi and Smith[2] inspected the results of the "irrational theory" to observe that "the stability properties of the Blasius boundary layer are governed by the behavior on the streamwise length scale $O(Re^{-9/20})$ as far as the upper branch of the neutral curve is concerned". Consequently, they used $\sigma = Re^{-1/20}$ as their perturbation parameter and used the streamwise scale X defined by $x = 1 + \sigma^9 X$ and the time scale $t = \sigma^8 T$. This choice leads to a five-zoned structure. To account for the nonparallel effects, one needs to carry out the expansion to $O(\sigma^9)$. In view of the logarithmic terms, one needs 13 terms in the expansion. With three variables and five decks, one needs to derive and solve 195 equations and then match the results. Bodonyi and Smith gave up after four terms. Their calculated neutral stability curve, which is intended to approximate the upper branch, is below the lower branch!! We note that for an Re = 10^6, $\sigma \approx 0.5$, which is not small.

For the case of an accelerating boundary layer, Smith and Bodonyi[3] assumed a streamwise variation $O(Re^{-5/12})$ and a time scale $O(Re^{-1/3})$ near the upper branch of the neutral stability curve. Using this streamwise variation leads to a five-zoned structure, with the nonparallel effects appearing at $O(Re^{-5/12})$.

It should be noted that the parallel flow assumption breaks down miserably for the case of Gortler instability. Floryan and Saric[4] and Ragab and Nayfeh[5] derived the appropriate equations for Gortler instability for the cases of zero and nonzero pressure gradients, respectively. Hall[6] questioned the solution of the resulting equations

using a normal-mode approach and suggested solving them as an initial-value problem.

Nonparallel Problem

A better agreement between the theoretical and experimental results can be obtained by accounting for the influence of the nonparallel terms[7-10]. To this end, we can use either the method of averaging or the WKB approximation or the method of multiple scales[11,12]. In this paper, we use the method of averaging and let

$$u = A(x,z,t)\zeta_1(y,x)e^{i\theta}, \quad v = A(x,z,t)\zeta_3(y,x)e^{i\theta} \tag{37}$$

$$p = A(x,z,t)\zeta_4(y,x)e^{i\theta}, \quad w = A(x,z,t)\zeta_5(y,x)e^{i\theta} \tag{38}$$

where A is a slowly varying function of x and t,

$$\frac{\partial\theta}{\partial x} = \alpha(x), \quad \frac{\partial\theta}{\partial z} = \beta, \quad \frac{\partial\theta}{\partial t} = -\omega \tag{39}$$

and the ζ_n are given by Eqs. (9)–(14). After a straightforward but lengthy algebra, one obtains[13-17]

$$h_1 \frac{\partial A}{\partial t} + h_2 \frac{\partial A}{\partial x} + h_3 \frac{\partial A}{\partial z} = h_4 A \tag{40}$$

where

$$h_1 = \int_0^\infty (\zeta_1\zeta_1^* + \zeta_3\zeta_3^* + \zeta_5\zeta_5^*)dy \tag{41}$$

$$h_2 = \int_0^\infty [\zeta_1\zeta_4^* + \zeta_4\zeta_1^* + U(\zeta_1\zeta_1^* + \zeta_3\zeta_3^* + \zeta_5\zeta_5^*)]dy \tag{42}$$

$$h_3 = \int_0^\infty [\zeta_5\zeta_4^* + \zeta_4\zeta_5^* + W(\zeta_1\zeta_1^* + \zeta_3\zeta_3^* + \zeta_5\zeta_5^*)]dy \tag{43}$$

$$h_4 = -\int_0^\infty [\frac{\partial\zeta_1}{\partial x}\zeta_4^* + \frac{\partial\zeta_5}{\partial z}\zeta_4^* + \frac{\partial\zeta_4}{\partial x}\zeta_1^* + \frac{\partial\zeta_4}{\partial z}\zeta_5^* + U(\frac{\partial\zeta_1}{\partial x}\zeta_1^*$$

$$+ \frac{\partial\zeta_3}{\partial x}\zeta_3^* + \frac{\partial\zeta_5}{\partial x}\zeta_5^*) + W(\frac{\partial\zeta_1}{\partial z}\zeta_1^* + \frac{\partial\zeta_3}{\partial z}\zeta_3^* + \frac{\partial\zeta_5}{\partial z}\zeta_5^*)$$

$$+ (\zeta_1\frac{\partial U}{\partial x} + VD\zeta_1 + \zeta_5\frac{\partial W}{\partial z})\zeta_1^* + (VD\zeta_3 + \zeta_3 DV + \zeta_3\frac{\partial V}{\partial x}$$

$$+ \zeta_5\frac{\partial V}{\partial z})\zeta_3^* + (\zeta_1\frac{\partial W}{\partial x} + VD\zeta_5 + \zeta_5\frac{\partial W}{\partial z})\zeta_5^*]dy \tag{44}$$

where the ζ_n^* are solutions of the adjoint homogeneous problem. Equation (40) can be rewritten as[13]

$$\frac{\partial A}{\partial t} + \omega_\alpha \frac{\partial A}{\partial x} + \omega_\beta \frac{\partial A}{\partial z} = hA \tag{45}$$

where

$$\omega_\alpha = \frac{h_2}{h_1} \ , \ \omega_\beta = \frac{h_3}{h_1} \ , \ h = \frac{h_4}{h_1}$$

Here, ω_α and ω_β are the components of the group velocity in the streamwise direction.

Equation (45) describes the propagation of a wavepacket centered at the frequency ω_r and the wavenumbers α_r and β_r, where the subscript r stands for the real part. Nayfeh[14] showed that for a physical problem, ω_α and ω_β in Eq. (45) must be real.

For a monochromatic wave, $\partial A/\partial t = 0$ and Eq. (45) reduces to

$$\omega_\alpha \frac{\partial A}{\partial x} + \omega_\beta \frac{\partial A}{\partial z} = hA \tag{46}$$

For a physical problem, Nayfeh[14] showed that $\omega_\beta/\omega_\alpha$ must be real. For the case of a parallel mean flow, this condition reduces to $d\alpha/d\beta$ being real, which was obtained by Nayfeh[14] and Cebici and Stewartson[18] using the saddle-point method.

Two-Dimensional Mean Flows

For the case of a monochromatic wave, $\partial A/\partial t = 0$ and Eq. (40) yields

$$A = A_0 \exp\left[\int_{x_0} (h_4/h_2) dx \right] \tag{47}$$

where A_0 is a constant. Hence,

$$u \approx A_0 \zeta_1(y,x) \exp\left[i(\int \alpha dx - \omega t) + \int \left(\frac{h_4}{h_2}\right) dx \right] \tag{48}$$

Consequently, the growth rate

$$\sigma = \text{Real} \left[\frac{\partial}{\partial x} (\ln u) \right]$$

is given by

$$\sigma = -\alpha_i + \text{Real} \left(\frac{h_4}{h_2}\right) + \text{Real} \left[\frac{\partial}{\partial x} (\ln \zeta_1) \right] \tag{49}$$

The first term is the quasiparallel contribution, whereas the last two terms are due to nonparallelism. It should be noted that the last term produces a variaton in the growth rate across the boundary layer.

Since ζ_1 is a function of y and, in general, distorts with streamwise distance, one may term stable disturbances unstable or vice versa. Morever, a different growth rate would be obtained if one replaces u with another variable. For example, using v or p or w, one obtains the growth rates

$$\sigma = -\alpha_i + \text{Real} \left(\frac{h_4}{h_2}\right) + \text{Real} \left[\frac{\partial}{\partial x} (\ln \zeta_m) \right] \tag{50}$$

where m = 3, 4, and 5, respectively. This raises the questions "What is meant by stability of a boundary layer?" If the stability criterion is based on σ, then which σ should be used? If one uses an N factor to compare the stabilizing or destabilizing influences of certain modifications to the boundary layer, then the contribution of the last term will not be significant.

In the case of parallel flows, the last terms in Eqs. (49) and (50) vanish and the growth rate is unique and independent of the variable being used. Consequently, one can speak of neutral disturbances or neutral stability curve given by the locus of $\alpha_i(R,\omega) = 0$. However, in the case of a nonparallel flow, the neutral stability is given by $\sigma(R,\omega) = 0$ and depends on the flow variable used to calculate the growth rate and the distance from the wall. To compare the analytical results with experimental data, one needs to make the calculations in the same manner in which the measurements are taken. Available experimental stability studies almost exclusively use hot-wire aneomometers. Usually, they measure the rms value $|u|$ of the streamwise velocity component u and use it to define the growth rate. Figure 2 compares the neutral stability curves calculated using $|u|$ and $\bar{u}^2 + \bar{v}^2$ with the experimental data of Kachanov, Kozlov and Levchenko[19]*. Since the experiment measured $|u|$, the calculations of Saric and Nayfeh[10], which were based on $|u|$, are in better agreement with the experimental data than the calculations of Bouthier[7], which were based on $\bar{u}^2 + \bar{v}^2$. Moreover, the growth rate is singular at the locations where $|u| = 0$. Figure 2 shows also that the calculated locations of the singular growth rates are in good agreement with the experimental results.

Some of the available experimental studies follow the maxima of $|u|$ whereas others follow a constant boundary-layer similarity variable η. Saric and Nayfeh[9,10] found that the contribution of the last terms in Eqs. (49) and (50) are significant if one follows a constant η whereas their contributions are negligible if one follows the maxima of $|u|$, yielding

$$\sigma = -\alpha_i + \text{Real}\left(\frac{h_4}{h_2}\right) \tag{51}$$

The neutral stability curve calculated by Saric and Nayfeh[9] using Eq. (51), and shown in Figure 1, is in very good agreement with the experimental data that follow the maxima of $|u|$, except near the minimum critical Reynolds number where the data may be suspect. However, in the case of experiments conducted by following trajectories of constant η such as those of Ross et al.[20], the effect of the distortion of the eigenfunction cancels the nonparallel effects, resulting in a better agreement between their data and the results of quasiparallel theory.

Saric and Nayfeh[10] made other comparisons of the growth rates calculated using Eq. (51) with the experimental data of Strazisar, Prahl and Reshotko[21] and Kachanov, Kozlov and Levchenko[19]. Strazisar et al.

---

* Also, private communication, June 1976.

conducted their experiments in a water tunnel and performed their measurements at the maxima of $|u|$, thereby minimizing the effects of the distortion of the eigenfunction. They measured the amplification rate as a function of the frequency at different locations on the plate, corresponding to different Reynolds numbers. Figure 3 shows a good agreement between the theoretical and experimental results. Kachanov et al. also followed the maxima of $|u|$ and measured the amplification factor $a = |u|/|u_0|$, where $|u_0|$ is the rms value of u at the first neutral point. Figure 4 shows a good agreement between the theoretical results calculated by Saric and Nayfeh[16] using Eq. (51) and the experimental results.

The present nonparallel analysis was extended by El-Hady and Nayfeh[22] to the case of two-dimensional compressible boundary layers, by Nayfeh[14] to the case of three-dimensional compressible boundary layers, and by Nayfeh and El-Hady[23] and Asrar and Nayfeh[24] to heated boundary layers.

References

1.   Smith, F. T.: Proceedings of the Royal Society - London, vol. A336, 1979, p. 91.

2.   Bodonyi, R. J.; and Smith, F. T.: Proceedings of the Royal Society - London, vol. A375, 1981, p. 65.

3.   Smith, F. T.; and Bodonyi, R. J.: Journal of Fluid Mechanics, vol. 118, 1982, p. 165.

4.   Floryan, J. M.; and Saric, W. S.: AIAA Journal, vol. 20, 1982, p. 316.

5.   Ragab, R. A.; and Nayfeh, A. H.: Physics of Fluids, vol. 24, 1981, p. 1405.

6.   Hall, P.: Journal of Fluid Mechanics, vol. 124, 1982, p. 475.

7.   Bouthier, M.: Journal de Mecanique, vol. 12, 1973, p. 75.

8.   Gaster, M.: Journal of Fluid Mechanics, vol. 66, 1974, p. 465.

9.   Saric, W. S.; and Nayfeh, A. H.: Physics of Fluids, vol. 18, 1975, p. 945.

10.   Saric, W. S.; and Nayfeh, A. H.: AGARD Conference Proceedings No. 224, May 2-4, 1977, Laminar-Turbulent Transition, Paper 6.

11.   Nayfeh, A. H.: Perturbation Methods, (Wiley-Interscience, New York, 1973).

12.   Nayfeh, A. H.: Introduction to Perturbation Techniques, (Wiley-Interscience, New York, 1981).

13.   Nayfeh, A. H.; and Padhye, A. R.: AIAA Journal, vol. 17, 1979, p. 1084.

14.   Nayfeh, A. H.: AIAA Journal, vol. 18, 1980, p. 406.

15.   Nayfeh, A. H.: International Union of Theoretical and Applied Mechanics Symposium on Laminar-Turbulent Transition, (E. Eppler and H. Fasel, Ed.), Springer-Verlag, Berlin, 1980, p. 201.

16.   Nayfeh, A. H.; and Padyne, A. R.: Physics of Fluids, vol. 23, 1980, p. 241.

17.   Padhye, A. R.; and Nayfeh, A. H.: AIAA Paper 81-1281, presented at the AIAA 14th Fluid and Plasma Dynamics Conference, Palo Alto, CA, June 23-25, 1981.

18.   Cebeci, T.; and Stewartson, K.: AIAA Journal, vol. 18, 1980, p. 398.

19. Kachanov, Yu. S.; Kozlov, V. V.; and Levchenko, V. Ya.: (In Russian), Ucheniye Zapiski TASGI, VI, 1975, p. 137.

20. Ross, J. A.; Barnes, F. H.; Burns, J. G.; and Ross, M. A. S.: Journal of Fluid Mechanics, vol. 43, 1970, p. 819.

21. Strazisar, A. J.; Reshotko, E.; and Prahl, J. M.: Journal of Fluid Mechanics, vol. 83, 1975, p. 225.

22. El-Hady, N. M.; and Nayfeh, A. H.: AIAA Paper No. 80-0277, presented at the AIAA 18th Aerospace Sciences Meeting, Pasadena, CA, January 14-16, 1980.

23. Nayfeh, A. H.; and El-Hady, N. M.: Physics of Fluids, vol. 23, 1980, p. 10.

24. Asrar, W.; and Nayfeh, A. H.: Physics of Fluids, vol. 28, 1985, p. 1263.

25. Schubauer, G. B.; and Skramstad, H. K.: Journal of Research of National Bureau of Standards, vol. 38, 1947, p. 251.

26. Wortmann, F. X: 50 Jahre Grenzschichtforchung, Braunschweig, F. Vieweg & Sohn, 1955, p. 460.
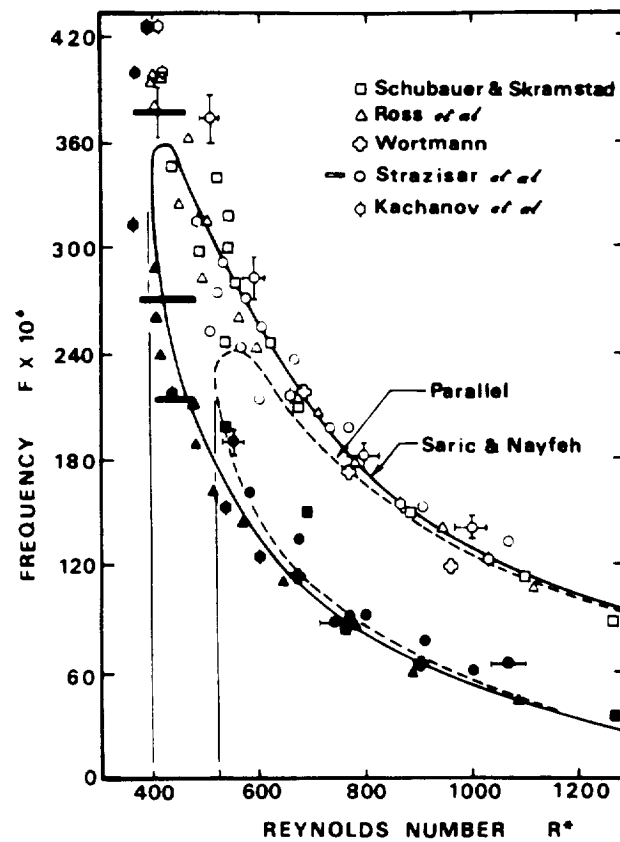
Figure 1. Neutral stability curve for Blasius boundary layer. Solid symbols are Branch I experimental points. Open symbols are Branch II. The critical Reynolds number is 400 for nonparallel calculations, 520 for parallel calculations (Saric and Nayfeh[9]).
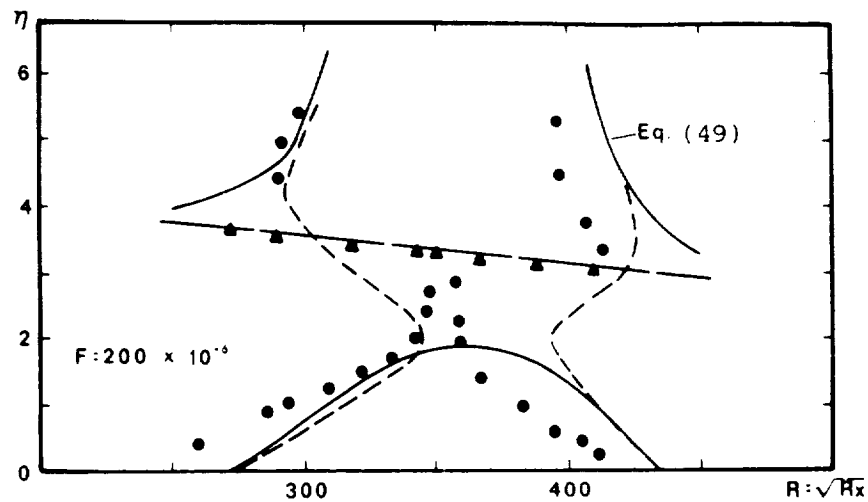
Figure 2. Vertical variation of neutral stability points at F = 200x10^{-6}. Experimental points from Kachanov, Kozlov and Levchenko[17]. Dashed lines are calculations of Bouthier[7] based on energy. Solid lines are calculations of Saric and Nayfeh[10] based on |u|. Streamwise position is the Reynolds number based on δ_r which is the ξ of Refs. 7 and 17. Solid triangles give the locus of |u| = 0 and the broken line is the calculation[10] for |u| = 0.
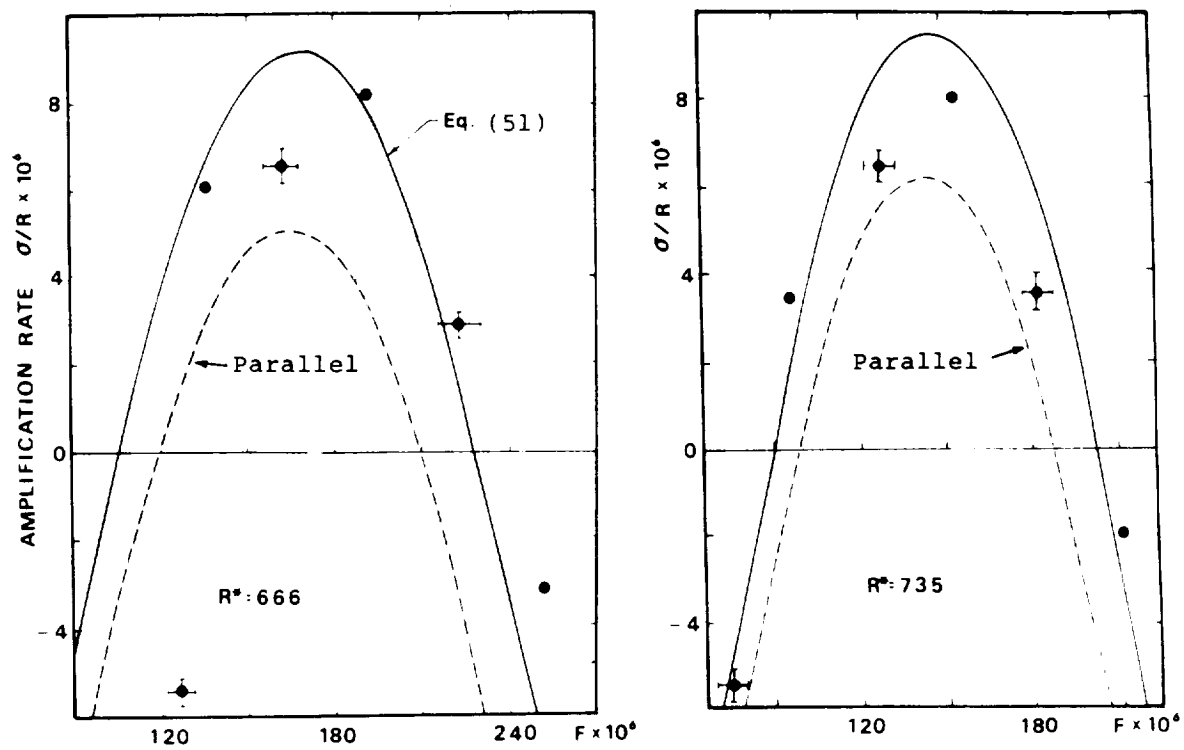
Figure 3. Amplification rate as a function of frequency: Theory of
           Saric and Nayfeh; Experimental data of Strazisar, Prahl
           and Reshotko following maximum of |u|.
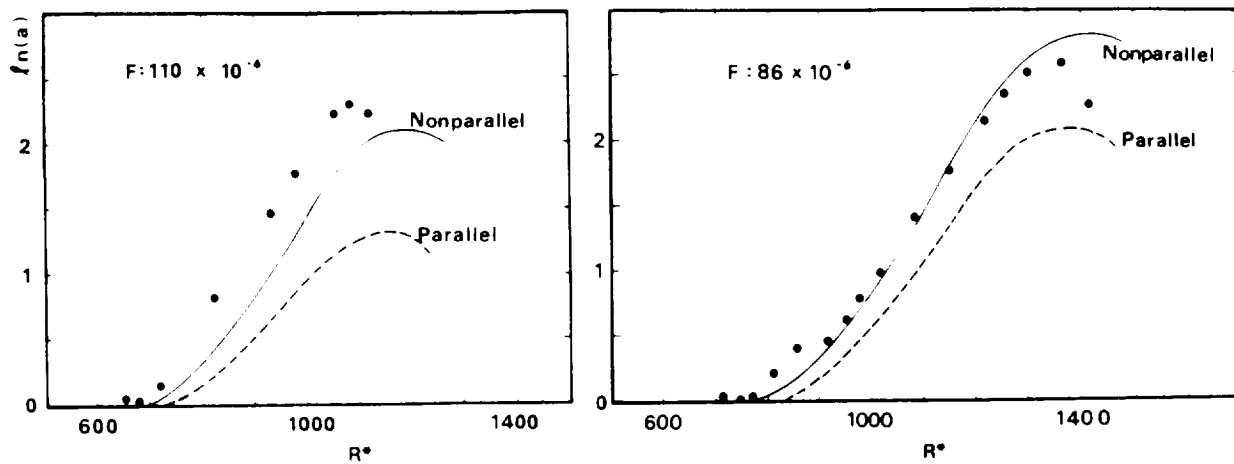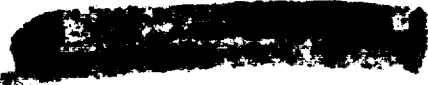
Figure 4. Amplification factor a as a function of streamwise position
           at F = 110x10^{-6} and F = 86 x 10^{-6}. Experimental points from
           Kachanov, Kozlov and Levchenko following maximum of |u| and
           nonparallel results of Saric and Nayfeh based on following
           maximum of |u|.

INTERACTION OF TOLLMIEN-SCHLICHTING WAVES AND GÖRTLER VORTICES

P. Hall
Institute for Computer Applications in Science and Engineering
NASA Langley Research Center
Hampton, Virginia
and Department of Mathematics
Exeter University
Exeter, England

List of Symbols

$\underline{\mu}_B(x,y,z)$ mean velocity

$\delta\underline{\mu}'\exp[i\{\alpha x + \beta y - \Omega t\}]$ perturbation velocity

α complex streamwise wavenumber

β spanwise wavenumber of Görtler perturbation

k spanwise wavenumber of TS wave

Ω temporal frequency

T Taylor number

TS   Tollmien-Schlichting

M^o angle between TS wave propagation and the mean flow direction

262

There are many fluid flows of practical interest where transition can be caused by competing hydrodynamic instabilities. Thus in three-dimensional boundary-layer flows over curved walls, instability might be caused by Tollmien-Schlichting waves, Görtler vortices or crossflow vortices. If a particular type of instability is suppressed by some means, there is the possibility that another one might be stimulated. Hence it is important to understand the mechanisms by which these different instabilities interact. Here we shall discuss some properties of the interaction which can take place between Görtler vortices and Tollmien-Schlichting waves.

INTERACTION OF TOLLMIEN-SCHLICHTING WAVES AND GÖRTLER VORTICES

1. Large amplitude Görtler vortices, small linear Tollmien-Schlichting (TS) waves

2. Weakly nonlinear interaction of small amplitude Görtler vortices and small amplitude Tollmien-Schlichting waves

3. Large amplitude TS waves, 3-D breakdown induced by unsteady Görtler instability

263

We discuss the linear stability of large amplitude Görtler vortices to Tollmien-Schlichting waves. In order to avoid technical difficulties associated with boundary-layer growth, we shall concentrate on fully developed flows in curved channels. However, the corresponding external flow problem can be treated in essentially the same way and gives similar results. Some discussion will also be given about the secondary instability of large amplitude Tollmien-Schlichting waves to Görtler vortices. In this case, instability occurs in the presence of convex or concave curvature.

Secondary instabilities of large Görtler vortices

- Basic state is now a spatially periodic flow in z direction. We calculate this flow by integrating the Navier-Stokes equations numerically

- In external flows basic state is a function of x, y, z

- Now perturb the basic state by writing

$$\underline{u} = \underline{u}_B (x, y, z) + \delta \underline{u}' \exp \left[i \{\alpha x + \beta y - \Omega t\} \right]$$

- Solve the linearized equations at high Reynolds numbers using Triple Deck Theory

- For spatially varying flows write

$$\alpha x = \int^{x} \alpha (x') dx'$$

and calculate α as the disturbance moves downstream

Here we show the dependence of the wave number of neutral TS waves on frequency at different values of the Taylor number T. The results for T = 0 correspond to zero curvature. The wave number at a given frequency increases monotonically with the curvature.
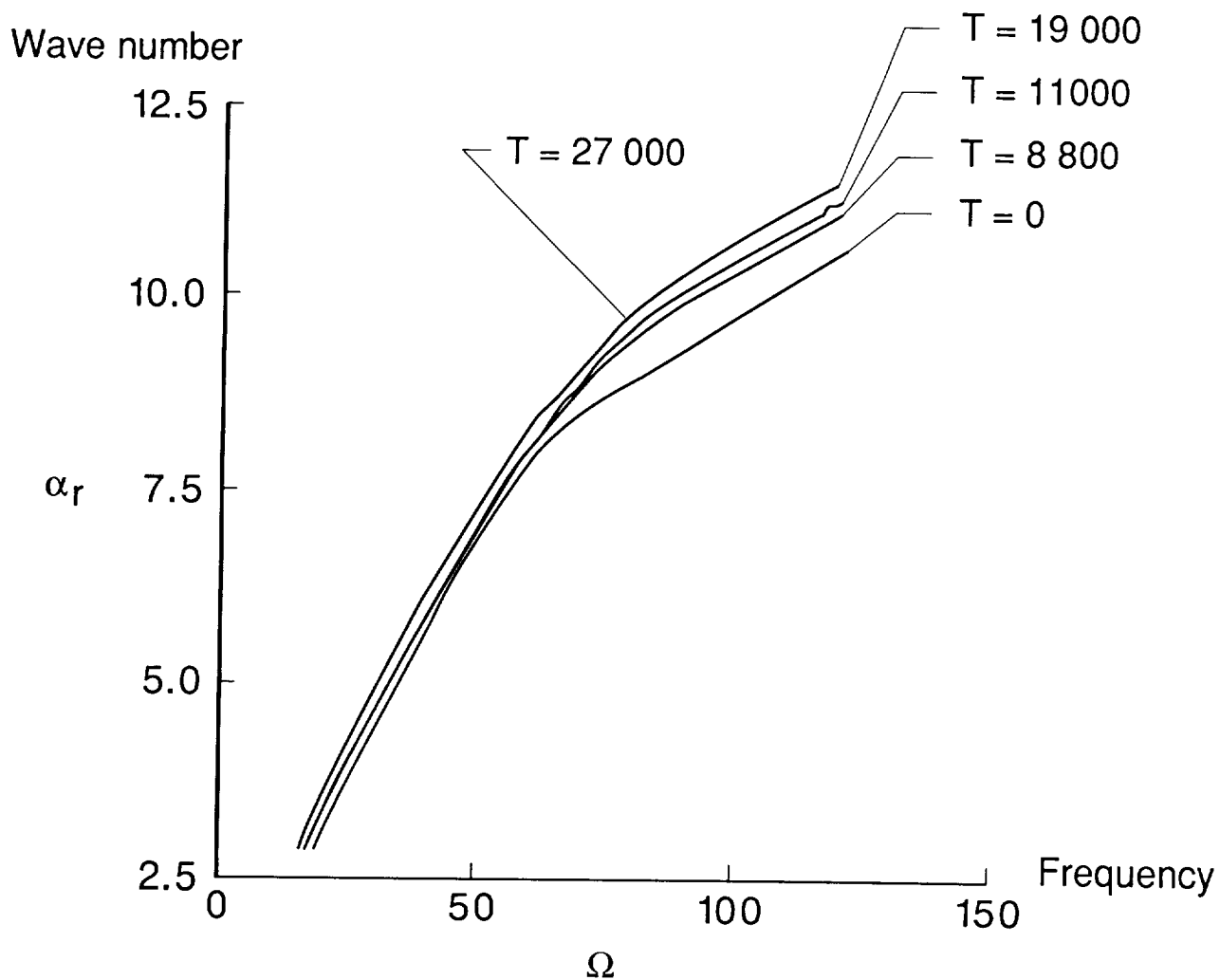
This figure shows the growth rate of unstable TS waves as a function of frequency at different Taylor numbers. Note the significant destabilization effect of the vortices on the growth rate. At the larger values of T the area under the unstable part of the curve is typically increased by 40-50%.

Growth rate

$-\alpha_i$

T = 27 000
T = 19 000
T = 11 000
T = 8800
T = 0

.5

0

Frequency

-.5

0   50   100

Ω
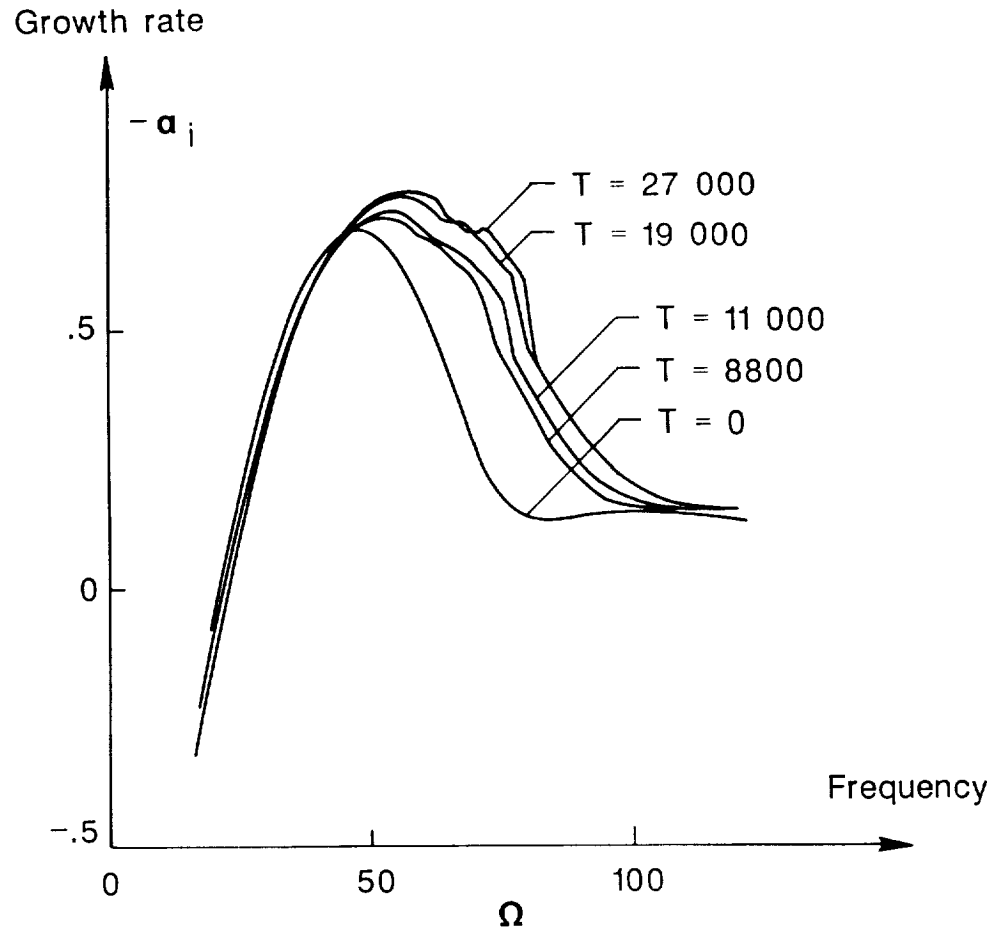
The wave numbers for a 3-D TS wave at T = 0 and T = 11000 are shown below. Note the increase in the wave number produced by the curvature. Calculations at different values of T produce similar results.

Wave number
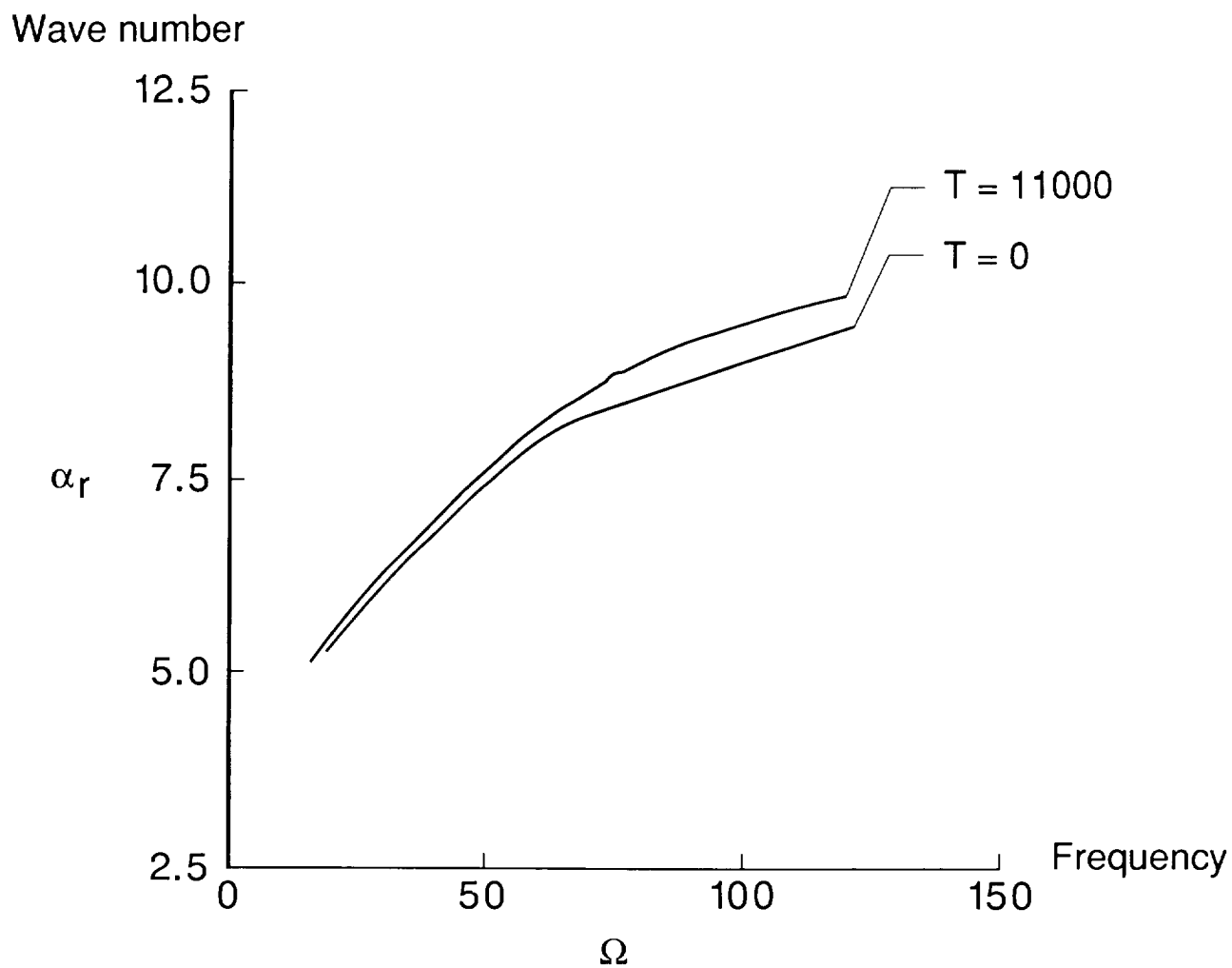
This figure shows the growth rate of a 3-D TS wave at   T = 11000 at
different values of the frequency. The vortex flow again destabilizes the TS
wave and the unstable area under the curve is again increased by 40-50%. This
result is typical of the effect of vortices on 3-D TS waves.
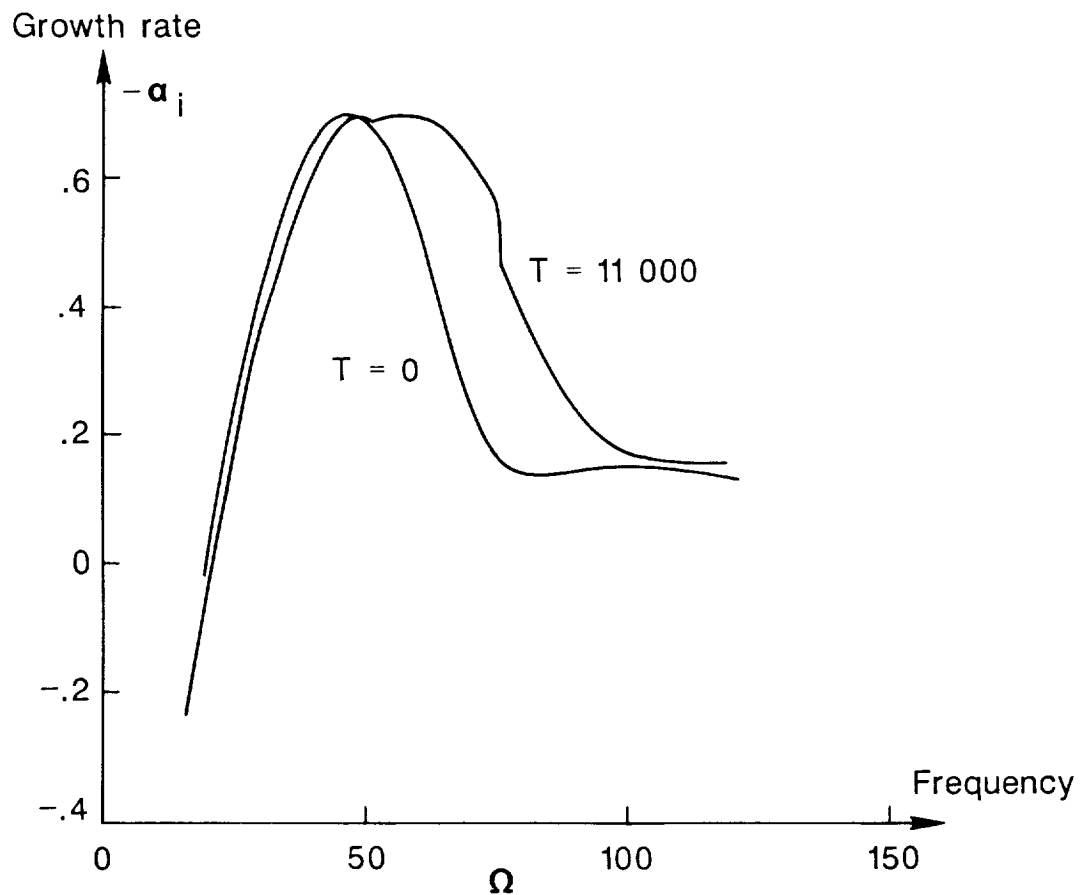
The interaction of a Görtler vortex of spanwise wave number β with a pair of skewed Tollmien-Schlichting waves with wave numbers α and $\pm k$ in the x and z directions was considered. A particularly strong interaction was found to occur when $\beta = k/2$. In fact there is a "resonant triad" interaction between the different modes in this case. The amplitudes a, b, and c of the Tollmien-Schlichting waves over the Görtler vortex were found to satisfy the equations

$$\frac{da}{dt} = e\,a + f_0 b_c,$$

$$\frac{db}{dt} = g_0 b + h_0 a\bar{c},$$

$$\frac{dc}{dt} = g_1 c + h_1 a\bar{b},$$

where e, f, g_0, h_0, g_1, h_1 are constants. These constants were calculated numerically and determine the nature of the solutions to these equations. For the values of these constants appropriate to channel flows, we find that any solution of these equations terminates in a singularity at a finite time. Physically this means that the disturbance amplitude becomes unbounded at that time.

Weakly nonlinear interaction of TS and Görtler
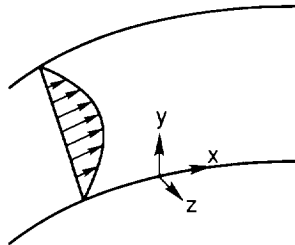
TS waves $\sim e^{i\{\alpha x \pm kz - \Omega t\}}$

Görtler vortices $\sim e^{i\beta z}$

Triad interactions involving 2 TS waves and a Görtler vortex dominate nonlinear growth. TS waves are inclined at an angle M° to flow direction. Interaction governed by triple deck theory

In fact, at this stage a much stronger interaction takes place. The interaction is governed by a coupled partial differential system and an ordinary integro-differential equation. The nature of the solutions to this system again depends on numerical values of the constants appearing in this equation. The resulting behavior is characterized in terms of M, the angle between the direction of propagation of the waves and the flow direction. If M is less than $41.6°$, a much weaker blow-up occurs in an infinite time. Thus, the system stays in the smaller amplitude state for a much longer time if M < 41.6. Indeed the strong interaction for M > $41.6°$ can take place in the absence of curvature. We conclude that in shear flows this is a nonlinear interaction mechanism involving two skewed Tollmien-Schlichting waves and a longitudinal vortex which produces unbounded growth of the disturbance after a finite time in a channel flow or after a finite distance in an external flow.

Stage 1

- Small amplitude TS and Görtler interact and develop
  a finite time singularity

Stage 2

- Large amplitude disturbances, blow up if M > 41.6
- Curvature not needed, mechanism occurs in
  straight channels & flat plate boundary layers

$M°$
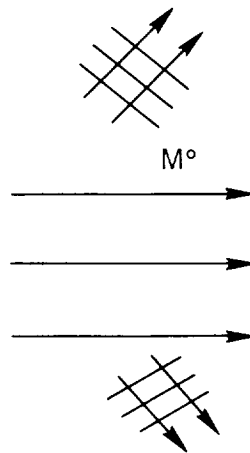
Now let us consider the instability of large amplitude Tollmien-Schlichting waves to Görtler vortices. The linearized form of the Görtler equations applies to interacting boundary layers or Triple-Deck flows. Thus since it has been shown that large amplitude two and three-dimensional Tollmien-Schlichting waves are governed by Triple Deck theory, we can use these equations to investigate the instability of these flows.

The surprising feature of the large amplitude structure of Tollmien-Schlichting waves is that they have a wall layer essentially identical to a Stokes layer induced by oscillating a flat plate in a viscous fluid. However, it was shown that in the presence of curvature, Stokes layers are unstable to Görtler vortices. The vortices are confined to the Stokes layer and have axes aligned with the flow direction. Thus this instability mechanism occurs for large amplitude Tollmien-Schlichting waves. The instability can occur for either convex or concave curvature since for time-periodic flows there is no analogue of Rayleigh's criterion for the centrifugal instability of curved flows. It suffices to say that at moderate value of the curvature even relatively small amplitude Tollmien-Schlichting waves break up in this way.

Sublayer instabilities of large amplitude TS

waves interacting with surface curvature.

Convex or concave curvature causes breakdown.

3-D breakdown
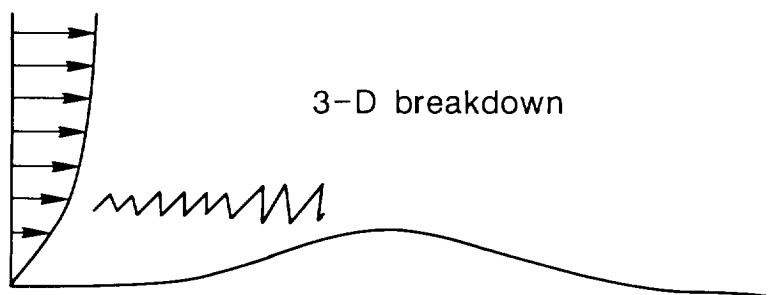
Use Smith-Burggraf theory to calculate large

amplitude 2- or 3-D TS waves. The Stokes

sublayer of these waves is unstable in presence

of convex or concave curvature.

BOUNDARY-LAYER RECEPTIVITY AND LAMINAR-FLOW AIRFOIL DESIGN

E. J. Kerschen
University of Arizona
Tucson, Arizona

C-4

273

BOUNDARY-LAYER RECEPTIVITY

Boundary-layer receptivity examines the processes by which unsteady disturbances in the free-stream flow enter the boundary layer. In contrast, classical stability theory examines the evolution of disturbances that are already present in the boundary layer. Unsteady environmental disturbances of importance include free-stream turbulence, sound waves, and body vibration. Experimental evidence suggests that the receptivity process and the initial growth of the instability waves are well described by linear equations. Hence we consider linear, time-harmonic disturbances to the steady boundary-layer flow. The mathematical description of the receptivity process has the form of a boundary value problem, since the free-stream disturbances are specified. In contrast, classical stability theory leads to an eigenvalue problem in which the growth or decay rate of the disturbance is found, but in which the actual amplitude of the instability wave cannot be determined.

RECEPTIVITY

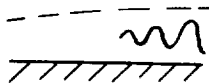- Examines the mechanisms by which external disturbances enter the boundary layer.

- Boundary value problem
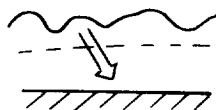
As Contrasted To

STABILITY THEORY

- Examines the evolution of disturbances that are already present in the boundary layer.

- Eigenvalue problem

IMPORTANCE OF RECEPTIVITY IN TRANSITION PREDICTION

Conceptually, the phenomenon of boundary-layer transition can be separated into three stages. These stages are the receptivity process, the linear growth of the instability wave, and the nonlinear breakdown into turbulence. The nonlinear breakdown is a violent process which occurs over a fairly short streamwise distance. Most of the distance between the airfoil leading edge and the transition point is covered by the receptivity and linear growth stages of the transition process. Hence, the details of the first two stages are most critical for prediction of the transition point.

Current transition prediction methods are based on linear stability theory, and hence consider only the second stage of the transition process. Linear stability theory cannot determine the amplitude of the instability waves, and hence the e^N criterion examines the ratio of the instability wave amplitude to its (unknown) amplitude at the neutral stability point. The amplitude ratio exponent N must be determined empirically by comparison with experiments and is found to be a strong function of the disturbance environment. A modified transition prediction method which combines receptivity with linear stability theory would have several advantages. The amplitude ratio criterion could be replaced by a critical amplitude criterion, the environmental disturbances would be directly accounted for, and the influence of the boundary-layer characteristics upstream of the neutral stability point would be included.

- Transition Involves Three Stages

  (1) Receptivity

  (2) Linear growth of instability

  (3) Nonlinear breakdown

- First Two Stages Most Critical for Transition Prediction

- Current e^N Methods Consider Only Stage (2)

  $$e^N = \frac{A_{tr}}{A_{nsp}} = \text{amplitude ratio}$$

  N = empirical function of disturbance environment

- Method Combining Receptivity and Linear Growth

  - utilitizes amplitude criterion (A_{tr})

  - directly accounts for disturbance environment

  - includes influence of boundary layer characteristics *upstream* of the neutral stability point
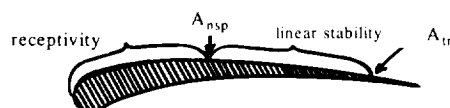
FUNDAMENTAL CONCEPTS OF RECEPTIVITY THEORY

While the importance of free-stream disturbances for the transition process has been recognized for many years, an appropriate mathematical description has been developed only recently (refs. 1, 2, 3 and 4). The fundamental ideas of this receptivity theory can be described as follows. The evolution of instability waves is governed by the Orr-Sommerfeld equation of linear stability theory. This equation assumes that, compared to the instability wave, the steady boundary-layer flow changes slowly in the streamwise direction. Boundary conditions representing free-stream disturbances may be imposed on the Orr-Sommerfeld equation, but these generate only particular solutions that are unrelated to the instability wave eigensolutions. This leads to the conclusion that the generation of the instability waves, or equivalently the receptivity process, must occur in regions where the boundary layer changes so rapidly that the Orr-Sommerfeld equation is invalid. The instability wave amplitude is then found by asymptotic matching of the receptivity region with the evolution region.

- Evolution of Instability Waves Governed by Orr-Sommerfeld Equation

  - assumes

    $$\frac{1}{\delta}\frac{d\delta}{dx} << \frac{1}{\lambda_{TS}}$$

  - free-stream disturbances produce particular solutions that are unrelated to instability waves

- Generation of Instability Waves Occurs in Regions where O.S. Equation is Invalid

  $$\frac{1}{\delta}\frac{d\delta}{dx} = O(\frac{1}{\lambda_{TS}})$$

- Amplitudes of Instability Waves Found by Asymptotic Matching of Generation and Evolution Regions

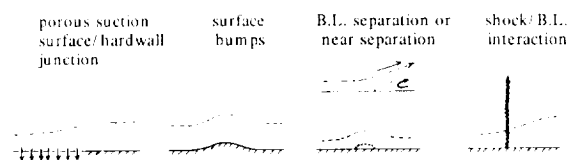# REGIONS WHERE RECEPTIVITY OCCURS

There are two classes of regions where receptivity occurs. The first is near leading edges, where the boundary layer is thin and growing rapidly. Since the boundary layer is thin, the pressure may be assumed constant across it and the disturbances are governed by the linearized, unsteady boundary-layer equation rather than by the Orr-Sommerfeld equation. In contrast to the O-S equation, the mean flow divergence enters at leading order in the unsteady boundary-layer equation. The interaction of the mean flow divergence with the unsteady disturbances imposed on the boundary layer by the free stream results in the generation of instability waves. The second class corresponds to regions further downstream where the boundary layer is forced to adjust on a streamwise length scale which is short compared to the body length. Examples of this class are wall suction - hardwall junctions, surface bumps and shock-boundary-layer interactions. In these situations both the mean flow and the unsteady flow exhibit triple deck structures (refs. 5 and 6). The unsteady flow in the lower deck adjacent to the wall is again governed by the unsteady boundary layer equation, and the instability wave is generated by interaction between the unsteady motion and the mean flow divergence.

- Near Leading Edges
  - Boundary layer thin and growing rapidly
  - Disturbances governed by unsteady boundary layer equation

$$\frac{\partial u'}{\partial t} + U\frac{\partial u'}{\partial x} + V\frac{\partial u'}{\partial y} + \underbrace{u'\frac{\partial U}{\partial x} + v'\frac{\partial U}{\partial y}}_{} = -\frac{1}{\rho}\frac{\partial p'}{\partial x} + v\frac{\partial^2 u'}{\partial y^2}$$
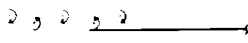
terms not present in O.S. equation

- In Regions of Rapid Boundary Layer Adjustment

| porous suction surface/hardwall junction | surface bumps | B.L. separation or near separation | shock/B.L. interaction |

- Mean flow and disturbance flow exhibit triple-deck structures
- Disturbance flow in lower deck governed by unsteady boundary layer equation

LEADING-EDGE RECEPTIVITY

In order to assess the relative importance of various leading-edge receptivity mechanisms, we have examined the case of the Blasius boundary layer at low Mach numbers. Three types of free-stream disturbances have been considered: convected gusts, which are the linear representation of turbulence, the von Kármán vortex street which is produced by a vibrating ribbon, and oblique acoustic waves. An oblique acoustic wave at $\theta = 90'$ also represents plate transverse vibration. For each of these free-stream disturbances, a closed form solution for the inviscid interaction with the semi-infinite flat plate is first determined. The slip velocity on the plate surface is then calculated. This slip velocity has two distinct components: the slip velocity that would occur for the interaction of the free-stream disturbance with an infinite plate and a cylindrical acoustic wave generated by interaction with the leading edge. The slip velocity then provides the boundary condition for the numerical solution of the unsteady boundary-layer equation, and the receptivity coefficient is extracted from the large x behavior of the solution.

- Flat Plate Geometry, $M_\infty \ll 1$

- Free Stream Disturbances
    - convected gust (turbulence)

    - Von Karman vortex street

    - acoustic wave
        $\theta = 90° \rightarrow$ plate transverse vibration

- Inviscid Interaction with Semi-Infinite Plate
    - analytical solutions
    - slip velocity on plate surface contains two components
        (1) infinite plate component
        (2) diffracted acoustic wave from leading edge

- Slip Velocity Provides Boundary Condition for Numerical
  Solution of Unsteady Boundary Layer Equation

- Receptivity Coefficient Extracted from Large x
  Behavior of Unsteady Boundary Layer

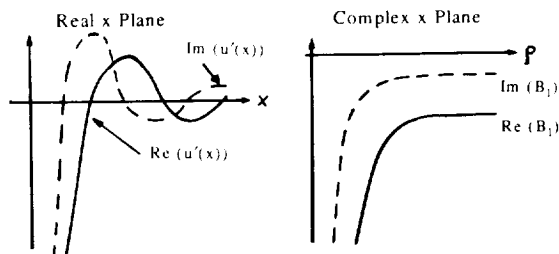# EXTRACTION OF RECEPTIVITY COEFFICIENT

The asymptotic structure of the unsteady boundary-layer equation for large x consists of a particular solution plus an infinite set of asymptotic eigensolutions. The eigensolutions are asymptotic in the sense that they do not satisfy the unsteady boundary-layer equation for all x, but only for large x. Hence the coefficients B_n are not arbitrary, but rather are determined by the full solution for all x. The asymptotic matching of the unsteady boundary layer and Orr-Sommerfeld regions shows that the n = 1 asymptotic eigensolution of the unsteady boundary-layer equation matches with the unstable Tollmien-Schlichting wave. Hence the amplitude of the T-S wave is linearly proportional to B_1, and we call B_1 the receptivity coefficient. We determine B_1 by solving the unsteady boundary-layer equation numerically, and then examining the solution for large x. The asymptotic eigenvalues λ_n are ordered such that the n = 1 eigensolution is exponentially small for large x, making direct extraction of its coefficient difficult. In order to overcome this, the unsteady boundary-layer equation is solved along a ray in the "complex x plane", where the n = 1 eigensolution grows exponentially with downstream distance.
The receptivity coefficient B_1 is found simply by examining the ratio of the numerical solution to the n = 1 asymptotic eigensolution.

- Analytical Structure of Unsteady Boundary Layer as $x \to \infty$

$$u' = u_p' + \sum_{n=1}^{n=\infty} B_n g_n(x,\eta) e^{-(1-i)\lambda_n x^{1/2}}$$

- n = 1 eigensolution matches with T.S. wave

  B_1 = receptivity coefficient $\to A_{nsp}$

- $\lambda_1 > \lambda_2 > \lambda_3 ... \to e^{-(1-i)\lambda_1 x^{1/2}}$ exponentially small as $x \to \infty$

- Numerical integration performed in "complex x" plane

  $(x = -i\rho)$ where first eigensolution is exponentially large

$$B_1 = \lim_{\rho \to \infty} \left(\frac{\text{numerical solution}}{g_1 e^{\sqrt{2}\lambda_1 \rho^{1/2}}} \right)$$

Real x Plane   Complex x Plane

The leading-edge receptivity coefficients for various free-stream distur-
bances are compared in the figure below. The disturbance characteristics are
chosen such that the instability wave has the same frequency in all cases, and
the amplitude of the velocity fluctuations at the location of the plate, but in
its absence, is identical. Both the convected gust and acoustic wave receptiv-
ities have a strong dependence on disturbance orientation θ. The null at θ =
55' for the convected gust results from destructive interference between the
instability waves generated by the infinite plate and leading-edge slip velocity
components. The von Karman vortex street produces a receptivity value approxi-
mately 4 times the convected gust result. The parallel acoustic wave (θ = 0)
receptivity is on the same order as that for the convected gust, but as θ incre-
ases the acoustic wave receptivity rises rapidly, by as much as two orders of
magnitude for M = 0.01. The explanation for this behavior is in the strength of
the cylindrical acoustic wave generated by the interaction of the free-stream
disturbance with the leading edge. At low Mach numbers the strength of this
scattered wave varies as $M^{-1/2}$. However, it should be noted that this behavior
occurs only for the case of an isolated semi-infinite flat plate. We are pre-
sently investigating the influences of finite plate length and wind tunnel walls
on leading-edge receptivity to acoustic waves at low Mach numbers.
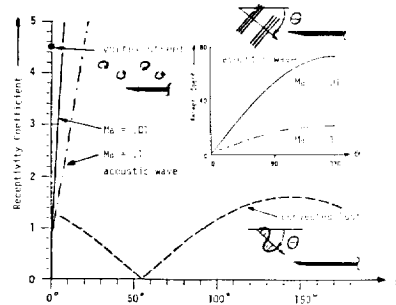
- Convected Gust Receptivity Strong Function of Gust Angle
  - θ dependence due to relative phase of diffracted and
    infinite plate components

- Acoustic Wave Receptivity Very Strong at Low M_∞
  - dominated by diffracted wave, strength $\sim \lambda_{ac}^{1/2} \sim M^{-1/2}$

- Finite Plate Length or Wind-Tunnel Walls Should
  Substantially Decrease Acoustic Receptivity
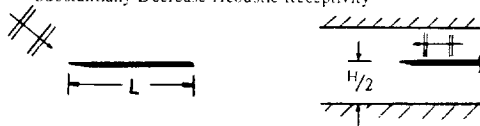
RECEPTIVITY TO ACOUSTIC WAVES AT A
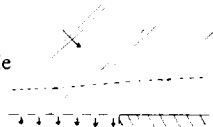# SUCTION SURFACE - HARD WALL JUNCTION

We are presently addressing one problem in the second class of receptivity mechanisms, namely the receptivity to free-stream acoustic waves which occurs at a junction between a suction surface and a hard wall. This particular problem is clearly relevant to hybrid laminar-flow design. In addition, since the instability waves decay exponentially upstream of the neutral stability point, even a weak receptivity mechanism close to the neutral stability point may be more important than a much stronger mechanism which occurs near the leading edge.

There are two receptivity mechanisms at the junction. The first is associated with the mean flow adjustment in the vicinity of the junction. This mean flow adjustment occurs over the triple deck length scale $L/Re^{3/8}$, where L is the body length and Re the Reynolds number. The T-S wavelength near the lower branch of the neutral stability curve is comparable, leading to efficient coupling. In addition to the mean flow adjustment, the change in wall admittance produces a diffracted acoustic wave whose short local length scale couples into the T-S wave. This second mechanism does not require wall suction. Since the phenomenon is linear, the two mechanisms can be linearly superposed.

- Motivations

  - relevant to hybrid laminar flow design

  - exponential decay upstream of neutral stability point

    $\rightarrow$ receptivity mechanisms closest to nsp dominate

- Two Receptivity Mechanisms at Junction

  (1) Mean Flow Adjustment
    - adjustment occurs over triple deck scale
      $(L/Re^{3/8})$
    - T.S. wavelength comparable

  (2) Wall Admittance Change

    - produces diffracted acoustic
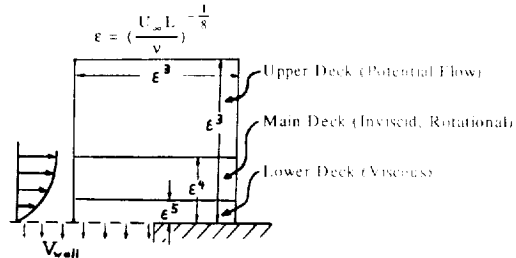   wave with short local scale
    - wall suction not required
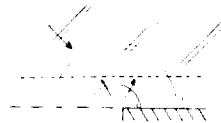
- Mechanisms Can Be Linearly Superposed

Near the suction surface – hard wall junction, both the mean flow and the unsteady flow exhibit a triple deck structure. An important characteristic of the triple-deck theory is that the pressure field is not imposed on the boundary layer, but is determined by an interactive relationship between the upper and lower deck solutions. The basic physics of the triple deck is as follows. The short streamwise length scale causes the original boundary layer or main deck to respond inviscidly. A new, thinner boundary layer or lower deck is then necessary to satisfy the no-slip wall boundary condition. Finally, the rapid variation in boundary-layer displacement thickness induces irrotational motion with this same scale outside the boundary layer. This latter region is called the upper deck. The streamwise length scale of $L/Re^{3/8}$ is necessary for consistency between the decks.

We consider wall suction velocities of the same order as the standard boundary-layer scaling. The mean flow adjustment then satisfies a linear set of equations, and the solution can be found in closed form by Fourier transform techniques. The unsteady flow is found to be a small perturbation of a Stokes shear wave. This perturbation satisfies an inhomogeneous equation with a source term involving interaction between the mean flow adjustment and the Stokes wave. The wall admittance variation enters as an inhomogeneous boundary condition. The solution for the unsteady flow adjustment (u_1', v_1') is found in terms of a Fourier transform, and the amplitude of the T-S wave generated by the interaction is given by the residue of the appropriate pole of the transform.

- Interactive Pressure-Displacement Relationship

- Asymptotic Description of Mean Flow, Unsteady Flow, T S, Waves

$$\varepsilon = \left(\frac{U_\infty L}{v}\right)^{-\frac{1}{8}}$$

Upper Deck (Potential Flow)

Main Deck (Inviscid, Rotational)

Lower Deck (Viscous)

V_{wall}

- $\dfrac{V_{wall}}{U_\infty \varepsilon^4} = O(1) \rightarrow$ mean flow adjustment (U_1, V_1) satisfies linear eqs

- Unsteady Flow

  - main and upper decks quasi-steady

  - lower deck small perturbation to Stokes wave $(u' = u_0' + \varepsilon u_1')$

$$L(u_1', v_1') = u_0' \frac{\partial U_1}{\partial x} + V_1 \frac{\partial u_0'}{\partial y}$$

unsteady b.l. eq — mean flow adjustment

$$u'(x,0) = 0 \qquad v'(x,0) = -\beta(x)p$$

— wall admittance change

  - T.S. wave = pole of Fourier Transform solution

  - Receptivity Coefficient — residue

SUCTION SURFACE JUNCTION RECEPTIVITY

The general structure of the T-S wave generated by the unsteady interaction at the junction is illustrated in the figure below. The amplitude of the instability wave is linear with respect to the free-stream acoustic wave and also with respect to the wall impedance and suction velocity. The two factors Λ_1 and Λ_2 are frequency dependent, while the junction geometry appears in the multiplicative factor $F(\kappa)$. The frequency dependence in Λ_1 and Λ_2 is fairly mild, with a maximum amplitude generated by frequencies corresponding to positions quite far upstream of the neutral stability point. In terms of proposed laminar-flow wall suction designs, the parameter $V_{wall}/U_\infty\epsilon^4$ is on the order of 0.1 for distributed suction systems, and on the order of 1 for strip suction systems. We have not yet explored the influence of wall admittance in detail, but it is interesting to note that the wall admittance β is divided by ϵ^2, while the wall suction parameter is multiplied by ϵ. Thus, even small admittances may be important in the receptivity process.
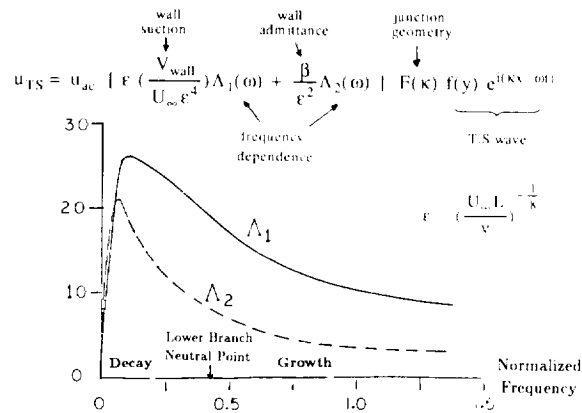
- Laminar Flow Designs

  - distributed suction $\dfrac{V_{wall}}{U_\infty\epsilon^4} = O(0.1)$

  - suction strips $\dfrac{V_{wall}}{U_\infty\epsilon^4} = O(1)$

- Even Small Wall Admittance May be Important

  $\beta = O(\epsilon^3)$ corresponds to $\dfrac{V_{wall}}{U_\infty\epsilon^4} = O(1)$

INFLUENCE OF SUCTION STRIP WIDTH

The figure below illustrates the influence of suction strip width on receptivity to free-stream acoustic waves. The total mass flow through the strip is held constant as strip width is varied, and hence the wall suction velocity is inversely proportional to the strip width. The Blasius profile is used for the undisturbed boundary layer. Results are shown for four strip locations. The quantity plotted is the receptivity coefficient divided by its narrow slot limit. It is seen that the maximum receptivity generally occurs for very narrow slots. For the slot located at the neutral stability point, a slot width equal to an integer number of T-S wavelengths produces a zero receptivity coefficient. Essentially, the instability wave generated at the front edge of the slot is cancelled by that generated at the rear edge.

Almost identical results are found for the slot located at 1/2 the distance from the leading edge to the neutral stability point and the slot located at the point of maximum instability growth rate. The general shape of these curves is similar to that for the neutral wave, but the minima at integer values of d/λ are nonzero. Basically, the growth or decay of the instability wave modifies the perfect cancellation between front and rear edges of the slot. However it can be seen that, by choosing a slot width equal to the instability wavelength, the receptivity can be reduced to 12% of the narrow slot limit. At the 1/4 point location closer to the leading edge the receptivity is not reduced as much by choosing $d/\lambda = 1$. Note also that, for sufficiently wide slots, the receptivity is actually higher than the narrow slot limit. This behavior is caused by the downstream displacement of the slot rear edge with increase in slot width.
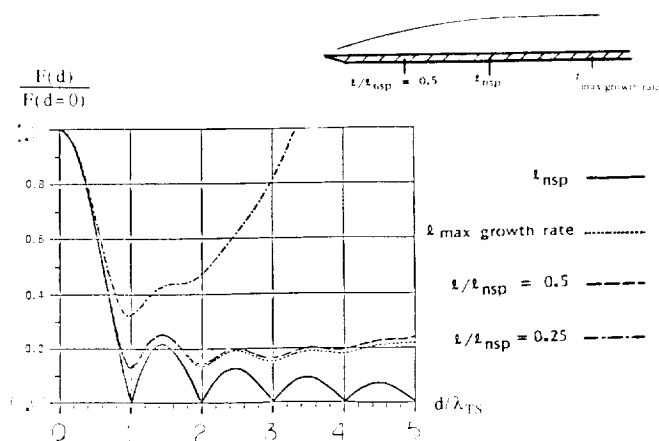
- $\dfrac{F(d)}{F(d=0)}$ $\dfrac{\text{Receptivity Coefficient}}{\text{Narrow Slot Limit}}$

- Maximum Receptivity for Narrow Strips

- Receptivity Minimized for $\dfrac{d}{\lambda_{TS}} = 1$

 - reduction most significant for near neutral waves

INFLUENCE OF JUNCTION SMOOTHING

For hybrid laminar-flow designs with distributed suction surfaces, the receptivity coefficient depends on the details of the transition from the suction surface to the downstream hard wall. To examine this dependence, we have compared the receptivity for a number of suction transition profiles. The case of a step discontinuity has been taken as the baseline. The additional profiles considered are a double step discontinuity, a linear variation and a cosine variation, as shown in the figure below. Three junction locations are considered: at the neutral stability point, at 1/2 the distance from the leading edge to the neutral stability point, and at the point of maximum growth rate. In all cases the ordinate is the receptivity coefficient normalized by the receptivity coefficient for the baseline case of the step discontinuity, and the abscissa is the transition length normalized by the instability wavelength.

The double step discontinuity generally has the largest receptivity coefficient and the cosine variation generally has the smallest. The results for the linear profile are surprisingly close to those for the cosine profile. A choice of transition profile length approximately equal to two instability wavelengths appears near optimum in most cases. Profile smoothing is less effective in reducing the receptivity coefficient for growing waves as compared to the neutral wave or decaying wave cases. In fact, for the maximally growing wave the double step discontinuity generally increases the receptivity coefficient as compared to the single step baseline case. Essentially, the double step junction has a discontinuity farther upstream, and the additional growth of this upstream generated wave negates the beneficial effects of spreading out the discontinuity in wall suction.

DISTRIBUTED SUCTION-HARD WALL JUNCTION

- Receptivity Normalized by Single Step Junction
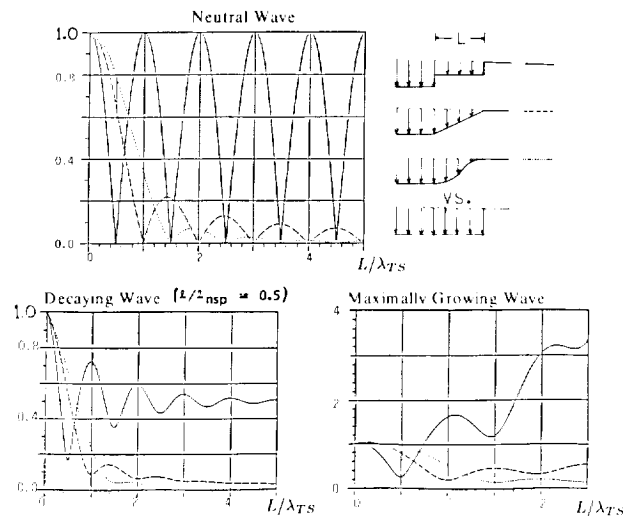
- Transition Lengths Greater Than λ_{TS} Significantly Reduce Receptivity

- Smooth Transition Generally Beneficial

- Multiple Step Transition Increases Receptivity in Growing Wave Case

285

SUMMARY

In summary, receptivity examines the way in which external disturbances generate instability waves in boundary layers. Receptivity theory is complementary to stability theory, which studies the evolution of disturbances that are already present in the boundary layer. A transition prediction method which combines receptivity with linear stability theory would directly account for the influence of free-stream disturbances and also consider the characteristics of the boundary layer upstream of the neutral stability point. The current e^N transition prediction methods require empirical correlations for the influence of environmental disturbances, and totally ignore the boundary layer characteristics upstream of the neutral stability point.

The regions where boundary-layer receptivity occurs can be separated into two classes, one near leading edges and the other at downstream points where the boundary layer undergoes rapid streamwise adjustments. Analyses have been developed for both types of regions, and parametric studies which examine the relative importance of different mechanisms have been carried out. The work presented here has focused on the low Mach number case. Extensions to high subsonic and supersonic conditions are presently under way.

- Instability Waves Generated
  - in leading edge region
  - in regions of rapid boundary layer adjustment

- Leading Edge Receptivity
  - strongly dependent on disturbance type
  - oblique acoustic waves dominant at low M_∞

- Junction Receptivity Dependent on Geometry

- Suction Slot Receptivity
  - maximum for narrow slots
  - minimum for $\dfrac{d}{\lambda_{TS}} = 1$

- Distributed Suction - Hard Wall Junction Receptivity
  - minimized by transition lengths greater than λ_{TS} smaller for smooth transitions

- Theories Currently Being Extended to Supersonic Conditions

REFERENCES

1. Goldstein, M. E.: The Evolution of Tollmien-Schlichting Waves Near a Leading Edge. J. Fluid Mech., vol. 127, 1983, pp. 59-81.

2. Goldstein, M. E.; Sockol, P. M.; and Sanz, J.: The Evolution of Tollmien-Schlichting Waves Near a Leading Edge. Part 2. Numerical Determination of Amplitudes. J. Fluid Mech., vol. 129, 1983, pp. 443-453.

3. Goldstein, M. E.: Scattering of Acoustic Waves into Tollmien-Schlichting Waves by Small Streamwise Variations in Surface Geometry. J. Fluid Mech., vol. 154, 1985, pp. 509-529.

4. Kerschen, E. J.; Choudhari, M. M.; and Heinrich, R.: A Comparison of Boundary Layer Receptivity Mechanisms. APS Annual Meeting of the Division of Fluid Dynamics (Columbus, Ohio), November 1986

5. Smith, F. T.: On the High Reynolds Number Theory of Laminar Flows. IMA Journal of Applied Mathematics, vol. 28, 1982, pp. 207-281.

6. Smith, F. T.: On the Non-Parallel Flow Stability of the Blasius Boundary Layer. Proc. R. Soc. Lond., vol. A 366, 1979, pp. 91-109.

ACKNOWLEDGMENTS

|

GÖRTLER INSTABILITY ON AN AIRFOIL

VIJAY KALBURGI
OLD DOMINION UNIVERSITY
NORFOLK, VIRGINIA

S. M. MANGALAM
A S & M, INC
HAMPTON, VIRGINIA

J. R. DAGENHART
NASA, LANGLEY RESEARCH CENTER
HAMPTON, VIRGINIA

S. N. TIWARI
OLD DOMINION UNIVERSITY
NORFOLK, VIRGINIA

INTRODUCTION

Görtler vortices arise in boundary layers along concave surfaces due to centrifugal forces. These counter-rotating streamwise vortices are one of the three known flow instabilities which lead to boundary-layer transition. Advanced supercritical Laminar Flow Control wings have concave regions on the lower surface near the leading and trailing edges. Görtler vortices coupled with T-S waves and crossflow vortices may play an important role in triggering early transition.

In earlier studies the linear development of Görtler vortices was reduced to an eigenvalue problem assuming the flow to be parallel or quasi-parallel (refs. 1-4). The shapes of the perturbation velocity components were assumed invariant in the streamwise direction while their amplitudes were assumed to grow at a common rate. The major differences in the approach, details of the formulations, as well as the computational results are discussed extensively by Herbert (ref. 5). In each of these investigations, a unique neutral curve was obtained. The major limitation of this method is that it cannot be used to determine the development of Görtler vortices in the presence of variable curvature, suction and pressure gradients. In such a general case it is necessary to solve the governing partial differential equations as an initial value problem as developed by Hall (ref. 6).

BACKGROUND

Hall obtains multiple neutral curves that depend strongly on the initial condition and their location (Fig. 1). However his conclusions are misleading because his initial conditions are mathematically correct but physically meaningless as shown in figures 2a - 2c below. If a physically meaningful vortex perturbation is introduced as the initial condition, then these multiple curves will coalesce into one curve. It will be shown subsequently that the resulting growth rates agree well with results obtained from the solution of the eigenvalue problem for the case of constant curvature.
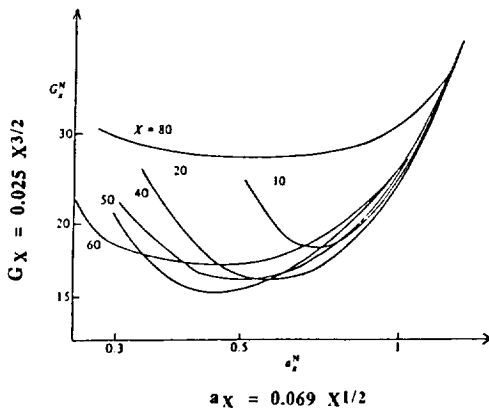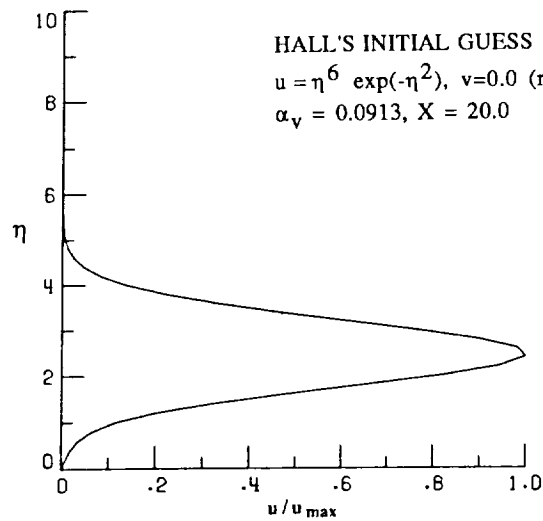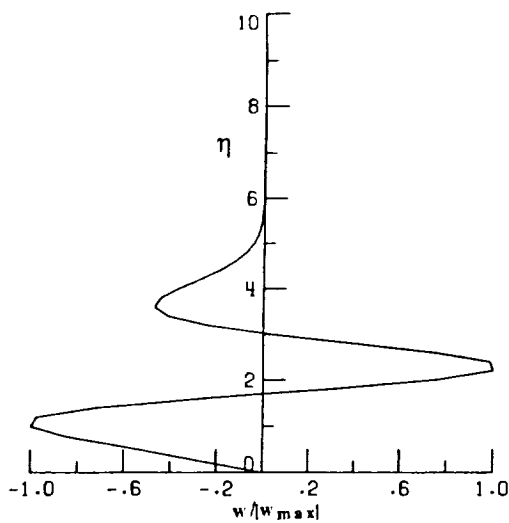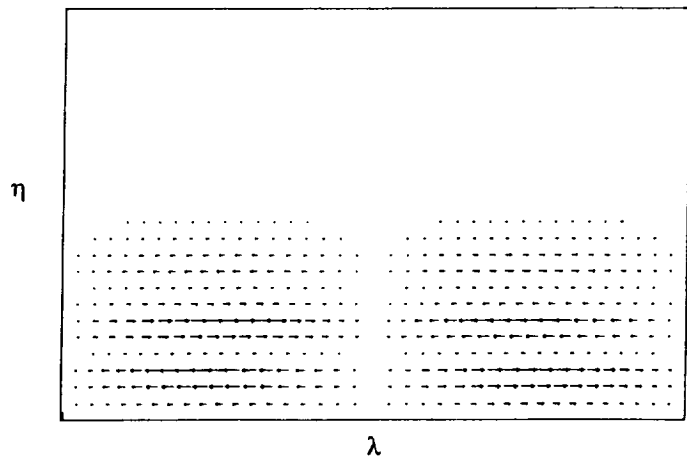

Figure 1

Figure 2a

Figure 2b

Figure 2c

GOVERNING EQUATIONS

The perturbation form and their linearized governing equations with appropriate boundary and initial conditions are given in figure 3. A second order accurate, implicit, iterative finite-difference scheme is used to solve the perturbation equations for the Blasius boundary layer. The governing equations are the same as those developed by Hall (ref. 6) but physically meaningful initial conditions have been used in the computations.

● **DISTURBANCE FORM**

$$U(X,Y,Z) = U(X,Y)\cos(\alpha_v Z)$$
$$V(X,Y,Z) = V(X,Y)\cos(\alpha_v Z)$$
$$W(X,Y,Z) = W(X,Y)\sin(\alpha_v Z)$$
$$P(X,Y,Z) = P(X,Y)\cos(\alpha_v Z)$$

● **GOVERNING EQUATIONS** $\qquad\qquad G_v = 21/R \sqrt{U_\infty l/v}$

$$U_X + V_Y + \alpha_v W = 0$$
$$u U_X + u_X U + v U_Y + V u_Y - U_{YY} + \alpha_v^2 U = 0$$
$$u V_X + v_X U + v V_Y + V v_Y + P_Y + G_v U u - V_{YY} + \alpha_v^2 V = 0$$
$$u W_X + v W_Y - \alpha_v P - W_{YY} + \alpha_v^2 W = 0$$

● **BOUNDARY CONDITIONS** $\qquad$ ● **INITIAL CONDITION**

$$U(X,0) = V(X,0) = W(X,0) = 0 \qquad U = U(Y)$$
$$U(X,\infty) = V(X,\infty) = W(X,\infty) = 0 \qquad V = V(Y) \qquad AT \ (X = \overline{X})$$
$$W = W(Y)$$

Figure 3

292

ᴿigure 4 below shows the normalized u- and v-perturbation velocities obtained from the present method and by solving the eigenvalue problem (ref. 3). Computed results based on Hall's initial guess have also been included to show the effect of physically incorrect input on the solution. The u-, v-, and w-perturbation velocities are assumed to grow at a common rate in the eigenvalue problem. If this approximation is true for the physical problem, then the v-perturbation velocity has to grow very rapidly to match the correct shape and amplitude if it is assumed to be zero initially as in reference 6. This may explain the behavior of the v-perturbation velocity in the following figures when it is assumed zero initially.
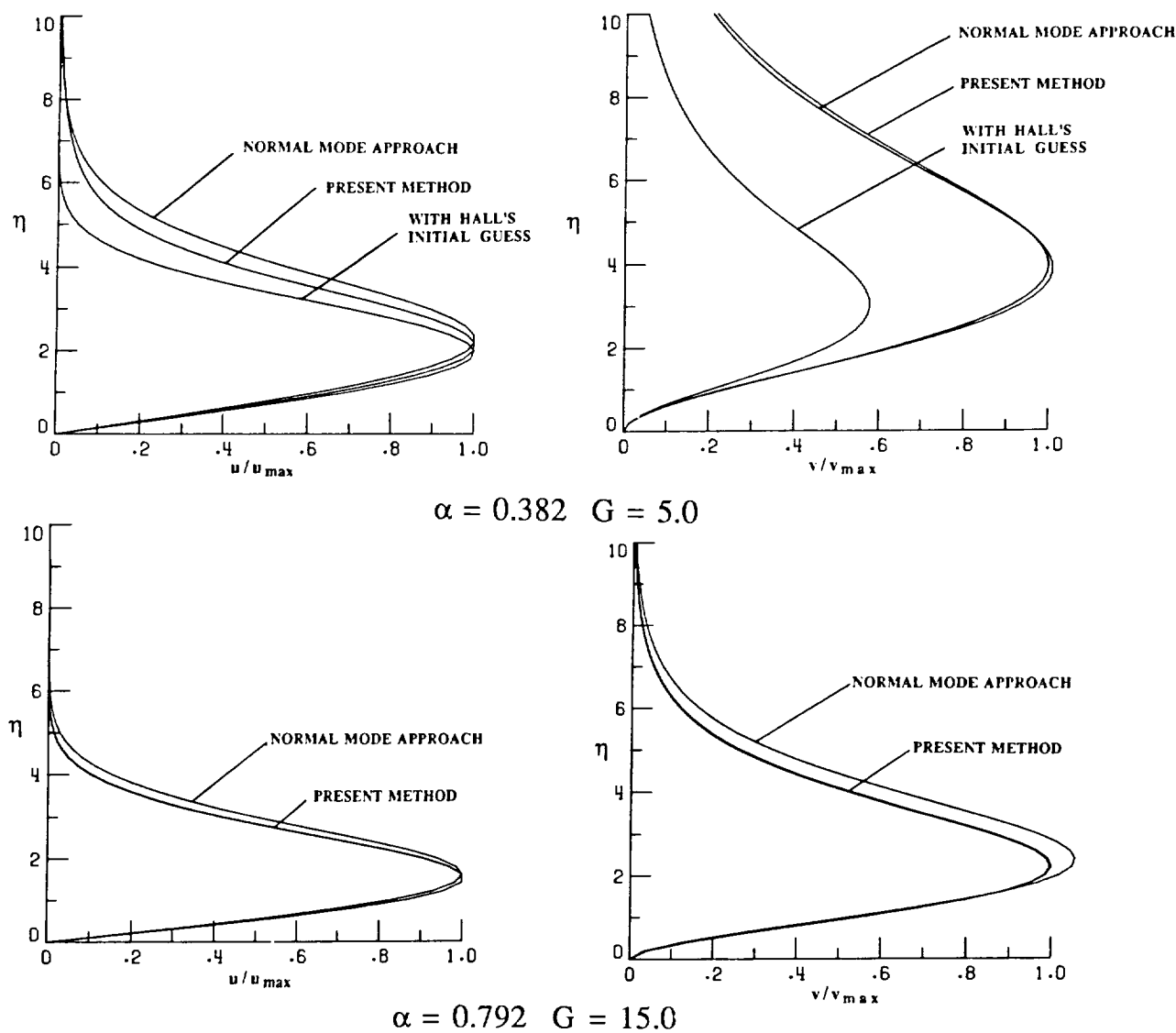

$$\alpha = 0.382 \quad G = 5.0$$

$$\alpha = 0.792 \quad G = 15.0$$

Figure 4

VARIATION OF AMPLIFICATION RATE WITH GÖRTLER NUMBER

This conclusion is further reinforced by figure 5 showing the variation of the amplification rates with Görtler number. A number of computational experiments showed that whenever the growth rates β_u and β_v matched (as assumed in the normal mode approach) the computed results from the initial value problem merged with results obtained from the normal mode approach, indicating that the assumptions made in the normal mode approach are reasonable for this problem (also, see ref. 2).
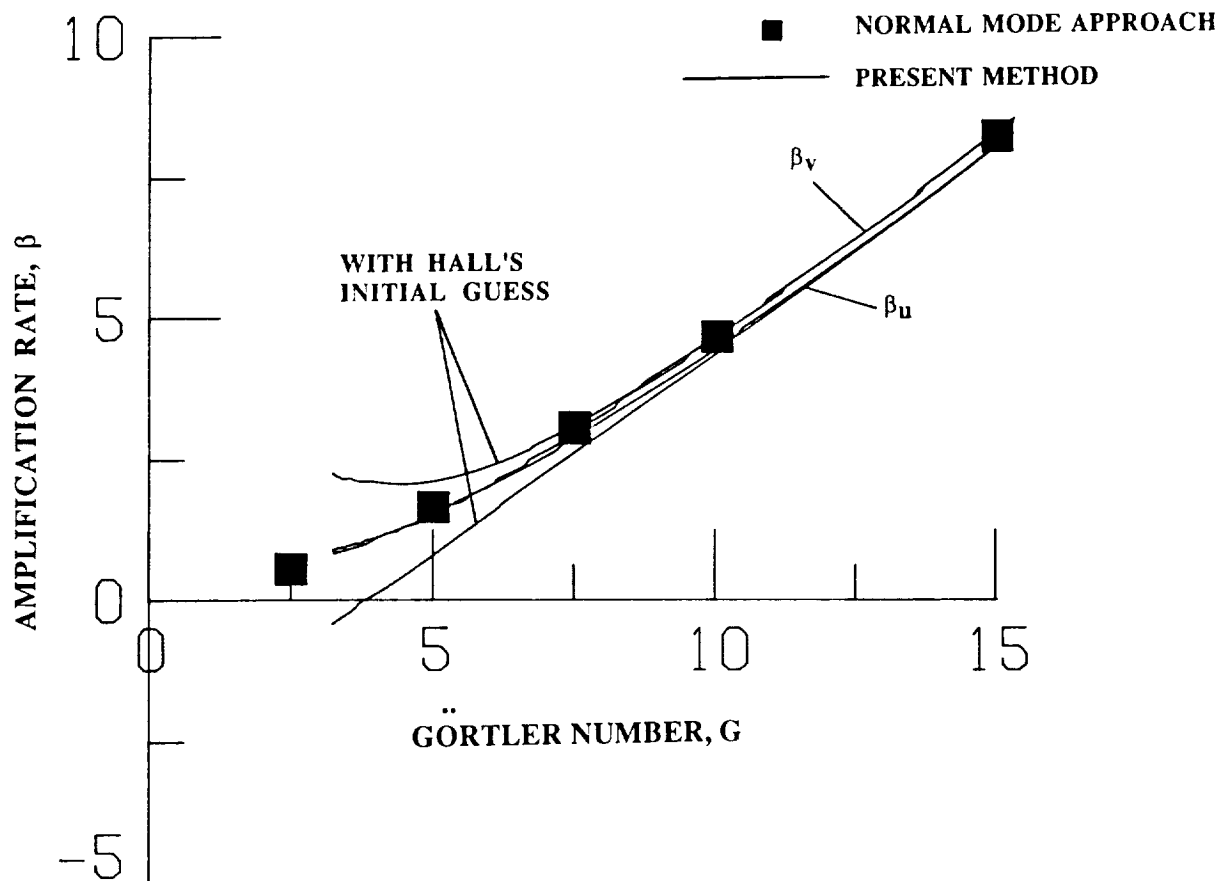

Figure 5

We now look at the growth/damping of Görtler vortices in the presence of a variable curvature distribution (Fig. 6). A Blasius boundary layer is assumed for the mean flow. The normal mode approach is not applicable to this problem. Computations were carried out for a number of curvature distributions, but only one case is considered here. Typical normalized perturbation functions and the perturbation velocity field along the span over one wavelength are shown in the following pages (Figs. 7a - 7f) for different streamwise locations. Note that a negative value of the Görtler number G_v denotes convex curvature, The Görtler vortices appear to lift off at the beginning of the convex region and a secondary, weaker vortex pair begins to emerge near the surface. The original vortex changes sign in this region and we observe counter-rotating vortices in the spanwise as well as normal direction. Further studies on more realistic problems are in progress.
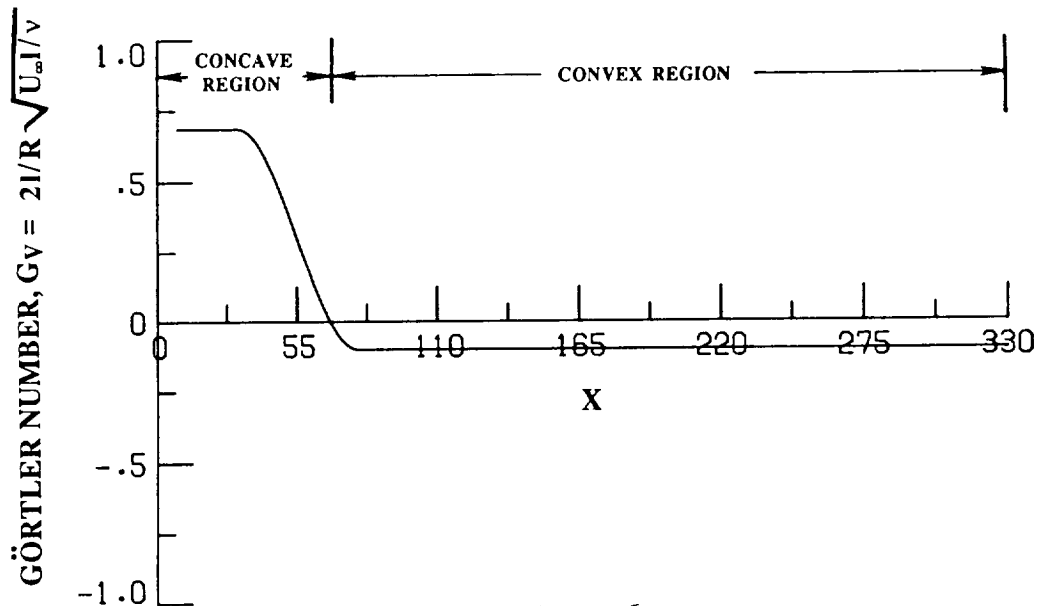
$$\alpha \, v \; = \; 0.0913$$

Figure 6
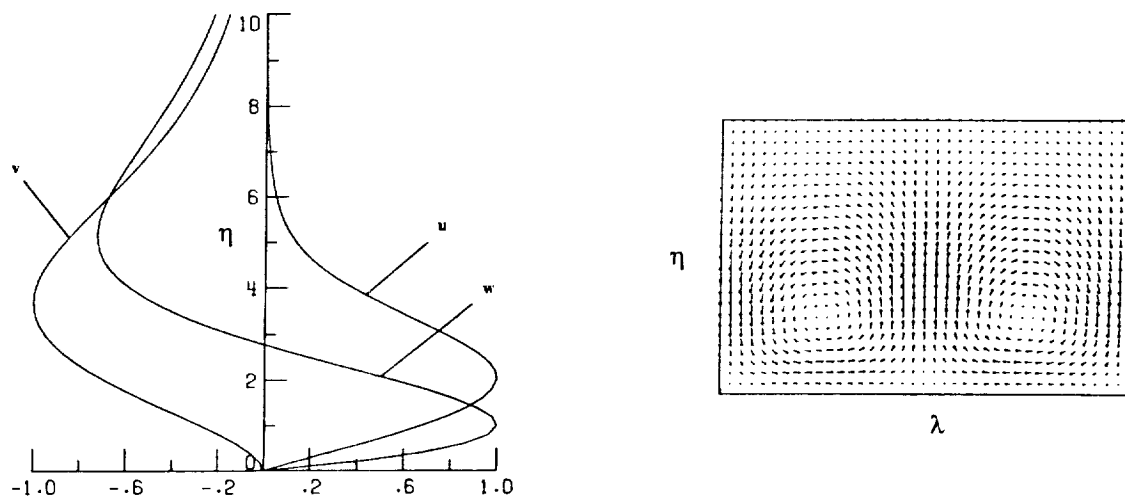
Fig. 7a $G_v = 0.685$, $X = 20.2$, $\alpha_v = 0.0913$
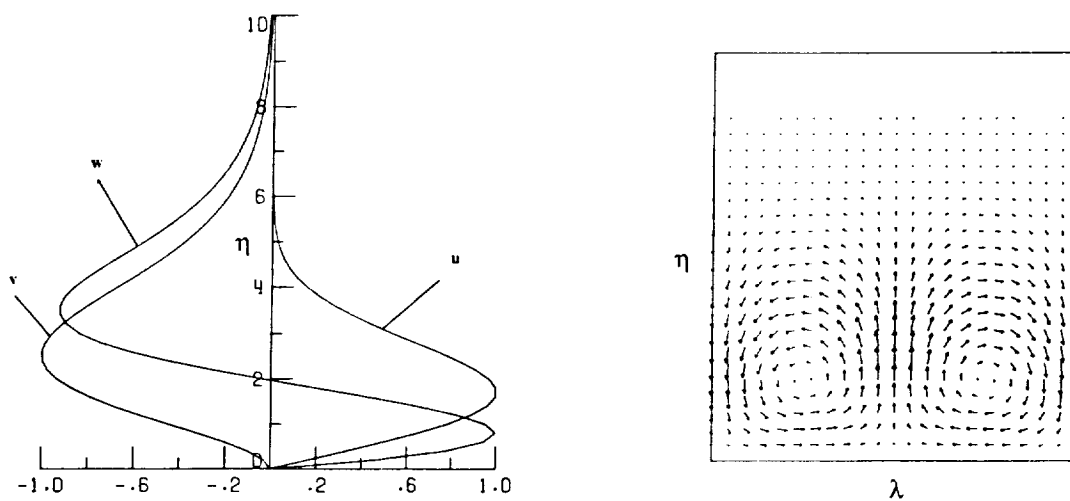
Fig. 7b $G_v = 0.165$, $X = 60.2$, $\alpha_v = 0.0913$
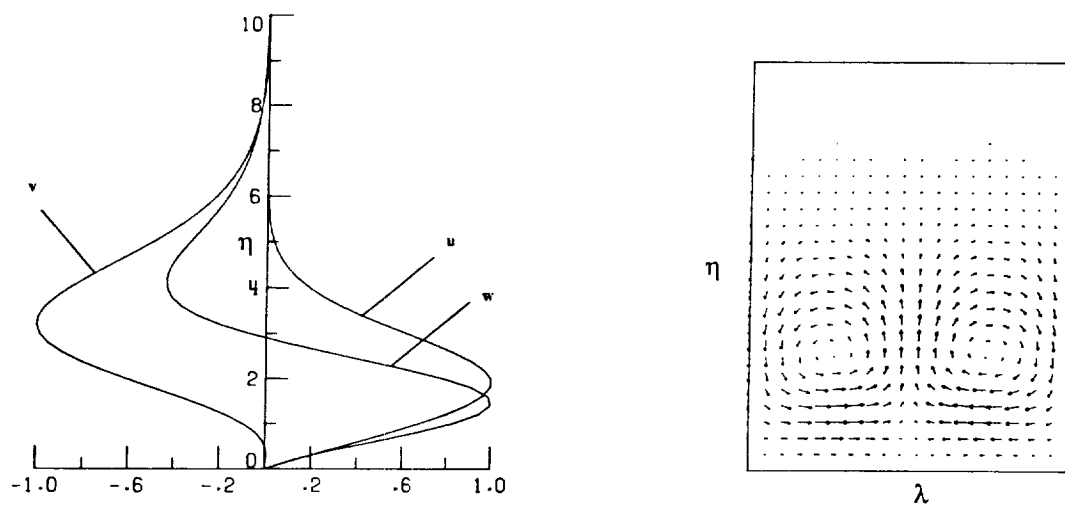
Fig. 7c $G_v = -0.10$, $X = 80.2$, $\alpha_v = 0.0913$
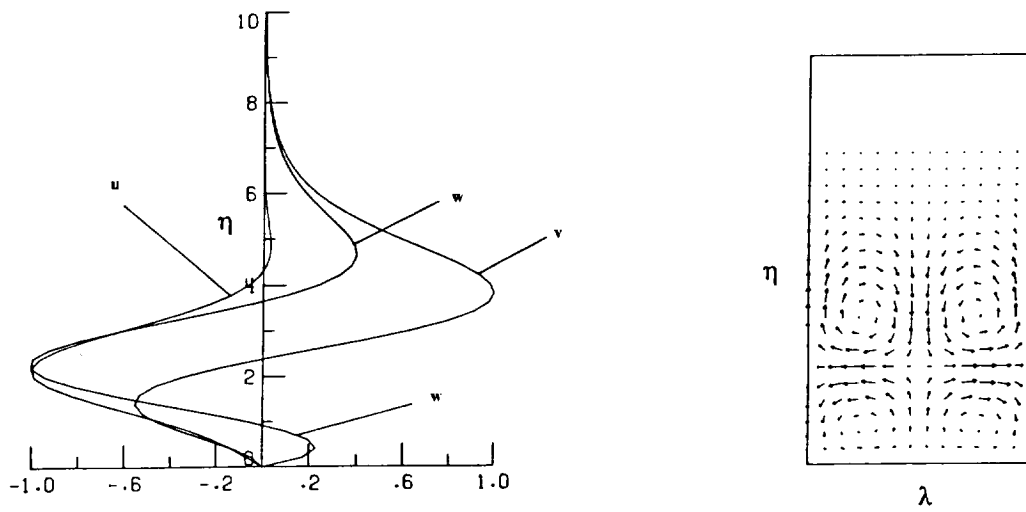
Fig. 7d $G_v = -0.10$, $X = 160.2$, $\alpha_v = 0.0913$
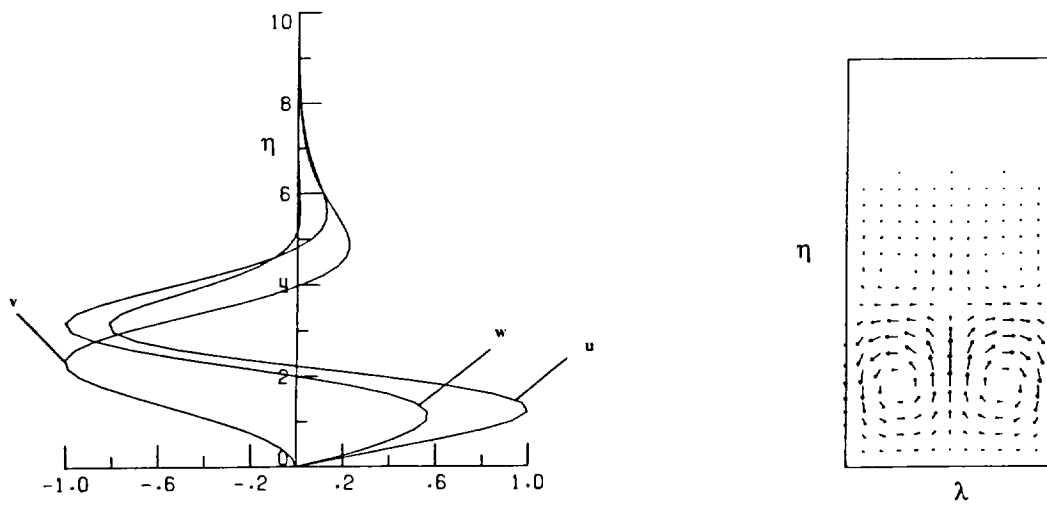
Fig. 7e $G_v = -0.10$, $X = 200.2$, $\alpha_v = 0.0913$
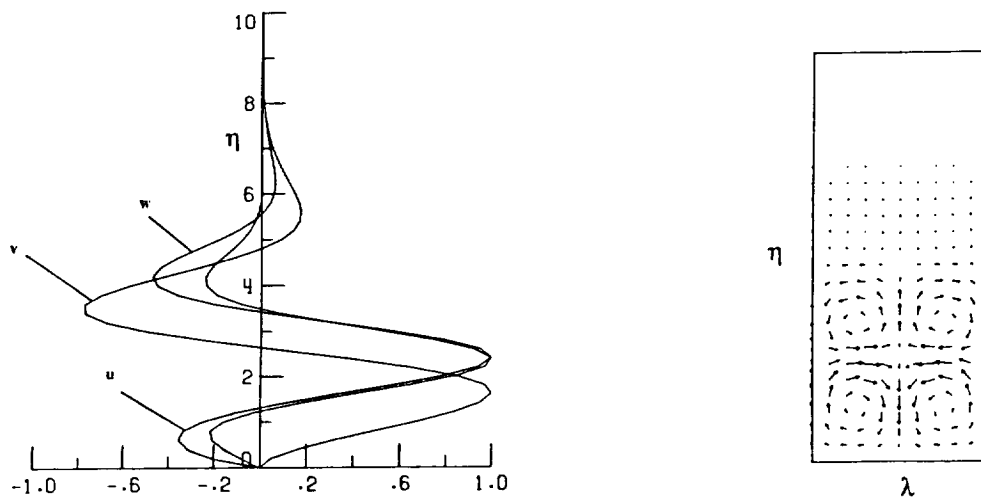
Fig. 7f $G_v = -0.10$, $X = 260.2$, $\alpha_v = 0.0913$

VARIATION OF ENERGY ALONG THE STREAMWISE DIRECTION

The variation in kinetic energy along the streamwise direction is shown in figure 8. As expected, the energy reaches a maximum at the end of the concave region followed by a rapid damping in the convex zone.

$$\alpha_V = 0.0913$$
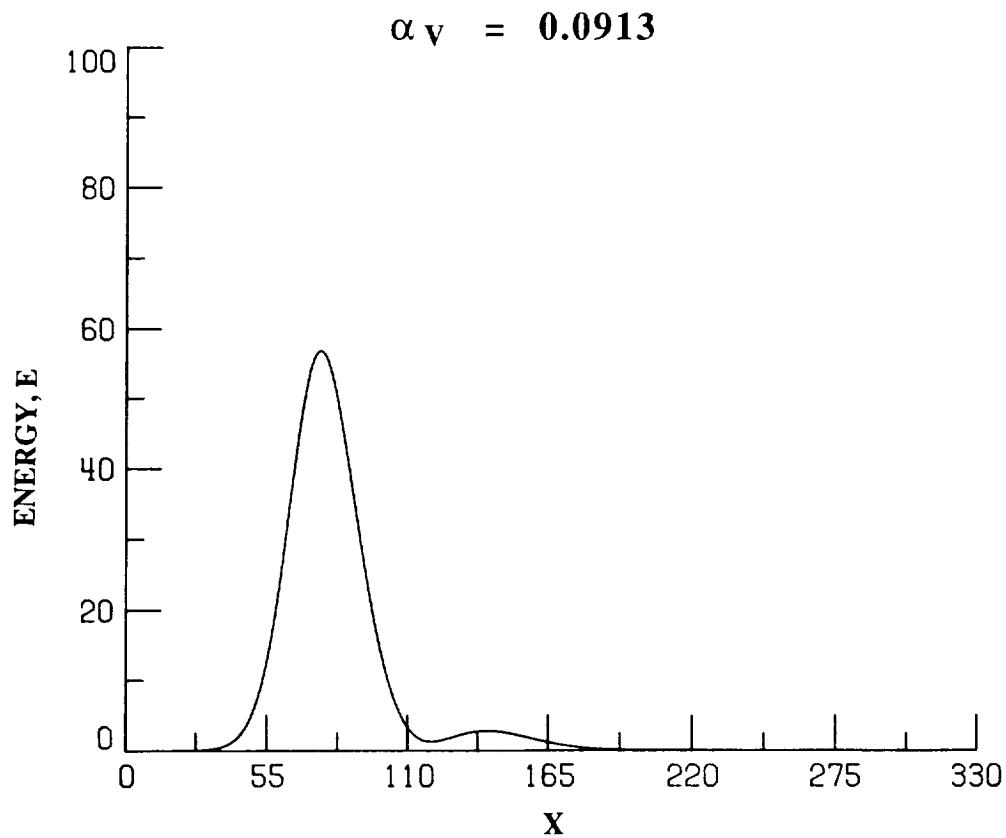
Figure 8

CONCLUSIONS

An effective computational scheme has been developed to study the growth/damping of Görtler vortices along walls of variable curvature.

Computational experiments indicate that when the amplification rates for the u-, v-, and w-perturbations are the same, the finite-difference approach to solve the initial value problem and the normal mode approach give identical results for the Blasius boundary layer on constant curvature concave walls.

The growth of Görtler vortices was rapid in the concave region and was followed by sharp damping in the convex region. However, multiple sets of counter-rotating vortices were formed and remained far downstream in the convex region.

The current computational scheme can be easily extended to more realistic problems including variable pressure gradients and suction effects.

REFERENCES

1. Görtler, H. :   On the Three-Dimensional Instability of Laminar Boundary Layers on Concave Walls.   NACA-TM-1375,   1954.

2. Smith, A. M. O. :   On the Growth of Taylor-Görtler Vortices Along Highly Concave Walls.   Quart.   J.   Math.,   Vol. 13,   pp. 233-262,   1955.

3. Floryan, J. M. :   Stability of Boundary Layer Flows Over Curved Walls. Ph.d.   Dissertation,   Virginia Polytechnic and State University, Virginia,   1980.

4. Ragab, S. A.   and   Nayfeh, A. H. :   Effect of Pressure Gradients on Görtler Instability.   AIAA paper No. 80-1377,   AIAA 13th Fluid and Plasma Dynamics Conference, Snowmass, Colorado, July 14-16, 1980.

5. Herbert, T. :   On the Stability of the Boundary Layer along a Concave Wall.   Arch. Mechaniki Stosowanej, Vol. 28, pp. 1039-1055, 1976.

6. Hall, P. :   The Linear Development of Görtler Vortices in Growing Boundary Layers.   Journal of Fluid Mechanics, Vol. 130, pp. 44-58, 1983.

EFFECT OF ROUGHNESS ON THE STABILITY OF BOUNDARY LAYERS

Ali H. Nayfeh, Saad A. Ragab, and Ayman Al-Maaitah
Department of Engineering Science and Mechanics
Virginia Polytechnic Institute and State University
Blacksburg, Virginia

The instability of flows around hump and dip imperfections is investigated. The mean flow is calculated using interacting boundary layers, thereby accounting for viscous/inviscid interaction and separation bubbles. Then, the two-dimensional linear instability of this flow is analyzed, and the amplification factors are computed. Results are obtained for several height/width ratios and locations. The theoretical results have been used to correlate the experimental results of Walker and Greening.[1] The observed transition locations are found to correspond to amplification factors varying between 7.4 and 10, consistent with previous results for flat plates. The method accounts for Tollmien-Schlichting waves, the shear layer instability, and their interaction. Separation is found to significantly increase the amplification factor.

1. INTRODUCTION

The performance of natural laminar flow (NLF) airfoils is critically dependent on the location of transition, which may be strongly influenced by surface imperfections. Although modern metal and composite manufacturing techniques can provide smooth surfaces that are compatible with NLF, manufacturing tolerance criteria are needed for other unavoidable surface imperfections. These imperfections include waviness and bulges, steps and gaps at junctions, and three-dimensional roughness elements such as flush screw head slots and incorrectly installed flush rivets. Other unavoidable discontinuities arise from the installation of leading edge panels on wings, nacelles, and empennage surfaces and the installation of access panels, doors, and windows on fuselage noses and engine nacelles[2-4]. Because discontinuities cannot be avoided, a guide is needed for manufacturing tolerances. The guide is not related to the drag generated by these discontinuities, but it is related to their allowable sizes so that laminar flow can be maintained. The mechanisms by which these imperfections cause transition include amplification of Tollmien-Schlichting waves, Kelvin-Helmholtz instability (for separated flows), amplification of crossflow vorticity, Gortler instability, enhancement of receptivity of freestream turbulence and acoustic disturbances, and any interaction between two or more of these mechanisms[4-9].

Walker and Greening[1] made wind tunnel experiments to determine the effect of two-dimensional smooth bulges and hollows on the transition of the flow over a flat plate. They used surface tubes to determine the location of transition from laminar to turbulent flow. Their bulges and hollows were mounted on one side of a smooth flat aluminum plate, having an elliptic leading edge. Hislop[10] carried out similar experiments for narrow spanwise surface ridge corrugations on a flat plate. Walker and Cox[11] made wind tunnel experiments to study the effect of spanwise corrugations on an airfoil. These experiments were made for three forms of narrow corrugations (flat, arch and wire) situated in the laminar boundary layer of a large symmetric airfoil (EQH 1260 section), mounted at zero angle of attack.

Fage[5] collected the three previous works[1,10-11] and established criteria for the critical heights of these imperfections that cause transition from laminar to turbulent flow. He found out that the flow conditions near a corrugation which affect transition are associated with a separation of the laminar boundary layer from its surface. Carmichael[6-8] also developed empirically based criteria for allowable waviness and roughnesses that cause either laminar separation or amplification of Tollmien-Schlichting waves. His criteria are for allowable single and multiple bulges or sinusoidal waviness for both swept and unswept wing surfaces. His experiments include the influence of compressibility, suction, pressure gradients, multiple imperfections, and wing sweep. The flight experiments of Holmes, Obara, Martin and Domack[4] demonstrate the strong influence of shapes of steps on the transition location and hence on the allowable heights of such imperfections. They found that by rounding a foward-facing step, the transition Reynolds number increases from 1800 to 2700. Carmichael's criteria are based on experimental results for waves located more than 25-percent chord downstream of the leading edge and hence they will underpredict allowable imperfections in the leading edge region and overpredict allowable imperfections in regions of unaccelerated flows. Klebanoff and Tidstrom[12] used a spanwise trip wire as a roughness element, which causes local upstream and downstream separations, the latter extending forty to fifty times the height of the wire before reattachment to the wall.

Inspite of all these investigations, an understanding of the physics of the instability of flows around surface imperfections is still lacking. As a first step toward such an understanding, this work investigates the influence of a two-dimensional hump or dip on the two-dimensional stability. This work uses a combination of linear stability theory and the exp(N) criterion that has proven to be a valuable tool for correlating transition and for evaluating natural laminar flow as well as laminar flow control concepts. Since linear stability of parallel as well as nonparallel incompressible and compressible flows is well established, the major task in evaluating the influence of imperfections is an accurate prediction of the mean flow.

For smooth surfaces, one can use a conventional boundary-layer formulation to solve for the mean flow over swept and unswept wing surfaces. However, conventional boundary-layer formulations cannot predict flow over surfaces with imperfections, such as suction strips and slots, waviness and bulges, steps and gaps at junctions, and three-dimensional roughness elements because of the strong viscous/inviscid coupling and flow separation. Instead, one needs to use a triple-deck formulation, an interacting boundary-layer formulation, or a Navier-Stokes solver. All these approaches account for the viscous/inviscid interaction as well as separation bubbles, but Navier-Stokes solvers are very expensive compared with triple-deck and interacting boundary-layer formulations. In this work, we use an interacting boundary-layer formulation, which already had been used to compute compressible as well as incompressible flows over smooth steps, wavy surfaces and humps, convex and concave corners, suction or blowing slots, and finite-angle trailing edges. In most of these applications separation bubbles and upstream influence exist and comparisons with solutions of the Navier-

Stokes equations and/or experiments had shown good agreement. Gleyzes, Cousteix and Bonnet[13], Vatsa and Carter[14], and Davis and Carter[15] used interacting boundary-layer theory to analyze separation bubbles near the leading edges of airfoils. Davis, Carter and Reshotko[16] developed an interacting boundary-layer technique for the calculation of transitional separation bubbles over infinite swept wings; the results are in good agreement with Horton's[17] detailed experimental data for separated flow over a swept plate.

The purpose of this work is to study the effect of a two-dimensional roughness element or a two-dimensional surface waviness, represented by a hump or a dip, on the two-dimensional stability of boundary layers over flat plates. Quartic humps with different sizes and locations are studied first. Then, the theory is used to correlate the experimental data of Walker and Greening.

2. MEAN FLOW

The two-dimensional incompressible laminar boundary layer over the plate and the hump is determined by solving the interacting boundary-layer equations[18,19]. These equations account for upstream influence through the interaction of the viscous flow with the inviscid flow outside the boundary layer. Moreover, they are also capable of capturing separation bubbles without difficulties. Solutions are obtained by using a finite-difference method in which the grid spacings acknowledge the scalings predicted by the triple-deck theory in the interaction region.

Figure 1 shows a small symmetric hump of height h^* and width $2b^*$ whose center is located at x_m^*. We introduce dimensonless variables using L^* and U_∞^*, where L^* is the distance from the leading edge to a reference point, as reference quantities. In terms of dimensionless variables, the hump shape is given by

$$y = \frac{y^*}{L^*} = \frac{h^*}{L^*} f(\zeta)$$

(1)

where

$$\zeta = \frac{x^* - x_m^*}{b^*} = \frac{x - x_m}{b}$$

(2)

We present numerical results for a quadratic hump given by

$$f(\zeta) = \begin{cases} (1 - \zeta^2)^2 & \text{if } |\zeta| \leq 1 \\ 0 & \text{if } |\zeta| > 1 \end{cases}$$

(3)

and the Walker and Greening hump

$$f(\zeta) = \begin{cases} 1 - 3\zeta^2 + 2|\zeta|^3 & \text{if } |\zeta| \leq 1 \\ 0 & \text{if } |\zeta| > 1 \end{cases}$$

(4)

Figure 2 shows the variation of the height of a hump, corresponding to h = 3 in triple-deck variables, and the resulting displacement thickness. Figure 3 shows the distributions of the skin friction and pressure coefficients for the hump shown in Fig. 2. A small separation bubble is formed on the lee side of the hump.

Tables 1 and 2 show some of the mean-flow properties for the humps and dips of Walker and Greening. The velocity u outside the boundary layer for the undistorted surface varies from 15.9 m/sec (53.0 ft/sec) to 28.5 m/sec (95.0 ft/sec) for the humps, and from 18.57 m/sec (61.9 ft/sec) to 25.47 m/sec (84.9 ft/sec) for the dips. The maximum transverse dimension h* varies from 0.75 mm (0.03 in) to 1.75 mm (0.07 in) for the humps and from 1.425 mm (0.057 in) to 1.675 mm (0.067 in) for the dips. The observed transition length is denoted by L_T; it is measured from the leading edge to the observed transition location. The Reynolds numbers at the middle of the humps or dips R_m and at the transition location R_T are based on the reference length δ^* so that

$$R_m = (Re)^{\frac{1}{2}}, \qquad R_T = (\frac{L_T}{L^*} Re)^{\frac{1}{2}} \tag{5}$$

All of the previous quantities were calculated directly from the experimental data given by Walker and Greening, but the streamwise extents of the separation bubbles are expressed as the difference in the Reynolds numbers at separation and reattachment; that is, ΔR = R(reattachment) - R(separation) and ΔR is calculated using the interacting boundary-layer code. Except for hump No. 1 all the humps and dips in Tables 1 and 2 have separation bubbles.

Figure 4 shows the variation of the streamwise velocity profiles for hump No. 14. The first and the last velocity profiles are at locations away from the hump; they are essentially Blasius profiles.

3. STABILITY ANALYSIS

We consider the two-dimensional spatial quasi-parallel stability of the basic state determined by the interacting boundary-layer code. To this end, we superimpose on it a two-dimensional unsteady disturbance. Thus, we let

$$\tilde{q}(x,y,t) = Q(y) + \hat{q}(x,y,t) \tag{6}$$

where q refers to the pressure p and the velocity components u and v in the streamwise direction x and the transverse direction y, respectively. Substituting the assumed flow into the Navier-Stokes equations, subtracting the basic-flow quantities, and linearizing the resulting equations, we obtain equations describing the disturbance. We consider the case of spatial stability and determine the amplification rate - α_i, where α_i is the imaginary part of the complex wavenumber α.

For a given U, ω, and R, we determine α and then calculate the N factor from

$$N = - 2 \int_{R_o}^{R} \alpha_i dR \tag{7}$$

305

where R_0 is the Reynolds number corresponding to branch I of the neutral stability curve.

Figure 5 shows the variation of the growth rate with streamwise distance for the hump shown in Fig. 2. Shown also is the growth rate of the Blasius flow at the same frequency. The presence of the hump first increases the growth rate then it decreases the growth rate and finally increases the growth rate again. The stabilizing and destabilizing effects are consistent with the gradients of the pressure distributions shown in Fig. 3.

The amplification of two-dimensional disturbances is the result of a complex interaction of Tollmien-Schlichting waves and shear-layer (laminar separation) instability as evident from Figs. 4 and 6. They show the variation of the streamwise velocity profile and the corresponding eigenfunction of the instability wave, respectively, with distance along the plate. Ahead of the separation region, the eigenfunction has a character typical of T-S waves with two peaks, a large one at the critical layer and a small peak near the edge of the boundary layer. In the separation region, the eigenfunctions develop a third peak at the inflection point of the mean-flow profile. This peak increases with distance from the separation point, achieves a maximum which can be comparable to the peak at the critical layer, and decreases to zero at the reattachment point. The effects of the shear-layer instability are to increase the growth rates and the dangerous frequency.

Table 3 shows the variations of the Reynolds number R_g at which $N = 9$ and the computed amplification factor N_T at the experimentally measured transition location with the dimensionless frequency F for hump No. 5 in Table 1. For $F = 45 \times 10^{-6}$, the maximum value of N is 8.4. It is clear that the most dangerous frequency has shifted from $F = 25 \times 10^{-6}$ for the Blasius flow to $F = 37.5 \times 10^{-6}$ for the disturbed flow. Moreover, the maximum computed amplification factor at the experimental transition location is 8.7.

Tables 4 and 5 summarize the computed results for all the hump and dip configurations of Walker and Greening. They show the maximum (maximized over all frequencies) amplification factor N_T and its corresponding frequency at the measured transition location. The values of N_T range from 7.4 to 10, consistent with previous results for flat plates.

4. CONCLUSIONS AND RECOMMENDATIONS

An analysis is conducted of the effect of imperfections consisting of humps and dips on the stability of incompressible flows over flat plates. The mean flow is calculated using interacting boundary layers. Linear quasiparallel spatial stability is used to calculate the growth rates and mode shapes of two-dimensional disturbances. Then, the amplification factor is computed. A search for the most dangerous frequency is conducted based on an amplification factor of 9 in the shortest distance. Correlations are made with the transition experiment of Walker and Greening using the e^9 method.

Based on the present investigations, it can be concluded that:

1. The e^9 method gives a good estimate of the transition location.

2. Increasing the size of the separation bubble, by increasing either the height-to-width ratio or the freestream Reynolds number, causes transition to occur sooner.

3. In the separation bubble, the calculated growth rates of the disturbances account for both the T-S and shear-layer instabilities.

4. The shape of a smooth hump or dip does not have a significant effect on the growth rates.

5. The geometrical factors of the imperfection that govern the instability are:

    a. the height-to-width ratio.

    b. the location of the imperfection element from the leading edge of the plate and Branch I of the Blasius stability curve.

6. The most dangerous frequency in the presence of the roughness element is not the same as that for the Blasius flow.

    The present study needs to be extended by accounting for:

    a. nonlinear effects (in view of the large growth rates encountered in separation regions).

    b. nonparallel effects.

    c. the effects of concave curvature (i.e., Görtler instability).

    d. the receptivity to acoustic and free-stream disturbances.

    e. the interaction between any of the instability mechanisms.

More experiments need to be conducted to provide detailed measurements of the mean profiles, mode shapes, growth rates, etc. that can be used to corroborate the theoretical results.

REFERENCES

1. Walker, W. S.; and Greening, J. R.: Brit. A.R.C. 5950, 1942.

2. Holmes, B. J.; Obara, C. J.; and Yip, L. P.: NASA TP 2256, 1984.

3. Obara, C. J.; and Holmes, B. J.: NASA TP 2417, 1985.

4. Holmes, B. J.; Obara, C. J.; Martin, G. L.; and Domack, C. S.: presented at the 1985 SAE General Aviation Meeting and Exposition, Wichita, Kansas, SAE Paper No. 850863, 1985.

5. Fage, A.: Report and Memorandum No. 2120, Brit. A.R.C., 1943.

6. Carmichael, B. H.; Whites, R. C.; and Pfenninger, W.: Northrup Aircraft Inc. Rep. No. NAI-57-1163 (BLC-101), 1957.

7. Carmichael, B. H.: Norair Rep. No. NOR-59-438 (BLC-123), 1959.

8. Carmichael, B. H.; and Pfenninger, W.: "Surface Imperfection Experiments on a Swept Laminar Suction Wing", Norair Rep. No. NOR-59-454 (BLC-124), 1959.

9. Goldstein, M. E.: Journal of Fluid Mechanics, vol. 154, 1985, p. 509.

10. Hilsop, G. S.: Brit. A.R.C. 6443, 1943.

11. Walker, W. S.; and Cox, R. J.: Brit. A.R.C. 6126, 1942.

12. Klebanoff, P. S.; and Tidstrom, K. P.: Physics of Fluids, vol. 15, 1972, p. 1173.

13. Gleyzes, C.; Cousteix, J.; and Bonnet, J. L.: in Second Symposium on Numerical and Physical Aspects of Aerodynamic Flows, (Proceedings, Springer-Verlag, 1983).

14. Vatsa, V. N.; and Carter, J. E.: AIAA Journal, vol. 22, 1984, p. 1697.

15. Davis, R. L.; and Carter, J. E.: AIAA Journal, vol. 25, 1986, p. 850.

16. Davis, R. L.; Carter, J. E.; and Reshotko, E.: AIAA Journal, vol. 25, 1987, p. 421.

17. Horton, H. P.: Ph.D. Thesis, University of London, (Queen Mary College, 1968).

18. Davis, R. L.; and Werle, M. J.: "Progress on Interacting Boundary-Layer Computations atHigh Reynolds Number", in the Numerical and Physical Aspects of Aerodynamic Flows, (ed. T. Cebeci, Springer-Verlag, New York, 1982).

19. Ragab, S. A.; and Nayfeh, A. H.: "A Comparison of the Second-Order Triple-Deck Theory with Interacting Boundary Layers", in Numerical and Physical Aspects of Aerodynamic Flows, (ed. T. Cebeci, Springer-Verlag, New York, 1982).

Table 1. Hump configurations in the experiments of
Walker and Greening

Number	u ft/sec	h in	L_T ft	h*/b*	R_m	R_T	Bubble size ΔR
1	82.6	0.031	4.58	0.0155	812	1346	00.0
2	69.4	0.0525	4.58	0.0263	830	1376	18.0
3	70.4	.0555	4.58	0.0278	860	1426	29.6
4	53.0	0.0620	4.58	0.0310	744	1234	25.7
5	56.2	0.0665	4.58	0.0332	764	1267	28.8
6	53.8	0.0700	4.58	0.0350	753	1249	36.1
7	78.0	0.0530	3.75	0.0265	904	1357	26.9
8	76.0	0.0555	3.75	0.0278	892	1337	32.5
9	61.5	0.0620	3.75	0.0310	803	1205	31.6
10	62.4	0.0630	3.75	0.0315	810	1215	34.5
11	55.5	0.0680	3.75	0.0340	761	1142	34.6
12	95.0	0.0525	2.92	0.0263	997	1319	32.6
13	70.0	0.0620	2.92	0.0310	860	1138	32.8
14	92.4	0.0620	2.08	0.0310	983	1098	49.9

Table 2. Dip configurations in the experiments of Walker and Greening

Number	u ft/sec	h in	L_T ft	h*/b*	R_m	R_T	Bubble size ΔR
1	76.4	-0.057	4.58	0.0285	894	1483	37.7
2	65.8	-0.067	4.58	0.0335	831	1377	41.6
3	82.7	-0.057	3.75	0.0285	930	1395	39.8
4	61.9	-0.067	3.75	0.0335	807	1210	36.5
5	84.9	-0.057	2.92	0.0285	943	1248	41.3
6	69.7	-0.067	2.92	0.0285	855	1132	39.0

310

Table 3. Variation of the maximum N-factor and the location
at which $N = 9$ with the height of a quartic hump of
half-width $\frac{b^*}{L^*_m} = 2.274 \times 10^{-2}$ $(\frac{b^*}{\delta} = 4.430)$ whose center

is at $R_m = 975$: $\delta = 5 \frac{\nu L^*}{U}$

$\frac{h^*}{L^*}$	$\frac{h^*}{\delta}$	$\frac{h^*}{b^*}$	R_9	N_{max}	Bubble length ΔR
0	0	0	1792	9.84	0
4.198×10^{-4}	0.082	0.019	1779	10.04	0
5.457×10^{-4}	0.106	0.024	1750	10.25	0
8.395×10^{-4}	0.164	0.037	1680	11.02	6.7
12.593×10^{-4}	0.246	0.055	1552	12.67	22.1

Table 4. Correlation of the theoretical and experimental
results for the transition location for the
humps in Table 1

Hump#	h^* in	$\frac{h^*}{b^*}$	R_m	Separation bubble ΔR	R_T	N_T	$F_T \times 10^6$
1	0.0310	0.0155	812	00.0	1346	10.03	20.0
2	0.0525	0.0262	830	18.0	1376	8.20	37.5
3	0.0555	0.0278	860	29.6	1426	9.09	35.0
4	0.062	0.0319	744	25.7	1234	7.95	40.0
5	0.0665	0.0333	764	28.8	1267	8.70	37.5
6	0.0700	0.0350	753	36.1	1249	9.10	40.0
7	0.0530	0.0265	904	26.9	1356	8.30	37.5
8	0.0555	0.0278	892	32.5	1337	8.19	35.0
9	0.0620	0.0310	803	31.7	1205	7.90	45.0
10	0.0630	0.0315	810	34.5	1215	8.00	42.5
11	0.0680	0.0340	761	34.6	1142	7.85	45.0
12	0.0525	0.0263	997	32.0	1319	9.20	35.0
13	0.0620	0.0310	860	32.8	1138	7.40	45.0
14	0.0620	0.0310	983	49.9	1098	9.00	55.0

Table 5. Correlation of the theoretical and experimental results for the transition location for the dips in Table 2

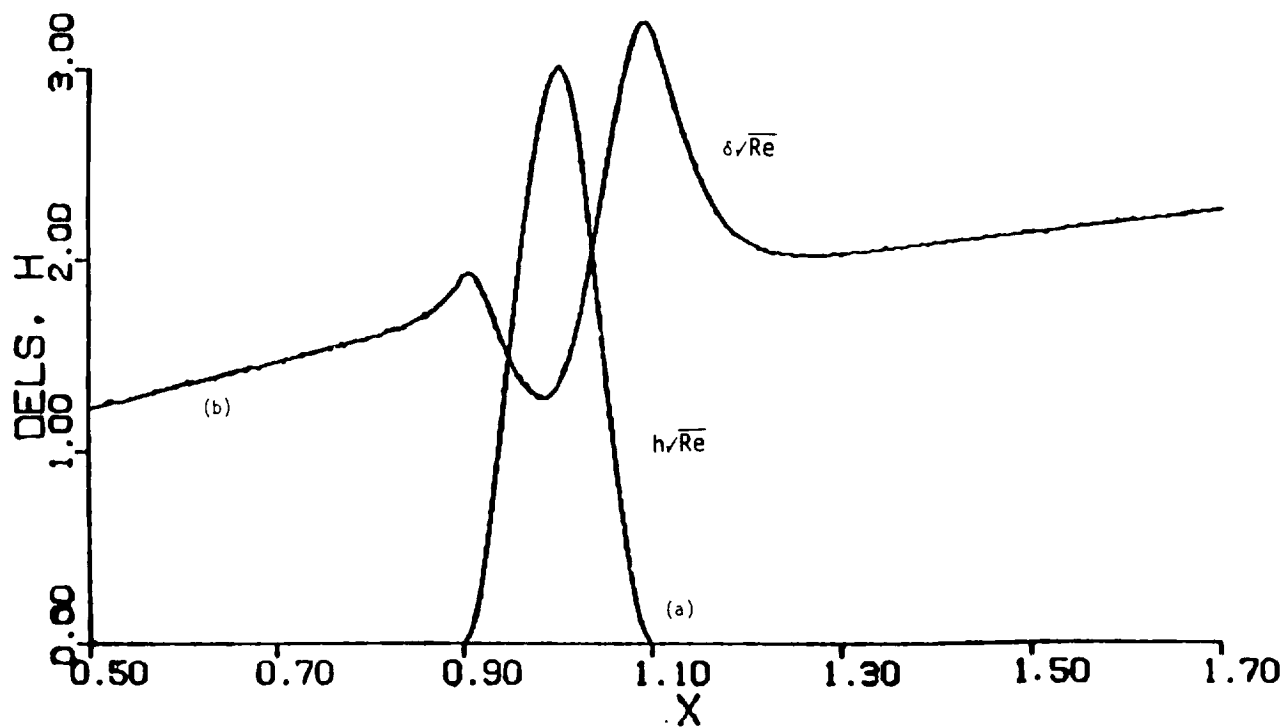| Dip#	$-h^*$	$\dfrac{h^*}{b^*}$	R_m	Separation bubble ΔR	R_T	N_T	$F_T \times 10^6$
1	0.057	0.0285	894	37.7	1483	9.2	30
2	0.067	0.0335	831	41.6	1377	8.9	35
3	0.057	0.0285	930	39.8	1395	8.31	35
4	0.067	0.0335	807	36.5	1210	7.5	40
5	0.057	0.0285	943	41.3	1248	7.3	45
6	0.067	0.0335	855	39.0	1132	6.69	50
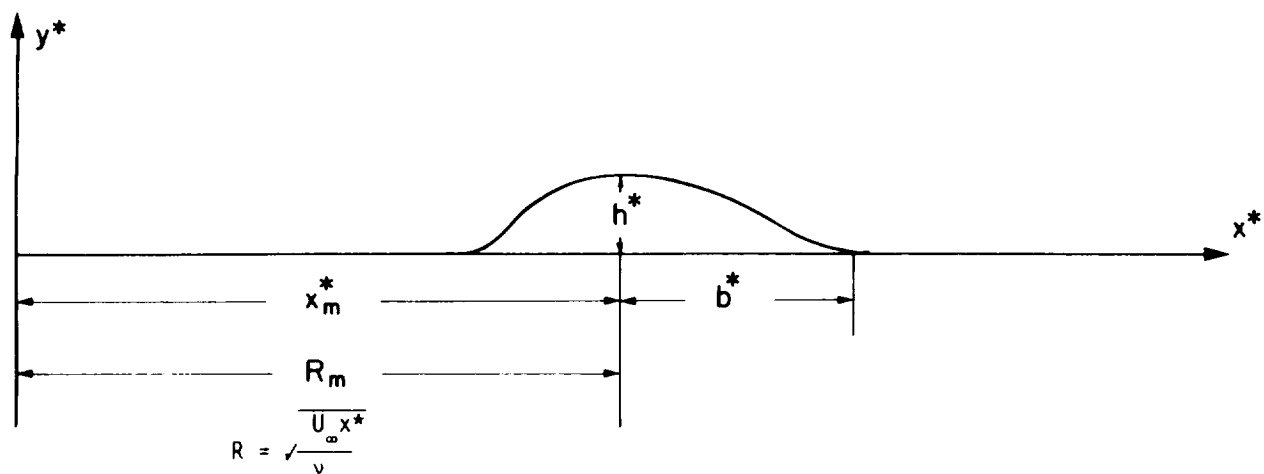
Figure 1. Hump configuration.

Figure 2. (a) Hump shape for h = 3, and

(b) corresponding displacement surface $\delta\sqrt{Re}$; Re = 10^6.
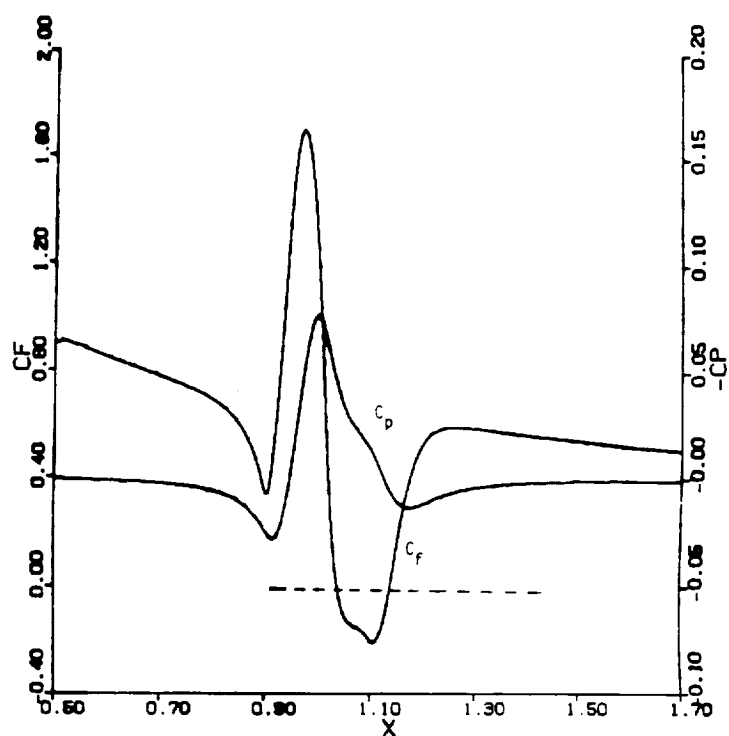
Figure 3. Distributions of (a) skin friction coefficient $c_f\sqrt{Re}$,
and (b) pressure coefficient c_p for $h = 3$, $Re = 10^6$;
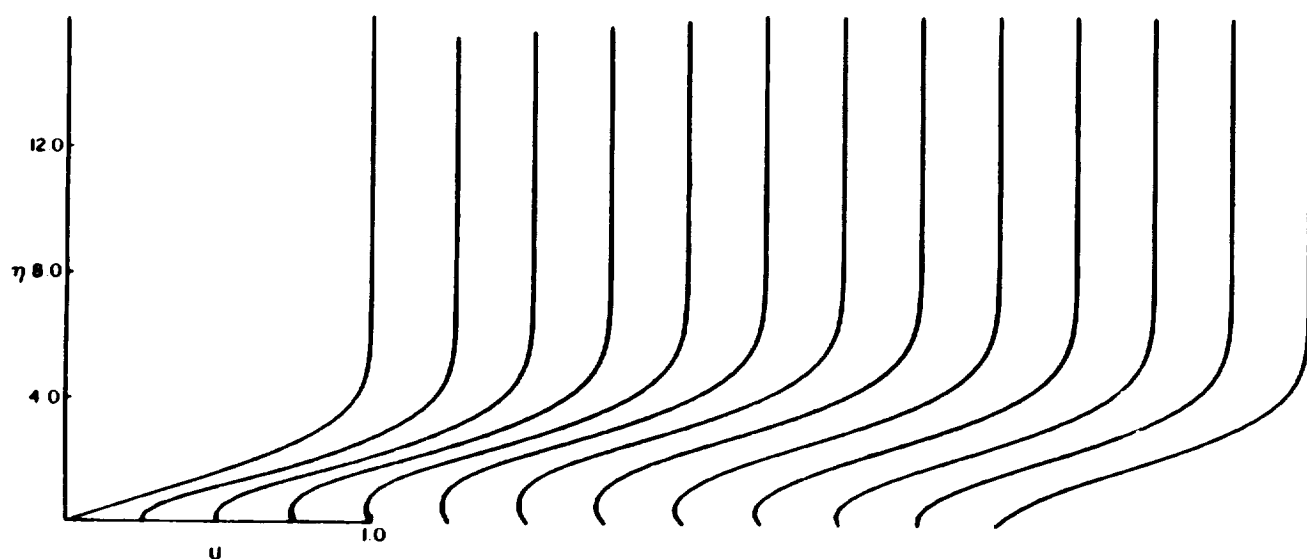small separation bubble.

Figure 4. Variation of streamwise velocity profiles along the plate
for hump No. 14 in Table 1. The hump is centered at
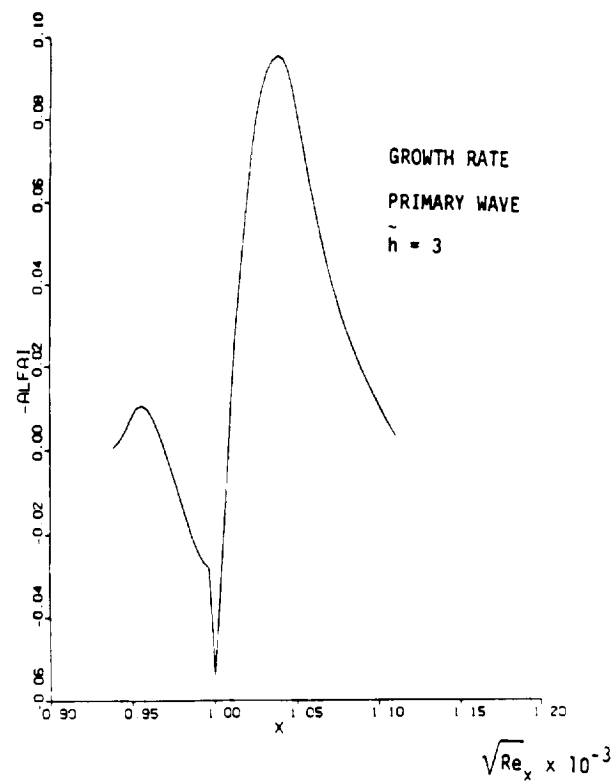$X_m^*/L^* = 1.0(R = 983)$, $h^*/b^* = 0.031$, $b^*/L^* = 0.1$.

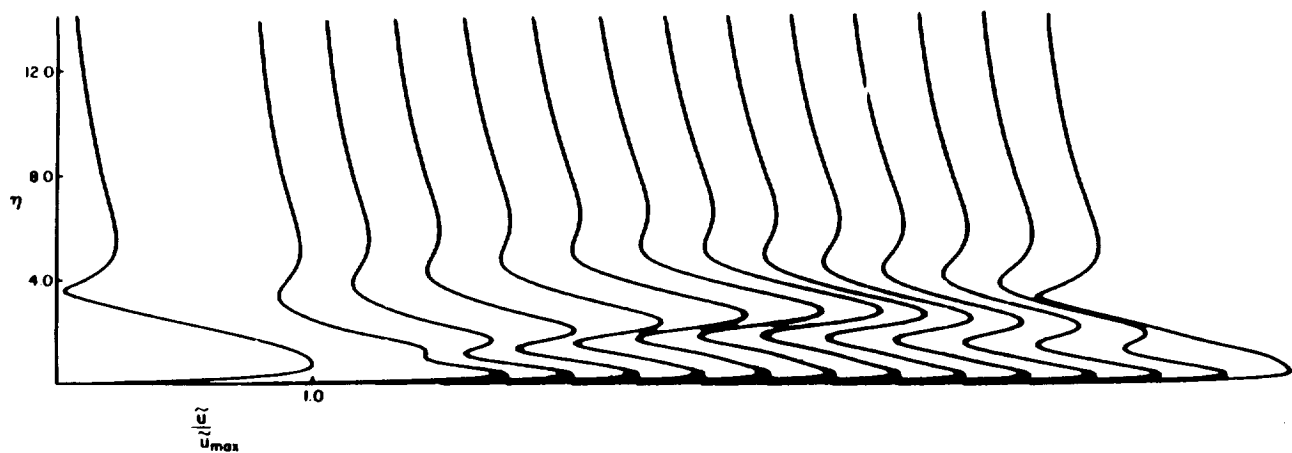Figure 5. Variation of the growth rate with streamwise position.

Figure 6. Variation of the eigenfunction of hump No. 14 in Table 1
along the plate at frequency $F = 55 \times 10^{-6}$.

315

|

NASA

Report Documentation Page

1. Report No. NASA CP-2487, Part 1	2. Government Accession No.	3. Recipient's Catalog No.

4. Title and Subtitle	5. Report Date
Research in Natural Laminar Flow and Laminar-Flow Control	December 1987
	6. Performing Organization Code

7. Author(s)	8. Performing Organization Report No.
Jerry N. Hefner and Frances E. Sabo, Compilers	L-16350
	10. Work Unit No. 505-60-31-06

9. Performing Organization Name and Address	11. Contract or Grant No.
NASA Langley Research Center Hampton, VA 23665-5225	
	13. Type of Report and Period Covered

12. Sponsoring Agency Name and Address	Conference Publication
National Aeronautics and Space Administration Washington, DC 20546-0001	14. Sponsoring Agency Code

15. Supplementary Notes

16. Abstract

Since the mid 1970's, NASA, industry, and universities have worked together to conduct important research focused at developing laminar-flow technology that could reduce fuel consumption for general aviation, commuter, and transport aircraft by as much as 40 to 50 percent. This research, which was initiated under the NASA Aircraft Energy Efficiency Program and continued through the Research and Technology Base Program, has proved very successful with many very significant and impressive results having been obtained.

This symposium was planned in view of the recent accomplishments within the areas of laminar-flow control and natural laminar flow, and the potential benefits of laminar-flow technology to the civil and military aircraft communities in the United States. The symposium included technical sessions on advanced theory and design tool development, wind tunnel and flight research, transition measurement and detection techniques, low and high Reynolds number research, and subsonic and supersonic research.

17. Key Words (Suggested by Author(s))	18. Distribution Statement
Laminar flow Natural laminar flow Aerodynamics	▓▓▓▓▓▓▓ Subject Category 02

19. Security Classif. (of this report)	20. Security Classif. (of this page)	21. No. of pages	22. Price
Unclassified	Unclassified	329	